Vol. 63 December, 1959 No. 12

THE JOURNAL OF PHYSICAL CHEMISTRY

(Registered in U. S. Patent Office)

CONTENTS

NOTES

Communication to the Editor

THE JOURNAL OF PHYSICAL CHEMISTRY

(Registered in U. S. Patent Office)

Published monthly by the American Chemical Society at 20th and Northampton Sts., Easton, Pa.

Second-class mail privileges authorized at Easton, Pa. This publication is authorized to be mailed at the special rates of postage prescribed by Section 131.122.

The *Journal of Physical Chemistry* is devoted to the publication of selected symposia in the broad field of physical chemistry and to other contributed papers.

Manuscripts originating in the British Isles, Europe and Africa should be sent to F. C. Tompkins, The Faraday Society, 6 Gray's Inn Square, London W. C. 1, England.

Manuscripts originating elsewhere should be sent to W. Albert Noyes, Jr., Department of Chemistry, University of Rochester, Rochester 20, N. Y.

Correspondence regarding accepted copy, proofs and reprints should be directed to Assistant Editor, Allen D. Bliss, Department of Chemistry, Simmons College, 300 the Fenway, Boston 15, Mass.

Business Office: Alden H. Emery, Executive Secretary, American Chemical Society, 1155 Sixteenth St., N. W., Washington 6, D. C.

Advertising Office: Reinhold Publishing Corporation, 430 Park Avenue, New York 22, N. Y.

Articles must be submitted in duplicate, typed and double spaced. They should have at the beginning a brief Abstract, in no case exceeding 300 words. Original drawings should accompany the manuscript. Lettering at the sides of graphs (black on white or blue) may be pencilled in and will be typeset. Figures and tables should be held to a minimum consistent with adequate presentation of information. Photographs will not be printed on glossy paper except by special arrangement. All footnotes and references to the literature should be numbered consecutively and placed in the manuscript at the proper places. Initials of authors referred to in citations should be given. Nomenclature should conform to that used in *Chemical Abstracts*, mathematical characters marked for italic, Greek letters carefully made or annotated, and subscripts and superscripts clearly shown. Articles should be written as briefly as possible consistent with clarity and should avoid historical background unnecessary for specialists.

Notes describe fragmentary or incomplete studies but do not otherwise differ fundamentally from articles and are subjected to the same editorial appraisal as are articles. In their preparation particular attention should be paid to brevity and conciseness. Material included in Notes must be definitive and may not be republished subsequently.

Communications to the Editor are designed to afford prompt preliminary publication of observations or discoveries whose value to science is so great that immediate publication is imperative. The appearance of related work from other laboratories is in itself not considered sufficient justification for the publication of a Communication, which must in addition meet special requirements of timeliness and significance. Their total length may in no case exceed 500 words or their equivalent. They differ from Articles and Notes in that their subject matter may be republished.

Symposium papers should be sent in all cases to Secretaries of Divisions sponsoring the symposium, who will be responsible for their transmittal to the Editor. The Secretary of the Division by agreement with the Editor will specify a time after which symposium papers cannot be accepted. The Editor reserves the right to refuse to publish symposium articles, for valid scientific reasons. Each symposium paper may not exceed four printed pages (about sixteen double spaced typewritten pages) in length except by prior arrangement with the Editor.

Remittances and orders for subscriptions and for single copies, notices of changes of address and new professional connections, and claims for missing numbers should be sent to the American Chemical Society, 1155 Sixteenth St., N. W., Washington 6, D. C. Changes of address for the *Journal of Physical Chemistry* must be received on or before the 30th of the preceding month.

Claims for missing numbers will not be allowed (1) if received more than sixty days from date of issue (because of delivery hazards, no claims can be honored from subscribers in Central Europe, Asia, or Pacific Islands other than Hawaii), (2) if loss was due to failure of notice of change of address to be received before the date specified in the preceding paragraph, or (3) if the reason for the claim is "missing from files."

Subscription Rates (1959): members of American Chemical Society, $8.00 for 1 year; to non-members, $16.00 for 1 year. Postage free to countries in the Pan American Union; Canada, $0.40; all other countries, $1.20. Single copies, current volume, $1.35; foreign postage, $0.15; Canadian postage $0.05. Back volumes (Vol. 56–59) $15.00 per volume; (starting with Vol. 60) $18.00 per volume; foreign postage, per volume $1.20, Canadian, $0.15; Pan-American Union, $0.25. Single copies: back issues, $1.75; for current year, $1.35; postage, single copies: foreign, $0.15; Canadian, $0.05; Pan American Union, $0.05.

The American Chemical Society also publishes *Journal of the American Chemical Society, Chemical Abstracts, Industrial and Engineering Chemistry, Chemical and Engineering News, Analytical Chemistry, Journal of Agricultural and Food Chemistry, Journal of Organic Chemistry* and *Journal of Chemical and Engineering Data*. Rates on request.

THE JOURNAL OF PHYSICAL CHEMISTRY

VOL. LXIII

1959

EASTON, PA.
MACK PRINTING COMPANY
1959

THE JOURNAL OF
PHYSICAL CHEMISTRY

(Registered in U. S. Patent Office) (© Copyright, 1959, by the American Chemical Society)

VOLUME 63 DECEMBER 30, 1959 NUMBER 12

EXCHANGE OF DEUTERIUM AND HEAVY OXYGEN AMONG HYDROGEN, WATER VAPOR AND OXIDE CATALYSTS OF SPINEL TYPE

BY YUKIO YONEDA, AKIO FUJIMOTO[1] AND SHOJI MAKISHIMA

Department of Applied Chemistry, Faculty of Engineering, University of Tokyo, Tokyo, Japan

Received January 14, 1959

The exchange of D and ^{18}O among H_2, $D_2{}^{18}O$ and oxide catalysts of the spinel type, $MgAl_2O_4$, $MgCr_2O_4$, $ZnCr_2O_4$ and $ZnFe_2O_4$ was studied by a flow method. The total exchange rate of hydrogen, R, and that of oxygen, R', were calculated. R'/R of a catalyst is approximately independent of temperature, was about 0.1 for $MgAl_2O_4$ and 0.2–0.4 for the other catalysts. It was concluded that the common rate-determining step in the exchange of hydrogen and of oxygen in the regeneration of oxygen vacancies in the catalyst which is accompanied by the release of water molecules. There is a correlation between the exchange rate and the oxidizing power of the catalyst, *i.e.*, $ZnFe_2O_4 > ZrCr_2O_4 > MgCr_2O_4 > MgAl_2O_4$. The mechanism of hydrogen exchange on the surface of the catalyst is discussed.

Introduction

It has been desired to discover an active catalyst for hydrogen exchange in a dual temperature method.[2] Although there is considerable literature on the catalytic exchange reaction between H_2 and D_2,[3] little work has been done on the exchange between hydrogen and water, especially with oxide catalysts.

In a previous study of the exchange of oxygen atoms among carbon dioxide, carbon monoxide and oxide catalysts,[4] the authors concluded that the catalyst should be considered to be a reactant and not merely as a *field* for a heterogeneous reaction.

In the present paper, we have tried to elucidate the mechanism by which the catalyst, a solid phase, takes part in the catalytic reaction. Simultaneous measurements were made of the exchange rate of hydrogen atoms between hydrogen and water vapor and that of oxygen atoms between the *bulk* of the catalyst and water vapor, with $D_2{}^{18}O$ as one of the starting materials.

Experimental

Materials.—Four oxide spinels, $MgAl_2O_4$, $MgCr_2O_4$, $ZnCr_2O_4$ and $ZnFe_2O_4$, were prepared by a solid phase reaction between appropriate pairs of simple compounds: Mg, basic magnesium carbonate precipitated with sodium carbonate; Al, Cr and Fe, respective hydroxides precipitated with NH_4OH; Zn, $Zn(OH)_2$ of A.R. grade. The spinels were obtained by heating a stoichiometric, well-ground mixture of above-mentioned materials at temperatures and durations indicated in parentheses: $MgAl_2O_4$ (1300°, 4 hr.), $MgCr_2O_3$ and $ZnCr_2O_4$ (1200°, 5 hr.), $ZnFe_2O_4$ (1100°, 3 hr.). X-Ray diffraction analyses showed that the spinel formation was complete except in the case of $MgAl_2O_4$, which contained a small quantity of MgO and Al_2O_3.

The heavy water contained 9.49% of D and 0.332% of ^{18}O.

Exchange Reaction System and Procedures.—The exchange reaction was studied by a flow method. A weighed amount of the catalyst (volume 3 cc.) which had been outgassed for 50 min. at 400° and 10^{-2}–10^{-3} mm. was placed on a sintered glass disk in a glass reactor. Tank hydrogen, purified in a common train of heated palladium asbestos and a trap, was saturated with the vapor of heavy water in a saturator kept at the boiling point of ethanol. After the temperature of the reactor had been adjusted, a stream of saturated hydrogen was introduced at a rate of 28 cc./min. for 75 min. The calculated value of the flow rate of heavy water was 1.265 g./75 min., the ratio hydrogen/water being 57/43; the observed values agreed with those calculated within ±1.5%. After the reaction the heavy water was separated by a trap kept at −78°, and hydrogen was sampled when necessary. The isotope content of trapped water was measured in the form of hydrogen or carbon dioxide with a mass spectrometer, Model 21-103A of Consolidated Electrodynamics, Inc.; the accuracy of the determination was ±1%. The surface area was measured by the B.E.T. method with carbon dioxide as the adsorbate; this method is not sufficiently accurate for areas smaller than 0.5 m.²/g.

Calculation

In this calculation, all the heavy water molecules are assumed as HDO. Following the conventional

(1) Asahi Kasei Kogyo, Ltd., Nobeoka, Miyazaki-ken, Japan.

(2) M. Benedict, First Intern. Conf. on Peaceful Uses of Atomic Energy, 1955, Publ. 819.

(3) A. H. Kimball, *et al.*, "Bibliography of Research on Heavy Hydrogen Compounds," NNES, III-4C, 1949, McGraw-Hill Book Co., New York, N. Y.; NBS Circular, No. 562 (1956).

(4) Y. Yoneda, S. Makishima and K. Hirasa, *J. Am. Chem. Soc.*, **80**, 4503 (1958).

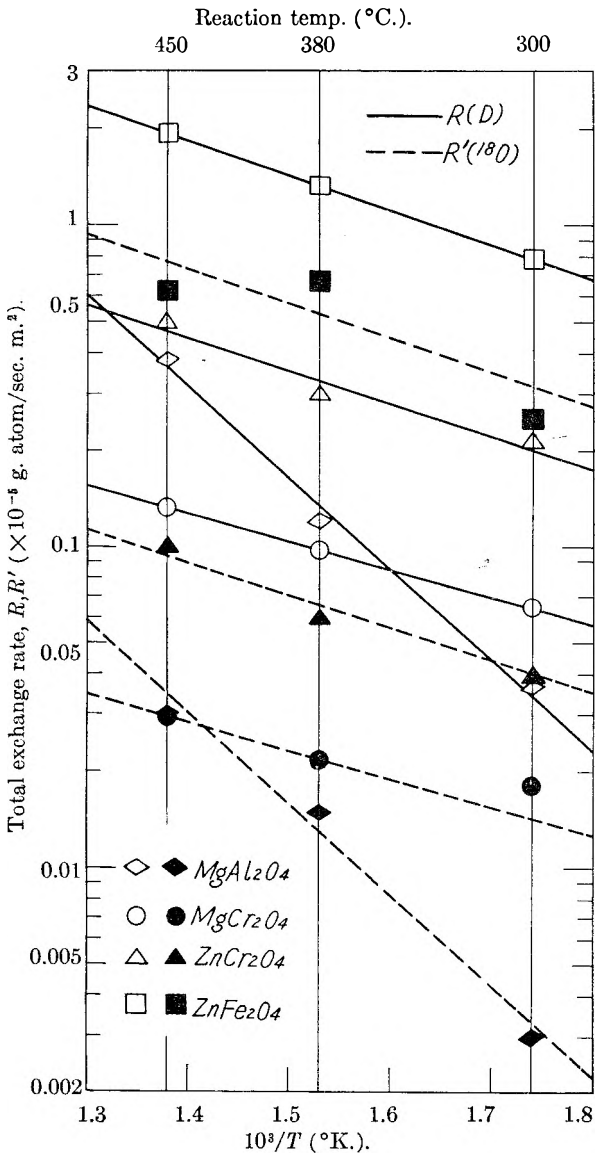

Fig. 1.—Total exchange rate, R or R' *vs.* temperature.

calculation of a flow reaction, we have rate equation 2 for the deuterium exchange 1

$$\underset{\alpha}{HDO} + \underset{1-\beta}{H_2} \underset{R_r}{\overset{R}{\rightleftharpoons}} \underset{1-\alpha}{H_2O} + \underset{\beta}{HD} \qquad (1)$$

$$-a^0_w d\alpha = [R\alpha(1-\beta) - R_r(1-\alpha)\beta]\, dS \qquad (2)$$

where α and β represent the atomic fractions of deuterium of water vapor and hydrogen, respectively; a^0_w is gram atoms of hydrogen in the passed water per unit time, 3.035×10^{-5} g. atom/sec.; and S is the surface area of the catalyst, (m.²). Then since $R/R_r = 1/K$ where $1/K$ is the equilibrium constant of eq. 1 ($K = 1.38 - 1.75$ at these temperatures), and α and β are less than 0.1, we can abbreviate eq. 2 to eq. 3, a term $(K-1)\alpha\beta$ being neglected

$$-a^0_w\, d\alpha = R(\alpha - K\beta)\, dS \qquad (3)$$

When the isotopic effect between hydrogen and deuterium is neglected, the forward total exchange rate of hydrogen without discrimination between isotopes is to be represented by R. As the hydrogen exchange ratio in water vapor, x, must be equal to that in gaseous hydrogen, we have eq. 4.

$$x = (\alpha_0 - \alpha)/(\alpha_0 - \alpha_\infty) = (\beta - \beta_0)/(\beta_\infty - \beta_0) \fallingdotseq \beta/\beta_\infty \qquad (4)$$

where the suffixes 0 and ∞ denote the beginning of the reaction and equilibrium, respectively; $\beta_0 = 0.005\%$ is neglected in the last term. Substituting β from eq. 4 in eq. 3 and remembering $K = \alpha_\infty/\beta_\infty$, which is derived from eq. 3 at $d\alpha/dS = 0$, we have

$$-a^0_w\, d\alpha = \alpha_0/(\alpha_0 - \alpha_\infty) \times R(\alpha - \alpha_\infty)\, dS \qquad (5)$$

Integration gives

$$R = (\alpha_0 - \alpha_\infty)/\alpha_0 \times (a^0_w/S)[-\ln(1 - x_f)] \qquad (6)$$

where suffix f denotes the end of reaction, *e.g.*, x_f is the hydrogen exchange ratio of the trapped water.

It is shown readily that

$$R = (\alpha_0 - \alpha_\infty)/\alpha_0 \times a^0_w \tau k_e/S \qquad (7)$$

where k_e is the experimental rate constant (sec.$^{-1}$) so that $-d\alpha/dt = k_e(\alpha - \alpha_\infty)$, and τ is an average contact time (sec.). The values of K, α and τ are summarized in Table I.

TABLE I

HYDROGEN EXCHANGE

$1/K$ is the equilibrium constant, α_∞ the atomic fraction of D in the water vapor at equilibrium, and τ the average contact time

Temp. (°C.)	450	380	300
K	1.38	1.53	1.75
α_∞ (%)	4.77	5.00	5.29
τ (sec.)	1.46	1.61	1.84

Exchange Rate of Heavy Oxygen.—If we express the exchange reaction of heavy oxygen as

$$\underset{\alpha'}{HD^{18}O} + \underset{1-\beta'}{{}^{16}O_s} \underset{R'_r}{\overset{R'}{\rightleftharpoons}} \underset{1-\alpha'}{HD^{16}O} + \underset{\beta'}{{}^{18}O_s} \qquad (8)$$

and assume that there is no appeciable isotope effect and that α', which is not less than $0.9\alpha'_0$, is equal to α'_0 throughout the reaction, $R' = R'_r$ and the velocity of the exchange is

$$a'_s d\beta'/dt = R'(\alpha'_0 - \beta')S \qquad (9)$$

where O_s is an oxygen atom in the catalyst, α' and β' are the atomic fractions of ^{18}O of water vapor and the catalysts, respectively, a'_s is gram atoms of oxygen in the catalyst, and R' represents the total exchange rate of oxygen, without discrimination between isotopes (g. atom/sec. m.²).

From a material balance of ^{18}O

$$a'_s(\beta'_f - \beta'_0) = a'_w(\alpha'_0 - \alpha'_f) \qquad (10)$$

where α'_f and β'_f are the atomic fractions of ^{18}O of the trapped water and the catalyst, respectively, after the reaction, and a'_w is gram atoms of oxygen in the passed water. Since $\beta'_\infty = \alpha'_0$ at equilibrium, the oxygen exchange ratio after the reaction, x'_f, is

$$x'_f = (\beta'_f - \beta'_0)/(\beta'_\infty - \beta'_0) = (\beta'_f - \beta'_0)/(\alpha'_0 - \beta'_0) \qquad (11)$$

Integrating eq. 9, we have

$$R' = (a'_s/tS)[-\ln(1 - x'_f)] \qquad (12)$$

It is readily shown that

$$R' = a_s' k'_e / S \qquad (13)$$

where k'_e is the experimental rate constant (sec.$^{-1}$) so that $d\beta'/dt = k'_e(\beta'_\infty - \beta')$.

Results and Discussion

The experimental results are summarized in Table II and Figs. 1 and 2; the apparent heat of activation $\Delta H^\ddagger$ and the frequency factor R_0, where $R = R_0 \exp(-\Delta H^\ddagger/RT)$, are given in Table III.

Figure 2 shows that (i) R'/R of a catalyst is almost constant throughout the temperature range and (ii) R'/R is 0.1–0.4 for the catalysts studied. The density of oxygen atoms in the surface was calculated to be 2×10^{-5} g. atom/m.,^{2} assuming the lattice constant of these spinels to be 8.3 Å. It is shown readily from the values of R' in Fig. 1 that (iii) at least 6–60 layers of oxygen atoms in $MgAl_2O_4$ or at most 700–1600 layers in $ZnFe_2O_4$ have been exchanged in 75 min. with those of water vapor.

From (i) and (ii) it is reasonable to conclude that the hydrogen and oxygen exchange reactions proceed through the common rate-determining step and that the solid phase is involved in the exchange of hydrogen atoms as well as in that of oxygen atoms (iii).

As ΔH^*, R'/R and Θ-plot[5] of $MgAl_2O_4$ are qualitatively different from corresponding values of the other catalysts, two reaction mechanisms are proposed; exchange with $MgAl_2O_4$ is attributed to an acid–base mechanism and exchange with the other catalysts to an oxidation–reduction mechanism.

TABLE II

ISOTOPIC CONTENT AND HYDROGEN EXCHANGE RATIO OF THE TRAPPED WATER

Exp. no.	Catalyst	Surface area, S_0 (m.^{2}/g.)	Wt. of catalyst (g.)	Reaction temp. (°C.)	α_f (%)	α'_f (%)	x_f (%)
11	$MgAl_2O_4$	2.4	3.554	450	5.30	0.312	88.7
24				380	7.15	.323	52.1
12				300	8.60	.329	21.2
15	$MgCr_2O_4$	1.8	2.980	450	7.69	.320	38.1
14				380	8.10	.322	31.0
16				300	8.51	.324	23.3
2	$ZnCr_2O_4$	0.8	3.217	450	6.75[a]	.314[a]	58.0
5			3.217	380	7.60	.321	42.1
6			3.012	300	8.04	.324	34.5
8	$ZnFe_2O_4$	(0.1)[c]	5.497	450	7.10[b]	.319[b]	50.6
7			6.407	380	7.47	.317	45.0
9			6.033	300	8.22	.318	30.2

[a] Time of reaction 90 min. [b] Time of reaction 45 min. [c] Not very accurate value. $\alpha_0 = 9.49\%$, $\alpha'_0 = 0.332\%$.

TABLE III

HEAT OF ACTIVATION $\Delta H^\ddagger$ AND FREQUENCY FACTOR R_0 FOR HYDROGEN EXCHANGE

Catalyst	$MgAl_2O_4$	$MgCr_2O_4$	$ZnCr_2O_4$	$ZnFe_2O_4$
$\Delta H^\ddagger$ (kcal./mole)	12.9	4.0	4.6	4.9
log R_0 (g. atom/sec. m.^{2})	3.46	0.32	1.06	1.77

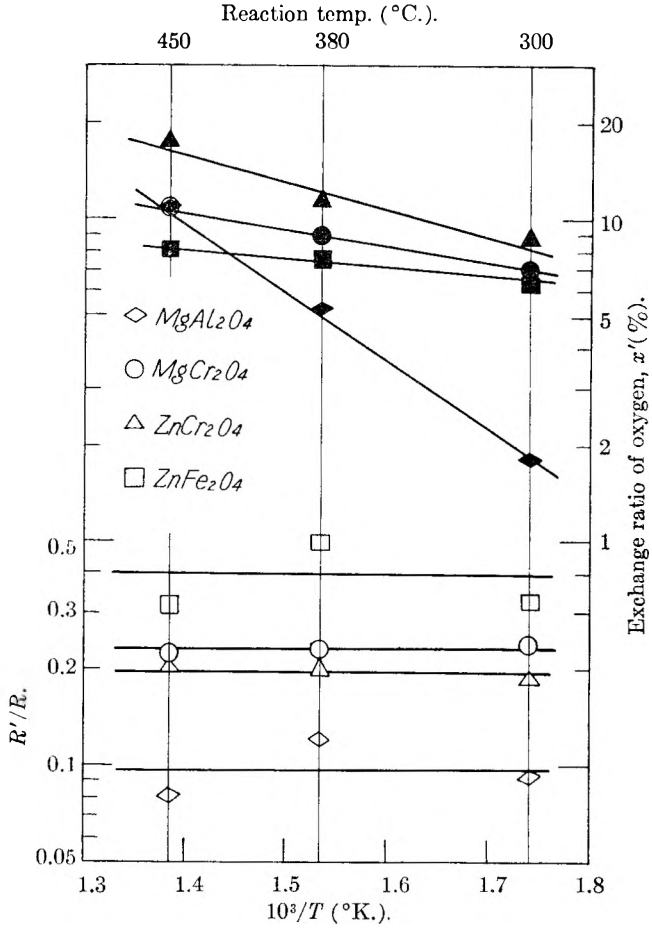

Fig. 2.—R'/R and exchange ratio of oxygen x'.

a. Oxidation–Reduction Mechanism. ($MgCr_2O_4$, $ZnCr_2O_4$, $ZnFe_2O_4$).—The over-all exchange reaction of hydrogen or oxygen atoms is assumed to proceed through rapid repetition of reaction 14

$$H_2O + (K) \rightleftarrows H_2 + (K)O \qquad (14)$$

which in a more detailed form is

$$H_2O + (K) \underset{I_r}{\overset{I_f}{\rightleftarrows}} H_2O(K) \underset{II_r}{\overset{II_f}{\rightleftarrows}} H_2 + (K)O \qquad (15)$$

where (K) and (K)O represent the catalyst with some oxygen vacancies on the surface and the catalyst without such vacancies, respectively, while $H_2O(K)$ represents a state where the vacancies are filled by water molecules. Since the experimental value for R'/R (Fig. 2) is in substantial agreement with the predicted value of unity, regardless of the reaction temperature and the catalyst, these two exchange reactions must have a common rate-determining step which involves the exchange of both hydrogen and oxygen at the same time. As the heat of reaction between H_2O and (K) is positive, the rate of I_f will be larger than that of I_r. Therefore, I_r is the rate-determining step of reaction 14.

According to the above discussion, hydrogen atoms in $H_2O(K)$ must exchange with gaseous hydrogen through a rapid step II. It is assumed

(5) A correlation diagram between R_0 and ΔH^*; *cf.* E. Cremer, "Advances in Catalysis," Vol. 7, Academic Press, Inc., New York, N. Y., 1955, p. 75.

that the step I_r is a process whereby a vacancy of oxygen is reproduced by fluctuation somewhere else on the surface, releasing a water molecule. If an oxygen atom in $H_2O(K)$ were rapidly exchanged with oxygen in the bulk and never returned to the gaseous phase, R'/R would be unity. The values of R'/R in Fig. 2 are understandable if 0.2–0.4 of oxygen atoms in $H_2O(K)$ are assumed to exchange with those in the bulk, while the remainder returns to the gaseous phase.

The concentration of oxygen vacancies in a catalyst may increase with its oxidizing power, $MgCr_2O_4 < ZnCr_2O_4 < ZnFe_2O_4$. This concentration may be particularly high in $ZnFe_2O_4$, as this spinel is reduced or oxidized by an hydrogen–water vapor mixture depending upon the composition and temperature. Since R and R' should also increase with the concentration of oxygen vacancies, it is reasonable that R and R'/R are in qualitative agreement with the order of the oxidizing power of the catalysts.

We shall now consider the oxygen exchange ratio x'_f. Cameron, Farkas and Litz[6] found that the rate of oxygen exchange in a V_2O_5–$H_2{}^{18}O$ system was 20–30 times more rapid than in a V_2O_5–$^{18}O_2$ or V_2O_5–$H_2{}^{18}O$–O_2 system. Weller and Voltz[7] reported that oxygen exchange between Cr_2O_3 (surface area = 200 m.²/g.) and $H_2{}^{18}O$ at 350° occurred to a depth of 2–3 atomic layers in a 30 minutes run. However, our results (Figs. 1 and 2) show that the exchange occurred to a depth of about 250 layers in a $ZnCr_2O_4$–$D_2{}^{18}O$–H_2 system at 350° in the same period of time.

Apparently the more reductive is the atmosphere around a catalyst, the more rapid is the rate of regeneration of vacancies on the surface and in the bulk, a tendency which is readily understood.

b. Acid–Base Mechanism ($MgAl_2O_4$).—Exchange reactions on acid catalysts between water and D_2[8] and between $H_2{}^{18}O$ and oxygen atoms of the catalysts[9] have been observed; Wright, Weller and Mills[10] reported that heterolytic splitting is the mechanism by which hydrogen exchange occurs between D_2 and water on an aluminum chloride catalyst.

As is shown in a previous paper[11] the work function of alumina is decreased by the adsorption of water vapor. It is certain, therefore, that in the case of a water molecule in an oxygen vacancy on the surface the hydrogen atom is oriented above the plane of the catalyst. Such a water molecule may cause heterolytic splitting of a hydrogen molecule and exchange a proton with it according to reaction 16, which is similar to the reaction on aluminum chloride.[8]

$$\text{H-H} + \text{D}^+[\text{HO(K)}] \rightleftharpoons \text{H}^+\text{H}^- + \text{D}^+[\text{HO(K)}] \rightleftharpoons \text{D-H} + \text{H}^+[\text{HO(K)}] \quad (16)$$

Equation 16 is merely a substitution for II in (15); if a rapid exchange of protons on the surface through prototropy is assumed, I_r, in this case also, may be a rate-determining step. The large heat of activation and the small value of R'/R of $MgAl_2O_4$ are due to the low concentration and the small rate of regeneration of the vacancies, characteristics which one might predict from the relatively low oxidizing power and high melting point of this spinel.

Acknowledgments.—The authors are indebted to Dr. Shun Araki for help with isotopic analyses and for making the mass spectrometer available, to Mr. Fujio Mochizuki for technical assistance and Mrs. Weissberger for her elaborate revising of the manuscript. Messrs. Akira Kumai, Katsuyoshi Hirasa and Hitoshi Hirokane collaborated with us in the preliminary experiments. The expenses were partially defrayed by a Grant in Aid from the Ministry of Education, Japan.

(6) W. C. Cameron, A. Farkas and L. M. Litz, THIS JOURNAL, **57**, 229 (1953).

(7) S. W. Weller and S. E. Voltz, *J. Am. Chem. Soc.*, **76**, 4695 (1954).

(8) H. S. Taylor and H. Diamond, *ibid.*, **57**, 1256 (1935).

(9) G. A. Mills and S. G. Hindin, *ibid.*, **72**, 5549 (1950).

(10) L. W. Wright, S. W. Weller and G. A. Mills, *Ind. Eng. Chem.*, **49**, 1054 (1957).

(11) Y. Yoneda, *Oyo-Buturi* (*J. Applied Phys., Japan*), **22**, 307 (1953).

THE CALORIMETRIC DETERMINATION OF PURITY. THEORY AND CALCULATION METHODS

BY J. H. BADLEY

Shell Development Co., Emeryville, Calif.

Received February 2, 1959

The theoretical basis for purity calculation is extended to include samples forming moderately non-ideal solutions. Two cases are considered involving: (1) moderately concentrated, solid-insoluble impurities, and (2) a single, dilute, solid-soluble impurity. Equations relating fraction melted or heat content of the sample and temperature are developed from mass and energy conservation equations and thermodynamic relations for solid–liquid phase compositions. A new purity calculating method (designated the HCT method) is described which appears to be superior to methods in current use. An experimental study of known mixtures showed that this method gives reliable results for samples containing as much as 2 mole per cent. of a solid-insoluble impurity. Tests of known mixtures of solid-soluble components failed to give good results, presumably because the solid formed during sample freezing was non-uniform in composition.

Introduction

The melting or freezing behavior of organic compounds has been used for judging their purity for over 35 years. Reviews of the literature are given by Sturtevant,[1] Cines[2] and Mathieu.[3] Two general experimental methods have evolved; in one, the sample is placed in a controlled environment, either hotter or colder than the sample, and the temperature of the sample measured as a function of time. Under suitable conditions, the time–temperature curve gives useful information about the purity of the sample. The second experimental method employs a calorimeter to measure the increase in heat content of the sample during melting over that of the corresponding solid. This quantity is used to calculate the melting curve, *i.e.*, the fraction melted as a function of temperature. The melting curve is related through general thermodynamic relations to the purity of the sample, provided that certain experimental conditions are met. The major concern of the present work is the extension of calorimetric purity calculation methods to cover a wider range of systems and experimental conditions than is now accessible. While parallel methods could be developed for time–temperature data, they are not considered in this paper.

In previous derivations of purity calculation methods, it has been assumed that the major component and impurity form ideal solutions. In this work, equations are derived which are valid for systems showing moderate departures from ideality. Two cases are considered: (1) the impurity is solid-insoluble, moderately non-ideal and its concentration is less than 0.2 mole fraction, and (2) the impurity is a single component which is solid-soluble, dilute, ideal in the liquid phase and non-ideal in the solid phase. While these conditions are, of course, not completely general, they include many real systems for which the ideal solution treatment is not valid. The derivations are based on three types of relations. The first two are conservation equations for mass and for energy, and the third is a relation between phase composition and temperature. Specific phase composition relations for each of the two cases described above are combined with the mass conservation equation to yield relations between the fraction melted and the temperature. By substituting these latter equations into the energy conservation equation, new relations are obtained between the temperature and heat content of the calorimeter and sample. Both the fraction melted and heat content equations contain the sample impurity content as a parameter which can be evaluated by curve fitting methods.

Somewhat surprisingly, the heat content–temperature equations for both non-ideal cases are, to an acceptable degree of approximation, identical to each other, and to a similar equation derived for the limiting case of ideal, dilute solutions. Furthermore, there exists a relatively simple method for evaluating the parameter of the equation related to the sample impurity content. This evaluation method serves as a more general, yet no more laborious calculation of purity from calorimetric data. The wider range of applicability of the heat content–temperature equation makes possible the quantitative estimation of markedly greater impurity concentrations than were accessible before. In fact, it is applicable to impurity contents which frequently make determination of the heat of fusion difficult or impossible. However, the heat content–temperature equation does not include the heat of fusion explicitly so it is not made inapplicable by this experimental difficulty. The method developed for using the heat content–temperature equation for the analysis of calorimetric purity data has been designated the HCT method.

Theory

Conservation of Mass During Melting.—Consider a system consisting of N moles of test sample and a container. The sample consists of N_1 moles of a major component and N_2 moles of a minor component or of several minor components which together behave as a single quasi-component. The pressure is constant and the temperature is within the range for which the sample is a mixture of solid and liquid with a negligible fraction in the vapor phase. Then

$$N^s + N^l = N \qquad (1)$$

(1) J. M. Sturtevant, "Calorimetry" in "Technique of Organic Chemistry," A. Weissberger, Editor, Vol. I, 2nd Ed., Interscience Publishers, Inc., New York, N. Y., 1949, part 1, page 731.

(2) M. R. Cines, "Solid-Liquid Equilibria of Hydrocarbons" in "Physical Chemistry of Hydrocarbons," A. Farkas, Editor, Vol. I, Academic Press, Inc., New York, N. Y., 1950, Chapter 8.

(3) M. P. Mathieu, *Acad. roy. Belg., Memoires (Sciences)*, **28**, No. 2 (1953).

$$N^s X_1^s + N^l X_1^l = N X_1^0 \qquad (2)$$
$$N^s X_2^s + N^l X_2^l = N X_2^0$$

where

N^s = moles of solid sample
N^l = moles of liquid sample
N = total moles of samples
X_1^s, X_2^s = mole fractions of components 1 and 2 in the solid phase
X_1^l, X_2^l = mole fractions of components 1 and 2 in the liquid phase
X_1^0, X_2^0 = mole fractions of components 1 and 2 in the total sample

Conservation of Energy During Melting.—Adding heat to the sample and container results in the melting of a small portion of the solid and a rise in temperature of the system. When component 2 is solid-insoluble or dilute, its contribution to the heat of melting is zero or negligible. Assuming that the liquid molal heat can be represented by that of the major component, the conservation equation becomes

$$dh = \Delta H_1\, dN^l + (N^s C^s + N^l C^l + C^c)\, dT + d(N^l H^m) \qquad (3)$$

where

dh = increment of heat
ΔH_1 = heat of fusion of component 1 at temp. T
dN^l = increase in the no. of moles of liquid
C^c = heat capacity of the sample container
C^s = molal heat of solid component 1
C^l = molal heat of liquid component 1
dT = temperature rise
H^m = excess molal heat content of liquid soln.

Hildebrand and Scott[4] discuss theoretical expressions for estimating H^m. Sufficient for the present purpose is

$$H^m = B_1^l R T X_1^l X_2 \qquad (4)$$

where

B_1^l = second Margules coefficient for component 1 in the liquid

Taking the partial derivative of (4) with respect to the amount of component 1 leads to a curtailed Margules equation which Hildebrand[4] has found useful in expressing the solution behavior of a large number of binary systems. As this term is only a small part of the heat added and X_2^l is postulated to be less than 0.2, equation 4 can be approximated by an expression in which $X_1^l = 1$. When the components form non-ideal liquid solutions, it is very unlikely that they will form solid solutions. Hence from (2)

$$X_2^l = \frac{X_2^0 N}{N^l}$$

and

$$N^l H^m = N B_1^l R T X_2^0 \qquad (5)$$

The change in $N^l H^m$ on melting a portion of the solid is

$$d(N^l H^m) = N B_1^l R X_2^0\, dT \qquad (6)$$

Now letting Y equal the fraction melted and substituting YN for N^l and equation 6 in 3 and writing the heat of fusion in terms of its value at the freezing point of the major component, ΔC_p, and the temperature gives

$$dh = N(\Delta H_1^0 - \Delta C_p \Delta T)dY + [N(C^s + \Delta C_p Y + B_1^l R X_2^0) + C^c]dT \qquad (7)$$

where

$\Delta C_p = C^l - C^s$
$\Delta T = T_1^0 - T$
T_1^0 = freezing point of the major component
ΔH_1^0 = molal heat of fusion of the major component at T_1^0
$A_1^0 = \Delta H_1^0 / R(T_1^0)^2$

Over the temperature ranges employed in purity testing ΔC_p can be assumed constant. Integration of (7) gives

$$h = N(\Delta H_1^0 - \Delta C_p \Delta T)Y + [N(C^s + B_1^l R X_2^0) + C^c]T + \text{Const.} \qquad (8)$$

Evaluating the integration constant at a point h^a, T^a, Y^a yields

$$h - h^a = N(\Delta H_1^0 - \Delta C_p \Delta T)(Y - Y^a) + [N(C^s + Y^a \Delta C_p + B_1^l R X_2^0) + C^c)](T - T^a) \qquad (9)$$

This equation holds for $0 < Y < 1$ and T greater than the eutectic temperature. The principal approximations made in its derivation are: (1) the excess heat content of the sample is assumed proportional to the impurity concentration in the total sample, (2) the liquid molal heat of the sample is assumed equal to that of the major component, (3) the molal heats of the solid and liquid major component are assumed to be independent of temperature. These approximations seem unlikely to impair the validity of equation 9 when applied to the systems postulated at the beginning of the derivation.

Phase Composition Relations.—In a two-phase condensed system at equilibrium, the compositions of the phases are related through the fact that the partial molal free energy of each component is the same in both phases. By writing separate expressions for this quantity for each component in each phase and equating, the desired relations are obtained. For real systems, the appropriate partial molal free energy equations differ in detail according to the kind of interaction between components and the concentration range of interest. Hildebrand and Scott[4] discuss this approach to the derivation of phase composition relations. For the two cases considered here, the composition of the liquid or liquid and solid phases is related to the temperature by the equations shown below. For case 1, postulating solid insoluble impurities with $X_2^l < 0.2$ and $-2 < B_1^l < 2$

$$-\ln X_1^l = \frac{\Delta H_1^0}{R}\left[\frac{1}{T_1^0} - \frac{1}{T}\right]\left[1 - \frac{\Delta C_p \Delta T}{2\Delta H_1^0}\right] + B_1^l (1 - X_1^l)^2 \qquad (10)$$

and for case 2 postulating a dilute, solid-soluble impurity which is ideal in the liquid phase but non-ideal in the solid phase with $-2 < B_1^s < 2$

$$\ln \frac{X_1^s}{X_1^l} = \frac{\Delta H_1^0}{R}\left[\frac{1}{T_1^0} - \frac{1}{T}\right] + B_1^s (1 - X_1^s)^2 \qquad (11)$$

In the latter case, by writing an additional equation of the form of (11) for the minor component, a relation is found between X_1^s and X_1^l. Although this shows that the ratio X_2^s/X_1^l, conventionally defined as the distribution ratio k, is theoretically temperature dependent, the temperature variation is small in a purity test involving the postulated

(4) J. H. Hildebrand and R. L. Scott, "The Solubility of Non-Electrolytes," 3rd Ed., Reinhold Publ. Corp., New York, N. Y., 1950, Chapters 3, 17 and 18.

dilute solutions, so k can be assumed constant without error.

Combinations of Basic Equations

The basic equations derived or stated above can be combined to yield relations between either fraction melted or heat content of the sample and temperature.

Fraction Melted—Temperature Relations.—Considering first case 1, employing $X_1^l + X_2^l = 1$, expansion of the $-\ln X_1^l$ in a power series gives

$$-\ln X_1^l = X_2^l + \frac{1}{2}(X_2^l)^2 + \frac{1}{3}(X_2^l)^3 + \ldots \quad (12)$$

For $X_2^l < 0.2$, the sum of the cubic and higher terms amounts to less than 1.6% of X_2^l and therefore may be discarded for the present work. Substituting in equation 10

$$X_2^l + \left(\frac{1}{2} - B_1^l\right)(X_2^l)^2 = \frac{\Delta H_1^0}{R}\left(\frac{1}{T} - \frac{1}{T_1^0}\right) \times \left(1 - \frac{\Delta C_p \Delta T}{2\Delta H_1^0}\right) \quad (13)$$

Rearranging the right-hand side of the equation

$$X_2^l + \left(\frac{1}{2} - B_1^l\right)(X_2^l)^2 = A_1^0 \Delta T(1 + A_1' \Delta T) \quad (14)$$

where

$$A_1' = \frac{1}{T_1^0} - \frac{\Delta C_p}{2\Delta H_1^0}$$

Because $A_1' \Delta T$ is always small compared to one, it can be shown that equation 14 can be written with little loss in validity as

$$X_2^l + \left(\frac{1}{2} - \frac{A_1'}{A_1^0} - B_1^l\right)(X_2^l)^2 = A_1^0 \Delta T \quad (15)$$

Provided the temperature is always above that of the highest eutectic temperature involving the major component

$$X_2^l = \frac{X_2^0}{Y} \quad (16)$$

Substitution in (16) gives

$$\frac{X_2^0}{Y} + \left(\frac{1}{2} - \frac{A_1'}{A_1^0} - B_1^l\right)\left(\frac{X_2^0}{Y}\right)^2 = A_1^0 \Delta T \quad (17)$$

When the solution is ideal, $B_1^l = 0$, hence

$$\frac{X_2^0}{Y} + \left(\frac{1}{2} - \frac{A_1'}{A_1^0}\right)\left(\frac{X_2^0}{Y}\right)^2 = A_1^0 \Delta T \quad (18)$$

In case 2, in order to justify the assumption that the heat of melting of the solid solution is the heat of fusion of the major component, it is necessary to limit the discussion to dilute solutions. Hence the quadratic term in the expansion of $\ln X_1$ becomes negligible. Expanding equation 11 one obtains

$$X_2^l - X_2^s = A_1^0 \Delta T + B_1^s (X_2^s)^2 \quad (19)$$

The magnitude of the proportionality constant B_1^s is difficult to estimate and no data appear to be available for organic systems. Although development of cryoscopic equations containing this constant is thus of qualitative interest only at the present time, such equations are more general than those based solely on the laws of dilute solutions. Eliminating X_2^l and X_2^s one obtains

$$\frac{X_2^0}{Y + \frac{k}{1-k}} - B_1^s\left(\frac{k}{1-k}\right)^2\left(\frac{X_2^0}{Y + \frac{k}{1-k}}\right)^2 = A_1^0 \Delta T \quad (20)$$

For an ideal solid solution $B_1^s = 0$ and equation 20 reduces to

$$\frac{X_2^0}{Y + \frac{k}{1-k}} = A_1^0 \Delta T \quad (21)$$

This equation has been previously derived by Mastrangelo and Dornte.[5]

Heat Content–Temperature Relations.—As shown earlier, the heat content of the calorimeter and sample in the melting region is given by equation 9. By substituting a relation between T and Y, appropriate for the system under consideration, equations for heat content as a function of temperature can be derived. Considering in turn the cases discussed above, these results are obtained.

For case 1, the fraction melted-temperature relation is given by equation 17. For the present derivation it is necessary to solve this equation for Y in a form which avoids the square root term obtained by use of the general quadratic equation formula. Many approximate solutions are possible because the ranges of $A_1^0 \Delta T$ and the term $(1/2 - A_1'/A_1^0 - B_1^l)$, denoted henceforth by E, can be fairly well defined. For the present purposes, the maximum value of X_2^l is postulated to be 0.2. With $E = 0$, this corresponds to $A_1^0 \Delta T = 0.2$ also. The value of B_1^l is postulated to fall within the range $-2 < B_1^l < 2$. The value of A_1'/A_1^0 is generally small compared to 1/2. Consequently, the limits for E can be reasonably assigned to be $-1.5 < E < 2.5$. Within these limits for $A_1^0 \Delta T$ and E, it can be shown that the approximation

$$X_2^l = \frac{X_2^0}{Y} \cong \frac{A_1^0 \Delta T(1 + EA_1^0 \Delta T)}{(1 + 2EA_1^0 \Delta T)} \quad (22)$$

yields results for X_2^0/Y with 5% error or less. Equation 22 arises from the continued fraction expansion of (17).

$$\frac{X_2^0}{Y} = \cfrac{A_1^0 \Delta T}{1 + \cfrac{EA_1^0 \Delta T}{1 + \cfrac{EA_1^0 \Delta T}{1 + \ldots}}} \quad (23)$$

Substituting in (9) gives

$$h - h^a = \frac{NR(T_1^0)^2 X_2^0 (T - T^a)}{(T_1^0 - T^a)(T_1^0 - T)} \times \left\{1 + \frac{(E_1^l)^2 (A_1^0)^2 (T_1^0 - T)(T_1^0 - T^a)}{[1 + E_1^l A_1^0 (T_1^0 - T)][1 + E_1^l A_1^0 (T_1^0 - T^a)]}\right\} + \{N[C^s + Y^a \Delta C_p + B_1^l RX_2^0] + C^c\}[T - T^a] \quad (24)$$

This equation is a good approximation to the relation between the heat content and temperature under the following conditions: (1) equation 9 is valid. The validity of this equation has already been discussed, (2) the impurity is solid-insoluble and forms liquid solutions with $-2.0 < B_1^l < 2.0$ and less than 0.2 mole fraction in concentration, and (3) the temperature is always above that of

(5) S. V. R. Mastrangelo and R. W. Dornte, *J. Am. Chem. Soc.*, **77**, 6200 (1955).

the highest eutectic temperature involving the major component. Under certain additional conditions the term

$$\frac{(E_1^1)^2(A_1^0)^2(T_1^0 - T)(T_1^0 - T^a)}{[1 + E_1^1A_1^0(T_1^0 - T)][1 + E_1^1A_1^0(T_1^0 - T^a)]}$$

in equation 24 becomes small compared to 1. These correspond to values of $E_1^1A_1^0\Delta T$ between -0.1 and $+0.4$ and are realized when the solutions are relatively dilute, or $-1.0 < B_1^1 < 1.5$ and $A_1^0\Delta T \cong X_2^1$ is less than 0.2. Under these further conditions, and dropping the sub and superscript for B, the systems described in case 1 are adequately represented by

$$h - h^a = \frac{NR(T_1^0)^2X_2^0(T - T^a)}{(T_1^0 - T^a)(T_1^0 - T)} + [N\{C^s + Y^a\Delta C_p + BRX_2^0] + C^c\}[T - T^a] \quad (25)$$

In case 2, solving equation 20 for $[X_2^0/Y + k(1 - k)]$ by the approximation used in case 1 and substituting for Y in (9) with the heat of mixing term = 0, one obtains an equation of the form of equation 24. Provided that $-1.5 < B_1^s(k/1 - k)^2 < 2.5$, this equation is a good approximation to the heat content–temperature relation. The range of validity of equation 25 for this case is similar to that in case 1.

The preceding discussion has shown that equation 25 is a valid relation between the heat content and temperature under the following conditions: (1) the concentration of the minor component is less than 0.2 mole fraction throughout the melting of the sample, (2) the reference temperature used to evaluate the integration constant is selected to be not too far from the freezing point of the sample, (3) the liquid or solid solutions formed do not depart too far from ideality. It is interesting to see that equation 25 is, except for the unimportant term in B, identical to the heat content–temperature relation derived assuming dilute ideal liquid solutions. The preceding development has established that the range of validity of this equation is greater than one might suspect if he derived it only on the simplest but most restrictive assumptions. It is particularly noteworthy that it is applicable to equilibrium data for dilute binary systems which form solid solutions. It is not, however, applicable to multicomponent systems in which one or more components form solid solutions.

Purity Calculation

Methods Based on the Fraction Melted Transform.—Solving equation 9 for the fraction melted, one obtains

$$Y = Y^a + \frac{h - h^a - [N(C^s + Y^a\Delta C_p + B_1^1RX_2^0) + C^c][T - T^a]}{N(\Delta H_1^0 - \Delta C_p\Delta T)} \quad (26)$$

Conventionally, the point Y^a, h^a, T^a is taken as the freezing point of the sample, *i.e.*, 1, h^f, T^f, and the heat of mixing and ΔC_p are assumed to be negligible. Hence

$$Y = 1 - \frac{h^f - h - (NC^s + C^c)(T - T^a)}{N\Delta H_1^0} \quad (27)$$

Many numerical procedures utilizing the fraction melted transform have been described for reducing experimental data for the ideal binary or quasi-binary systems. These are discussed in one or more of the review papers cited earlier.[1–3] More complicated systems are best treated by elimination of the parameter T_1^0 in terms of the coördinates of a point on the T, Y curve. Then it frequently becomes possible to find pairs of functions of Y and T which give linear plots with each other and involve the impurity concentration as a parameter. For case 1, this treatment results in the transformation of equation 17 to give

$$X_2^0\frac{(Y^a - Y)}{Y^aY} + \left(\frac{1}{2} - \frac{A_1'}{A_1^0} - B_1^1\right)(X_2^0)^2 \times \frac{[(Y^a)^2 - Y^2]}{(Y^aY)^2} = A_1^0(T^a - T) \quad (28)$$

A plot of $[Y(T^a - T)/(Y^a - Y)]$ *versus* $(Y^a + Y)/Y$ is a straight line with intercept $X_2^0/A_1^0Y^a$ and slope $[1/2 - A_1/A_1^0 - B_1^1](X_2^0)_2^1/Y^a)1/A_1^0$. Means for applying the limiting ideal solution equation have been discussed elsewhere.[6–8]

The ideal solution form of case 2 has been discussed by Mastrangelo and Dornte.[5] An alternative calculation method based on their equation can be obtained by elimination of the parameter T_1^0 in terms of the point T^a, Y^a. This shows that a plot of $(Y^a - Y)/(T^a - T)$ *versus* Y is a straight line with intercept $k/(1 - k)$ and slope $X_2^0/[A_1^0(Y^a + k/1 - k)]$.

Methods Based on the Heat Content–Temperature Relation.—In view of the generality of equation 25 it is unnecessary to distinguish between the two cases based on differing phase composition relations in utilizing the heat content–temperature relation for the calculation of purity. It can be transformed in at least three ways to obtain practical data reduction methods. The first was discussed over 40 years ago by Dickinson and Osborne[9] and by Sturtevant.[1] The second method is similar to the earlier calculation procedure in that it is based on the derivative of the heat content–temperature equation; that is

$$\frac{dh}{dT} = \frac{NR(T_1^0)^2X_2^0}{(T_1^0 - T)^2} + J^s \quad (29)$$

where

$$J^s = N(C^s + Y^a\Delta C_p + BRX_2^0) + C^c$$

Solving for the temperature, one obtains

$$T = T_1^0\left(1 - \sqrt{\frac{NRX_2^0}{dh/dT - J^s}}\right) \quad (30)$$

This shows that a plot of $1/\sqrt{dh/dT - J^s}$ *versus* T is linear and has the slope $T_1^0\sqrt{NRX_2^0}$ and intercept T_1^0. While this computation method has several inherent advantages stemming from the broad range of validity of the parent equation, the derivative form is probably not the most satisfactory one for evaluation of new experimental

(6) F. W. Schwab and E. Wichers, "Precise Measurement of the Freezing Range as a Means of Determining the Purity of a Substance" in "Temperature—Its Measurement and Control in Science and Industry," Reinhold Publ. Corp., New York, N. Y., 1941, p. 256.

(7) B. J. Mair, A. R. Glasgow, Jr., and F. D. Rossini, *J. Research Natl. Bur. Standards*, **26**, 591 (1941).

(8) W. J. Taylor and F. D. Rossini, *ibid.*, **32**, 197 (1944).

(9) H. C. Dickinson and N. S. Osborne, *Bull. Natl. Bur. Standards*, **12**, 49 (1915).

data. It has little to recommend it in preference to the transform described below when the experimentally measured quantities are heat content and temperature.

The HCT Method.—Equation 25 can be rearranged as

$$T_1^0 - T = \frac{NR(T_1^0)^2X_2^0}{T_1^0 - T^a} \times \frac{1}{\frac{h - h^a}{T - T^a} - J^s} = \frac{NR(T_1^0)^2X_2^0}{T_1^0 - T^a} \times U \quad (31)$$

The variable $1/[(h - h^a)/(T - T^a) - J^s]$ is represented by the symbol U in the following discussion. A plot of U *versus* T has slope $-[NR(T_1^0)^2X_2^0/(T_1^0 - T^a)]$ and intercept T_1^0. Denoting the slope of the line through a set of experimental points by W, the concentration of impurity in the sample is given by

$$X_2^0 = \frac{(-W)(T_1^0 - T^a)}{NR(T_1^0)^2} \quad (32)$$

The experimental evaluation of the terms in equation 31 is clear for all except J^s. For most of the melting region $(h - h^a)/(T - T^a)$ is large compared to J^s. Consequently, J^s need not be accurately evaluated. Usually the approximation $J^s \cong NC^1 + C^c$ is sufficiently accurate.

Failure of this approximation is most likely when the heat of fusion of the sample is abnormally low and the amount of impurity is relatively high. Then accurate estimation of the specific heat of the solid is required in order to evaluate J^s. The term $B_1^1RX_2^0$ is nearly always negligible compared to C^s under the conditions of this discussion. A reasonably linear plot of T *vs.* U is good evidence that the estimate of J^s employed is sufficiently accurate. However, the contrary, *i.e.*, curvature in the T, U plot is not proof that J^s is in error.

The freezing point of the sample is found by solving equation 31 and the equation relating heat content and temperature for the liquid sample for the temperature at which both equations are satisfied by the same value of the heat content. Provided the liquid specific heat is constant near the melting point and ΔC_p is negligible

$$T^f = T^a + \frac{K(T_1^0 - T^a)}{K - W} \quad (33)$$

where

$K = h^b - h^a - J^1(T^b - T^a)$
h^b, T^b = coördinates of a point on the heat content–temperature curve for the liquid sample
J^1 = heat capacity of calorimeter plus the liquid sample = $NC^1 + C^c$

Equation 25 holds for binary systems which form a solid solution. Provided that an independent estimate of the heat of fusion is available, and the solid solution is ideal, the distribution ratio of the impurity can be estimated. The freezing point depression caused by the impurity is given by

$$T_1^0 - T^f = \frac{R(T_1^0)^2X_2^0(1 - k)}{\Delta H_1^0} \quad (34)$$

Eliminating $R(T_1^0)^2X_2^0$ between equations 25, 33 and 34 gives

$$k = 1 - \frac{K - W}{N\Delta H_1^0} \quad (35)$$

The relation between the variable U and the fraction melted, Y, is found from the defining equations for them. This is

$$U = \frac{T - T^a}{(Y - Y^a)N\Delta H_1^0} \quad (36)$$

Calorimetric data for purity calculation generally have been published in the form of temperature–fraction melted values. Equation 36 suggests an improved means for analyzing such data. Combination of equations 36 and 31 to eliminate U and N gives

$$T = T_1^0 - \frac{R(T_1^0)^2X_2^0(T - T^a)}{\Delta H_1^0(T_1^0 - T^a)(Y - Y^a)} \quad (37)$$

In the light of the broader basis of the validity of equation 31, computations based on this equation should yield more reliable values for the impurity concentration than does the conventional plot of $1/Y$ *vs.* T or the method of Mastrangelo and Dornte.[5]

In addition to its broad range of validity, the calculation scheme outlined here has at least two additional advantages when compared to conventional purity calculation methods. The parent equation does not require the explicit evaluation of heat of fusion. This is quite important for a method intended for use with impure samples, as the heat of fusion of the major component frequently cannot be evaluated easily for such materials. Secondly, the new functions can be calculated directly from the heat content–temperature data without an intervening step such as the evaluation of the heat of fusion of the sample. This results in a simpler and shorter calculation procedure compared to the conventional computing method.

Experimental

The apparatus and procedure employed were essentially those of Tunnicliff and Stone.[10] This apparatus, while not suitable nor intended for accurate specific heat or heat of fusion measurement, is equipped with a sensitive temperature difference measuring device and provides heat content measurements of sufficient reliability for the determination of purity.

A special means for pretreating the sample in the calorimeter cell was found necessary to avoid systematic departure from thermodynamic equilibrium during melting of the sample. This consisted in melting the sample in the cell, mixing it thoroughly by partially removing the cell and replacing, then chilling the sample rapidly by immersing the cell in liquid nitrogen. This process is called "quick freezing" and is practical only in an apparatus in which the well-mixed sample is distributed in a thin film which can be chilled by withdrawing heat in a direction perpendicular to the film surface. Tunnicliff and Stone's 1/2-ml. cell was used in tests reported here involving quick freezing.

The materials employed were: 1,4-bromochlorobenzene, 1,4-dibromobenzene, bibenzyl, *trans*-stilbene and benzene. The first four were purified by zone melting in a single zone, vertical tube, multiple pass apparatus. A dye was added to the samples and zone refining continued until about 80% of the sample was water white. The benzene was a highly purified material of petroleum origin.

Mixtures of known composition were prepared by weight. Homogeneity of the stock solution and samples taken from it was ensured by taking all samples in the liquid state.

(10) D. D. Tunnicliff and H. Stone, *Anal. Chem.*, **27**, 73 (1955).

Discussion of Experimental Results

Accuracy of HCT Method for Solid-insoluble Impurities.—The accuracy of the heat content–temperature (HCT) purity calculation method (*i.e.*, the method based on equations 31 to 35) for solid-insoluble impurities is shown by the data in Table I. These data show that the HCT method gives results within 20% of the synthesis value. Cetane was used as an impurity in these tests because it was solid insoluble and likely to form moderately non-ideal solutions with the aromatic major components. The sample was quick frozen in all tests. Owing to the difficulty of preparing and maintaining reference materials of sufficiently high purity, no attempt was made to synthesize mixtures of lower impurity content. There is no reason to doubt the reliability of the HCT calculation method for such mixtures, however.

TABLE I

ACCURACY OF HCT IMPURITY CALCULATION METHOD

Test	Sample	Impurity, % Synthesis	Impurity, % Found	Difference	Relative error, %
98	Benzene + cetane	1.51	1.60	0.09	6
109	1,4-Bromochlorobenzene + cetane	1.42	1.45	.03	2
102	1,4-Bromochlorobenzene + cetane	1.83	2.17	.34	19
104	1,4-Bromochlorobenzene + cetane	1.65	1.72	.07	4
105	1,4-Dibromobenzene + cetane	1.07	1.14	.07	7
108	1,4-Dibromobenzene + cetane	1.18	0.99	.19	16
110	1,4-Dibromobenzene + cetane	1.18	1.42	.24	20
99	Bibenzyl + cetane	1.93	2.17	.24	12
100	Bibenzyl + cetane	1.58	1.62	.04	3
112	*trans*-Stilbene + cetane	1.43	1.50	.07	5

Solid-soluble Impurities.—When the impurities form solid solutions with the major component, it is apparently quite difficult to obtain equilibrium melting data in a calorimeter. In fact, in the series of tests summarized in Table II, the impurity recovery was very poor, the highest value being a little over 50% of the impurity added. Phase data for the bromochlorobenzene–dibromobenzene systems[11] and the bibenzyl–*trans*-stilbene systems[12] show that small amounts of dibromobenzene in bromochlorobenzene and of *trans*-stilbene in bibenzyl, should have distribution ratios greater than one. Such values were not found in this work. It seems likely that the impurity distribution was non-uniform in either or both phases in these tests and that no numerical analysis of the data is capable of yielding the correct impurity content.

TABLE II

LOW RECOVERY OF ADDED SOLID-SOLUBLE IMPURITIES (HCT CALCULATION)

Test	Sample	Impurity concn. Added	Impurity concn. Found	% impurity recovered	Apparent distribution ratio, k
125	Benzene + thiophene	1.05	0.13	12	0.06
123	1,4-Bromochlorobenzene + 1,4-dibromobenzene	1.04	.06	6	.07
124	1,4-Bromochlorobenzene + 1,4-dibromobenzene	0.18	.05	27	.03
121	1,4-Dibromobenzene + 1,4-bromochlorobenzene	1.20	.07	6	.05
122	1,4-Dibromobenzene + 1,4-bromochlorobenzene	0.21	.02	10	.01
114	Bibenzyl + *trans*-stilbene	2.14	.12	6	.04
119	Bibenzyl + *trans*-stilbene	0.26	.07	27	.02
118	*trans*-Stilbene + bibenzyl	2.27	1.24	55	.11
120	*trans*-Stilbene + bibenzyl	0.27	0.15	56	.07

The data employed by Mastrangelo and Dornte[5] to test their computing method were taken from a plot of reciprocal fraction melted and temperature data for a mixture containing 0.046 mole fraction impurity and include only four data points. These data do not appear adequate for a critical test of a purity calculation procedure applicable to dilute solid-soluble impurity systems. There appear to be no such data in the literature. In the light of the present work, solid-soluble impurities seem likely to go undetected in large part. Additional experimental work is required to establish cryoscopic purity methods which can be applied safely to systems forming solid solutions.

Acknowledgments.—The author is indebted to Mr. W. B. Quigley for aid in the experimental work and to Dr. F. H. Stross for many helpful discussions during the course of the investigation.

(11) A. N. Campbell and L. A. Prodan, *J. Am. Chem. Soc.*, **70**, 553 (1948).

(12) A. Kofler and M. Brandstätter, *Z. physik. Chem.*, **190**, 346 (1942).

VAPOR PRESSURE OF DIBORANE

BY LEO J. PARIDON AND GEORGE E. MACWOOD

Contribution from the McPherson Chemical Laboratory, The Ohio State University, Columbus 10, Ohio

Received February 27, 1959

The vapor pressure of diborane has been measured from 151.2 to 288.5°K. In this range, it varied from 0.14 to 38.3 atm. The normal boiling point was found to be 180.59 ± 0.04°K.

Introduction

As a part of the program to obtain the necessary data for the construction of a Mollier diagram for diborane, it was decided to remeasure the vapor pressure on carefully purified diborane The vapor pressure had previously been measured by Stock,[1] Clarke, Rifkin and Johnston,[2] Rifkin, Kerr and Johnston,[3] and Wirth and Palmer.[4]

Experimental

The equipment used for these measurements is the same as that described by Johnston and White.[5] Pressures below 3 atm. were read from a mercury manometer, while above 3 atm. a MIT-type dead-weight gage was used.

Diborane of 99.91 mole % purity was condensed into the pipet until it was approximately one-half filled. The pipet temperature was adjusted to the desired operating temperature as were the upper, lower and auxiliary blocks and can. Pressure and temperature readings were recorded at one-minute intervals over a ten-minute period. The precision of the pressure readings was 0.01% The normal temperature drift during this time was less than 0.02°K.

After completion of a set of measurements, the valve at the top of the pipet was closed and the material above it removed. In this way subsequent measurements did not involve material which had been at room temperature for more than approximately one hour. Operating difficulties made it impractical to remove the material above the pipet valve when the temperature of the measurements exceeded 250°K. Measurements above this temperature involved some diborane which had been at room temperature for four hours. That decomposition is slight at this temperature over this period of time is evidenced from the inability to detect any non-condensable gas in the sample at the end of the measurements.

Results

The vapor pressure results are given in Table I. Pressures below 3 atm. are measured with a precision of 0.05 mm., while the precision at greater pressures varied from approximately 0.05% below 10 atm. to 0.01% at the higher pressures. The accuracy is limited by the purity of the diborane. This is shown by the results of duplicate determinations made at 251, 260 and 273°K. on different samples. The material used was of the same initial purity, but the amount of decomposition which could occur in the pipet and measuring system during each determination could vary, since the time required for each measurement was dependent upon the rapidity with which equilibrium was attained. It is estimated that the measurements above 250°K. are accurate to 0.1% and those at the lower temperatures to 0.05%.

In the temperature range 151.23°K. $\leqslant T \leqslant$ 219.75°K., the vapor pressure data were fitted by the equation

$$\log p = 3.8262 - \frac{598.30}{T} - \frac{1.6733 \times 10^4}{T^2} \quad (1)$$

with an average deviation of 0.02%. In the range 151.2°K. $\leqslant T \leqslant$ 288.46°K., the data were fitted by means of the equation

$$\log p = 4.8600 - \frac{1236.2}{T} + \frac{1.2215 \times 10^5}{T^2} - \frac{1.2247 \times 10^7}{T^3} + \frac{3.4141 \times 10^8}{T^4} \quad (2)$$

with an average deviation 0.06%.

The calculated value of the normal boiling point using eq. 1 is 180.59 ± 0.04°K.

TABLE I

VAPOR PRESSURE OF DIBORANE

Run No.	Temp., °K.	Pressure, atm.
1	151.23	0.1375
2	160.39	0.2787
4	169.92	0.5325
3	180.64	1.0025
5	194.54	2.0339
6	205.17	3.2523
7	209.96	3.9568
8	219.75	5.7167
9	229.58	8.0182
10	240.15	11.1735
16	246.07	13.2924
11	251.39	15.4418
15	251.40	15.4756
17	256.02	17.5118
12	260.47	19.6553
20	260.49	19.6960
21	264.53	21.8520
19	268.53	24.1090
18	273.16	26.9859
13	273.19	26.9734
27	276.31	29.0888
28	279.85	31.6676
25	282.89	33.8443
24	285.63	36.0677
14	288.46	38.3354

Discussion

The low pressure values are in good agreement with those of Wirth and Palmer,[4] and the value of the normal boiling point agrees with their value, 180.63°K., within the precision of the temperature scale in this temperature range.

The high pressure values are somewhat higher than those of Rifkin, Kerr and Johnston.[2] Considering the greater precision in the measurement of pressure in this research, the differences are about what one should expect.

(1) A. Stock and E. Kass, *Ber.*, **56**, 789 (1923).

(2) John T. Clarke, E. C. Kerr and H. L. Johnston, *J. Am. Chem. Soc.*, **75**, 781 (1953).

(3) E. B. Rifkin and H. L. Johnston, *ibid.*, **75**, 785 (1953).

(4) Henry E. Wirth and Emiel D. Palmer, THIS JOURNAL, **60**, 911 (1956).

(5) H. L. Johnston and David White, *Trans. A.S.M.E.*, **77**, 785 (1950).

THE HEAT OF VAPORIZATION OF DIBORANE

BY LEO J. PARIDON, GEORGE E. MACWOOD AND JIH-HENG HU

Contribution from the McPherson Chemical Laboratory of the Ohio State University, Columbus 10, Ohio

Received March 4, 1959

The heat of vaporization of diborane has been measured calorimetrically from the normal boiling point to within four degrees of the critical point. Over this range, the heat of vaporization as a function is given quite well by the expression $L_v = 546.2\,(T_c - T)^{0.39}$ cal. mole^{-1}, where T_c is the critical temperature, 289.7°K.

Introduction

As a part of this laboratory's program for the investigation of the thermodynamic properties of diborane, its heat of vaporization was determined calorimetrically from the normal boiling point to the critical point.

Experimental

Apparatus.—The condensed gas calorimeter used in this work is the same as that of Hu, White and Johnston.[1]

Procedure.—Diborane of 99.91 mole % purity was condensed into the calorimeter from a calibrated volume. The quantity of material was determined to 0.4% by measuring the pressure with a mercury manometer and a Gaertner cathetometer. All pressure readings were referred to a standard meter bar, and the observed pressures were corrected for capillary depression, the temperature of the mercury and scale, and for local value of g.

The temperature of the calorimeter was determined using a standard copper-constantan thermocouple and a Wenner potentiometer. The energy input for vaporizing diborane was determined, using a double White potentiometer and a resistance thermometer.

At the start of a determination, the temperatures of the calorimeter blocks, which had been adjusted previously to the temperature of the calorimeter, were recorded. The current through the resistance thermometer was read, as well as its drift rate and the galvanometer sensitivity. The potential drop across the resistance thermometer and the e.m.f. of the thermocouple were read alternately at 30-sec. intervals until steady drift rates were obtained.

The valve at the top of the calorimeter was cracked open at the same time that the heating period began. By throttling this valve it was possible to maintain the temperature of the calorimeter constant to ±0.05° throughout the heating period. The vaporized diborane was collected in an evacuated calibrated volume. At the end of the heating period the material remaining in the lines outside the calorimeter was transferred into the calibrated volume by means of a Toepler pump.

The heating period was adjusted to approximately 15 min. duration. The rate of energy input was determined by measuring the potential drop across the heater at the midpoint of the heating period, and the current was taken as the average of that obtained at 0.21 and 0.79 of the heating period. The energy input so obtained was corrected for heat leak as well as for the drift in temperature from the beginning to the end of the heating period.

Results

The molar heat of vaporization L_v is related to the experimentally observed Q and m by[2]

$$L_v = \frac{QM}{m} - TV^l \frac{dp}{dT} \qquad (1)$$

or

$$L_v = \frac{QM}{m}\left(1 - \frac{V^l}{V^g}\right) \qquad (2)$$

where Q is the energy input necessary to vaporize m grams of diborane, M the molecular weight, p the vapor pressure, V^g and V^l, the molar volume of diborane vapor and liquid, respectively. The vapor pressure data used are reported in the preceding paper.[3] The molar volumes were taken from unpublished measurements made in this Laboratory. The corrections of $\frac{QM}{m}$ were calculated using both eq. 1 and 2 and were consistent.

TABLE I

HEAT OF VAPORIZATION OF DIBORANE

T, °K.	QM/M, cal. mole^{-1}	$TV^l\,dp$ cal. mole^{-1}	L_v (exp), cal. mole^{-1}	L_v (eq. 3), cal. mole^{-1}
179.79	3412	15	3397	3405
179.37	3430	15	3415	3404
179.38	3417	15	3402	3404
190.06	3312	25	3287	3286
199.77	3198	38	3160	3158
209.98	3066	56	3010	3013
220.03	2946	81	2865	2858
229.99	2808	112	2696	2692
239.89	2664	155	2509	2508
250.03	2511	207	2304	2295
259.92	2326	277	2049	2052
264.97	2236	320	1916	1908
270.07	2121	371	1750	1744
274.87	1988	418	1570	1563
277.94	1900	468	1432	1428
280.98	1809	531	1278	1271
284.01	1646	576	1070	1076

TABLE II

HEAT AND ENTROPY OF VAPORIZATION OF DIBORANE

T, °K.	L_v, cal. mole^{-1}	ΔS_v, cal. mole^{-1} deg.$^{-1}$
180.57	3405	18.85
180.60	3405	18.85
190.00	3287	17.30
200.00	3155	15.78
210.00	3012	14.34
220.00	2859	13.00
230.00	2691	11.70
240.00	2506	10.44
250.00	2296	9.18
260.00	2050	7.88
270.00	1747	6.47
273.16	1631	5.97
280.00	1325	4.73
285.00	999	3.51
288.00	672	2.3
289.7	0	0

The results of the heat of vaporization measurements and calculations are given in Table I. Considering the precision of the measurements and various sources of systematic error, the maximum error

(1) J. Hu, D. White and H. L. Johnston, *J. Am. Chem. Soc.*, **75**, 5642 (1953).

(2) N. S. Osborne and D. C. Ginnings, *J. Research Natl. Bur. Standards*, **39**, 453 (1947).

(3) Leo J. Paridon and George E MacWood, THIS JOURNAL, **81**, 1997 (1959).

in the molar heat of vaporization is estimated to be ±10 cal./mole.

To smooth the data, they were fitted to the equation

$$L_v = 546.2\,(T_c - T)^{0.39}\ \text{cal. mole}^{-1} \qquad (3)$$

where $T_c = 289.7$°K. Table II gives the values of L_v, calculated using eq. 3, and ΔS_v, the entropy of vaporization.

There have been several previous determinations of the heat of vaporization of diborane at the normal boiling point.[4,5] Clarke, *et al.*, determined it both calorimetrically and from their vapor pressure measurements, reporting 3412 and 3431 cal./mole, respectively. The first value is in good agreement with the value reported here considering the uncertainty in the two values. Wirth and Palmer calculated a value of the heat of vaporization at the normal boiling point from their vapor pressure measurements, estimating the gas imperfection using the Bertholet equation. Their value is 3413 cal./mole and is in exceptional agreement with the other two.

(4) John T. Clarke, E. B. Rifkin and H. L. Johnston, *J. Am. Chem. Soc.*, **75**, 781 (1953).

(5) Henry E. Wirth and Emiel D. Palmer, THIS JOURNAL, **60**, 911 (1956).

SOLUBILITY OF HYDROGEN FLUORIDE IN MOLTEN FLUORIDES. I. IN MIXTURES OF NaF–ZrF$_4$

BY J. H. SHAFFER, W. R. GRIMES AND G. M. WATSON

Oak Ridge National Laboratory,[1] *Oak Ridge, Tennessee*

Received March 5, 1959

Solubilities of HF have been determined at pressures from 0.5 to 3 atmospheres over a temperature range 550 to 800° in NaF–ZrF$_4$ mixtures containing 45 to 80.5 mole % NaF. Henry's law is obeyed and the solubility decreases with increasing temperature. The solubility of HF increases approximately tenfold as the mole % of NaF in the solvent is increased from 45 to 80.5 mole %. Henry's law constants in moles HF per cc. of solution per atmosphere at 600, 700 and 800° are $(1.23 \pm 0.04) \times 10^{-5}$ and $(0.93 \pm 0.02) \times 10^{-5}$ and $(0.73 \pm 0.01) \times 10^{-5}$ in NaF–ZrF$_4$ (53 mole % NaF). The enthalpies of solution in kcal. per mole also increase in magnitude from −3.85 to −9.70 as the mole % of NaF is changed from 45 to 80.5. The entropies of solution vary from −5.2 to −6.5 e.u. over the same range of solvent compositions.

Introduction

This investigation constitutes part of a systematic study of the solubilities of gases in molten salts. In this study an attempt is being made to elucidate the solvent characteristics which have an effect on gas solubility. The results of measurements on the solubility of HF in various mixtures of NaF–ZrF$_4$ at pressures from 0.5 to 3 atmospheres over the temperature range 550 to 800° are presented here.

Solubilities of gases in liquids have been studied by many investigators; reviews covering much of this work are available.[2–4] Solubilities of noble gases in molten fluoride mixtures have been reported.[5] Burkhard and Corbett[6] recently determined the solubility of water in molten LiCl–KCl mixtures and presented an approximate value of the solubility of HCl at 480° in a mixture containing 60% LiCl. No information regarding the solubilities of HF in molten fluorides in the range of pressures, temperatures and solvent compositions presented here has been found in the literature. Related investigations on some of the properties and phase behavior of acid fluorides of LiF,[7] NaF,[8–10] KF,[11] RbF,[12] CsF[13] and NH_4F[14] have been reported. Information on liquid–liquid solubilities and liquid–vapor equilibrium of HF–UF$_6$ mixtures is available.[15,16]

Mixtures of NaF and ZrF$_4$ were chosen for this investigation because of their value in nuclear fuel element reprocessing[17–21] and their use (with added UF$_4$) as fuel for an experimental nuclear reactor.[22]

(1) Operated for the United States Atomic Energy Commission by the Union Carbide Corporation.

(2) A. E. Markham and K. A. Kobe, *Chem. Revs.*, **28**, 519 (1941).

(3) J. H. Hildebrand and R. L. Scott, "The Solubility of Non-Electrolytes," Chapter XV, 3rd Ed., Reinhold Publ. Corp., New York, N. Y., 1950.

(4) M. W. Cook, U. S. Atomic Energy Commission, UCRL-2459 (1954).

(5) (a) W. R. Grimes, N. V. Smith and G. M. Watson, THIS JOURNAL, **62**, 862 (1958); (b) M. Blander, W. R. Grimes, N. V. Smith and G. M. Watson, *ibid.*, **63**, 1164 (1959).

(6) W. J. Burkhard and J. D. Corbett, *J. Am. Chem. Soc.*, **79**, 6361 (1957).

(7) H. V. Wartenberg and O. Bosse, *Z. Elektrochem.*, **28**, 386 (1922).

(8) J. F. Froning, M. K. Richards, T. W. Stricklin and S. G. Turnbull, *Ind. Eng. Chem.*, **39**, 275 (1947).

(9) D. G. Hill, unpublished work, Oak Ridge National Laboratory, Oak Ridge, Tennessee.

(10) W. Davis, Jr., KLI-2552, "Vapor Pressure-Temperature Relations in the System NaF–HF," Union Carbide Nuclear Company, Oak Ridge Gaseous Diffusion Plant.

(11) G. H. Cady, *J. Am. Chem. Soc.*, **56**, 1431 (1934).

(12) E. B. R. Prideaux and K. R. Webb, *J. Chem. Soc.*, 1 (1937); 111 (1939).

(13) R. V. Winsor and G. H. Cady, *J. Am. Chem. Soc.*, **70**, 1500 (1948).

(14) O. Ruff and L. Staub, *Z. anorg. allgem. Chem.*, **212**, 399 (1933).

(15) G. P. Rutledge, R. L. Jarry and W. Davis, Jr., THIS JOURNAL, **57**, 541 (1953).

(16) R. L. Jarry, F. D. Rosen, C. F. Hale and W. Davis, Jr., *ibid.*, **57**, 905 (1953).

(17) G. I. Cathers and R. E. Leuze, "A Volatilization Process for Uranium Recovery in Reactor Operational Problems," Vol. II, Pergamon Press, New York, N. Y., 1957, pp. 157–163.

(18) G. I. Cathers, *Nuclear Sci. and Eng.*, **2**, 768 (1957).

(19) R. P. Milford, *Ind. Eng. Chem.*, **50**, 187 (1958).

(20) S. Lawroski, "Non-aqueous Processing—An Introduction," Symposium on the Reprocessing of Irradiated Fuels Held at Brussels, Belgium, May 20–25, 1957, pp. 479–497, Book II, TID-7534.

(21) R. C. Vogel and R. K. Steunenberg, "Fluoride Volatility Processes for Low Alloy Fuels," ref. 20, pp. 498–559.

(22) A. M. Weinberg and R. C. Briant, *Nuclear Sci. and Eng.*, **2**, 795 (1957).

Experimental

Materials.—The HF was obtained from cylinders each containing 6 lb. of anhydrous liquid hydrogen fluoride supplied by the Harshaw Chemical Company, Cincinnati, Ohio. The liquid HF had a specified minimum purity of 99.9%. The vapor was found to contain less than 0.2 mole % of gases insoluble in aqueous KOH solution; it was used without purification.

The fluoride mixtures were prepared from sodium fluoride of reagent grade and ZrF_4 which had been prepared by hydrofluorination of $ZrCl_4$ at 500° in equipment of nickel. The mixtures were purified, transferred, sampled and analyzed by procedures previously described.[5]

Apparatus.—The apparatus consists of saturating and stripping sections connected by a section of metal tubing which could be sealed as desired by freezing a portion of the fluoride. All sections of the apparatus in contact with the molten fluoride or at high temperature were of nickel; welded construction and commercial Swagelok fittings were used throughout this metal portion. Some sections that the gas contacted only at low temperature were of copper or Teflon tubing. The saturatior and accessories, the connecting tube, the nickel vessel into which the solution was transferred, and the furnace assembly were identical to those used in a previous study.[5]

Pressures were measured on Bourdon pressure indicators of bronze, known as Ashcroft Laboratory Test Gauges. Pressures above atmospheric were read from a gage of 4.5 in. diameter face reading 0–30 lb./sq. in. in 0.1 lb./sq. in. subdivisions. Low pressures were read from a gage with a 7-in. diameter face showing 0–30 in. Hg in $^1/_8$-in. subdivisions. These gages were calibrated in place by periodic comparison with a mercury U-tube manometer having a scale graduated in 1 mm. subdivisions.

The line through which HF was admitted to the saturator contained a filter made from a disc of sintered nickel (0.0004-in.-diameter pores) and a 2-liter surge tank of nickel. The filter effectively removed finely divided solid particles which were detached from the surfaces of heated lines carrying HF vapor. The surge tank diminished the pressure decrease when a portion of the melt was transferred to the stripping section.

Temperatures were controlled and recorded from chromel–alumel thermocouples as in previous investigations.[6] Once per day the melt temperature was checked with a standard platinum to platinum–rhodium thermocouple connected to a Leeds & Northrup type K-2 potentiometer. The temperatures probably were known to 5°.

Procedure.—The internal surfaces of the empty saturator, stripping section and connecting tube were treated at 600° with flowing hydrogen for 2 hours. A charge of approximately 2.5 l. (5 to 7.5 kg.) of molten salt was transferred to the saturator which was then isolated from the empty stripping section by establishing the frozen seal. The internal surfaces of the stripping section were conditioned by treatment at 600° with anhydrous HF vapor. The empty stripping section and the saturator containing the molten charge were flushed with He until the HF concentrations in the effluent streams diminished to values below 4×10^{-6} mole HF/l. The melt, at thermal equilibrium in the saturator, was saturated by sparging with HF at the desired pressure for 6 hours. After sparging was discontinued the HF was maintained at pressure as a covering atmosphere. The liquid level was measured by use of the electrical probe.[5] Meanwhile the stripping section, which had been continually flushed with a stream of He, was closed and filled with He at a predetermined pressure such that about one-half the salt would transfer from the saturator when the frozen seal was destroyed. The frozen seal was melted and the molten salt was allowed to transfer until hydrostatic equilibrium was achieved. The frozen seal was immediately re-established and the final liquid level in the saturator was determined. The dissolved HF was stripped from the salt and absorbed in a standard solution of KOH in water. Stripping with He was discontinued (after about 75 l. had been passed) when the concentration of HF in the effluent stream dropped to about 4×10^{-6} mole/l. The HF absorbed in the KOH solution was determined by back titration with standard acid solution.

No attempts were made in the routine determinations to continue the final stripping until negligibly small quantities of HF remained in the molten salt. Instead, in several separate experiments, a portion of molten salt which had been transferred under identical experimental conditions of temperature and pressure, but which had been saturated with helium instead of HF, was used to establish that about 0.3 mmole of HF was recovered by sparging with 75 l. of helium. This "blank," which amounted to 1 to 2% of the HF recovered by the regular procedure, was used to correct all the data presented in this report.

The volume of transferred salt was established from the

TABLE I

SOLUBILITY OF HF IN MOLTEN NaF–ZrF_4 (53 MOLE % NaF)

Saturating temperature, °C.	Saturating pressure, (atm.)	HF solubility $\times 10^5$, moles/(cc. melt)	$K \times 10^5$, moles HF (cc. melt)(atm.)
550	2.09	2.91	1.39
	2.56	3.62	1.41
	2.96	3.98	1.35
		Av.	1.38 ± 0.02
		Calcd. from eq. 1	1.45
600	0.494	0.57	1.16
	0.550	0.66	1.19
	0.565	0.69	1.23
	1.05	1.39	1.32
	1.05	1.33	1.27
	1.34	1.62	1.21
	1.50	1.75	1.17
	1.55	1.92	1.24
	2.05	2.72	1.33
	2.05	2.45	1.19
	2.52	3.07	1.22
	2.52	3.02	1.20
	2.53	3.11	1.23
	2.95	3.52	1.20
		Av.	1.23 ± 0.04
		Calcd. from eq. 1	1.22
650	0.43	0.47	1.10
	1.03	1.02	1.00
	1.47	1.49	1.01
	2.14	2.20	1.03
	2.36	2.41	1.02
	2.74	2.81	1.03
		Av.	1.03 ± 0.02
		Calcd. from eq. 1	1.06
700	0.62	0.58	0.93
	1.16	1.08	.93
	1.40	1.32	.95
	1.79	1.68	.94
	1.86	1.80	.97
	2.75	2.42	.88
		Av.	.93 ± 0.02
		Calcd. from eq. 1	.93
750	0.83	0.73	.88
	1.15	1.00	.87
	1.96	1.63	.84
		Av.	.86 ± 0.02
		Calcd. from eq. 1	.83
800	0.42	0.31	.74
	0.84	0.62	.74
	1.51	1.14	.75
	2.18	1.54	.73
	2.48	1.75	.71
		Av.	.73 ± 0.01
		Caled. from eq. 1	.74

TABLE II

EFFECT OF SOLVENT COMPOSITION ON THE SOLUBILITY, ENTHALPY AND ENTROPY OF SOLUTION OF HF IN NaF–ZrF_4 MIXTURES

Solvent compn., mole % NaF	$K \times 10^3$ at 600°	$K \times 10^3$ at 700°	$K \times 10^3$ at 800°	ΔS_c,[b] e.u.	Const. for eq. $\ln K = \frac{\Delta S_p}{R} - \frac{\Delta H}{RT}$: ΔH, kcal./mole	ΔS_p,[c] e.u.	δ[d]
45	0.78	0.65	0.51	−5.2	−3.85	−14.0	3.65
53	1.23	0.93	0.73	−5.4	−4.70	−14.1	2.85
60	1.53	1.03	0.81	−6.2	−5.80	−14.9	2.51
65	2.17[a]	1.46	1.06	−6.4	−6.60	−15.1	0.90
80.5	12.80[a]	7.20[a]	4.43	−6.5	−9.70	−15.2	1.19

[a] Extrapolated from measurements at higher temperatures. [b] ΔS_c, entropies of solution calculated for equal concentrations of HF in gas and liquid phases at 1000°K. [c] ΔS_p, entropies of solution calculated from equal pressures of HF in the gas and liquid phases at 1000°K. [d] δ, per cent. standard deviation of experimental values of K from values calculated by the equation $\ln K = \Delta S_p/R - \Delta H/RT$.

initial and final levels in the saturator. The concentration of HF in the saturated melt was available from this volume and the corrected absolute quantity of HF recovered.

Results

The solubility of HF in molten NaF–ZrF_4 (53 mole % NaF) has been examined at 50° intervals over the range 550 to 800° at pressures from about 0.5 to 3 atmospheres. Linear dependence of solubility on HF pressure was observed from the experimental data shown in Table I. The temperature dependence of the Henry's law constant for this system is expressed by the equation

$$\ln K = -\frac{\Delta H}{R}\frac{1}{T} + \frac{(\Delta S_p)}{R} \qquad (1)$$

The calculated Henry's law constants from this equation are also shown in Table I. The solubility of HF has been measured over the same range of pressures at 600, 700 and 800° in NaF–ZrF_4 mixtures containing 45 and 60 mole % NaF, at 650, 750 and 850° in mixtures containing 65 mole % NaF, and at 800, 850 and 900° in mixtures containing 80.5 mole % NaF. Because of the high liquidus temperatures[23] of NaF–ZrF_4 mixtures containing more than 60 mole % NaF, it was not possible to make a direct measurement of the solubilities at 600 and 700°. For purposes of comparison, Henry's law constants for these gases were extrapolated from measurements at higher temperatures. The arithmetic averages of Henry's law constants and calculated enthalpies and entropies of solution in different solvent mixtures are shown in Table II. The standard deviation of the experimental with the calculated values of Henry's law constants are also shown to be within 4%.

Table III shows values of the constants for the equation[24]

$$\rho(\text{g./cc.}) = A - Bt(°\text{C.}) \qquad (2)$$

from which densities of these liquids can be calculated over the temperature interval used in this study. The data presented can, by use of these values, be converted to mole fraction or to moles HF per gram of solvent as desired.

As in the studies of noble gas solubility,[4] sparging of the melt for 6 hours was shown to be ample to

(23) C. J. Barton, W. R. Grimes, H. Insley, R. E. Moore and R. E. Thoma, THIS JOURNAL, 62, 665 (1958).

(24) H. F. Poppendiek, Oak Ridge National Laboratory, personal communication.

TABLE III

CONSTANTS FOR DENSITY–TEMPERATURE EQUATION OF MIXTURES INVESTIGATED[24]

ρ (g./cc.) = $A - Bt$ (°C.)

Soln. compn., mole % ZrF_4	A	$B \times 10^{+3}$
55	3.83	0.91
47	3.71	.89
40	3.61	.87
35	3.52	.86
19.5	3.23	.81

ensure saturation; no evidence of entrainment of gas bubbles in the liquid was observed.

Temperatures should have been accurate to ±5° and the volume of salt transferred could be measured to ±2%. Uncertainties in the acidimetric titration were negligibly small while the blank, which could hardly have been in error by ±25%, contributed less than 2% to the solubility values. The solubility values and Henry's law constants shown in Table I are representative of the precision of the experiments.

Discussion

Within the precision of the measurements the solubility of HF in all mixtures studied follows Henry's law. In contrast with the behavior of noble gases in similar solvents,[4] the solubility of HF decreases as the temperature is increased. The dependence of the solubility of HF on solvent composition is far greater than that exhibited by the noble gases[4] in related solvents. As shown in Table II, the solubility increases by approximately tenfold as the mole per cent. of NaF in the solvent is increased from 45 to 80.5. Table II also shows that the enthalpy of solution is strongly dependent on the solvent composition. The values of the entropies of solution[25] are all negative and change only 1 e.u. over the range of solvent compositions investigated but are considerably larger in magnitude than those observed for the noble gases in NaF–ZrF_4[4a] and in NaF–KF–LiF ternary eutectic.[4b]

The observed strong dependence of the solubility of HF on solvent composition may be related to the relatively high stability of NaF–HF compounds. It may be possible, when more data are

(25) The entropies of solution have been calculated for equal concentrations of HF in the gas and liquid phases in the same manner as described elsewhere.[4]

available, to relate the observed strong dependence of HF solubility on solvent composition with the relative stabilities of some of the alkali metal acid fluorides noted previously at lower temperatures.[13] Since LiF_4 forms quite unstable bifluorides[7,13] it might be predicted that the solubility of HF in $LiF–ZrF_4$ mixtures would be smaller and less dependent on the composition of the solvent than in the corresponding $NaF–ZrF_4$ mixtures. Present plans are to study HF solubility in related mixtures of $LiF–ZrF_4$, $LiF–BeF_2$, $NaF–BeF_2$ and LiF–NaF.

Acknowledgments.—The authors are especially indebted to Drs. F. F. Blankenship, M. Blander and R. F. Newton for many interesting and valuable discussions. Dr. Max Bredig's review of the manuscript is also gratefully acknowledged.

INTRINSIC VISCOSITY–MOLECULAR WEIGHT RELATIONSHIPS FOR ISOTACTIC AND ATACTIC POLYPROPYLENE. I[1]

BY J. B. KINSINGER[2] AND R. E. HUGHES

Contribution from the John Harrison Laboratory of Chemistry, University of Pennsylvania, Philadelphia, Pennsylvania

Received April 17, 1959

Number average molecular weight–intrinsic viscosity relationships have been determined for atactic polypropylene in three solvents. High temperature light scattering studies of polypropylene in 1-chloronaphthalene at 125° have provided weight average molecular weight–intrinsic viscosity relationships for atactic and isotactic polypropylene. In a thermodynamically good solvent the "K" and "a" constants from the Mark–Houwink expression are found identical for these geometrical isomers. The root-mean-square-end-to-end-distances for atactic and isotactic polypropylene in 1-chloronaphthalene at 125° were found to have experimental values in reasonable agreement with hydrodynamical theory. The calculated values of the universal hydrodynamic interaction constant (Φ) were in good agreement with those reported for other atactic polymers. The second virial coefficients for atactic polypropylene differed from those of the isotactic polymer reflecting differences in thermodynamic interaction between polymer and solvent and possibly molecular size.

Introduction

While several viscosity–molecular weight relationships for polypropylene have appeared in the literature,[3–6] all of these investigations are limited in nature and none embrace concomitant studies on the atactic and isotactic polymers. The importance of conducting experiments in this manner has been emphasized by Danusso,[7] who noted differences in the second virial coefficient for two geometrical isomers of polystyrene. The purpose of this work was to provide intrinsic viscosity–molecular weight relationships for polypropylene so that further investigations on the dilute solution properties and their dependence on geometrical configuration might be facilitated.

While variations in geometrical structure account for wide differences in behavior of the polymers in the solid state, additional interest is now centered on the characteristics of the various geometrical forms of the same polymer in dilute solution where the polymer configuration and thermodynamic properties can be measured. In particular, differences in configuration may be characterized by the thermodynamic parameters and unperturbed dimensions which arise from the dilute solution theory for linear macromolecules.

(1) Presented before the Division of Polymer Chemistry, 132nd National Meeting, American Chemical Society, New York City, September 8–13, 1957.

(2) Hercules Powder Co. Fellow; University of Pennsylvania, 1956–1957. Department of Chemistry, Michigan State University, East Lansing, Michigan.

(3) G. Ciampa, *Chim. e ind. (Milan)*, **38**, 298 (1956).

(4) F. Ang and H. Mark, *Monatsh. Chem.*, **88**, 427 (1957).

(5) R. Chiang, *J. Polymer Sci.*, **28**, 235 (1958).

(6) F. Danusso and G. Moraglio, *Makromol. Chem.*, **28**, 250 (1958).

(7) F. Danusso and G. Moraglio, *J. Polymer Sci.*, **24**, 161 (1957).

Experimental

Samples of atactic and crystalline (isotactic) polypropylene were generously provided by the Hercules Powder Company of Wilmington, Delaware. The atactic samples were clear, colorless and characteristically rubbery whereas the crystalline polymers were fluffy, white, non-tacky powders. According to their source, these polymers were prepared with Zeigler type catalysts. No residual metals (very low ash content) were noted in the polymer; however, the purification and the atactic–isotactic separation procedure was not revealed. All samples appeared pure and homogeneous. The three samples investigated are designated as:

Sample A	Atactic, $[\eta]$ = 1.10 (benzene) 25°
Sample B	Atactic, $[\eta]$ = 1.10 (benzene) 25°
Sample C	Isotactic, $[\eta]$ = 1.69 (decalin) 135°

As indicated by the limiting viscosity number and later confirmed by the source, the two atactic samples were taken from a common master batch and are therefore identical.

Fractionation. A. Atactic Polymer.—The solubility parameter (δ = square root of the cohesive energy density) of polypropylene was determined previously in this Laboratory to be approximately 8.2.

Both atactic samples were fractionated by the addition of a non-solvent to a dilute solution of the polymer by the precipitation procedure described by Flory.[8]

Sample A was fractionated at 30° with a solvent–non-solvent pair consisting of benzene and methanol, respectively. Each of the resulting fractions was redissolved in benzene, filtered and freeze dried. All fractions were dried to a constant weight *in vacuo* at 50°.

To circumvent earlier separation difficulties, a new solvent–non-solvent system consisting of cyclohexane and acetone, respectively, was chosen for the fractionation of Sample B. In this mixture the concentrated polymer phase settled to the bottom of the flask so the clear dilute solution phase could be decanted easily. Eight fractions were recovered and each was redissolved in benzene and recovered by freeze drying. The large initial fraction subsequently was separated by refractionation into two fractions.

(8) P. J. Flory, "Principles of Polymer Chemistry," Cornell Univ. Press, Ithaca, New York, N. Y., 1953, pp. 339–342.

During the fractionation it was noted the atactic polymer behaved in all respects like a true amorphous material with no evidence for any crystalline type separations or even a small portion of crystalline polymer in the initial fractions. The high molecular weight atactic fractions were transparent, non-tacky rubbers, whereas the low molecular weight atactic fractions were viscous, slightly tacky oils. There was no noticeable change in the transparency or the rubbery or viscous nature of the atactic fractions even months after they had been purified and dried and examination under crossed polaroids revealed no crystalline regions.

B. Isotactic Polymer.—As recommended in a recent study,[9] fractions of crystalline (isotactic) polypropylene were prepared by the method of fractional precipitation at high temperature. Since it had been shown that polyethylene could be fractionated in this manner as much as 60° below the melting point of the polymer, a fractionation temperature range of 130 to 135° was chosen for polypropylene (~30° below the melting point).

The fractionation was performed in standard equipment in a constant temperature oil-bath. A two liter, three necked flask was fitted at the bottom with a moderate size stopcock and was lubricated with a coating of powdered graphite to prevent sticking and leaking in the hot oil. With the addition of a pressure spring and careful manipulation no difficulties with the stopcock were encountered during the high temperature fractionation. A variable speed motor drove a standard taper ground glass stirrer mounted through the center neck of the flask. A standard taper dropping and measuring funnel was fitted to one of the other two necks and the third was occupied by a thermometer.

The polymer solution was agitated vigorously during the slow addition of the non-solvent until a non-vanishing precipitate appeared. *In all instances* this phase would vanish when the solution was warmed slightly. Finally the mixture was cooled slowly with stirring to the preferred temperature and the polymer allowed to settle overnight. Since the precipitated phase could be transposed easily to a true solution merely by a slight temperature increase it appeared the *initial* separation was liquid–liquid in nature.[10]

Cyclohexanone, a theta solvent for the atactic polymer at a lower temperature, was used as the solvent and ethylene glycol as the non-solvent. This combination gave clean fractionation, especially for medium to low molecular weight species. To aid the initial dissolution of polymer in cyclohexanone, a small amount of tetralin (tetrahydronaphthalene) was added to the concentrated mixture to form a viscous solution before the cyclohexanone was added further as a diluent (1% or less in polymer).

Although the initial separations appeared liquid–liquid, after settling overnight the precipitated polymer in the more concentrated phase would crystallize and was easily separated from the remaining solution by draining the latter away through the stopcock into another preheated flask.

To circumvent the problem of over-stepping the initial addition of non-solvent, a less drastic non-solvent, dimethyl phthalate, was chosen for a second run with sample C (denoted C′). In this case a larger portion of non-solvent was needed to reach the point of initial phase separation and two moderate sized fractions of high molecular weight polymer were obtained to complete the range of fractions sought.

Oxidative degradation of the polymer was prevented by the addition of stabilizers to the solutions (preferably 2,6-di-*t*-butyl-*p*-cresol).

The crystalline polymer fractions could be recovered as white fluffy powders or friable fibers by dissolving the fractions in tetralin at 130° and immediately pouring the solution into cold, rapidly stirred methanol. Upon completion of the precipitation, the mixture was stirred slowly for a half hour, after which the polymer was placed into fresh methanol for a period of 24 hours. Thereafter the polymer was filtered free of excess solvent, washed with additional fresh methanol and finally dried in a vacuum oven at 70 to 90° until the sample reached constant weight (usually 48 hours). At this stage, all fractions were extremely porous and would dissolve almost instantaneously when placed in either decalin or tetralin at 130°. The fractions were *free of color*. Although other methods of fraction recovery were attempted, none was found to leave the samples in as pure a condition or as easily redissolvable. This latter point proved especially important because it reduced the time the polymers had to remain at high temperatures by a considerable extent and thus helped minimize the degradation problem.

A summary of the fractionation data is given in Table I.

TABLE I

FRACTIONATION OF ATACTIC (A, B[a]) AND ISOTACTIC (C, C′) POLYPROPYLENE

Sample	G./ Fract.	Wt. %/ Fract.	Solv.	Non-solv.	Temp., °C.
A-1	0.9	4.5	Benzene	Methanol	25
2	0.56	2.8			
3	2.90	14.5			
4	2.96	14.8			
5	3.04	15.2			
6	1.96	9.8			
7	1.92	9.6			
8	0.76	3.8			
9	0.50	2.5			
B-1a	0.30	3.0	Cyclohexane	Acetone + methanol for 7 and 8	30
1b	1.10	11.0			
2	2.8	28.0			
3	0.4	4.0			
4	0.9	9.0			
5	0.6	6.0			
6	1.65	16.5			
7	0.56	5.6			
8	1.24	12.4			
C-1	4.1	41.	Cyclohexanone	Ethylene glycol	130
2	1.26	12.6			
3	1.14	11.4			
4	0.66	6.6			
5	0.63	6.3			
6	0.25	2.5			
C′1	0.31	2.8	Cyclohexanone	Dimethyl phthalate	130
2a	1.68	15.0			
2b	2.35	21.0			

[a] $\Sigma[\eta_i]W_i = 1.99$ for $[\eta]$ in cyclohexane at 25° (see Table II); $[\eta]$ bulk-polymer = 2.01.

Viscosity Measurements.—Polymer solutions were prepared so the relative viscosity fell within the limits 1.2 to 1.9. Both η_{sp}/C and $(\ln \eta_{rel}/C)$ were calculated and plotted against the concentration and a double extrapolation to zero concentration was performed where the two curves met at a common intercept $[\eta]$. These two initial extrapolations were drawn by eye to a best fit. Afterwards the k and k' values of the Huggins viscosity relationships were calculated from the slopes and the intercept. In all cases these values when summed equalled 0.5 ± 0.03.

Generally three or more concentrations of each fraction were prepared *individually* (the dilution technique was never used) for each intrinsic viscosity determination.

Special techniques were required for handling the crystalline polymer at high temperature. Severe degradation in decalin resulted when it was necessary to maintain the polymer at solution temperatures (120° or higher) for a considerable time (~30 minutes). The polymer fractions dissolved rapidly in the solvent and the solutions were immediately filtered through a heated glass frit into the viscometer and measured so that the total time lapse from dissolution to completion of the viscosity measurement was less than 15 minutes.

Degradation was further prevented by adding a stabilizer to the solutions (2,6-di-*t*-butyl-*p*-cresol). With this compound as a stabilizer, (1%), a constant efflux time could be maintained in decalin in the viscometer for over half an hour at 135°. If left exposed to air in the viscometer overnight at this temperature the polymer degraded even with stabilizer.

Viscosity data were taken in several solvents and at several temperatures and are recorded in Table II.

(9) A. Nasini and C. Mussa, *Makromol. Chem.*, **20**, 59 (1957).

(10) Recent experiments have verified that these phase separations occurred in the liquid–liquid region.

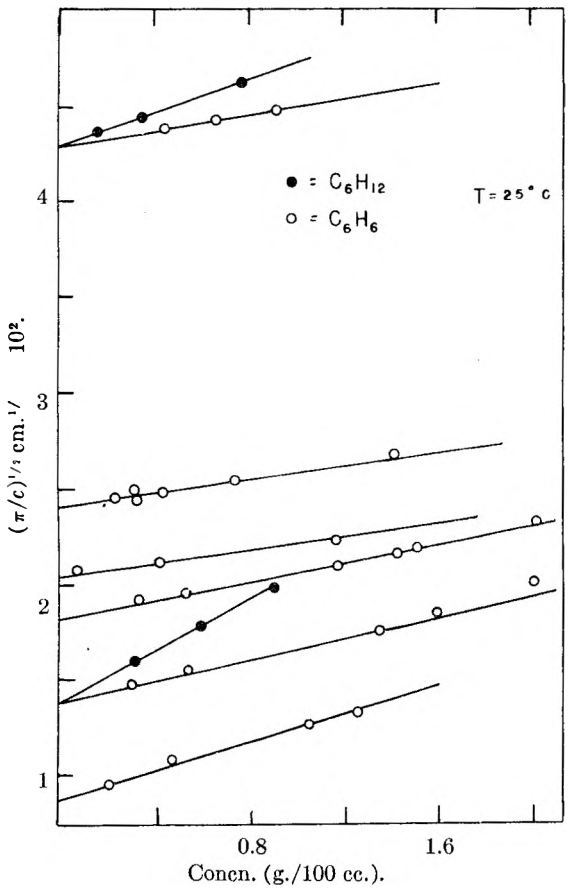

Fig. 1.—Osmotic pressure *vs.* concentration for atactic polypropylene in (○) benzene and (●) cyclohexane at 25°.

TABLE II

INTRINSIC VISCOSITY OF FRACTIONS OF ATACTIC AND ISOTACTIC POLYPROPYLENE

	(Units are deciliters/g.)		
Fract.	Benzene 25°	Decalin 135°	Cyclohexane 25°
A-1	2.45		
A-2	3.20		
A-3	2.14	3.70	4.08
A-4	1.20	1.70	2.30
A-5	0.75	1.10	1.35
A-6	.49	0.63	0.80
A-7	.305		.296
A-8	.17		
A-9	...		
A-7, 8[a]	.23	0.26	.32
B-5	.64		1.03
C-1		3.90	
C-2		1.85	
C-3		1.34	
C-4		0.63	
C-5		0.27	
C-6		...	
C′-1		4.99	
C′-2a		4.80	
C′-2b		2.35	
C′-3		...	
C′-4		...	

[a] Mixture of 7 and 8.

Osmometry.—Osmotic pressure measurements were carried out with the atactic polymer only, in a modified Bureau of Standards type osmometer at 25°. Membranes were prepared from very dense grade "Ultracella" which were treated successively with caustic solution, water, ethyl alcohol, acetone and finally benzene. The membrane treatment followed an elaboration of a scheme suggested by Yanko.[11] Redistilled white label grade solvents were used for all osmotic pressure measurements.

Most of the osmotic pressure data were taken with a single osmometer and membrane. At least 24 hours were required to attain equilibrium but readings were generally extended from 48 to 72 hours. The final values, which fluctuated slightly because of temperature variations, were averaged to obtain an equilibrium value. The membranes were sufficiently non-permeable that only one fraction showed any appreciable diffusion of polymer (A-7, 8). The diffusion rate of the lowest molecular weight fraction was found to be 1% per 24 hours and the equilibrium value for this fraction was taken as the intercept of the extrapolated steady diffusion curve to zero time.

The number average molecular weight ($\bar{M}_n$) was determined for six atactic fractions in benzene at 25°, two of which were also measured at the same temperature in cyclohexane. For these two fractions the extrapolated reduced osmotic pressure *vs.* concentration curves were found within experimental error to meet at a common intercept (Fig. 1).

Light Scattering.—Light scattering measurements were performed in a Brice Phoenix Light Scattering Photometer fitted with a Brice Phoenix high temperature thermostat designed after a model used by Trementozzi.[12] The thermostat was lagged on the outside with sheet asbestos and the temperature within the unit was maintained by circulating ethylene glycol through the thermostat from a regulated external bath. The glycol was transported through asbestos lagged quarter inch copper tubing and all connections were made with silicone rubber tubing. A commercial pump successfully transferred the hot fluid up to 140° without modification. The polymer solution temperature lagged ten degrees below that of the regulated external bath but once equilibrium was established the solution temperature did not vary throughout the measurements more than ±2° for a single fraction.

The thermostat was not operated at high temperature for extended periods of time and except when measurements were actually in progress the lid to the photometer was left open. In this manner the photomultiplier tube housing never became hotter than slightly warm to the touch. Neither erratic behavior nor excessive drift in galvanometer readings was noted, which indicated the photomultiplier tube apparently was not affected by the slight temperature rise during the measurements. Data taken intermittently over a 15-minute period for a given concentration of polymer were reproducible.

The photometer was calibrated by two methods: the first based on the standard opal glass reference as explained in the Brice Phoenix handbook, the second consisted of measuring the turbidity of a standard sample of Cornell polystyrene. Both methods agreed within 1%.

Technical grade 1-chloronaphthalene was distilled twice through a short Vigreux column at 15 mm., each time collecting the middle third of the distillate. The final distillation was carried out in a 24 inch packed column and the center third retained for scattering measurements. The refractive index of each batch of solvent was taken with an Abbe refractometer at 25°. These values were found to agree with the literature within two units in the third decimal place.

Since the crystalline polymer precipitated just 15 to 20° below the measurement temperature, it was necessary to handle these solutions in a somewhat different fashion. Before dissolving the fractions at high temperature all equipment was prepared so that measurements could be performed in minimum time. The polymer and solvent then were weighed into a volumetric flask and heated to 130° to dissolve the polymer. After solution was complete (usually 10 to 15 minutes with intermittent agitation) it was forced with nitrogen through a preheated ultrafine filter directly into the preheated cylindrical cell set into the thermostat. When filtration was complete, the cell was covered

(11) J. A. Yanko, *J. Polymer Sci.*, **19**, 437 (1956).
(12) Q. A. Trementozzi, *ibid.*, **22**, 187 (1956).

with a ground glass plate and the measurements taken after allowing ten minutes for temperature equilibrium. The heated filter was later flushed three times at high temperature with hot xylene and dried with air.

After the first concentration was measured, the cell was quickly removed, weighed and returned to the thermostat. Preheated, filtered solvent then was added to the cell, the amount measured by difference in weight of the solvent flask. If during successive additions, dust contaminated the solution, it was refiltered into the cell and the contents reweighed. The measurement of a fraction took from 30 minutes to an hour to complete. Although solvent was generally added to the initial polymer solution, one run was carried out by adding concentrated polymer solution to pure solvent. There was no indication from the data taken by these two methods that degradation was occurring. A single pass through the ultrafine filter was sufficient to clarify the 1-chloronaphthalene solutions.

All light scattering measurements were taken with unpolarized light in the Wittnauer type cell sold by the Phoenix Instrument Company. Angular deviations due to cell imperfections were checked by measuring the scattering of a dilute solution of fluorescein in water.

A Zeiss–Rayleigh type interferometer was used to measure the refractive index increment at two temperatures (25 and 50°) for solutions of atactic polypropylene in 1-chloronaphthalene and the data extrapolated to 125° to obtain (dn/dc). This extrapolated value also agreed closely with a value calculated with the Dale–Gladstone relationship using measured densities for both the polymer and the solvent. However, the uncertainty in the high temperature refractive index increment values represent the major source of error in the weight average values for the various atactic and crystalline fractions in this study (dn/dc in 1-chloronaphthalene at 125°; 5460 Å. = −0.227, 4380 Å. = −0.228).

Considerable fluorescence in blue light developed in the 1-chloronaphthalene solutions when they were exposed to air at 140° or higher for short periods. Considerable effort was expended to restrict access of air to the solutions and all measurements were made with green light (546 mμ).

At the high temperature the 1-chloronaphthalene produced strong penetrating fumes when the cell was opened at the top to add solvent. These vapors condensed inside the apparatus and were especially noticeable on the working standard which thus required regular cleaning before each run.

Results and Discussion

Number Average Molecular Weight.—Several equations relating the reduced osmotic pressure to concentration appear in the literature. In particular the two virial expansions used are

$$(\pi/C) = (\pi/C)_0[1 + \Gamma_2 C_2 + g\,\Gamma_2 C_2^2 + \ldots] \quad (1)$$

$$(\pi/C) = RT\left[\frac{1}{M_n} + A_2 C + A_3 C_2^2 + \ldots\right] \quad (2)$$

By neglecting terms higher than C^2 in the expansion and setting $g = 1/4$, equation 1 can be reduced to

$$(\pi/C)^{1/2} = (\pi/C)_0^{1/2}[1 + \Gamma_2 C/2] \quad (3)$$

where the second virial coefficients of (1) and (2) are related as $A_2 = \Gamma_2/\bar{M}_n$. According to the simple polymer theory $A_2 = (\bar{v}^2/V_1)(1/2 - \chi_1)$ where $\bar{v}$ is the specific volume of the polymer, V_1 is the molar volume of the polymer and χ_1 is the thermodynamic interaction parameter.

The number average molecular weight and second virial coefficients were determined for six atactic fractions from data plotted according to equation 3 (Fig. 1). The values of (π/C) were always less than three times $(\pi/C)_0$ as suggested for this procedure.[13] The data which are given in Table III show a twenty-fold molecular weight range for the fractions measured.

(13) See ref. 7, Chapter .

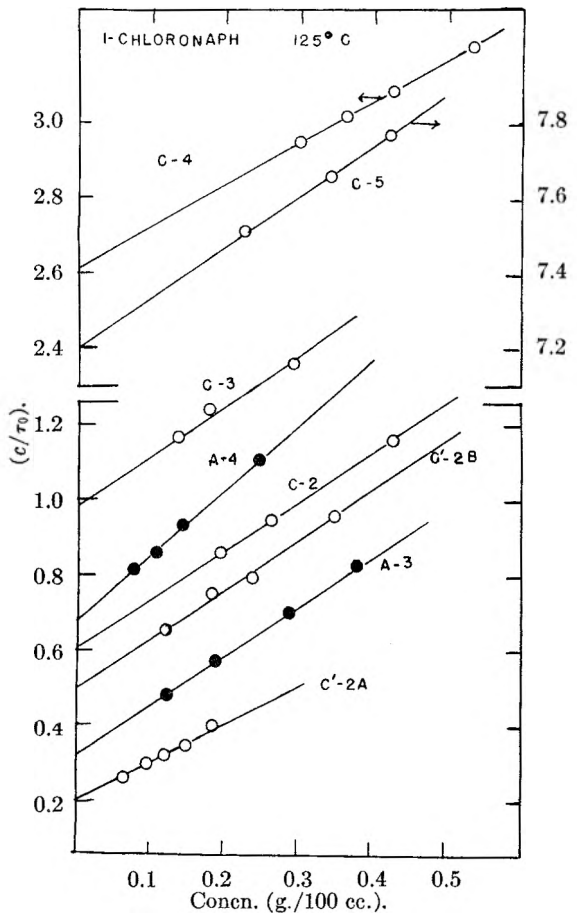

Fig. 2.—(C/τ_0) at $(\theta) = 0$ *vs.* concentration for two (●) atactic fractions and 6 (○) isotactic fractions of polypropylene. Solvent was 1-chloronaphthalene at 125°.

TABLE III

OSMOTIC PRESSURE DATA AT 25° FOR ATACTIC POLYPROPYLENE

Fract.	Solv.	$M_n \times 10^{-4}$	Γ_2 (cc./g.)	A_2 (cc. mole/g.^{2}) $\times 10^4$	χ_1
A-3	Benzene	30 8	75	2.44	0.498
A-4	Benzene	13.8	39	2.72	.498
A-5	Benzene	7.58	25	3.30	.498
A-6	Benzene	4.38	16	3.65	.497
A-7, 8	Benzene	1.42	8	5.60	.496
B-5	Benzene	6.00	15	2.52	.498
A-7, 8	Cyclohexane	1.42	23	9.0	.35
A-4	Cyclohexane	13.8	124	16.5	.42

Weight Average Molecular Weight.—$\bar{M}_w$ was obtained graphically by plotting (C/τ) against $\sin^2\theta/2$ for each concentration and extrapolating the resulting curves to $\theta = 0$. The zero angle values (C/τ_0) were then plotted against concentration and the resulting curves extrapolated to zero concentration $(C/\tau)^0$ in accordance with the relationship

$$(C/\tau_0) = (C/\tau_0)^0(1 + 2\Gamma_2 C + \ldots) \quad (4)$$

The weight average molecular weight then was calculated from the relationship

$$M_w = \frac{1}{H(C/\tau_0)^0} \quad (5)$$

where

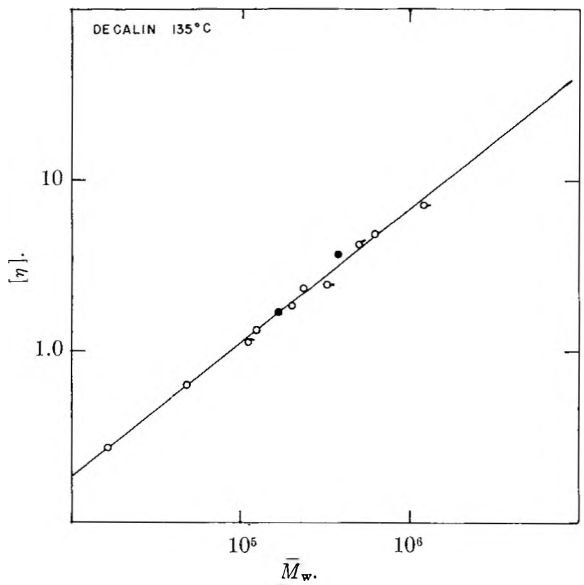

Fig. 3.—log $[\eta]$ *vs.* log $\bar{M}_w$ for atactic (●) and isotactic (○, this work; ○-, ref. 3) polypropylene fractions in decalin at 135°.

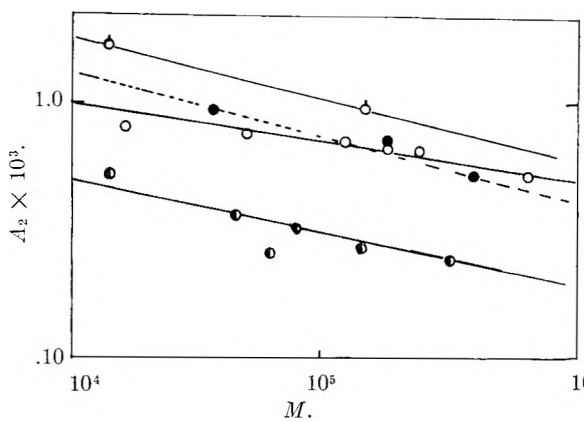

Fig. 4.—Second virial coefficient A_2 *vs.* log M for atactic polypropylene in benzene (◐), cyclohexane (♂) at 25° and 1-chloronapthalene (●) at 135°. Open circles are for isotactic polypropylene in 1-chloronaphthalene (○) at 125°.

$$H = 32\pi^3 n_0^2 (dn/dc)^2 / 3\lambda^4 N$$

Examples of these data are shown in Fig. 2. From the slopes and the values of $\bar{M}_w$, A_2 was calculated from the relationship $A_2 = \Gamma_2/\bar{M}_w$. The pertinent light scattering results are summarized in Table IV where the data of Chiang[5] are included for comparison.

Although Chiang's light scattering data were taken in the same solvent at 140° our values of the second virial coefficient appear to be in reasonable agreement.

Intrinsic viscosity–molecular weight relationships were established by combining the viscosity data of Table A with the $\bar{M}_n$ and $\bar{M}_w$ of Tables III and IV, respectively, on a log–log plot. The two constants a and K from the empirical Mark–Houwink expression

$$[\eta] = KM^a \qquad (6)$$

were evaluated from the slope and intercept respectively and are summarized for both weight and number average molecular weights in Table V. The two constants for benzene and cyclohexane in the weight average value relationship were calculated from intrinsic viscosity data alone.

TABLE IV

LIGHT SCATTERING DATA IN 1-CHLORONAPHTHALENE AT 125°

Fract.	$\bar{M}_w$	$\bar{M}_w/\bar{M}_n$	Γ_2 (cc./g.)	A_2 (cc. mole/g.²) × 10⁴
C'-2a	618,000		31.5	5.1
C'-2b	235,000		15.5	6.6
A-3	383,000	1.23	22.4	5.8
A-4	170,000	1.26	14.1	8.3
C-2	200,000		13.2	6.6
C-3	124,000		8.5	6.8
C-4	49,000		2.9	6.0
C-5	16,500		1.1	6.9
B-6	39,500	1.27	4.1	10.2
F-1[a]	107,000		4.5	4.2
F-2[a]	333,000		12.6	3.8
F-3[a]	500,000		17.5	3.5
F-4[a]	1,100,000		45.0	4.1

[a] From ref. 5 (data taken in 1-chloronaphthalene at 140°).

TABLE V

Solv.	Temp., °C.	$K \times 10^4$	"a"	Fract.
		$\bar{M}_n$		
Benzene	25	2.70	0.71	6
Cyclohexane	25	1.60	.80	6
Decalin	135	1.38	.80	5
		$\bar{M}_w$		
Decalin	135	1.10	0.80	8
Benzene	250	2.55	.70	5
Cyclohexane	25	1.43	.80	5

The weight average molecular weight relationship for decalin taken from Fig. 3 shows excellent agreement with the relationship given by Chiang[5] and his data are found to correspond closely to ours. This good correlation obtains despite the fact that our reported (dn/dc) values differ by enough to allow a 40% error in measured molecular weights. Since the agreement is generally good this variation in (dn/dc) must result from differences in measurement temperature plus solvent preparation and purity.

The high values of "a" for cyclohexane and decalin reflect their behavior as thermodynamically good solvents. This is expected since the cohesive energy density parameter of polypropylene, cyclohexane and decalin are nearly identical. The lower value for K in decalin at 135° suggests the chain is somewhat smaller under these conditions as the polymer molecule would possess greater flexibility at the higher temperature.[14] Benzene is only a moderately good solvent for atactic polypropylene and dissolution is slow unless the sample is warmed.

The data in decalin confirm the work of Danusso[7] and Krigbaum[15] on atactic and isotactic polystyrene that the intrinsic viscosity–molecular weight relationships for the two conformations are identical in a thermodynamically good solvent. This is especially gratifying since the measure-

(14) See ref. 7, Chapter 14.

(15) W. R. Krigbaum, D. K. Carpenter and S. Newman, THIS JOURNAL, **62**, 1586 (1958).

ments with isotactic polystyrene were taken while the polymer was in a metastable condition with respect to crystallization from solution.

The molecular weight heterogeneity of the fractions as shown in column 3 of Table IV indicate a fairly narrow molecular weight distribution. There was no evidence from the fractionation or molecular weight data that either conformation of the polymer chain was highly branched.

The Second Virial Coefficients.—The dependence of the second virial coefficient A_2 on the conformation of the polymer chain recently has been confirmed by Krigbaum, Carpenter and Newman.[15] The work of these authors shows the second virial coefficient of the atactic polystyrene chain to be larger than an isotactic chain of identical molecular weight. They further propose that these data can be justified if the unperturbed dimensions ($\bar{L}_0^2/M$) of the isotactic polystyrene are larger than those of the atactic polymer.

In Fig. 4 our log A_2 values as measured both osmotically and by light scattering are plotted against log M. The slight dependence of A_2 on molecular weight noted in most other synthetic polymers is verified for polypropylene. The curves for 1-chloronaphthalene at 125° show a noticeable difference in slope for the atactic and isotactic polymer; however, the general scatter in the data which reflects the high temperature and general experimental problems associated with light scattering measurements on crystalline polymers does not justify further comment on the relative chain dimensions from these data. The postulation that the isotactic polymer may have large unperturbed dimensions implies that, (1) the theta or "Flory" temperature may differ from the atactic and (2) either the second coefficient or the θ temperature may ultimately reflect the degree of stereoregularity within the polymer chain. In a future paper we plan to discuss the results in thermodynamically poor solvents where segment–segment interactions are favored.

Size of the Polymer Chain.—The $\langle z \rangle$ average radius of gyration has been calculated from both Zimm plots (for the highest molecular weights) and by the dissymmetry technique. Table VI compiles this data where the $\langle z \rangle$ average radius of gyration is given in cm.

TABLE VI

Fract.[a]	$(\bar{R}_z^2)^{1/2}$ Zimm $\times 10^8$, cm.	$(\bar{R}_z^2)^{1/2}$ Dissy. $\times 10^8$, cm.	$\Phi \times 10^{-21}$ (av. value)
C′-2A	920	852	2.35
C′-2B	860	855	1.90
A-3	900	835	
A-4	520	485	2.1
C-2	...	452	
C-3	...	350	2.5

[a] Solvent is 1-chloronaphthalene at 125°.

The Zimm plots gave a somewhat larger radius of the polymer and for dimensions of chains this size little advantage was found in using this type of evaluation to determine the radius of the molecule. The dissymmetry method was simpler and gave radii which resulted in a calculated Φ value somewhat nearer the accepted value measured for other polymer–solvent systems. An especially large $\langle z \rangle$ average radius value was obtained for the atactic sample A-3 and the reason for this is unknown.

The data show some variation in the value of the universal hydrodynamic interaction parameter Φ; however, the average value corresponds to that measured in other systems.[12] Under these conditions, the distribution of segments about the center of gravity of the molecule appears to remain Gaussian whether the polymer is atactic or isotactic. There is no evidence that the isotactic polymer is assuming the shape of stiff rods but this does not mean that some extended segments in the chain may not already be in the helical conformation found in the crystalline state. The viscosity also shows no sign of an overt change near the precipitation temperature as has been observed for cellulose polymers near the critical miscibility temperature. A transition from a Gaussian distribution of segments to a stiff rod-like molecule for the cellulosics under these conditions has been proposed to account for the sizable increase in the viscosity of the polymer.[16]

(16) A. M. Holtzer, H. Benoit and P. Doty, THIS JOURNAL, **58**, 624, 635 (1954).

THE THERMAL TRANSITION OF RIBONUCLEASE IN UREA SOLUTIONS

BY JOHN G. FOSS AND JOHN A. SCHELLMAN

Department of Chemistry, University of Oregon, Eugene, Oregon

Received May 4, 1959

The temperature dependence of optical activity of ribonuclease has been measured in water and in several concentrated urea solutions. The observed features of the rotation–temperature curves are discussed qualitatively in terms of an "inverted transition" followed by a "normal transition." The importance of refractive index corrections in the interpretation of rotation data is demonstrated.

The heat and urea denaturations of proteins have been widely investigated as separate phenomena. If the hypothesis of Kauzmann is accepted[1] that in most cases the effect of urea or of high temperature is to destroy the stability of a hydrogen-bonded structure in favor of a flexible polypeptide chain, it must be concluded that the processes are closely related. In fact a qualitative description of denaturation in agreement with most facts can be obtained with the simple as-

(1) W. Kauzmann, "Mechanism of Enzyme Action," W. McElroy and B. Glass, Eds., John Hopkins Press, Baltimore, Md., 1954.

sumption that the hydrogen-bonded structures of most proteins have only a marginal stability because of the hydrogen bonding properties of water and that this slight stability can be destroyed either by heating or the addition of a more powerful breaker of hydrogen bonds, *e.g.*, urea, etc.[2] Investigations simultaneously involving denaturing agents and the variation of temperature are relatively rare in the literature, though the results are often intriguing. For example, Christensen found that β-lactoglobulin placed in concentrated urea solution at 0° undergoes a large change in optical rotation which is *reversed* by heating to 30°.[3] A similar effect is implied in the results of Simpson and Kauzmann[4] in their kinetic investigations of the urea denaturation of ovalbumin where an increase in temperature resulted in a partial reversion to a more folded form (indicated by a change in optical rotation). If it is admitted that the urea denaturation of proteins is a special case of the disruption of a hydrogen-bonded structure by a solvent component capable itself of forming strong hydrogen bonds, then related investigations may be found in the field of synthetic polypeptides. Bamford, Hanby and Happey[5,6] found that polypeptides which exist in the α-form in solvents such as $CHCl_3$, never do so in formic acid, which forms very strong hydrogen bonds. Subsequent work, involving a continuous transformation from one type solvent to another, has shown that the addition of formic acid in sufficient quantities converts the α-helix into a flexible polypeptide chain.[7] A very illuminating parallel to the work of Jacobsen and Christensen is to be found in the paper of Doty and Yang[8] in which the transition of the helix to a flexible chain is found to be inverted, *i.e.*, the helix is the high temperature form.

The present work is an attempt to investigate, rather more thoroughly than is usual, the combined effect of urea and high temperatures on a protein. Ribonuclease was chosen because of its stability as a chemical species. We avoid the frequent remark that ribonuclease has a high stability toward heat denaturation, since this and other investigations show that ribonuclease undergoes profound structural changes at about 60°. This protein maintains its structural integrity after exposure to denaturing conditions because of the reversibility of its transitions rather than from any inherent stability.

Experimental

Armour crystalline ribonuclease lot 81-059 was used for all of the experiments. A sample of the protein was dried to constant weight at 105° and found to contain 9.7% moisture. This figure was used for all of the calculations of specific rotations. When solutions were not made up in volumetric flasks the data of Gucker, Gage and Moser[9] for apparent molal volumes of urea were used to determine concentrations. For these calculations a value of 0.7 ml./g. was used for the specific volume of ribonuclease. The solvent for all of the protein solutions was 0.1 *M* potassium chloride. The urea was J. T. Baker C.P., recrystallized once from U.S.P. ethanol and dried at 45° in a vacuum oven.

A Rudolph precision polarimeter with a monochrometer, 1P28 photomultiplier and a rocking prism[10] was used for all of the measurements. The solutions used for the temperature measurements contained about 3% protein and measurements were made in a jacketed 1 dm. polarimeter tube. The urea-free solution had a *p*H of 4.8. When the dispersion measurements were made, this 1 dm. tube was not available so the 2 dm. tube was used with about half the protein concentration. One serious difficulty arises with the concentrated urea solutions that is not commonly observed with dilute aqueous solutions. When the temperature is changed there are marked fluctuations in the light coming through the polarimeter tube which make it impossible to measure the rotation. Normally in less than 10 min. after changing temperature rotations can be measured. These light fluctuations seem to result from refractive index gradients set up by temperature gradients. Since the polarimeter tubes used have glass linings the rate of heat transfer to the solution is slow, which means it may take some time to establish final temperature equilibrium. As would be expected, the light fluctuations are less marked in the 1 dm. tube. (Very recently some experiments have been performed in an all metal tube which clearly demonstrates its superiority to the glass-lined tubes in this respect.)

When this work was started the initial measurements were made visually using the 546 mμ mercury green line. Consequently when the careful photoelectric measurements were started we continued using this line. This does not permit direct comparison with other work done at the sodium-D line except at 25° where we also have dispersion data. However, since larger specific rotations normally are observed for proteins at shorter wave lengths, we feel the green line is preferable.

Results

The temperature *versus* rotation data are summarized in Fig. 1. Although these changes appear large in terms of specific rotations, the largest measured changes were of the order of half a degree.

Looking at the curves we observe these several features.

(A) A thermal transition, presumably an unfolding or swelling of some sort, is occurring as the solutions are heated. The transition temperature is lowered as more urea is added. (We will show the transition is complete at the maximum in the $-[\alpha]$ *vs.* T curves.)

(B) Below the minima large increases in levorotation occur on adding more urea.

(C) The changes in rotation on going through the thermal transitions decrease as more urea is added, except that the change in the 3.72 *M* solution is slightly larger than that for the zero molar solution This will be discussed below.

(D) Above the transition temperatures the slopes are parallel.

(E) Below the minima in the $-[\alpha]$ *vs.* T curves the slopes are steeper at higher urea concentrations.

Since we wish to discuss data in thermodynamic terms it is necessary that the thermal transitions be reversible or at least largely reversible. All of the data on the curves of Fig. 1 were taken as the temperature rose. Usually the temperature was

(2) W. H. Harrington and John A. Schellman, *Compt. rend. trav. lab. Carlsberg, Ser. chim.*, **30**, 21 (1956).

(3) L. K. Christensen, *ibid.*, **28**, 39 (1952).

(4) R. B. Simpson and W. Kauzmann, *J. Am. Chem. Soc.*, **75**, 5139 (1953).

(5) C. H. Bamford, W. E. Hanby and F. Happey, *Proc. Roy. Soc. (London)*, **A205**, 30 (1951).

(6) C. H. Bamford, A. Elliott and W. E. Hanby, "Synthetic Polypeptides," Academic Press, New York, N. Y., 1956.

(7) P. Doty, A. Holtzer, J. Bradbury and E. Blout, *J. Am. Chem. Soc.*, **76**, 4493 (1954).

(8) P. Doty and J. T. Yang, *ibid.*, **78**, 498 (1956).

(9) F. T. Gucker, F. W. Gage and C. E. Moser, *ibid.*, **60**, 2583 (1938).

(10) H. Rudolph, *J. Opt. Soc. Am.*, **45**, 50 (1955).

permitted to rise as rapidly as possible but occasionally the temperature would be fixed for intervals ranging from 15 minutes to an hour to see whether the rotations remained constant. In all cases they did.

On cooling rapidly the rotations generally did not return to their original values immediately. The slowness of the reversal is not surprising since there must be a large decrease in entropy in going from the unfolded states to the intermediate activated complexes. The most carefully studied case was in 6.79 *M* urea. Here the temperature was quickly changed from 50 to 20° by running tap water through the polarimeter tube jacket. The first measured rotation almost coincided with an extension of the high temperature slope of Fig. 1 to 20°. Apparently the protein was temporarily trapped in a thermodynamically unstable state. After 90 minutes the rotation was exactly that found on the way up. The 3.72 *M* urea solution was cooled rapidly from 70 to 20° and in 20 minutes the levorotation was +97° (about 77% reversed to its original value). With no urea the levorotation went to +93° (over 60% reversed) in 20 minutes on being cooled from 78 to 20°. All of this suggests that the reaction is probably almost completely reversible.

However, as with most protein kinetics, there are some interesting complications. For example, in the 3.72 *M* solution the rotation was within 23% of its value on the ascending curve after 20 minutes. No more measurements were made that evening but the next morning the levorotation had increased to about 125°. Furthermore, the apparently well behaved 6.79 *M* solution did not continue behaving. At the end of the 90 minute period mentioned above the solution was rapidly cooled to 6°. After 2 minutes the levorotation had changed from 114.0 to 118.8°. Nine minutes later it was at +117.5° and when left overnight at 6° it went to +113.4°.

We do regard these difficulties as important but the reactions apparently are largely reversible over a period of a few hours. So for simplicity we will neglect these peculiarities in most of our discussion.

The rotatory dispersions of the four solutions were measured. (Only four wave lengths were used: 546, 436, 365 and 313 mμ.) These data fitted a Heller plot[11] with values of 232, 234, 220 and 223 mμ for λ_c for the 0, 3.72, 6.79, and 7.75 molar solutions. Since the λ_c values were based on only four points and a line fitted visually they are not too accurate but they should be useful for extrapolations.

Discussion

In order to interpret the results in a reasonably simple way we have chosen to use a two state model, *i.e.*, the protein is either native or denatured. This is almost certainly an approximation since there will be a number of intermediate, partially unfolded molecules.[12,13] But this simple model is adequate to explain the observations of Fig. 1. We assume

$$[\alpha] = f_I[\alpha]_I + (1 - f_I)[\alpha]_E \qquad (1)$$

where f_I is the fraction of the protein molecules internally hydrogen bonded, *i.e.*, in the native state.[14] $[\alpha]_I$ and $[\alpha]_E$ are the specific rotations of the native and denatured states. The subscripts I and E represent the state of peptide hydrogen bonding, partially internal for native ribonuclease, according to current beliefs, mostly external for the denatured form. Rearranging the equation gives

$$f_I = \frac{[\alpha] - [\alpha]_E}{[\alpha]_I - [\alpha]_E}$$

which may be used to evaluate a thermodynamic variable f_I from the observed rotations. In order to do this we need to know the values of $[\alpha]_I$ and $[\alpha]_E$ as functions of temperature.

The protein will be most stable at low temperatures in the absence of urea. Looking at Fig. 1 it can be seen that from 5 to 32° the levorotation is approximately constant at 87.3°. This value will be used as the specific rotation of the native ribonuclease.

In the high temperature, high urea concentration region there is a striking similarity in the slopes which we attribute to the intrinsic temperature dependence of rotation for the denatured protein.

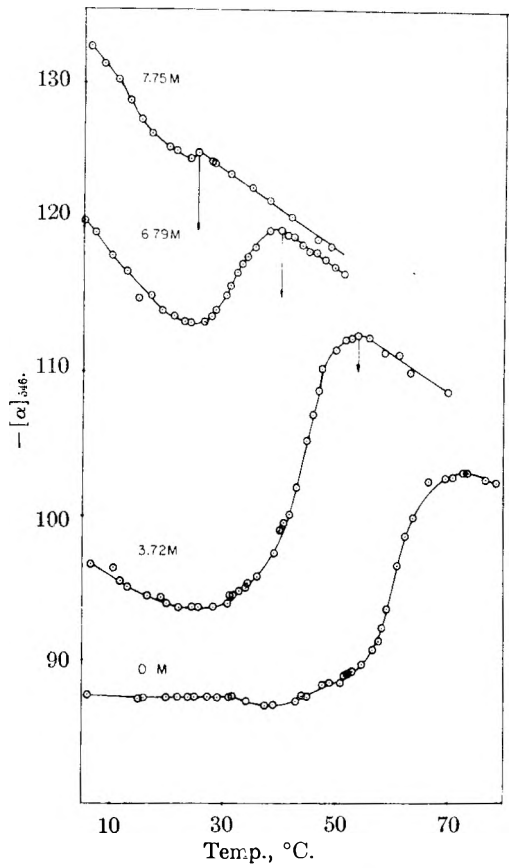

Fig. 1.—The temperature dependence of levorotation of ribonuclease. Refractive index corrections are indicated for three points by arrows.

(11) W. Heller, THIS JOURNAL, **62**, 1569 (1958).

(12) J. A. Schellman, *ibid.*, **62**, 1485 (1958).

(13) J. A. Schellman, *Compt. rend. trav. lab. Carlsberg, Ser. chim.*, **30**, 363 (1958).

(14) This is the equivalent of f_h used previously in a discussion of helices.

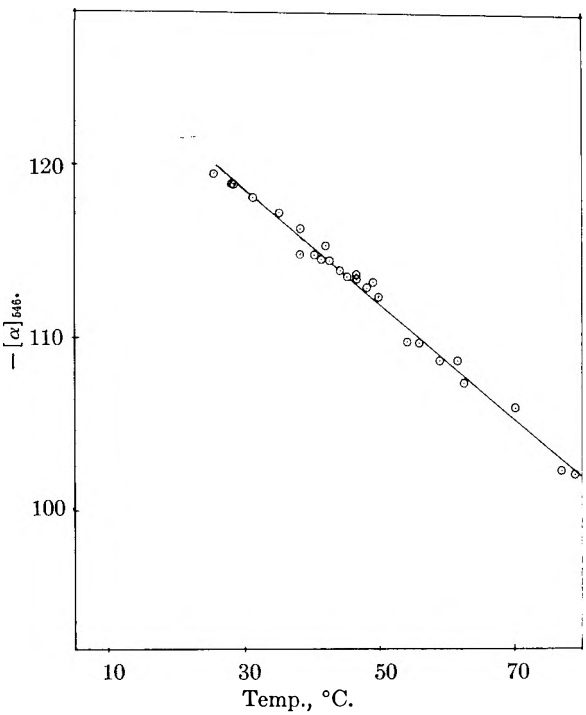

Fig. 2.—The temperature dependence of levorotation of denatured ribonuclease corrected for refractive index differences.

The upper slopes do not lie on a common line because the refractive index differences of the urea solutions give rise to differences in the absolute values of rotations. By multiplying each rotation by

$$\frac{n_w^2 + 2}{n_u^2 + 2}$$

(where n_w and n_u are the refractive indices of the water and urea solutions) we are effectively comparing the rotations of the denatured protein molecules when they are in water.[13] Figure 2 shows the slopes above the maxima corrected in this way. The straight line is given by $[\alpha]_E = -128.5 + 0.33T(°C.)$.

One important conclusion to be drawn from the continuity of this upper slope through a large range of temperatures and urea concentration is that the specific rotation of the denatured form is completely independent of the presence of urea. The urea serves only to destroy the internally hydrogen-bonded protein structure. Once the protein is unfolded it makes no difference in rotation whether few or many urea molecules are combined with it. Further evidence for the view that the upper slope represents the temperature dependence of rotation of a random polypeptide chain comes from a consideration of the rotation–temperature data already in the literature. Oxidized ribonuclease lacks the stabilizing influence of the four disulfide links in native ribonuclease and should behave as a random chain in water. Recently reported data for its temperature dependence[2] show a value of 0.25 between 20 and 30° compared to our value of 0.33 for denatured ribonuclease. Clupein in 0.1 *M* potassium chloride, chymotrypsinogen in 8 *M* urea and α-chymotrypsin in 8 *M* urea all have a similar temperature coefficient of rotation.[13] (All of these values were measured at the sodium-D line while our measurements were made at the 546 mμ mercury green line where the slopes will be about 20% greater. This difference may be calculated from a single Drude equation with the λ_c value given above of 223 mμ.)

Figure 3 shows f_I *versus* temperature (with refractive index corrections applied to all the urea values). The most interesting feature of these curves is that in the urea solutions f_I increases with temperature at low temperatures. This means that some of the denatured protein is being refolded as the temperature is increased! Since this behavior is contrary to that normally observed with proteins it has been termed an "inverted transition."[8] It can be seen in Fig. 3 that these inverted transitions are followed by "normal transitions" as the temperature is raised. We will now discuss qualitatively the reasons for this behavior in terms of a two state model.

When a protein is reversibly denatured we may represent the reaction occurring by

$$\text{P(folded)} \rightleftharpoons \text{P(unfolded)}$$

If there is only one solvent present, *e.g.*, water, what happens when this reaction takes place is that internal hydrogen bonds are replaced by external hydrogen bonds to water. This is, of course, a very crude picture which neglects, among other things, the possible effects of side chains, ionization, etc., on denaturation. The free energy of unfolding in pure solvent will be designated by $\Delta F_{unf}(s)$ and is given by

$$\Delta F_{unf}(s) = \Delta H_{unf}(s) - T\Delta S_{unf}(s)$$

It is known that for proteins $\Delta H_{unf}(s)$ is positive, *i.e.*, energy is required to break the internal bonds and replace them with water.[1] However, there is a large increase in entropy on unfolding so that as the temperature is raised this term will eventually predominate as in any typical endothermic reaction.

If a denaturing agent such as urea is present this unfolding can be followed by a second step

$$\text{P(unfolded)} + r\text{D} \rightleftharpoons \text{PD}_r\text{(unfolded)}$$

in which r denaturant molecules displace water and are adsorbed on some of the ν adsorption sites which were not available on the unfolded protein. Although we have written this as a simple combination of r denaturant molecules with each unfolded protein molecule, this only represents an average number. There can be from zero to ν denaturant molecules adsorbed on the unfolded protein molecules, assuming one denaturant per site. The free energy for this reaction depends on r. This dependence is stressed by designating the free energy of combination by $\Delta F_{comb}(r)$.

The over-all ΔF_{unf} will now be given by

$$\Delta F_{unf} = \Delta F_{unf}(s) + \Delta F_{comb}(r) \qquad (2)$$

This new ΔF_{unf} will differ from the original value in pure solvent for two reasons. If the denaturant is more strongly adsorbed than the water it will decrease the heat of the unfolding. On the other hand, whenever a denaturant is adsorbed from solution it loses a good deal of its freedom and therefore there will be a decrease in entropy favoring

the folded state. The balance among these two heats and two entropies is a delicate one. If our interpretation of the ribonuclease data is correct it is just this balance that leads to the inverted transition. Perhaps the simplest way to see this is to start with an approximate relationship of the form

$$\Delta F_{unf} = \Delta H_{unf}(s) + r\Delta\langle H\rangle - T(\Delta S_{unf}(s) + r\Delta\langle S\rangle)$$

where $\Delta\langle H\rangle$ and $\Delta\langle S\rangle$ are average values for the heats and entropies of urea binding. If we assume a linear decrease in r with temperature this leads to a quadratic with a maximum in ΔF_{unf}. It is this maximum that corresponds to the end of the inverted transition.

We have now explained the more important features of Fig. 1 in terms of an inverted transition followed by a normal transition for the urea solutions and a normal transition alone for the water solution. There are a few points mentioned above in the results not specifically covered as yet. At temperatures below the minimum in $-[\alpha]$ *vs.* temperature there are large changes in the levorotation since the ΔF_{unf} is made more negative by the adsorption of urea on the unfolded form. This increases the fraction of unfolded form present and therefore increases the levorotation just as in the usual urea denaturation studies made at constant temperature.

As we go to higher urea concentrations the fraction of native protein present at the end of the inverted transition decreases (see Fig. 3). Consequently there will be smaller *changes* in rotation when the normal transition occurs. (The different temperature dependences of rotation for the two protein states would lead to larger changes in rotation at low temperatures if the normal transition always started with the same fraction folded. There is a small increase in $\Delta[\alpha]$ on going from 0 to 3.72 *M* urea which apparently is caused by this intrinsic increase not being quite overcome by the decrease in the fraction of native protein present at the start of the normal transition.)

From Fig. 1 it can be seen that the low temperature slopes increase as more urea is added to the protein solutions. These slopes increase because of an increase in the fraction of unfolded molecules with their large $d[\alpha]/dt$ of 0.33. However, the slopes for the 6.79 and 7.75 *M* solutions are actually greater than 0.33, since there are also contributions from the inverted transition. From Fig. 3 and the temperature derivative of eq. 1 the relative contributions of these two effects can be calculated. At 10° in 3.72 *M* urea the inverted transition accounts for 80% of the slope but in the 7.75 *M* solution it contributes only 35%.

Thus far we have only been concerned with the qualitative aspects of the denaturation. However it is possible to obtain some quantitative information quite readily for the case of denaturation in water from the temperature dependence of f_I and

$$\ln K(s) = \ln \frac{1 - f_I}{f_I} = -\frac{\Delta H_{unf}(S)}{RT} + \frac{\Delta S_{unf}(S)}{R} \quad (3)$$

If a transition temperature is defined as that temperature when $K = 1$, a heat and entropy of unfolding at this temperature can be determined. From a graph of eq. 3 (which is quite linear in the vicinity of $K = 1$) we obtain

$$\Delta H_{unf}(s) = 76.5 \text{ kcal.}$$

and

$$\Delta S_{unf}(s) = \frac{76.5 \times 10^3}{335.2} = 228 \text{ e.u.}$$

No great accuracy is claimed for these numbers since very small experimental errors have a marked influence on them. In a private communication Tanford reports 95 kcal. and 285 e.u. for the same reaction at the same *p*H.

In order to obtain quantitative data relating the other parameters used in the discussion (*viz.*, $\Delta\langle H\rangle$, $\Delta\langle S\rangle$ and ν) it is necessary to have an explicit form for eq. 2. Recently a number of authors have presented theoretical discussions of this very point.[12,15,16] However, at present we will not attempt to fit our data to the equations derived.

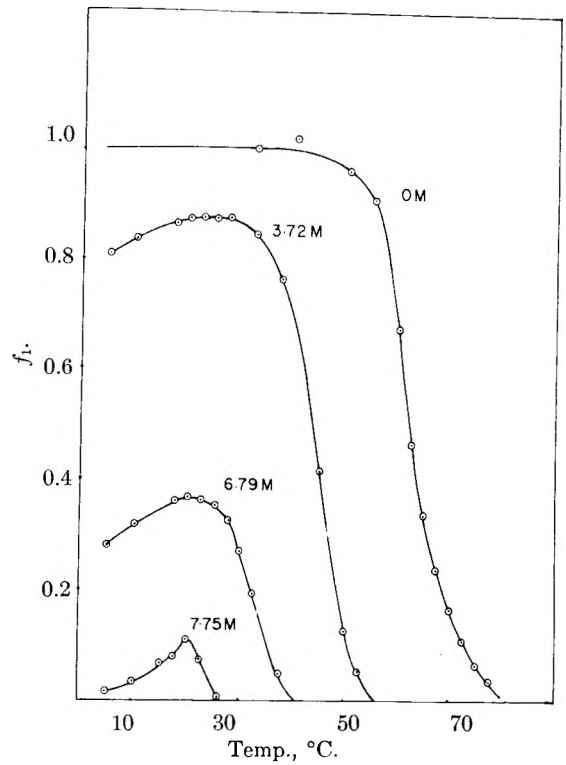

Fig. 3.—The fraction of internally hydrogen-bonded ribonuclease as a function of temperature.

Conclusions

We believe that our data show quite clearly that in a mixed solvent inverted transitions can occur in proteins. Doty and Yang were probably the first to recognize the occurrence of such transitions in a synthetic polypeptide of γ-benzyl-L-glutamic acid dissolved in an ethylene dichloride–dichloroacetic acid mixture. Since such polypeptides should be good model compounds for proteins it is not surprising that inverted transitions occur with them also. In fact this study was initiated in

(15) J. A. Schellman, *Compt. rend. trav. lab. Carlsberg, Ser. chim.*, **29**, 223 (1955).

(16) J. H. Gibbs and E. A. DiMarzio, *J. Chem. Phys.*, **30**, 271 (1959).

an attempt to find such a transition after Doty and Yang's results were first reported.

One of the differences between our results and theirs is that with ribonuclease the inverted transition is followed by a normal transition. In retrospect it now seems quite clear that all inverted transitions must be followed by a normal transition if the temperature is raised sufficiently. This is implicit in Doty and Yang's discussion of inverted transitions and is stated quite explicitly by Gibbs and DiMarzio. We are currently studying the temperature dependence of rotation and viscosity for lysozyme to see whether its behavior parallels that of ribonuclease in this respect.

If we now examine the data of L. K. Christensen[3] mentioned in the Introduction it is apparent that it can also be interpreted as the result of an inverted transition. One of the main differences between ribonuclease and lactoglobulin is that the latter exhibits irreversible effects more quickly. Christensen found that lactoglobulin in 38% urea underwent a slow change in rotation at 30°. The levorotation at the sodium-D line went from approximately 40 to 63° in six hours. Twice during this interval the solution was rapidly cooled to 10° and an increase was observed in levorotation. This brought its value to coincidence with a curve of a rotation–time experiment carried out at 10°. In terms of our Fig. 1 this would indicate that the 30° measurements were made near one of the minima. On cooling, an inverted transition occurred and levorotation increased as more denatured protein appeared. (Jacobsen and Christensen[17] have reported parallel measurements in which solubility changes were used as a criterion for denaturation. The results were essentially the same.)

Simpson and Kauzmann have reported an extensive series of measurements on the kinetics of the urea denaturation of ovalbumin.[4] This protein also appears to exhibit an inverted transition since heating an 8.3 *M* urea solution of ovalbumin from 0 to 30° causes a decrease in the levorotation. It should be emphasized that our results and interpretations are thermodynamic and not offered as an explanation of kinetic data. However it seems very probable that there is a connection between the maxima in our Fig. 3 and minima found by Simpson and Kauzmann in their rate–temperature data for ovalbumin (see their Fig. 4); but we will not attempt to interpret this point at present.

We have pointed out already that the data presented for ribonuclease, plus what published data are available, suggest that the observed marked temperature dependence of rotation for the unfolded protein may be generally true. In addition, the rules of Kauzmann and Eyring[18] also point to a larger temperature dependence of rotation for the unfolded compared to the folded form. (Briefly, these rules state that raising the temperature permits greater rotation about the bonds involved in optical activity which decreases their average asymmetry and therefore their contribution to the activity. The temperature effect on ring structures will be less marked since the rotation is more restricted. These rules have been shown to hold for a great many smaller molecules.) This temperature dependence is worth emphasizing since being unaware of it can lead to the erroneous interpretation of rotation data. An example of what we believe to be such an erroneous interpretation has just been published[16] in a discussion of Doty and Yang's data for poly-γ-benzyl-L-glutamate. As already mentioned, this polypeptide undergoes an inverted transition similar to that reported in this paper. However, they did not go to high enough temperatures to observe the normal transition and the large temperature of rotation for the unfolded polypeptide which we believe follows. If this prediction is correct then the values for the fraction of polypeptide folded as a function of temperature calculated by Gibbs and DiMarzio would be very badly in error. However, in this case they were only interested in showing that an explicit form of our eq. 2 could be made to fit a set of experimental data using reasonable parameters and this calculation is a minor point in their paper.

Finally, we would like to emphasize the potential importance of refractive index corrections for such studies. Figures 1 and 2 show that applying such corrections can largely eliminate solvent effects and thus permit legitimate comparison of rotations in different solvents. Unfortunately, refractometers for the ultraviolet are not commonly available at present.

Acknowledgment.—The authors wish to acknowledge the generous financial support of the National Institutes of Health.

(17) C. F. Jacobsen and L. K. Christensen, *Nature*, **161**, 30 (1948).

(18) W. Kauzmann and H. Eyring, *J. Chem. Phys.*, **9**, 41 (1941).

OXYGEN SORPTION AND ELECTRICAL CONDUCTIVITY OF COPPER OXIDE FILMS

BY A. W. SMITH AND H. WIEDER

Contribution from the Research Laboratories, National Carbon Company, Division of Union Carbide Corporation, Cleveland, Ohio

Received May 21, 1959

An experimental apparatus has been constructed that allows the simultaneous measurement of the electrical conductance of thin films and the uptake of gases by these films. This apparatus has been used to study the kinetics of oxygen uptake by copper oxide films and the effect of this uptake on the electrical conductance of the film. The results obtained show that the rate of oxygen uptake depends on the conductance of the film, that the relationship between conductance and gas uptake is not simple and that an incorporation step, which is not apparent from gas uptake measurements alone, can be followed by conductance changes.

I. Introduction

The measurement of the electrical conductance of solid films during sorption reactions is a means of obtaining information about the "electronic factor" in chemisorption and catalysis. The importance of the work discussed here is that gas uptake as well as conductivity was measured. In previous kinetic work of this sort, only conductivity was reported.[1,2] The measurement of both these parameters not only adds new information for the study of reaction kinetics but also provides data for the determination of charge transfer effects on semiconductor surfaces.

This paper is an initial report of a study being made on this subject and is concerned principally with experimental techniques and experimental results.

II. Experimental Methods

1. **Vacuum System.**—The vacuum and gas handling system is of the ultrahigh vacuum type. A three-stage oil diffusion pump is used. The valves are either all metal or metal bodies with Teflon seats and gaskets. The part of the system containing the film tube and Pirani gauges can be baked out at 450° and pressures much less than 10^{-8} mm. can be attained. During the experiments reported here, there was no baking out, but pressures of $1\text{–}3 \times 10^{-8}$ mm. were attained regularly. Because of the Teflon gaskets, the gas handling part of the system could not be heated above 100–125° and this part was limited to pressures of 10^{-7} mm.

2. **Pirani Gauge.**—An important part of this experiment was the development of a vacuum gauge capable of measuring pressures accurately over a wide pressure region. This gauge is described elsewhere.[3] It is sufficient to say here that the accuracy of our data was in no case limited by the vacuum gauge. The actual variations in pressure due to temperature fluctuation of other parts of the system were always greater than the uncertainty in the pressure measurements. For example, fluctuations in pressure due to cycling of the room air conditioner were easily visible even though this effect was less than 0.1%.

3. **Film Preparation and Measurement.**—The film tube consists of a Pyrex tube, 51 mm. in diameter and 300 mm. long, which is sealed at one end with four tungsten leads and connected to the vacuum system at the other end with 10 mm. tubing. Four thin strips of platinum on the inside walls of the tube are used as contacts for the conductance measurements. These strips are 2 mm. wide and 5 mm. apart, extend almost the length of the tube and make contact to specially prepared tungsten-to-glass seals.[4] The platinum strips are prepared by painting on "Liquid Bright Platinum" and heating to obtain a thin uniform layer of the metal.

Copper was plated onto a molybdenum filament from an acid sulfate bath prepared with reagent grade chemicals. The filament was mounted along the axis of the film tube and the copper was evaporated over the cylindrical surface of the tube, as well as over the platinum strip. Evaporation was carried out in an auxiliary vacuum system, the filament then being removed and the tube sealed onto the primary system.

The film tube is surrounded by a closely fitting aluminum block, 5 inches in outside diameter. The block is first wrapped with asbestos, then provided with Nichrome heating wires and finally covered with a 2-inch layer of insulating material. The furnace is on a track and may be raised or lowered from the tube as desired. The temperature of the block is controlled by a variable transformer in series with a constant voltage transformer and it can be varied from room temperature to 500°.

During the experiment, the temperature of the film was monitored by a 10-junction thermopile; the hot junctions were buried in the aluminum block and the cold junctions were immersed in an ice-bath. Most of the e.m.f. of the thermopile was bucked out by a potentiometer, the difference being registered on a 10 mv. recorder. With this apparatus, the temperature can be read to ±0.1°. It was generally held constant within 0.2° during a run. A timing mechanism attached to the furnace allowed the film to reach operating temperature by morning after an overnight bake-out.

The conductance of the film was measured by applying a current between the two outer platinum strips and measuring the voltage across the inner two. The film voltage and the Pirani voltage were recorded simultaneously on a two-pen recorder. The film current, which changed slightly during a run, was measured periodically.[5]

The film contained 23 μg. of copper per cm.^{2} which implies a thickness of Cu_2O of about 5×10^{-6} cm. using the bulk density. The voltage probes were 0.5 cm. apart and 25 cm. long. The conductivity is thus on the order of 4×10^3 times the conductance. Because of the uncertainty in the exact film thickness, only the conductance values are presented in the results.

4. **Sorption and Desorption Measurements.**—Gas used for sorption was obtained by purifying ordinary tank oxygen in the following way: After the gas lines were flushed, oxygen was condensed in a liquid nitrogen trap, warmed until part of it filled the gas-handling system and then this was pumped out. This procedure was repeated several times and finally the gas was retained in the system for later use.

During sorption measurements, a small amount of oxygen was allowed to leak into the section containing the Pirani gauge. This section will be referred to as the gauge section. The gas was then allowed to expand into the previously evacuated film tube section and its pressure was continuously followed on a recorder. In the constant pressure runs, the valve to the gas-handling system was repeatedly adjusted to maintain constant pressure in the tube.

The amount of sorption Δp reported in the Experimental Results section of this paper, is simply the change in pressure measured by the Pirani gauge in a constant volume system. The major error in these values (except

(1) W. E. Garner, T. J. Gray and F. S. Stone, *Disc. Faraday Soc.*, **8**, 246 (1950).

(2) V. I. Lyashenko and I. I. Stepko, *Zhur. Fiz. Khim.*, **31**, 1825 (1957).

(3) A. W. Smith, *Rev. Sci. Instr.*, **30**, 485 (1959).

(4) H. Wieder and A. W. Smith, *ibid.*, **29**, 794 (1958).

(5) We thank P. C. Claspy for early work on the conductance measurements.

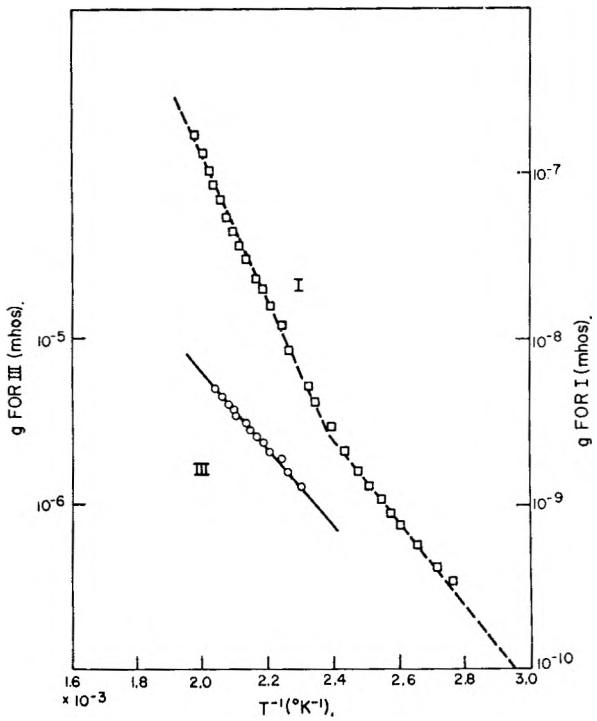

Fig. 1.—Temperature dependence of electrical conductance.

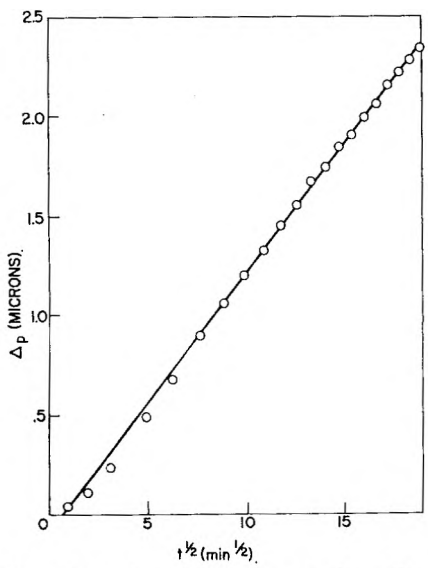

Fig. 2.—Time dependence of oxygen uptake; film in State III.

for uncertainty in pressure differences when very small amounts were sorbed) is due to the temperature difference in the two parts of the system. The temperature difference can be used to calculate gas concentration differences in the two parts of the system. Also, thermomolecular flow effects are important in this pressure region. Corrections for thermomolecular flow were computed for a large number of temperatures and pressures using the equation given by Porter.[6,7] Both this correction and the normal gas concentration correction were applied in several cases and the effect was shown to be small. For this reason, the results to be presented here do not include these corrections except in the calculation of desorption. Systematic errors of a few per cent. can arise from this source but they are not large enough to affect the interpretation in any way.

(6) A. S. Porter, *Disc. Faraday Soc.*, **8**, 358 (1950).

(7) For this computation, we thank J. W. McClure and L. B. Smith of these Laboratories.

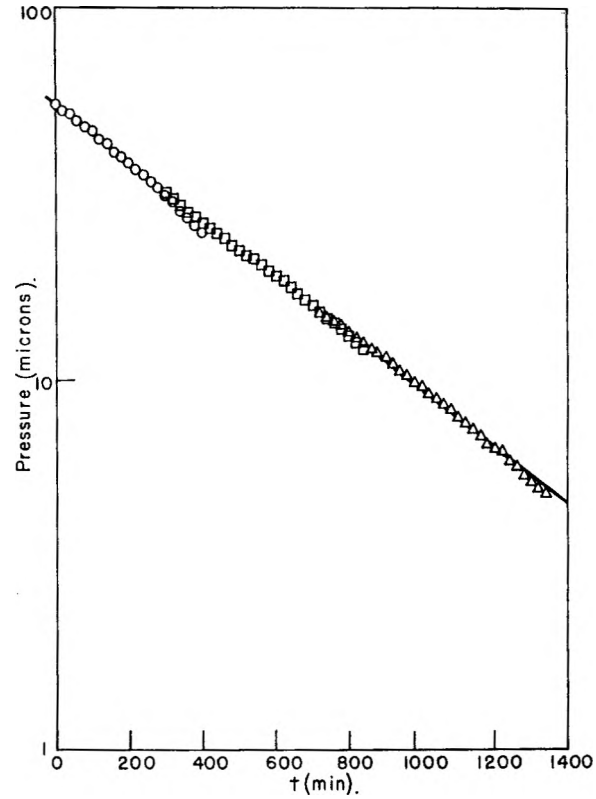

Fig. 3.—Time dependence of oxygen uptake; film in State I; three separate runs.

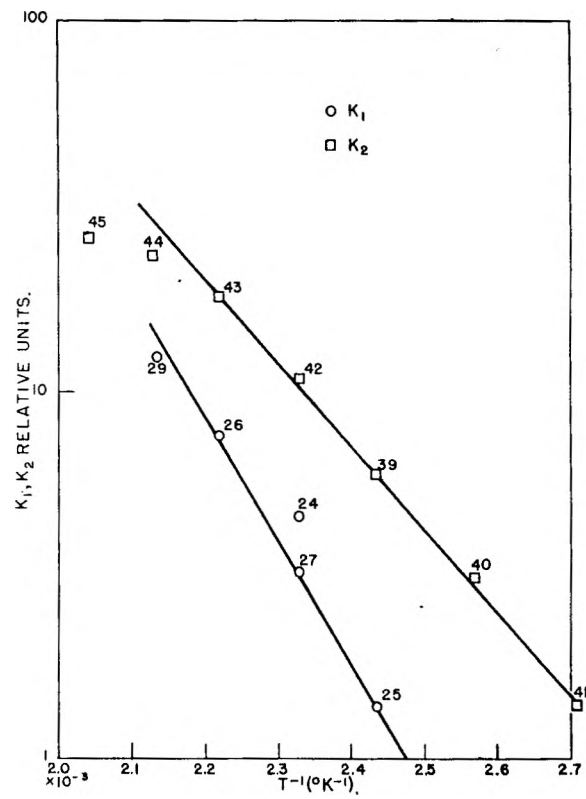

Fig. 4.—Temperature dependence of rate constants: K_1 is rate constant for State III, K_2 is rate constant for State I. The numbers indicate runs.

Desorption measurements were made by expanding the gas from the film tube into the gauge section, measuring the

new over-all pressure, and then pumping out just the gauge section, the cycles continuing until the pressure was too low to be measured.

III. Experimental Results

The copper oxide films are light yellow when first oxidized, becoming darker with further oxidation and ultimately reaching a dark brown color. Reduced to their lowest conductivity using hydrogen at 200°, the films have a reddish cast. In terms of sorption and conductance behavior, we can distinguish four states. In the reduced state (State I), there is rapid sorption of oxygen accompanied by negligible conductance change. After some oxygen is incorporated into the film, State II is reached, at which point rapid oxygen sorption is now accompanied by a definite conductance change, the two being related almost parabolically. With further incorporation of oxygen, State III is reached, as determined by the nearly linear relationship between sorption and conductance. State IV, which appears after strong oxidation, shows negligible oxygen sorption and conductance change, while for the first time permitting rapid hydrogen sorption.

In passing from the reduced state to the oxidized state, the electrical conductance changes in a way typical of polycrystalline oxides, which is described by Meyer's rule.[8] This states that the increased conductivity upon departure from stoichiometry is due largely to a decrease in the exponential temperature factor, the activation energy for conduction. For the copper oxide film, the conduction in all cases was *p*-type, determined both by the sign of the conductance change during sorption of oxygen or hydrogen and in a few cases by the sign of the thermoelectric power.

The results to be presented here refer to one film in States I, II and III. The electrical conductance measured in States I and III is plotted logarithmically *versus* the reciprocal temperature in Fig. 1. Activation energies for conduction determined from the slopes of these lines yield values of 0.87 and 0.50 e.v. for State I and 0.45 e.v. for State III. Results for other films indicate that the break in the curve for State I is atypical.

The kinetics of the uptake of oxygen on copper oxides has been studied by the Bristol workers.[9] Both a Langmuir type adsorption curve and an Elovich (also called Rojinski–Zeldowich) type curve have been used. In some cases an Elovich type plot fits our data, but a better and less arbitrary fit is a simple parabolic curve for State III and a simple first-order curve of logarithm pressure *versus* time for State I. These curves are shown in Figs. 2 and 3. The small amount of scatter to these points shows the accuracy of the pressure measurements. An attempt has been made to relate the experimental kinetics to a reaction mechanism. This problem will be discussed in a later communication, since these data alone do not establish an unequivocal mechanism. Since surface areas were measured only on subsequent films, one can only estimate that in the present case the largest uptake of oxygen during a run corresponded to less than 0.2 monolayer.

(8) W. Meyer and H. Neldel, *Z. Tech. Phys.*, **18**, 588 (1937).

(9) T. J. Jennings and F. S. Stone, *Adv. in Catalysis*, **9**, 441 (1957).

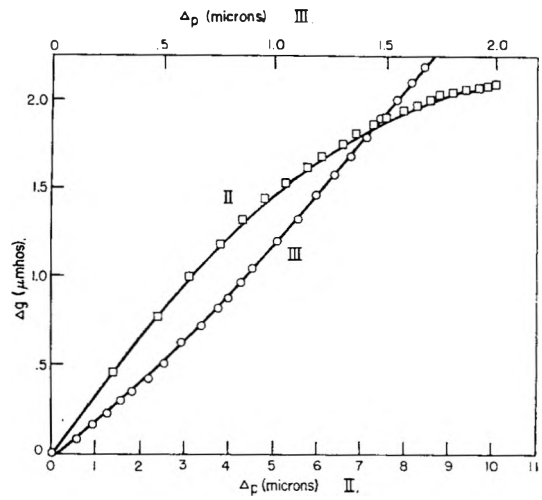

Fig. 5.—Conductance change *versus* gas uptake.

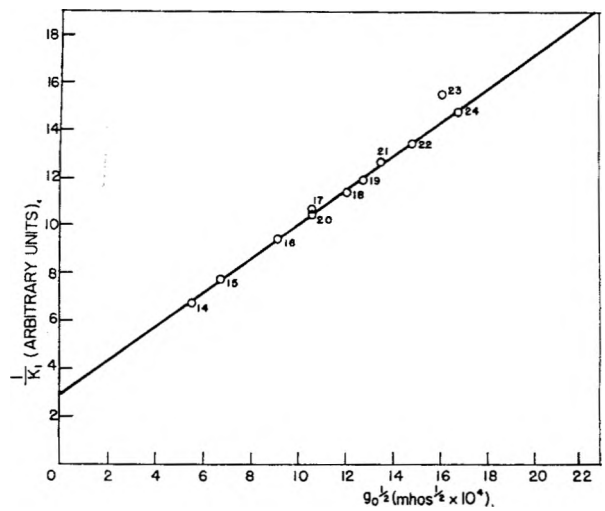

Fig. 6.—Variation of rate constant with initial conductance; film in State III; the numbers indicate the runs.

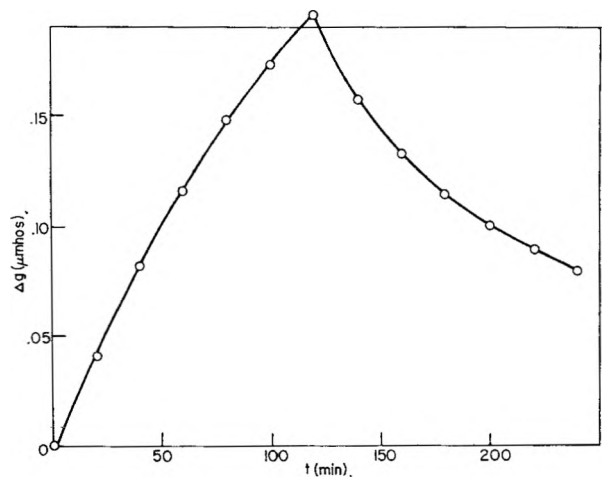

Fig. 7.—Conductance change during sorption and incorporation.

Data of the type shown in Figs. 2 and 3 have been recorded at a number of temperatures and the resultant curves are used to obtain rate constants from which activation energies may be calculated. The plots of the logarithm of the rate constants

K_1 and K_2 *versus* reciprocal temperature, shown in Fig. 4, yield activation energies for sorption of 10 and 16 kcal. for States I and III, respectively. This does not imply that only one activation energy would be found in each state; more likely the activation energy increases continuously as oxygen is incorporated. Jennings and Stone found an activation energy of 7 kcal. for cuprous oxide on copper metal.[9]

The electrical conductance may be plotted against time or against gas uptake. Figure 5 shows typical plots of the conductance change *versus* the gas uptake. In State II, this is more or less parabolic while the data for State III can be fit by a more complex function. The most important point is that the conductance change is not directly proportional to the gas uptake, the shape of the curve depending strongly on the state of the film.

Many measurements were made to show that the rate of oxygen sorption depends on the stoichiometry of the film as determined by the conductance. Figure 6 shows how the rate constant in State III varies with the conductance at the beginning of a sorption run. Since each run followed an overnight bakeout in vacuum, the initial conductance is due to changes in the bulk stoichiometry rather than being just a surface effect. The good fit of the data as shown in Fig. 6 is typical of these results.

An interesting and unexpected consequence of these measurements was the conductance change observed at the end of a run when the oxygen was pumped out of the system. The conductance change at that point reversed direction and started to decrease. This effect is shown in Fig. 7. In one run, the desorption was followed carefully. In six hours the conductance decrease was 75% of the original increase while only 5% of the adsorbed gas was desorbed. This behavior was noticed particularly in State II. In State III, there was little change in conductance on pumping out the oxygen. This effect can only be explained by some incorporation process in which the oxygen is presumably diffusing into the film.

Adsorption–incorporation runs similar to those shown in Fig. 7 were made for varying durations of sorption. The effect was present even for very short times. This shows that adsorption and incorporation occur simultaneously even at very low coverages. Thus the conductance change normally measured is a result of both adsorption and incorporation.

IV. Conclusions

The results presented here show the interesting possibilities resulting from the measurement of the electrical conductance simultaneously with the usual reaction kinetics. While these results cannot be applied rigorously to any theory, due to uncertainties in such factors as electron mobility and film porosity, they do show the role of the electronic factor in chemisorption. With further knowledge of these presently uncertain factors, the results can be used in a quantitative way.

The results do show that measurements of conductance alone cannot be used for kinetic expressions based on an assumed relation of conductance change to gas uptake since different relations are obtained for even one sample under different oxidation conditions. On the other hand, measurement of gas uptake alone will not reveal the presence or extent of electronic interactions.

The significant decrease in conductance without a correspondingly significant desorption during oxygen pump-out shows the presence of an additional, incorporation step in the gas uptake. It also shows the need for both measurements in correctly distinguishing between desorption and incorporation.

KINETICS OF BROMINE ADDITION TO SOME UNSATURATED SULFONES

BY V. BALIAH AND SP. SHANMUGANATHAN

Department of Chemistry, Annamalai University, Annamalainagar, Madras State, India

Received May 25, 1959

The kinetics of bromine addition to α,β- and β,γ-unsaturated sulfones in carbon tetrachloride at 30° has been studied. It is found to be approximately second order. α,β-Unsaturated sulfones add bromine at a slightly lower rate than β,γ-unsaturated sulfones. There is no evidence of any significant conjugation between the sulfonyl and ethenyl groups in α,β-unsaturated sulfones in the ground state. The data obtained can be interpreted on the basis of the inductive effect of the sulfonyl group.

Introduction

Sudborough and Gittins,[1] from a study of rates of esterification of α,β-unsaturated acids, showed that conjugation of a carboxyl group with an ethylenic linkage decreases the reactivity of the carboxyl group. Similarly the effect of conjugation with a carboxyl group on the reactivity of an ethylenic linkage was established by the determination of the rates of addition of bromine to unsaturated acids; α,β-unsaturated acids add bromine at a much lower rate than β,γ- or γ,δ-unsaturated acids.[2] Furthermore, the addition of hypochlorous acid to ethylenic double bonds is also much retarded if the double bonds are conjugated with the carboxyl group.[3–6]

(1) J. J. Sudborough and J. M. Gittins, *J. Chem. Soc.*; **95**, 315 (1909).

(2) J. J. Sudborough and J. Thomas, *ibid.*, **97**, 715, 2450 (1910).

(3) G. F. Bloomfield, E. H. Farmer and C. G. B. Hose, *ibid.*, 800 (1933).

The present investigation deals with the rates of addition of bromine to some α,β- and β,γ-unsaturated sulfones in carbon tetrachloride solution at 30°. It was thought that a comparison of these rates would reveal whether there is effective conjugation or not between the sulfonyl group and ethylenic double bonds in α,β-unsaturated sulfones.

Experimental

Materials.—Methyl vinyl sulfone was prepared according to the method of Buckley, Charlish and Rose[6]; allyl methyl sulfone was obtained according to the method of Price and Gillis[7]; the procedure of Smith and Davis[8] was employed for the preparation of phenyl vinyl sulfone and *p*-tolyl vinyl sulfone. Allyl phenyl sulfone and allyl *p*-tolyl sulfone were prepared according to the method of Otto.[9] The method of Balasubramanian, Baliah and Rangarajan[10] was used for the preparation of methyl styryl sulfone; phenyl styryl sulfone and styryl *p*-tolyl sulfone were obtained following the method of Balasubramanian and Baliah.[11] Cinnamyl phenyl sulfone, cinnamyl *p*-tolyl sulfone and cinnamyl methyl sulfone were obtained as already reported.[12]

Purification of Carbon Tetrachloride.—B.D.H. "Analar" carbon tetrachloride was shaken with 5% sodium hydroxide solution, then with 5% hydrochloric acid solution, washed several times with water and dried over fused calcium chloride for a day. It was thendistilled over phosphorus pentoxide, the distillation unit being provided with a calcium chloride guard-tube. Only the middle portion of the distillate was employed.

Purification of Bromine.—About 150 ml. of analytical grade bromine was shaken thrice with an equal volume of sulfuric acid, the bromine layer separated and frozen in a bath of ice and calcium chloride. When the bromine had completely solidified, it was taken out of the bath and partly melted. The supernatant liquid was decanted off and the rest of the solid bromine was allowed to melt completely. The liquid was once again frozen and the procedure repeated several times till about 50 g. of bromine freezing at −6 to −7° was obtained.

Measurement of Reaction Rate.—The general method of procedure was to prepare carbon tetrachloride solutions of the unsaturated sulfones and of bromine of the same concentration ($^1/_{30}$th or $^1/_{60}$th of the gram-molecular weight per liter of the solution, depending upon the solubility of the unsaturated sulfone in carbon tetrachloride). The bromine solution was standardized by means of sodium thiosulfate, potassium iodide and starch in the usual manner. One hundred ml. of each solution was placed in a ground-glass stoppered conical flask. The two solutions were placed in a thermostat regulated to 30 ± 0.1°. After the attainment of thermal equilibrium, the bromine solution was run into the solution of the unsaturated sulfone and when about half the bromine solution had been run, a stop-watch was started. The mixture was swirled gently to ensure complete mixing. At suitable intervals, 10 ml. of the mixture was withdrawn and run into a conical flask containing a solution of a slight excess of potassium iodide to arrest the reaction. It then was titrated immediately against $M/30$ or $M/60$ sodium thiosulfate solution using starch as indicator. The solutions of sodium thiosulfate, potassium iodide and starch were prepared in water from which carbon dioxide had been expelled.

Since the sulfone and bromine are both at the same concentration, the second-order rate constant k is given by the expression

$$k = \frac{1}{ta} \times \frac{x}{a - x}$$

where t is the time in minutes, a is the initial titer value (for zero time) expressed in mole/l. and $(a - x)$ is the titer value after time t. The average deviation in the value of the rate constant between duplicate determinations did not exceed 2%.

Trial runs with styryl *p*-tolyl sulfone and cinnamyl *p*-tolyl sulfone at both $M/30$ and $M/60$ concentrations of bromine and the sulfone indicated the rate constant to be independent of concentration. In the case of other sulfones either $M/30$ or $M/60$ solutions only were employed.

Results and Discussion

The bimolecular rate constants and the $k_{\beta,\gamma}/k_{\alpha,\beta}$ ratios are given in Table I.

TABLE I

RATE CONSTANTS FOR THE BROMINE ADDITION

Sulfone	$k \times 10^3$ (mole/l.)$^{-1}$ sec.$^{-1}$	$k_{\beta,\gamma}/k_{\alpha,\beta}$
$CH_3SO_2CH{=}CH_2$	6.1	4.42
$CH_3SO_2CH_2CH{=}CH_2$	27.0	
$C_6H_5SO_2CH{=}CH_2$	6.5	1.28
$C_6H_5O_2CH_2CH{=}CH_2$	8.3	
p-$CH_3C_6H_4SO_2CH{=}CH_2$	6.8	1.24
p-$CH_3C_6H_4SO_2CH_2CH{=}CH_2$	8.4	
$CH_3SO_2CH{=}CHC_6H_5$[a]	14.4	2.98
$CH_3SO_2CH_2CH{=}CHC_6H_5$[a]	42.9	
$C_6H_5SO_2CH{=}CHC_6H_5$[a]	3.3	1.63
$C_6H_5SO_2CH_2CH{=}CHC_6H_5$[a]	5.4	
p-$CH_3C_6H_4SO_2CH{=}CHC_6H_5$[a]	3.5	1.54
p-$CH_3C_6H_4SO_2CH_2CH{=}CHC_6H_5$[a]	5.4	

[a] *trans*-Isomer.[13]

It is seen that bromine adds to a β,γ-unsaturated sulfone only at a slightly faster rate than to an α,β-unsaturated sulfone. This is in marked contrast to what is observed in the case of β,γ- and α,β-unsaturated acids.[2] Thus there is no evidence of any significant conjugation of the sulfonyl group with the ethylenic link in the ground state of α,β-unsaturated sulfones. A similar conclusion was arrived at by earlier workers.[14,15] The slight increase in the value of $k_{\beta,\gamma}$ over $k_{\alpha,\beta}$ can be attributed to the weaker inductive influence of the sulfonyl group on the ethylenic bond in β,γ-unsaturated sulfones due to the intervening methylenic group.

It is significant to note that the sulfonyl group retards bromine addition more powerfully than the nitro group[14,16] in spite of the fact that the nitro group is a more "acidifying" substituent than the sulfonyl group.[17] This remarkable retarding influence of the sulfonyl group toward bromine addition may be explained by the high positive charge that the sulfur atom bears if the sulfur–oxygen bond is formulated as semi-polar.[18] The electrophilic attack will be inhibited by the positive sulfur.

The influence of structure on the rate of bromine addition is also interesting to note (Table I). The *p*-tolyl sulfones have slightly higher rates than the

(4) E. H. Farmer and C. G. B. Hose, *J. Chem. Soc.*, 962 (1933).
(5) G. F. Bloomfield and E. H. Farmer, *ibid.*, 2062, 2072 (1932).
(6) G. D. Buckley, J. L. Charlish and J. D. Rose, *ibid.* 1514 (1947).
(7) C. C. Price and R. G. Gillis, *J. Am. Chem. Soc.*, **75**, 4750 (1953).
(8) L. I. Smith and H. R. Davis, *J. Org. Chem.*, **15**, 824 (1950).
(9) R. Otto, *Ann.*, **283**, 181 (1894).
(10) M. Balasubramanian, V. Baliah and T. Rangarajan, *J. Chem. Soc.*, 3296 (1955).
(11) M. Balasubramanian and V. Baliah, *ibid.*, 1844 (1954).
(12) V. Baliah and Sp. Shanmuganathan, *J. Indian Chem. Soc.*, **35**, 31 (1958).
(13) V. Baliah and M. Seshapathirao, unpublished work.
(14) I. R. C. McDonald, E. M. Milburn and P. W. Robertson, *J. Chem. Soc.*, 2836 (1950).
(15) P. B. D. de la Mare and P. W. Robertson, *ibid.*, 2838 (1950).
(16) P. B. D. de la Mare, *Ann. Reports*, **47**, 127 (1950).
(17) W. Hückel, "Theoretical Principles of Organic Chemistry," Vol. I, Elsevier, New York, N. Y., 1955, p. 337.
(18) V. Baliah and Sp. Shanmuganathan, THIS JOURNAL, **62**, 255 (1958).

corresponding phenyl sulfones. The tolyl group is slightly more electron-releasing than the phenyl group. Thus the positive charge on sulfur is slightly less when the sulfonyl group is attached to *p*-tolyl than when it is attached to phenyl. Therefore the phenylsulfonyl group exerts relatively greater inductive effect on the ethylenic link than *p*-toluenesulfonyl.

Bromine adds to $CH_3SO_2CH{=}CHC_6H_5$ at a significantly faster rate than to $CH_3SO_2CH{=}CH_2$. Thus the nature of R in $CH_3SO_2CH{=}CHR$ influences the rate considerably. This effect of R is undoubtedly polar because phenyl group, which increases the electron accessibility on the ethylenic bond, causes an increase in the rate.

A careful examination of the rates of bromine addition to the various unsaturated sulfones listed in Table I reveals that steric effects also control the bromine addition. The rates of addition to $CH_3SO_2CH{=}CH_2$, $C_6H_5SO_2CH{=}CH_2$ and p-$CH_3C_6H_4SO_2CH{=}CH_2$ do not differ much, indicating that the nature of R in $RSO_2CH{=}CH_2$ does not have much effect on the rate. The same is not true of R in $RSO_2CH{=}CHC_6H_5$ because the rate of addition to $CH_3SO_2CH{=}CHC_6H_5$ is strikingly greater than that to $C_6H_5SO_2CH{=}CHC_6H_5$ and p-$CH_3C_6H_4SO_2CH{=}CHC_6H_5$. This is presumably a steric effect. Scale models of methyl styryl sulfone and phenyl styryl sulfone reveal that the two stages of bromine addition, electrophilic and nucleophilic, involved in the bromide formation are inhibited in phenyl styryl sulfone by the shielding phenyl group. A cyclic intermediate does not seem to be involved in the addition. This is to be inferred from the fact that bromine addition to methyl styryl sulfone, methyl cinnamyl sulfone, phenyl styryl sulfone and *p*-tolyl styryl sulfone results in the formation of a mixture of *erythro* and *threo* isomers of the addition product in each case.[13]

THE NON-STOICHIOMETRY OF LANTHANUM HYDRIDE[1]

BY EDWARD J. GOON[2]

Department of Chemistry, Tufts University, Medford 55, Mass.

Received May 26, 1959

An interpretation of the data from a high temperature X-ray diffraction study of lanthanum hydride indicates that the hydride exists as a non-stoichiometric compound at elevated temperatures. The non-stoichiometry may result from the movement of hydrogen out of the octahedral sites of the fluorite-type hydride lattice without the necessity of forming Schottky defects in the lanthanum lattice of the hydride. The energy which was required to create the hydrogen vacancy was calculated from thermal expansion data and found to be 0.10 e.v.

Introduction

To the author's knowledge, X-ray diffraction studies which have been performed on the rare earth hydrides have been conducted at room temperature.[3-8] The dihydrides of lanthanum, cerium, praseodymium and neodymium have the fluorite-type structure with the hydrogens located in the tetrahedral interstices. Neutron diffraction evidence[6] indicates that further absorption of hydrogen by the dihydride results in the filling of the octahedral interstices. Absorption of the additional hydrogen is accompanied by a contraction of the cell constant of the hydride without a change of symmetry of the metal atoms.

Many metallic hydrides are normally non-stoichiometric, containing a deficiency of hydrogen. The term non-stoichiometric as applied to lanthanum hydride, denotes a compound whose atomic ratio of hydrogen to lanthanum is between two and three. Since the lattice constant of lanthanum hydride, LaH_n ($2 \lesssim n \lesssim 3$), is sensitive to the number of hydrogen vacancies in the hydride lattice, it was believed that the information which would be obtained from a high temperature investigation, could be correlated with data from other physical chemical measurements to establish the stoichiometry of the hydride at elevated temperatures.

Experimental

Apparatus.—Diffraction patterns of metallic hydrides were obtained by the use of the high temperature assembly,[9] which was used in conjunction with the Straumanis type G. E. powder camera at temperatures up to 650° and pressures up to 600 p.s.i. The accuracy of the measurement of specimen temperatures was better than ±3°. Because the specimen was contained in a beryllium metal tube, films contained the diffraction pattern of beryllium metal superimposed on that of the specimen. Masking of some of the lanthanum hydride lines by beryllium diffraction bands was not a serious handicap to the method.

Usually the composition of a hydride specimen at elevated temperature is calculated from pressure–volume–temperature data. In the X-ray experiments this was not feasible because of the existence of a temperature gradient along the length of the specimen and the relatively large volume of the apparatus as compared to the small volume of hydrogen available from dissociation of the specimen. Since the temperature of that part of the specimen directly exposed to the X-ray beam and hydrogen pressure over the specimen were known, the composition of the hydride specimen was estimated whenever possible from available P–V–T data.

Materials.—The lanthanum metal was of high purity and was furnished by the Ames Laboratory of Iowa State College. To prepare the metal for hydriding, the surface

(1) This research was supported by the U. S. Atomic Energy Commission.

(2) National Research Corporation, Cambridge, Mass.

(3) A. Rossi, *Nature*, **133**, 174 (1934).

(4) B. Dreyfus-Alain, *Compt. rend.*, **235**, 540, 1295 (1952); **236**, 1265 (1953).

(5) B. Dreyfus-Alain and R. Viallard, *ibid.*, **237**, 806 (1953).

(6) F. H. Ellinger, C. E. Holley, Jr., R. N. R. Mulford, W. C. Koehler and W. H. Zachariasen, THIS JOURNAL, **59**, 1226 (1955).

(7) W. L. Korst and J. C. Warf, Dissertation, U. of Southern California, 1956.

(8) B. Stalinski, *Bull. acad. polon. sci.*, Classe III, **3**, 613 (1955).

(9) E. J. Goon, J. T. Mason and T. R. P. Gibb, Jr., *Rev. Sci. Instr.*, **28**, 342 (1957).

of the specimen was cleaned by abrading with Carborundum finishing paper No. 3/0 under mineral oil. Before transferring to a container for hydriding, the specimen was washed in anhydrous ethyl ether. Hydriding was carried out at room temperature under a hydrogen pressure of one atmosphere. Lanthanum hydrides of composition $LaH_{2.04}$ and $LaH_{3.04}$ were prepared. It is doubtful that the atomic ratio of hydrogen to lanthanum actually exceeded three so that the additional 0.04 is probably experimental error. The hydrogen was purified by passing it through a Deoxo purifier, Drierite and a hot uranium metal getter.

Calculation of Lattice Constant.—The lattice constant of the face-centered cubic structure of lanthanum hydride was calculated by use of the diffraction line 711,551. Parameter corrections for eccentricity and absorption were not necessary, the accuracy of the lattice constant measurements being ±0.001 Å.

Results.—Lattice constants of lanthanum hydride (LaH_2 to LaH_3) at elevated temperatures were calculated from diffraction patterns taken while the hydride was subjected to hydrogen gas pressures in excess of that needed to obtain a pressure-independent cell constant. The cell constant will be considered that of the hydride at limiting composition, which is defined as the composition at infinite hydrogen pressure and temperature T. If the magnitude of external gas pressure were insufficient to prevent the minimum amount of dissociation, larger values of cell constants would result. Hydrogen gas pressures ranged from 500 to 640 p.s.i. The linear variation of lattice constant of lanthanum hydride with temperature can be seen in Fig. 1, line AB.

The variation of lattice constant of a hydride of constant composition was desired. The experimental conditions necessary to obtain lanthanum dihydride, LaH_2, at various temperatures were available from the data of Korst and Warf.[7] The thermal expansion of the dihydride was observed to be linear (see line BC, Fig. 1) with the linear coefficient of thermal expansion equal to 1.07×10^{-5} per degree from room temperature to 650°.

Discussion

Due to experimental difficulties involved in the preparation of near stoichiometric LaH_3 and to the diffuseness of the diffraction lines, previous investigators have reported lattice constants which are in poor agreement. In the present study the diffuseness of the diffraction lines from a pattern of LaH_3 was verified and prevented a direct calculation of the lattice constant. However, the latter was obtained from an extrapolation of line AB to room temperature, Fig. 1, and found equal to 5.604 Å. A cell constant of 5.663 Å. was experimentally determined for stoichiometric LaH_2 in excellent agreement with a value of 5.661 Å. obtained by Korst and Warf.

The lattice constants of lanthanum hydride (LaH_2 to LaH_3) are plotted in Fig. 2. It is observed that the data obtained by other investigators are randomly distributed about the line drawn through the two points obtained in this research and that the variation between composition and cell constant is linear. From the slope of the line in Fig. 2, a change of lattice constant of 0.001 Å. is equivalent to a change in composition n of 0.017, where n is the atomic ratio of hydrogen to metal. Since the lattice constant is quite sensitive to a change in composition of lanthanum hydride, a graphical interpretation of Fig. 1 will be made to show the existence of non-stoichiometry at elevated temperatures.

Before a graphical interpretation can be attempted, several assumptions are necessary. (a) The change in lattice constant of lanthanum hydride at room temperature observed on varying the hydrogen content from LaH_2 to LaH_3 is invariant at a constant elevated temperature. (b) The thermal expansion of the dihydride remains linear above a temperature of 650°. (c) The intersection of lines AB and BC, Fig. 1, at point B may be interpreted to mean that dissociation of the trihydride has occurred at 908° to form the dihydride. In other words, the limiting composition of lanthanum hydride at 908° is $LaH_{2.0}$ at the pressures employed.

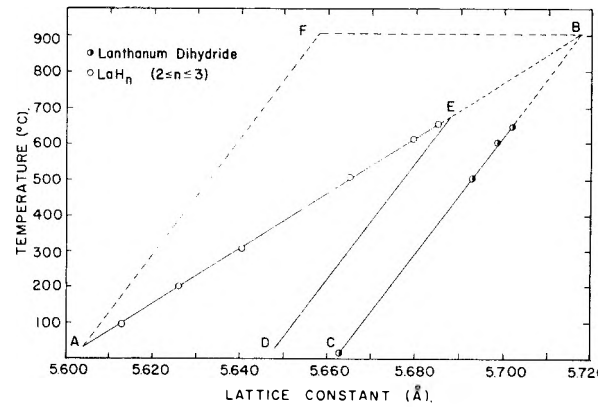

Fig. 1.—Lattice constant of lanthanum hydride *vs.* temperature.

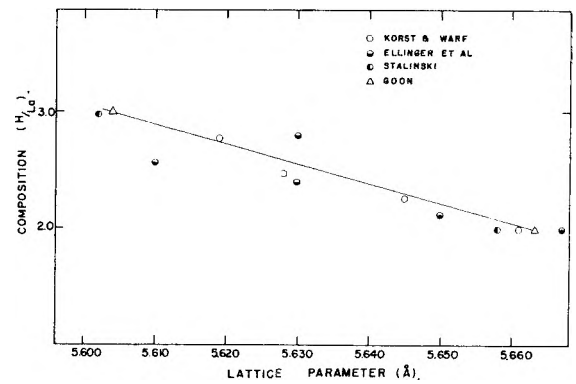

Fig. 2.—Lattice parameter of lanthanum hydride at room temperature *vs.* composition.

From Fig. 1 it is observed that the over-all change in lattice constant of the hydride is going from a composition of LaH_3 at point A to LaH_2 at point B is 0.113 Å. The change attributed only to the decrease of hydrogen content in going from the trihydride to the dihydride is 0.059 Å. (see Fig. 2). The difference between the values 0.113 and 0.059 Å. is the change in lattice constant that would have been observed for the thermal expansion of the trihydride, if it were stable at elevated temperatures. Graphically the dissociation of the trihydride can be visualized as occurring in two steps: (1) thermal expansion of the trihydride lattice to point F at 908° (represented by line AF) and (2) dissociation of the trihydride to the dihydride at a constant temperature of 908° (represented by line FB). It is interesting to note that the slopes of lines AF and BC are approximately equal. This indicates that the linear coefficients of thermal expansion of the dihydride and trihydride are equal. One may conclude that lanthanum hydride exists as a non-stoichiometric compound ($H/La < 3$) at elevated temperatures and infinite hydrogen pressures. The variation of limiting composition

of the hydride along line AB is also approximately linear.

From statistical mechanical considerations Rees[10] and Libowitz[11] have shown that hydrogen vacancies in the hydride lattices of zirconium and uranium, respectively, can be accounted for by the formation of Schottky defects in the metal atom lattice with the simultaneous formation of hydrogen vacancies. The assumption made is that a hydrogen atom cannot occupy a site next to a vacant metal atom site. The explanation is proposed to account for non-stoichiometry, *i.e.*, limiting compositions of the hydrides at elevated temperatures.

The application of a similar treatment to lanthanum trihydride does not seem warranted. First of all, there are two types of interstitial positions in the fluorite-type lattice of lanthanum hydride, tetrahedral and octahedral, which are available for occupancy by hydrogen. However, in the hydrides of uranium and zirconium there is only one type of interstice available for occupancy by hydrogen. Neutron diffraction studies[6] indicate that the tetrahedral interstices are filled preferably to the octahedral positions. Daou and Viallard[12] state that the hydrogens in the octahedral interstices of cerium hydride are more weakly bound than the hydrogen in the tetrahedral interstices. A simple picture of the formation of a Schottky defect in the metal atom lattice does not take into consideration the preference of hydrogen for one type of interstice over the other and a more rigorous theoretical treatment of this situation is not attempted. The formation of a hydride of limiting composition LaH_2 *via* the simple Schottky mechanism would result in a hydride lattice with both the tetrahedral and octahedral interstices partially filled. Although the evidence is not conclusive, a greater probability exists for finding only the tetrahedral interstices filled at composition LaH_2.

The energy of formation of a Schottky defect in the lanthanum lattice of the hydride was calculated from equation 1 derived by following a procedure similar to that employed by Rees and Libowitz.

$$E_{La} = 2.303\ RT \log \frac{11}{3 - s} \qquad (1)$$

where E_{La} = energy of formation of a Schottky defect in the lanthanum lattice of the hydride, s = limiting composition of hydride at infinite pressure. E_{La} is seen to be a function of s and T. By assuming that the linear coefficient of thermal expansion of a non-stoichiometric hydride is equal to that of the dihydride, values of s and T were obtained from Fig. 1. For example, $LaH_{2.25}$ at room temperature is represented by point D and a hydride of similar composition at a temperature of 678° is denoted by point E, the intersection of lines AB and DE. The values of E_{La} range from 3 to 5 kcal./mole. The rather small values for energy of formation of Schottky defects in the lanthanum lattice of the hydride leads one to believe that the procedure employed for calculating E_{La} may not be applicable to lanthanum hydride. The non-stoichiometry of lanthanum hydride in the composition range LaH_2 to LaH_3 must result from the dissociation of the hydride through another mechanism.

It is generally accepted that the presence of Schottky defects in a crystal lattice does not necessarily affect the magnitude of the cell constant. Mott and Gurney[13] have shown that the number of Schottky defects may contribute to the thermal expansion of a crystal lattice, particularly near the melting point. The non-linear thermal expansion of the crystal lattice of silver bromide was interpreted by Lawson[14] as due to Schottky defects in the crystal lattice. His method of analysis of the thermal expansion data makes it possible to calculate the formation energy of a lattice defect E_δ. The values of E_δ determined by Fischmeister[15] for the alkali halides do not compare favorably with activation energies for ionic conduction determined from electrical conductivity measurements and are too small compared to the formation energies of Schottky defects calculated by Kurosawa.[16] However, it appears that Lawson's method can be applied to the thermal expansion data of metallic hydrides as was done in the case of uranium hydride.[17]

The expression (equation 2) proposed by Lawson is of the same form as that for the number of lattice defects in equilibrium at a temperature T and relates the anomalous expansion δ to the formation energy of a lattice defect E_δ. Anomalous expansion is defined as total expansion $(l_T - l_r)/l_r$ minus regular expansion $\alpha_r(T - T_r)$, where α_r = linear coefficient of thermal expansion of lanthanum hydride, l_r = lattice constant of lanthanum hydride at room temperature, l_T = lattice constant of lanthanum hydride at temperature T.

$$\delta = \frac{l_T - l_r}{l_r} - \alpha_r (T - T_r) = e^{-E\delta/RT} \qquad (2)$$

On taking the logarithm of equation 2, equation 3 is obtained

$$\log \delta = -\frac{E_\delta}{2.303RT} \qquad (3)$$

Since the expansion of the lanthanum hydride lattice, which occurs on decreasing the hydrogen content from LaH_3 to LaH_2 (see Fig. 2 and line BF, Fig. 1), would come under the heading of anomalous expansion, equation 3 may be used to determine the energy of formation of a lattice defect E_δ. The regular or normal component of the thermal expansion of lanthanum trihydride, line AF, Fig. 1, was calculated by using a value of 1.061×10^{-5} per degree for α_r. The energy E_δ was determined from the slope of the line of Fig. 3 and appears to be constant in the temperature range from 100 to 650° with a value of 2.4 kcal./mole (0.10 e.v.). The deviation of the points from linearity at temperatures below 100° indicates an increase in the value of E_{La} as the composition of the hydride approaches stoichiometric LaH_3.

(10) A. L. G. Rees, *Trans. Faraday Soc.*, **50**, 335 (1954).
(11) G. G. Libowitz, *J. Chem. Phys.*, **27**, 514 (1957).
(12) J. Daou and R. Viallard, *Compt. rend.*, **243**, 2050 (1956).
(13) N. F. Mott and R. W. Gurney, "Electronic Processes in Ionic Crystals," Clarendon Press, Oxford, 1950.
(14) A. W. Lawson, *Phys. Rev.*, **78**, 185 (1950).
(15) H. F. Fischmeister, *Acta Cryst.*, **9**, 416 (1956).
(16) T. Kurosawa, *J. Phys. Soc. Japan*, **13**, 153 (1958).
(17) E. J. Goon, submitted for publication.

From the data obtained in an ultraviclet absorption study of the KBr–KH system,[18] Mott[19] has calculated the activation energy for the escape of a hydrogen atom from a KBr–KH lattice to be approximately 0.083 e.v. The latter value is the energy required to form an F-center. Since the energy E_δ obtained in this research is about the same as the value calculated by Mott for KBr–KH, this may indicate that a similar mechanism may be applied to the loss of hydrogen for the octahedral sites of the lanthanum hydride lattice. This is to say the hydrogens in the octahedral sites may leave the hydride lattice without the necessity of creating Schottky defects in the lanthanum lattice of the hydride.

In conclusion the good agreement between the energy E_δ and the activation energy for electrical conduction determined by Stalinski[20] in his electrical conductivity study of the lanthanum–hydrogen system (LaH_2 to LaH_3) should be mentioned. The order of magnitude of the conductivity at 80°K. ranged from 10 ohm^{-1} $cm.^{-1}$ at LaH_2 to 10^{-7} ohm^{-1} $cm.^{-1}$ at compositions close to LaH_3 so that lanthanum hydride would be classified as a semi-conductor. Values of the activation energy for electrical conduction ranged from 0.091 to 0.230 e.v. for composition of hydride $LaH_{2.86}$ to $LaH_{2.92}$. However, it was noted that the activation energy determined by Stalinski tended to zero at a composition of $LaH_{2.72}$, whereas in this research the value of E_δ appears to remain constant down to a hydride composition of $LaH_{2.28}$. Therefore, the good agreement may be fortuitous.

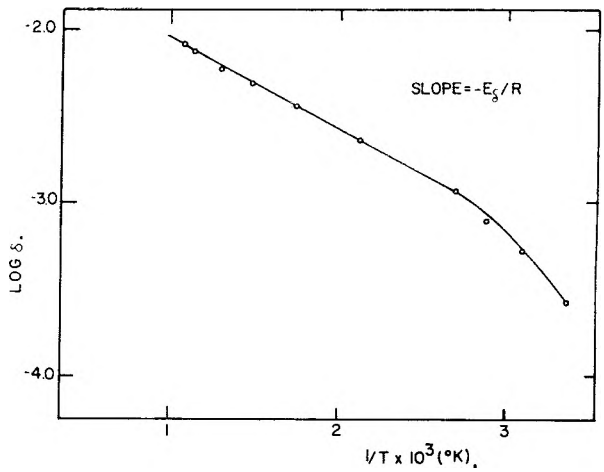

Fig. 3.—Anomalous expansion (α) of lanthanum hydride *vs.* temperature.

(18) R. Hilsch and R. W. Pohl, *Trans. Faraday Soc.*, **34**, 883 (1938).
(19) N. F. Mott, *ibid.*, **34**, 888 (1938).
(20) B. Stalinski, *Bull. acad. polon. sci.*, Classe III, **5**, 1001 (1957).

THE "HCl EFFECT" IN ANION-RESIN EXCHANGE[1]

BY BENJAMIN CHU AND

Chemistry Department, Cornell University, Ithaca, New York

RICHARD M. DIAMOND

Lawrence Radiation Laboratory, University of California, Berkeley, California

Received June 4, 1959

An explanation is offered for the interesting feature that distribution ratios of anions with strong-base exchange resins are generally lower from concentrated HCl solutions than from comparable LiCl solutions. It is suggested that this behavior is due to the invasion of the resin by non-exchange electrolyte at the high external-solution concentrations and to the partial association of the acid species in the resin phase. That is, because of the nature of the latter phase, normally strong acids are differentiated, the weaker ones partially associating. This does not occur as readily with the lithium salts, and so the preferential association of non-exchange H^+ with the weaker-acid anion (Cl^- in most of the cases studied) represses the absorption of the other anion as a non-exchange electrolyte. If the anion of interest were the anion of a weaker acid than that of the macroelectrolyte, the reverse of the usual behavior should occur, namely, exchange from acid solution should yield larger distribution ratios than exchange from lithium salt solutions. This is shown to be the case for Cl^- tracer exchanging with concentrated HBr and LiBr solutions.

Introduction

Hydrochloric acid is one of the commonest and most important eluents used in anion-exchange-resin separations and studies.[2] Since the aqueous activity coefficients of HCl and LiCl are moderately similar up to very concentrated solutions, it certainly might be expected that the exchange behavior of anions from LiCl and HCl solutions would also be similar. However, this has been found not to be true.[3,4] Most anions, and particularly the metal–chloride complex ions, show values of the distribution ratio D which are one to three orders of magnitude greater for concentrated LiCl solutions than those for HCl solutions of the same concentration. The distribution ratio is defined as

$$D = \frac{\text{amt. of ion of interest per g. of resin}}{\text{amt. of ion of interest per ml. of soln.}}$$

Examples are shown in Figs. 1 and 2, and other cases are in the literature.[3,4] Such behavior can be useful in metal-ion separations, and, for example, the larger D values obtained in LiCl solution have been used in the separation of the trans-

(1) This work was supported in part by the U. S. Atomic Energy Commission, Contract No. W-7405-eng-48.

(2) K. A. Kraus and F. Nelson, in "Proceedings of the International Conference on the Peaceful Uses of Atomic Energy," Vol. VII, Geneva, 1955 (United Nations, New York, 1955), pp. 113-125.

(3) S. G. Thompson, B. G. Harvey, G. R. Choppin and G. T. Seaborg, *J. Am. Chem. Soc.*, **76**, 6229 (1954).

(4) K. A. Kraus, F. Nelson, F. B. Clough and R. C. Carlston, *ibid.*, **77**, 1391 (1955).

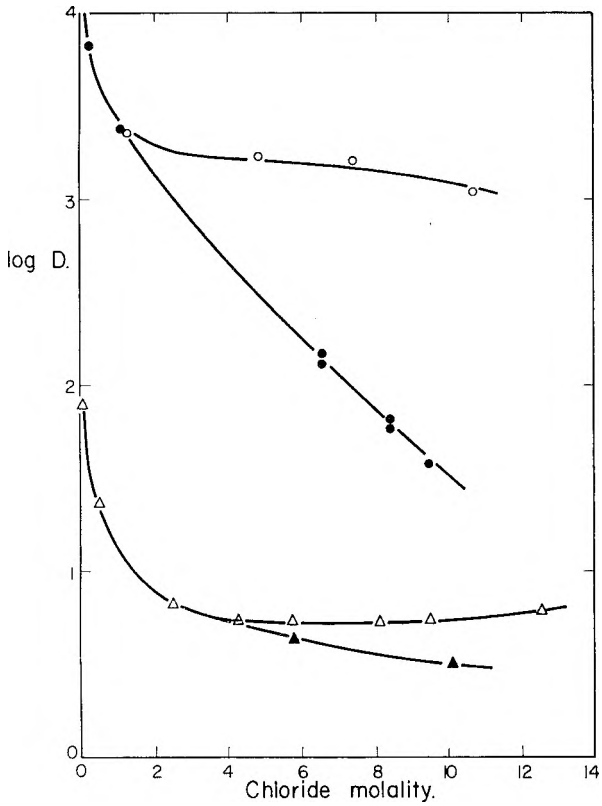

Fig. 1.—Distribution ratio *vs.* chloride molality for tracer bromide, △—△, and for tracer perrhenate, ○—○. Open symbols are LiCl solutions; closed symbols are HCl solutions.

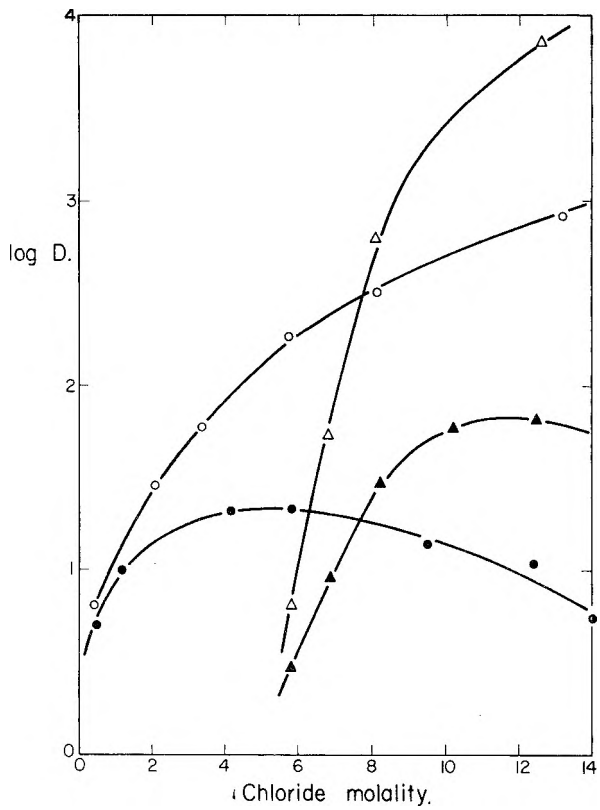

Fig. 2.—Distribution ratio *vs.* chloride molality for tracer indium(III), ○—○, and for tracer cobalt(II), △—△. Open symbols are LiCl solutions; closed symbols are HCl solutions.

plutonium ions from the rare earth ions.[3] But this difference in behavior is also an interesting feature to be explained in understanding the ion-exchange-resin process. An explanation that has been tentatively advanced[2,3] is that the complex metal anions are the anions of somewhat weak acids, and that at high HCl concentrations the undissociated complex acid forms in the external aqueous solution. Such association would lower the concentration of the distributing metal anion and so would lead to the observed lower value of D in HCl solutions.

But there are difficulties with this explanation. First the extraction behavior of the complex metal acids into oxygenated organic solvents indicates that they are not weak, but are very strong acids, stronger than HCl.[5,6] Their strength is of the order of that of $HClO_4$, which is indeed a good model acid for the metal-complex acids. Secondly, the distribution ratio of bromide ion is also larger from LiCl than from HCl solutions (ref. 2 and Fig. 1). But HBr is certainly a strong acid, stronger than HCl, and so by the above explanation should have a higher value of D from the HCl solution than from the LiCl solution. Curiously, the difference in the values of D for Br^- with HCl and LiCl is not as great as those for the chlorometallic complex ions such as $GaCl_4^-$, $FeCl_4^-$ and $InCl_4^-$. In fact, it appears that the magnitude of the difference in D between HCl and LiCl solutions increases with increasing acid strength of the anion under consideration. This is just the reverse behavior of that to be expected from the above explanation, but a clue to an alternative explanation to be presented in this paper.

Experimental

Resins.—The resins used in this work were of the strongly basic quaternary amine type, namely, Dowex-1 resins of 10 and 16% divinylbenzene content.[7] They were conditioned before use by alternate repeated washings with 3 M HCl and water and were then dried at 98 ± 1° overnight. After cooling, they were dry-sieved (10% DVB to 60 to 100 US mesh; 16% DVB to 200 to 400 US mesh), and stored in a desiccator over anhydrous $Mg(ClO_4)_2$.

Tracers.—The $(Re^{186}O_4)^-$ ($T_{1/2}$ = 89 hr.) and $(Br^{82})^-$ ($T_{1/2}$ = 36 hr.) were obtained from Union Carbide Nuclear Company, Oak Ridge, Tennessee. The $(Cl^{34})^-$ ($T_{1/2}$ = 32 min.) was produced by irradiating sodium hydrogen phosphate in the Berkeley 60-inch cyclotron. No detectable change in the γ-ray spectra of the tracers occurred during the period of their use, and the tracers decayed with the correct half lives, indicating that no appreciable radioactive impurities were present. The radioactive samples were counted with a well-type NaI scintillation counter employing a single-channel analyzer.

Method.—The values of D for ReO_4^- were obtained by the batch equilibration method, those for Cl^- by the column technique and those for Br^- by both methods. In the batch method, 50 μl. of the tracer in 10 ml. of the macro-electrolyte solution was shaken for 4 to 12 hr. with small amounts (0.03–0.2 g.) of resin. Duplicate 3-ml. aliquots of the solution were withdrawn through glass-wool filters and gamma-counted. After correction for background, comparison of the counting rates with those of aliquots of the initial solution before the introduction of the resin

(5) R. M. Diamond, THIS JOURNAL, **61**, 75 (1957), and unpublished work.

(6) E. Rudzitis, J. W. Irvine, Jr., and J. Mendez, "Annual Progress Report," June 1957 to May 1958, Laboratory for Nuclear Science, Massachusetts Institute of Technology.

(7) Thanks are expressed to the Dow Chemical Company, Midland, Michigan, for samples of the 16% DVB resin.

allowed the calculation of D. The method becomes quite inaccurate for small values of D and for such cases the column technique is more suitable. This consists of adsorbing a few microliters of the tracer on the top of a column of resin (pre-equilibrated with the macroelectrolyte solution at the concentration to be studied), and then eluting the tracer with the solution of macroelectrolyte. The volume of solution necessary to elute the tracer (neglecting one free-column volume) is proportional to the distribution ratio of the tracer.[8]

Results and Discussion

The variation in the distribution ratios for several tracer anions, Br^-, I^-, ReO_4^-, $InCl_4^-$, $CoCl_4^=$ and $ZnCl_4^=$, with Dowex-1 resins of 2, 10 and 16% DVB content from various chloride solutions, HCl, LiCl, NaCl, KCl, CsCl, $N(CH_3)_4Cl$ and $N(C_2H_5)_4Cl$ have been studied.[9] It has been found that the plot of log D *vs.* chloride concentration for HCl is anomalous. This curve always shows a more negative slope at high chloride concentrations than those for the alkali chlorides. Figure 3 is an example, showing some of the data for tracer ReO_4^-. Note that the curve for HCl falls steeply across the others.

For such exchange of univalent ions, X^- and Cl^-, the equilibrium expression may be written as

$$1 = \frac{(Cl)(\overline{X})\gamma_{MCl}\bar{\gamma}_{MX}}{(\overline{Cl})(X)\bar{\gamma}_{MCl}\gamma_{MX}} \qquad (i)$$

where the bar indicates the resin phase and MCl is the macroelectrolyte. A distribution ratio D' can be defined as

$$D' = \frac{\text{molality of ion in the resin phase}}{\text{molality of ion in the external soln.}} = \frac{(\overline{X})}{(X)} = \frac{(\overline{Cl})}{(Cl)}\frac{\bar{\gamma}_{MCl}}{\gamma_{MCl}}\frac{\gamma_{MX}}{\bar{\gamma}_{MX}} \qquad (2)$$

It should be noted that D' is not the same as the more easily measured ratio D which has already been defined, but D is equal to rD' where r is the ratio of the ml. of solution that contains 1 g. of water to the g. of resin that contains 1 g. of water. Then for dilute external solutions, where $\gamma_{MCl}/\gamma_{MX} \rightarrow 1$, we have

$$D' \approx \frac{(\overline{Cl})\bar{\gamma}_{MCl}}{(Cl)\bar{\gamma}_{MX}} \qquad (3)$$

Furthermore, if the ion of interest X^- is present in only tracer quantities and there is no resin invasion by non-exchange electrolyte, we have $(\overline{R'}) = (\overline{Cl})$ = constant, where $(\overline{R'})$ is the concentration of resin sites in meq. per gram of resin water, and $\bar{\gamma}_{MCl}/\bar{\gamma}_{MX}$ = constant. From these we obtain

$$D = rD' = K\frac{(\overline{R'})}{(Cl)} = K'/(Cl) \qquad (4)$$

At very low external solution concentrations, no dependence of the distribution ratio on the nature of the chloride solution is to be expected. The ratio depends only upon the chloride concentration. Experimentally, the difference between the HCl and LiCl (as well as the other alkali chloride) curves is negligible at low external solution concentrations but increases with increasing chloride concentration. This suggests that the effect may be

(8) S. W. Mayer and E. R. Tompkins, *J. Am. Chem. Soc.*, **69**, 2866 (1947).

(9) Benjamin Chu, Ph.D. Thesis, Cornell University, Feb. 1959.

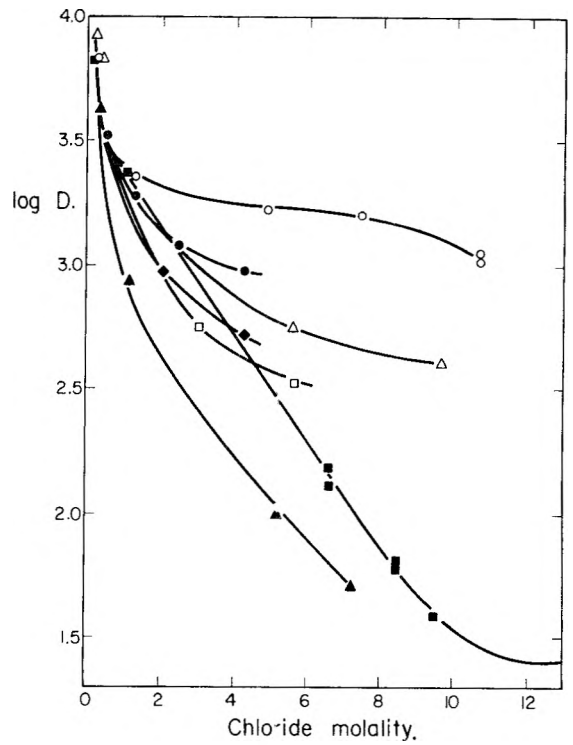

Fig. 3.—Distribution ratio *vs.* chloride molality for perrhenate ion from LiCl, ○—○; HCl, ■—■; NaCl, ●—●; KCl, ◆—◆; CsCl, □—□; Me_4NCl, △—△; NEt_4Cl, ▲—▲ solutions.

connected with the presence of non-exchange electrolyte in the resin phase, that is, with the increasing amount of electrolyte that invades the resin phase at increasing external solution concentrations.

The increasing amount of non-exchange electrolyte present in the resin phase makes the expression for D', eq. 3 or 4, more complicated. Equation 2 is still correct, but instead of $(\overline{Cl}) = (\overline{R'})$, we have $(\overline{Cl}) = (\overline{R'}) + (\overline{M})$. Thus we obtain

$$D' = \left[\frac{(\overline{R'})}{(Cl)} + \frac{(\overline{M})}{(Cl)}\right]\frac{\bar{\gamma}_{MCl}}{\bar{\gamma}_{MX}}\frac{\gamma_{MX}}{\gamma_{MCl}} = \left[\frac{(\overline{R'})}{(Cl)} + \frac{-(\overline{R'}) + \sqrt{(\overline{R'})^2 + 4(\gamma_{MCl})/(\bar{\gamma}_{MCl})(M)(Cl)}}{2(Cl)}\right]\frac{\bar{\gamma}_{MCl}}{\bar{\gamma}_{MX}}\frac{\gamma_{MX}}{\gamma_{MCl}} \qquad (5)$$

The first term on the right side gives the exchange contribution, but this decreases as $(Cl)^{-1}$, so that the second term, due to the resin-invasion electrolyte, may become dominant at high external-solution concentrations. Thus D' does not decrease as steeply with increasing (Cl^-) as the first term alone and becomes dependent on the nature of the cation of the macroelectrolyte solution. This dependence is reflected in variations in $(\overline{R'})$ and in the ratios of activity coefficients, $\gamma_{MCl}/\bar{\gamma}_{MCl}$ and $\gamma_{MX}/\bar{\gamma}_{MX}$.

For simple univalent tracer anions, the order of decreasing distribution ratios with the various concentrated alkali chloride solutions is the same as that of the resin invasion by the chloride salts themselves, namely, Li > Na > K > Cs > $NMe_4 \gtrsim$

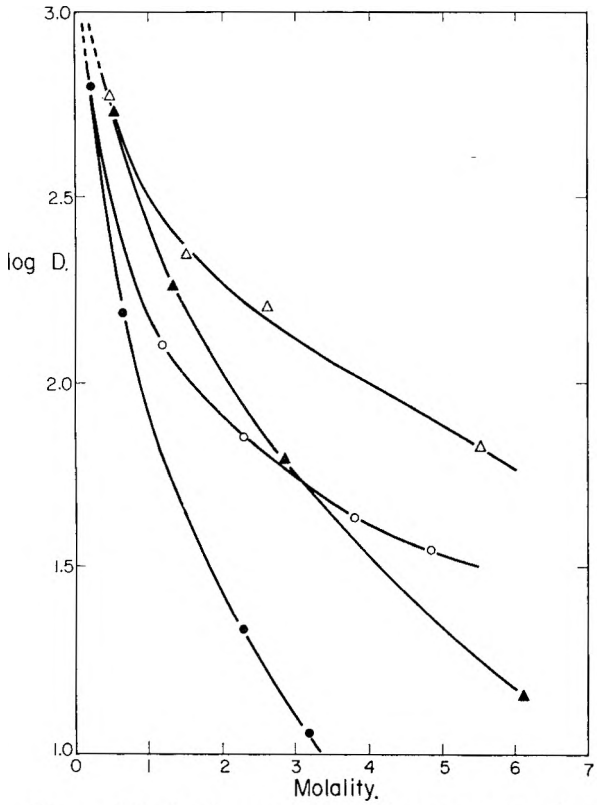

Fig. 4.—Distribution ratio for perrhenate tracer *vs.* bromide, △—△, and nitrate, ○—○, molality. Open symbols are for lithium salts; closed symbols are for acids.

NEt_4.[9] This is not surprising, as from eq. 5 it can be seen that the order of the distribution ratios depends upon the relative amount of resin-invasion cation, $(\overline{M})$. The reasons for the differing amounts of resin invasion and what effect this has on the distribution ratios will be discussed in greater detail in a later paper,[9] but for the present it is sufficient to point out the parallel between the amount of resin invasion by the macroelectrolyte, and the order of distribution ratios of a given tracer. In contrast to this general behavior, the distribution ratios for most tracer anions are lower from HCl than from LiCl solutions, even though the solubility of HCl in the resin phase is greater than that of LiCl from solutions of the same concentration.[9,10] This behavior becomes more marked as the external solution concentration increases. We believe that the origin of this anomaly lies in the formation of undissociated HCl in the resin-phase solution. This undissociated HCl may be either molecular HCl or an ion pair; it has not been possible to differentiate these cases. But there are several reasons for believing that association occurs. First, there is some association in any concentrated HCl solution and the amount increases with increasing total concentration. The resin phase solution is a very concentrated electrolyte. For example, when the external aqueous HCl concentration is ~12 *m*, the total ionic strength of the internal resin-phase solution is about double that, ~16 *m* in HCl and ~8 *m* in resin chloride. There is thus relatively less water in the resin phase than in the external solution to solvate the ions and keep the H^+ and Cl^- apart. Furthermore, the lower effective dielectric constant of the resin phase increases the electrostatic interaction between ions. The suggested association of HCl in the resin phase explains its greater solubility there than that of LiCl. In fact, this association explains both the greater amount of HCl over LiCl absorbed per unit weight of resin from solutions of the same molality, and the curious feature that the concentration of total HCl inside the resin is greater than that of the equilibrating solution, at high HCl concentrations. The resin solution contains more HCl in the form of a new (associated) species than the external solution. Experimentally, such acid association also has been observed with $SO_4^=$, since HSO_4^- appears to be a weaker acid in the resin phase than in an ordinary aqueous solution,[10] and should be a perfectly general phenomenon in the resin phase.

Of more importance for this discussion, it provides an explanation for the anomalously low values of the distribution ratios of tracer anions from concentrated HCl solutions. The association of the HCl in the resin phase results in a smaller number of "free" non-exchange cations there than with LiCl solutions. If the tracer anion of interest is from a stronger acid than HCl, few of these anions can enter the resin phase as non-exchange electrolyte from HCl solutions, because the chloride ion preferentially unites with the non-exchange hydrogen ion. A much smaller amount of association occurs with the non-exchange lithium ion in the resin phase and so the distribution ratio from HCl solutions falls increasingly below that from LiCl solutions as the amount of non-exchange electrolyte in the resin increases with increasing external solution concentration.

Such behavior follows directly from the present hypothesis that $\bar{\gamma}_{HCl}$ is less than $\bar{\gamma}_{LiCl}$ as long as the tracer anion is derived from an acid stronger than HCl. This can be seen from eq. 5 because γ_{LiX} and γ_{LiCl} are approximately equal to γ_{HX} and γ_{HCl}, respectively, so that $D'_{LiCl}/D'_{HCl} \propto \bar{\gamma}_{LiCl}\,\bar{\gamma}_{HX}/\bar{\gamma}_{LiX}\,\bar{\gamma}_{HCl}$. The difference in D between HCl and LiCl solutions should, in fact, increase with the strength of the acid HX and it appears that the magnitude of the "HCl effect" does increase from Br^- to I^- to ReO_4^- to $InCl_4^-$. This is the order of increasing acid strength for HCl, HBr and HI, and that expected for $HReO_4$ and $HInCl_4$. However, it is difficult to test this point with other anions from such strong acids as, because of their great strengths, they would not be expected to show great differences from each other in their resin behavior, and their exact acid strengths are not usually known.

However, if the hypothesis of relatively greater acid association in the resin phase than in the external solution is correct, the relative distribution ratios for a tracer anion from lithium and acid macroelectrolyte solutions should also be a function of the relative strength of the macroelectrolyte acid, as can be seen from eq. 5. If a weaker acid than HCl and its lithium salt were used, a greater

(10) F. Nelson and K. A. Kraus, *J. Am. Chem. Soc.*, 80, 4154 (1958)

variation in the distribution ratios of the tracer anion might be expected than from HCl and LiCl. If a stronger acid were used, less difference in the distribution ratios might be expected (as long as the macroacid were weaker than the tracer acid; see last paragraph below).[11] Figure 4 presents the results of such a study with ReO_4^- tracer using the acid–salt pairs HBr–LiBr and HNO_3–$LiNO_3$. Hydrobromic acid is stronger than HCl and HNO_3 is weaker, and it can be seen that the difference in D' values for the HNO_3–$LiNO_3$ case is indeed larger than that for the HBr–LiBr pair.

This larger difference between HNO_3–$LiNO_3$ solutions than between HCl–LiCl solutions has also been noted recently with the rare earth ions.[12] The idea that the resin phase solution is more conducive to ion association than the external solution because of its lower water content and effectively lower dielectric constant leads to an explanation for the absorption of the rare earth ions from $LiNO_3$ solutions and for their order of absorption. Since it is most unlikely that the rare earth ions form anionic complexes with nitrate, the absorption of the former by the resin is as non-exchange cations. Nitrate ion will preferentially associate with H^+, and so from HNO_3 solutions there will be little chance for the rare earth ions to enter the resin phase; the non-exchange electrolyte will be predominantly HNO_3. From $LiNO_3$ solutions, however, the non-exchange electrolyte cations are lithium and the rare earth ions. Observation of activity-coefficient tables[13] shows that nitrate salts have low values relative to chloride salts, and that this difference becomes more pronounced as one goes from the alkalies to the alkaline earths and, presumably, onto the rare earths. Such lower values are indicative of ion association and that the higher the charge on the cation, the larger the effect. Thus, although the rare earth ions cannot compete with H^+ for the non-exchange NO_3^-, they can do so very favorably with Li^+, and so go into the resin phase with nitrate ion as (partially ion associated) non-exchange electrolyte. The values of D should increase with increasing non-exchange electrolyte concentration and, hence, increasing external solution concentration, as is observed. Furthermore, the strength or degree of the rare earth–nitrate ion association should be a function of the ionic size of the rare earth ion, increasing with decreasing size of the hydrated ion. Since the hydrated size of the rare earth ions increases from La to Yb, as indicated by their limiting equivalent conductances,[14] greater association with nitrate ion should be expected in the reverse order. At a given nitrate concentration, the distribution ratios should decrease in the order La to Yb, which is the order observed experimentally. The striking effect of even very small amounts of HNO_3 (10^{-2} M) in reducing the values of D is also accounted for.

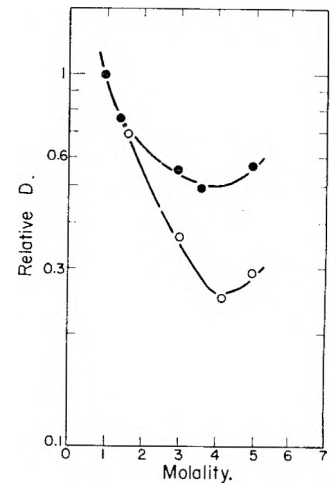

Fig. 5.—Distribution ratio *vs.* bromide molality for tracer chloride ion. Open symbols are for lithium salts; closed symbols are for acid.

Still one more test of the hypothesis of acid association predominantly in the resin phase has been made. The distribution ratios for a tracer anion derived from an acid the strength of which is weaker than that of the macroelectrolyte anion should show the opposite behavior from H^+ and Li^+ solutions than that shown in Figs. 1, 2, 3 and 4. Now the tracer anion associates in the resin phase with the non-exchange H^+ more than does the macroelectrolyte anion, yielding values of D which are larger from concentrated acid solutions than from lithium solutions of the same molality. This can be seen again from eq. 5. For example, the roles of Br^- and Cl^- as tracer anion and macroelectrolyte, respectively, (illustrated in Fig. 1) can be reversed, and the distribution behavior of tracer Cl^- can be studied from concentrated solutions of HBr and LiBr. The experimental results are shown in Fig. 5 and it can be seen that the expectation of larger D values for the HBr solutions than for those of LiBr are fulfilled.

Acknowledgment.—R.M.D. wishes to thank Mrs. Mab Tocher for help with some parts of this work.

(11) A complication in interpreting such an experiment is that the water activity may be quite different with the different macroelectrolytes, and this affects the degree of resin invasion, as, in general, the lower the water activity, the greater is the amount of resin invasion (*cf.* reference 9).

(12) Y. Marcus and F. Nelson, THIS JOURNAL, **63**, 77 (1959).

(13) R. A. Robinson and R. H. Stokes, "Electrolyte Solutions," Appendix 8.10, Butterworths Scientific Publications, London, 1955.

(14) F. H. Spedding and J. L. Dye, *J. Am. Chem. Soc.*, **76**, 879 (1954); F. H. Spedding and S. Jaffe, *ibid.*, **76**, 882, 884 (1954).

PASSIVITY IN THE IRON-CHROMIUM BINARY ALLOYS

BY P. F. KING AND H. H. UHLIG

Corrosion Laboratory, Department of Metallurgy, Massachusetts Institute of Technology, Cambridge, Massachusetts

Received June 8, 1959

Information is reported contributing to further knowledge of passivity in the Cr–Fe alloys containing up to 29% Cr. Data include (1) critical current densities for anodic passivation at *p*H 3 and 7 at 25°, and for *p*H 7 at 4, 25 and 50°, (2) coulombs of passive film substance per unit area, (3) activation potentials at which passivity breaks down. Critical current densities decrease with increasing Cr content, reaching a value equivalent to or less than the normal corrosion rate of iron at >12% Cr–Fe, hence these alloys are self-passivating (stainless steels). The equivalents of passive film substance on iron and Cr–Fe alloys average 0.01 coulomb/cm.^{2} If it is assumed that (1) the anodic passivation reaction is in accord with $M + 2H_2O \rightarrow O_2M + 4H^+ + 4e^-$, where O_2M signifies oxygen associated with metal as oxide or adsorbed gas, and (2) activation potentials correspond to equilibrium conditions for this reaction, then the calculated free energy of formation of O_2M is not in accord with the free energy of formation of any known iron oxide. It is concluded that the passive film on Fe, Cr and the stainless steels consists of a chemisorbed oxygen or oxygen–complex film.

Passivity in iron can be induced by concentrated HNO_3 or by anodic polarization in sulfuric acid, but the resulting resistance to chemical reaction is temporary, the metal reverting in short time to its original state. When 12 or more per cent. Cr is alloyed with Fe, passivity can be induced by simple air-exposure of the alloy and the resulting decrease in corrosion rate is relatively permanent. Alloys in this category are the basis of the so-called stainless steels.

The possible structure and composition of films on Cr–Fr alloys responsible for their passivity are still being discussed and constitute the basis of the present paper. Information is obtained from data presented herewith on the critical anodic current densities necessary to induce passivity in deaerated 3% Na_2SO_4 solution at *p*H 3 and 7 at 25°, and *p*H 7 at 4 and 50°. Data are also presented on the equivalent coulombs of passive film substance necessary to achieve passivity. Finally, the activation potentials (Flade potentials) at which the passive film breaks down are reported for 9.0, 18.6 and 29.1% Cr. This information combined with data by other investigators closely defines certain properties of the passive film with which any assumed structure and composition must be in accord.

Experimental Procedure

Alloys from which electrodes were prepared were melted in a vacuum induction furnace starting with pure iron (Ferrovac E, National Research Corporation) and electrolytic chromium. No deoxidizers were added. The alloys were cast by drawing into Vycor tubes, homogenized at 1100° in helium for 1 hour, rolled into strips, water-quenched from 1000°, cut to size and pickled.

The electrodes measuring about 1 cm.^{2} and 2 mm. thick were assembled with a nickel wire, silver soldered (keeping the alloy cold) to a stem machined on the alloy specimen. The wire was enclosed by an 8 mm. diameter glass tube. A Teflon gasket maintained a water-tight seal between electrode and glass at one end, with constant contact being effected by means of a screw, nut and rubber grommet attached to the wire at the other end.

Critical current densities for passivity were determined in an all-glass one-compartment cell, two components of which were joined by a ground glass seal. Two platinum electrodes about 3 cm. diameter were equally spaced on either side of the alloy anode. The probe of a salt bridge filled with 3% Na_2SO_4 was positioned near the surface of the alloy electrode. The salt bridge in turn made contact with a test-tube partly filled with the same solution and into which the tip of an Ag–AgCl, 0.1 *N* KCl electrode was immersed. The cell was similar to that described by Uhlig and Woodside[1] with the improvement that the alloy electrodes could be pickled within the cell using warm 15 vol. % HNO_3, 5 vol. % HF, washed three times with deaerated H_2O, and finally filled with deaerated 3% Na_2SO_4 without the electrode coming into contact with air. Deaeration of solutions was accomplished by bubbling through them, for 6 hours or more, nitrogen previously purified over copper turnings at 400°. Critical current densities obtained in this cell were somewhat higher than current densities determined after short exposure of the electrodes to air and were better reproducible. The cell and accompanying reservoirs of solutions, except for the pickle solution, were kept within a large constant temperature chamber maintained at 25 ± 0.2°, or at 4° or 50 ± 2°.

Activation or Flade potentials were recorded either by observing the final potential just before passivity spontaneously decayed in water of known *p*H (adjusted using H_2SO_4), or by cathodically reducing the alloy surface at slowly changing potentials until a sudden change of current through the cell indicated breakdown of passivity. The latter method was essential for the high chromium alloys which exhibited stable passivity even in acid media. Müller and Cupr[2] reported activation potentials of chromium which showed more active (less noble) values when the metal was cathodically activated, than when self-activated by simple immersion in acids of *p*H −0.2 to +1. Also the slope of activation potential, E_F *vs.* *p*H, for cathodically activated chromium was approximately twice (2 × 0.058) that for self-activated Cr. Rocha and Lennartz[3] similarly found a slope of about 2 × 0.058 volt for cathodically activated alloys of more than 14% Cr, and decreasing slopes for lower Cr alloys, eventually reaching a slope of 0.058 for Fe. One of us suggested[4] that the variation of slope with method of activation may be caused by differing chemical equilibria accompanying breakdown of passivity, triggered by a film thinning within pores in the case of self-activation, but thinning more generally over the surface in the case of cathodic activation. General thinning of the film may favor reaction of the passive film with the base metal and measurement of the corresponding potential involving reaction products, whereas with self-activation the potential is measured instead corresponding to equilibrium of only the passive film with electrolyte. An explanation along these lines is supported by the fact, as we found, that the slope can be altered by speed of cathodic reduction, higher speeds favoring local rather than general breakdown of the film, and hence accounting for lower slopes of E_F *vs.* *p*H. For currently reported measurements, we chose a speed of reduction which gave the same slope (0.059 volt, 25°) as is obtained for the same or neighboring alloys when self-activated. The same *p*H dependence of E_F indicates that passivity probably breaks down similarly by both methods of activation, and that the same chemical reactions are involved; hence the data are comparable. The method employed which gave the approximately correct slope consisted first of slightly polarizing the passive alloy specimen cathodically and retaining passivity at some definite potential with

(1) H. H. Uhlig and G. E. Woodside, THIS JOURNAL, **57**, 280 (1953).

(2) E. Müller and V. Cupr, *Z. Elektrochem.*, **43**, 42 (1937).

(3) H. Rocha and G. Lennartz, *Arch. Eisenhüttenw.*, **26**, 117 (1955).

(4) H. H. Uhlig, *Z. Elektrochem.*, **62**, 626 (1958).

reference to Ag–AgCl. The potential of the specimen was then made less noble, or more active, by about 20 mv. by appropriately adjusting the current and allowing time to reach steady-state conditions. This required about 5 minutes. The potential then was altered again in the active direction by another 20 mv. Eventually a critical potential E_F was reached at which the current changed direction within the cell accompanying breakdown of passivity, and the electrode became anode with respect to the auxiliary platinum electrodes.

The time–potential curves on passivating an active electrode at constant current were recorded manually using an electronic galvanometer, or if too rapid for potential measurements to be made in this manner, oscillograms were photographed. One of the manually recorded plots for a 13.6% Cr–Fe alloy is shown in Fig. 1. Plots of this kind usually showed two discontinuities in slope, each probably indicating a change in the nature of surface films formed anodically. The ratio of time to the first discontinuity T_1 to the second discontinuity T_2 averaged over 14 measurements for alloys between 2.7 and 39.1% Cr, was 0.27 with a standard deviation of 0.07. The change of potential between discontinuities was approximately linear with logarithm of time. On the basis that the potential change is proportional to the amount of surface oxygen (chemisorbed or as oxide), the log relation is in accord with the Elovich equation for rate of chemisorption or with the Tammann–Köster equation for the initial oxidation rate of metals. Not enough data were obtained to resolve with certainty the nature of the electrode processes initiating at each discontinuity.

Results

Critical Current Densities.—Critical current densities were obtained by noting the time t in seconds to reach the maximum passive potential for a given current density and obtaining such times for various current densities. The current densities then were plotted with $1/t$ in accord with the relation

$$I - I_c = \frac{K}{t} \qquad (1)$$

where I is the applied current density (amp./cm.^{2}), I_c is the critical current density below which passivity is not achieved in any time and K represents coulomb/cm.^{2} to achieve the passive state. (Time is chosen to reach the passive potential beyond which the potential is relatively constant. The corresponding coulombs/cm.^{2} are greater than the equivalents of passive film substance at the Flade potential.) This relation holds satisfactorily at current densities near the critical current density. It was used by Shutt and Walton[5] in their study of the passivation of gold in HCl, by Franck[6] in his study of the passivation of iron and by Olivier[7] for Cr–Fe alloys. A typical plot of potential E *vs.* time to passivity for various constant current densities is shown in Fig. 2 where t was chosen corresponding to the levelling off of potential at about 1.1 volt *vs.* Ag–AgCl 0.1 N KCl. The critical current densities obtained by plots of current density *vs.* $1/t$ for various alloys in deaerated 3% Na_2SO_4 are plotted as a function of chromium content in Fig. 3. The latter figure also shows critical current densities obtained *directly*, for which a specific applied anodic current density was applied below that required for passivation, then progressively higher values chosen until a c.d. was reached resulting in passivation. These

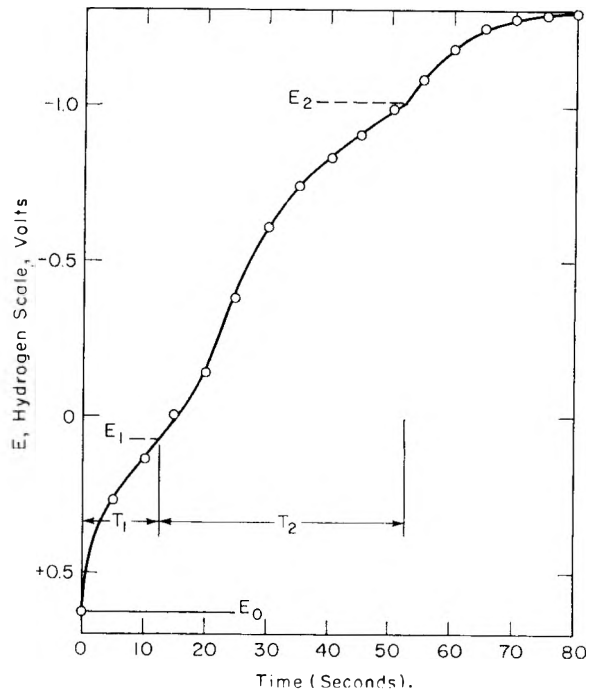

Fig. 1.—Tracing of oscillogram depicting change of potential with time for 13.6% Cr–Fe alloy anodically polarized in deaerated 3% Na_2SO_4, *p*H 7, at 0.18 ma./cm.^{2}, 25°.

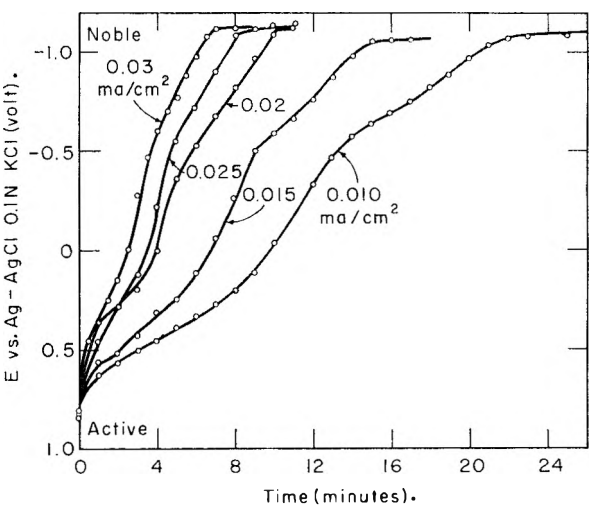

Fig. 2.—Relation of potential to time of passivation at various current densities for 13.6% Cr–Fe alloy in deaerated 3% Na_2SO_4, *p*H 7, 25°.

values are in good agreement with values obtained indirectly using equation 1. The present values tend to be somewhat higher but are in essential agreement with previously reported values of Uhlig and Woodside[1] up to 10% Cr. For higher chromium alloys, the latter authors did not find a critical current density by the direct method in contrast to the present data obtained by the indirect method. This can be accounted for in part by brief exposure of alloys to air in Uhlig and Woodside's measurements, inducing lower apparent values of the critical current density where critical current densities are already low, and where the alloy composition range >12% Cr corresponds to stable passivity, as is discussed later. In compari-

(5) W. Shutt and A. Walton, *Trans. Faraday Soc.* **30**, 914 (1934).
(6) U. F. Franck, *Z. Naturforsch.*, **4A**, 378 (1949).
(7) R. Olivier, "Int. Com. Electrochem. Therm. and Kinetics," Poitier. Butterworths, London, 1955, p. 34.

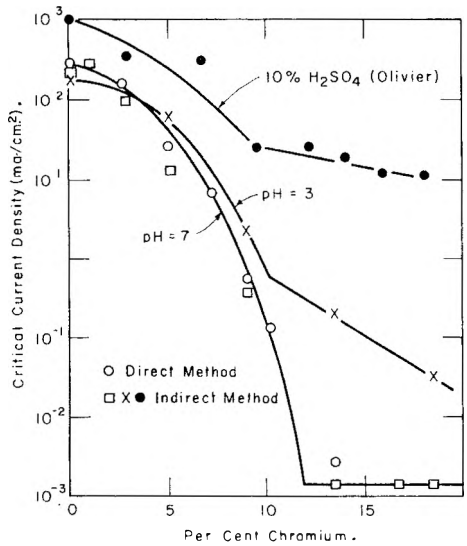

Fig. 3.—Critical current densities for passivation of Cr–Fe alloys, in deaerated 3% Na_2SO_4 at *p*H 3 and 7, 25°, including data of Olivier in 10% H_2SO_4, room temperature.

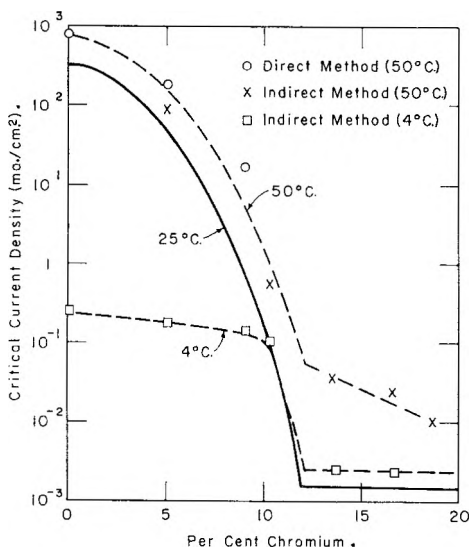

Fig. 4.—Critical current densities for passivation of Cr–Fe alloys in deaerated 3% Na_2SO_4, *p*H 7, at various temperatures.

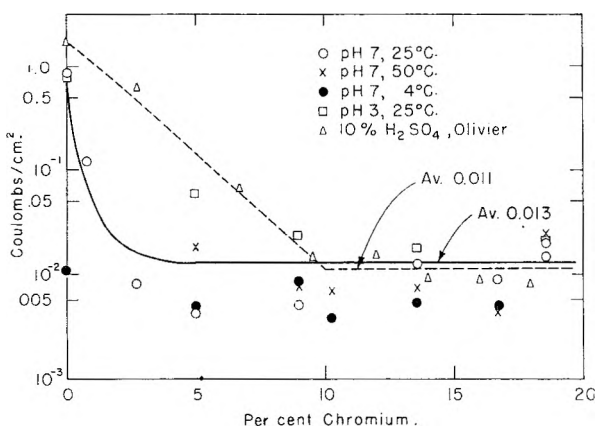

Fig. 5.—Electrochemical equivalents of passive film substance produced on Cr–Fe alloys by anodic polarization.

son, pickling within the cell and avoiding air-exposure, as was done presently, ensured the active state from the beginning of the measurement. The critical current densities presently obtained for alloys of greater than 12% Cr–Fe at *p*H 7, approximate 2 microamp./cm.²

Measurements at *p*H 3 are also shown in Fig. 3 together with data reported by Olivier obtained in 10% H_2SO_4 (*p*H approx. 0.13), both sets of data being obtained by plotting I *vs.* $1/t$ in accord with equation 1. Up to 9% Cr, critical current densities at *p*H 7 or 3 are the same within experimental error. Above 10% Cr, current densities at *p*H 3 are markedly higher than at *p*H 7, and similarly, critical current densities obtained by Olivier in 10% H_2SO_4 are still higher. It is not certain that Olivier's higher values below 9% chromium compared with values at *p*H 7 and 3 represent real differences. The three sets of data are consistent in showing a discontinuity in slope at 10 to 12% Cr.

Critical current densities at *p*H 7 for 4 and 50° are shown in Fig. 4. For alloys below 10% Cr, values at 4° are orders of magnitude lower than at the higher temperatures, but the 50° values are only slightly higher than those at 25°. Above 12% Cr, on the other hand, 4° values are slightly higher than the 25° values, but the differences fall within the expected experimental variation caused in large part by varying roughness factor after pickling. The corresponding values at 50° are definitely higher and qualitatively resemble the data of Fig. 3 for *p*H 3. A discontinuity of critical current density plotted with per cent. Cr appears at 12% Cr for all three temperatures. This critical composition, therefore, is not sensitive to small variations in temperature, nor to changes in *p*H of the environment.

From values of K in equation 1, coulombs/cm.² required for passivation of each alloy in sodium sulfate at *p*H 7 are plotted in Fig. 5 at 3 temperatures, and for *p*H 3 at 25°, including Olivier's data for 10% H_2SO_4 at room temperature. Values for iron are highest, ranging from 0.8 to 1.6 coulomb/cm.², except at 4° where the value is only 0.01 coulomb/cm.² Values decrease rapidly as Cr is alloyed with iron, reaching a value averaged for all alloys above 5% Cr of 0.013 coulomb/cm.² Olivier's data attain an average value above 9.5% Cr of 0.011 coulomb/cm.² Values at *p*H 3 tend to be higher than at *p*H 7; and values at 25 and 50° tend to be higher than at 4°, but experimental scatter is sufficiently large to discount any certain conclusions in this regard. The averages of present data and Olivier's data for the high range of Cr alloys are in good accord.

Flade potentials for 9.0, 18.6 and 29.1% Cr alloys as a function of *p*H of the solution in which activation takes place are shown in Fig. 6. Values for 9.0% Cr were obtained by self-activation, but for other alloys by cathodic activation. Values are also shown for iron passivated in concentrated HNO_3 or anodically in dilute H_2SO_4 based on our work reported previously.[8] The slopes of E_F *vs.* *p*H approximate 0.059. Standard Flade po-

(8) H. H. Uhlig and P. F. King, *J. Electrochem. Soc.*, **106**, 1 (1959).

tentials (pH 0) are in reasonably good accord with values reported by Rocha and Lennartz as shown in Fig. 7 despite differing techniques of activation; but, as discussed earlier, slopes of E_F vs. pH are lower. The "critical recovery potential" of a type 347 18-8 as measured by Cartledge[9] in 0.1 N H_2SO_4 is also close to the activation potential shown for 18% Cr, indicating that the two potentials are probably the same and are determined largely by the Cr content of the alloy as well as pH of the environment.

Discussion

Critical current densities mark a change in electrode reaction from anodic dissolution of active alloy forming Fe^{++} and Cr^{+++} in accord with Faraday's law, to a reaction resulting in oxygen evolution and Fe^{+++} plus CrO_4^{--} for the passive alloy. Oxygen is the major anodic reaction product for passive iron, but with higher chromium alloys formation of Fe^{+++} and CrO_4^{--} are the major products, and oxygen evolution may diminish to zero depending on the potential to which the electrode is polarized, this in turn being governed by current density and nature of the anion.[10-12] As discussed by Franck,[6] the true critical current density for passivation of iron lies considerably higher than the measured value. The initial anodic reaction product, probably $FeSO_4$, forms an insulating coating over the electrode, thereby raising the true current density within pores of this film. When about 17 amp./cm.^{2} is reached in pores, the true passive film forms accompanied by dissolution of the $FeSO_4$ film and a sudden potential change of about 2 volts in the noble direction. In accord with this mechanism we found that the critical current density for iron shifted from 450 ma./cm.^{2} in 5% H_2SO_4 to 100 ma./cm.^{2} in 5% H_2SO_4, 1.6 M $FeSO_4$. The same situation applies to low chromium alloys but at lower current densities. In solutions of pH 7 at about 12% Cr, the formation of an insulating film of corrosion products appears to be less important or no longer is required and the potential changes markedly toward the passive value on application of all but very small currents.

The critical current density can be considered that value which induces sufficient polarization at the anode to allow hydroxyl ions to discharge. For iron, the required polarization is considerable, but for chromium–iron alloys, where it can be reasonably assumed from properties of iron and chromium compounds (in accord with calculations presented later) that the affinity of the alloy for OH^- (or for oxygen) increases with chromium content, the required polarization is less. Above 12% Cr, the discharge of OH^- proceeds directly at current densities equivalent to or less than the corrosion rate of iron in water (approx. 25 mg./dm.^{2}/day equivalent to 10^{-2} ma./cm.^{2}), so that the alloy becomes self-passivating. In acid media, the critical current density required for passivation

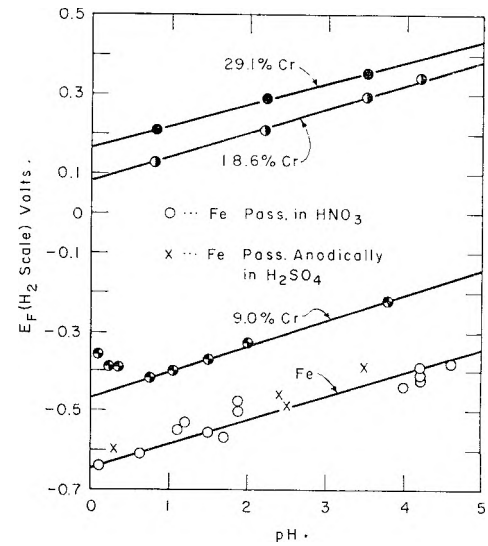

Fig. 6.—Activation (Flade) potentials of Fe and Cr–Fe alloys in H_2SO_4 as a function of pH (25°).

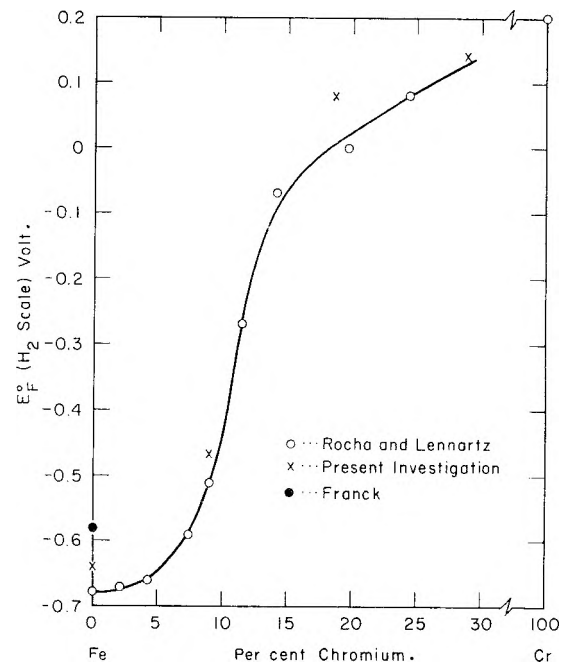

Fig. 7.—Standard activation (Flade) potentials of Fe, Cr–Fe alloys and Cr.

is higher because of lower hydroxyl ion concentration. Critical currents reported by Olivier are highest of all in accord with expected results in an acid environment of very low pH. Effect of pH is not so pronounced below 12% Cr, however, because, for one reason, the major film of reaction products first forming conditions the environment to the pH of saturated $FeSO_4$, regardless of external pH. Roberts and Shutt[13] and Heumann and Diekötter[14] found that the critical current densities for passivation of Cr are also higher the lower the pH.

(9) G. Cartledge, *ibid.*, **104**, 420 (1957).

(10) H. H. Uhlig and J. Wulff, *Trans. AIME*, **135**, 494 (1939).

(11) G. Masing, Th. Heumann and H. Jesper, *Arch. Eisenhüttenw.*, **25**, 169 (1954).

(12) Th. Heumann and W. Rösener, *Z. Elektrochem.*, **57**, 17 (1953).

(13) R. Roberts and W. Shutt, *Trans. Faraday Soc.*, **34**, 1455 (1938).

(14) Th. Heumann and F. Diekötter, *Z. Elektrochem.*, **62**, 745 (1958).

TABLE I

EQUIVALENTS OF PASSIVE FILM SUBSTANCE PER UNIT AREA (APPARENT SURFACE)

Metal	Method	Equiv. of pass. film, coulombs/cm.[2]	Ref.
Iron	Coulometry	0.008	Weil[17]
Iron	Max. oxidation of CrO_2^- to CrO_4^{--} by passive film	.012	Uhlig and O'Connor[18]
Iron	Anal. of iron entering soln.	< .003	Snavely and Hackerman[20]
>9% Cr–Fe alloys and 18-8	Coulometry	.011	Olivier[7]
>5% Cr–Fe alloys	Coulometry	.013	Present work
18-8	Consumption of O_2 on exposure of alloy to aerated H_2O[a]	.013	Uhlig and Lord[19]

[a] Based on alloy pickled in HCl–H_2SO_4, which gave a measured roughness factor of 4. The value for a measured roughness factor of 1.2 (18-8 pickled in HNO_3–HF) is 0.004 coulomb/cm.[2] The roughness factors of other metals listed in the table above have not been determined, but are expected to fall within the range 1.2–4.0.

At low temperatures, the initial film of ferrous sulfate is more viscous, diffusion is retarded, and the passive film forms at lower applied current densities. The corresponding critical current densities at 25° are lower than at 50° and still lower at 4°. Above 12% Cr, where the initial insulating film of reaction products is less important, critical current densities at 4 and 25° are about the same. But at 50° the values are higher, suggesting that passivity is less stable at this temperature, and that a reaction-product film must first partially insulate the surface before the true critical current density for passivity is attained.

The discontinuity in slopes at 10 to 12% chromium corresponds to the critical minimum concentration of Cr observed in practice for air-stable passivity. This critical chromium composition has been described by one of us[15,16] as the composition marking the filling of the surface d band of chromium energy levels by electrons of alloyed iron below 12% Cr but with d-electron vacancies present above 12% Cr. It is assumed that chromium d-electron vacancies favor optimum chemisorption of the environment (*e.g.*, O_2,), the resulting chemisorbed film constituting the passive layer.

Apparent coulombs required for passivity are higher for iron than for Cr–Fe alloys, because of the accompanying formation of a temporary $FeSO_4$ film. For Cr–Fe alloys, the initial insulating film is less important, and coulombs for passivity diminish as Cr content increases (or as temperature decreases), finally reaching at 5 to 10% Cr an average constant value of about 0.01 coulomb/cm.[2] This value is also the order of magnitude for the equivalents of the true passive film on iron as obtained from coulometric measurements of Weil[17] or from maximum oxidizing capacity of the passive film by Uhlig and O'Connor,[18] and is the value measured for 18-8 stainless steels as reported by Olivier by the same indirect method as was used in obtaining data for Cr–Fe alloys. It is also the value obtained by Uhlig and Lord[19] for the equivalent amount of oxygen consumed in forming the passive film on 18–8 stainless steel, first pickled, then washed in N_2-saturated H_2O and subsequently exposed to aerated water for several minutes up to several hours. Snavely and Hackerman[20] found 0.003 coulomb/cm.[2] based on a comparison of iron entering solution in a 0.1 *M* Na_2SO_4 + H_2SO_4, *p*H 3, and total coulombs passed during anodic passivation. They also state that the value at the Flade potential, based on cathodic reduction measurements, is much less than 0.003 coulomb/cm.[2] Several experimental factors, including local cell action during cathodic reduction, and factors entering anodic polarization as mentioned by the authors, may have combined to make their reported values too low. Except for this work, the total amount of passive film substance appears to be of the same order of magnitude whether the alloy is passivated by air exposure requiring up to 6 hours for complete passivity,[19] or by anodic polarization within as short a time as seconds or minutes. Data are summarized in Table I. The amount of passive film substance (0.01 coulomb/cm.[2]), allowing for a roughness factor of 4 as measured by the BET method[21] for 18-8 pickled in HCl–H_2SO_4, is equivalent to an oxide film about 17 Å. thick or an adsorbed close-packed nonatomic layer of O through gaps of which a monomolecular O_2 layer is chemisorbed. It is of interest in this connection that a two-layer structure has been suggested for O_2 adsorbed on W,[22] and for N_2 adsorbed on W, Mo, Ta, Nb, Cr and Fe.[23]

Structure of the Passive Film.—It can be assumed that the passivation of metal involves a typical anodic oxidation reaction

$$M + 2H_2O \longrightarrow O_2M + 4H^+ + 4e^- \qquad (2)$$

where O_2M signifies oxygen associated with metal as oxide or adsorbed gas. If it is further assumed that this reaction is at equilibrium at the activation potential, then the passive film is neither formed nor reduced at this potential. This assumption is consistent with the demonstration by others[24] that passivity cannot exist at potential

(15) H. H. Uhlig, *ibid.*, **61**, 700 (1958).

(16) "Corrosion Handbook," Edited by H. H. Uhlig, John Wiley and Sons, Inc., New York, N. Y., 1948, p. 20.

(17) K. Weil, *Z. Elektrochem.*, **59**, 11 (1955). (There has been discussion as to what Weil actually measured, the suggestion being made that he measured only the thickness of film supplementary to the passive film existing at the activation potential.)

(18) H. Uhlig and T. O'Connor, *J. Electrochem. Soc.*, **102**, 562 (1955).

(19) H. Uhlig and S. Lord, Jr., *ibid.*, **100**, 216 (1953).

(20) E. Snavely and N. Hackerman, *Can. J. Chem.*, **37**, 268 (1959).

(21) T. O'Connor and H. Uhlig, THIS JOURNAL, **61**, 402 (1957).

(22) J. Becker, *Ann. N. Y. Acad. Sci.*, **58**, 723 (1954).

(23) E. Greenhalgh, N. Slack and B. Trapnell, *Trans. Faraday Soc.*, **52**, 865 (1956).

(24) K. F. Bonhoeffer, *Z. Metallk.*, **44**, 77 (1953).

values more active than the activation or Flade potential, and that at more noble potentials, the passive film is thicker; hence at the activation potential the film is at minimum thickness consistent with passivity. It follows from the Nernst equation that the activation potential E_F for reaction 2 should be a linear function of pH or $E_F = E_F^0 + 0.059p$H, as is observed.

From values of E_F^0 one can calculate the standard free energy change.[4] For iron, E_F^0 is equal to -0.58 v. according to Franck, -0.68 v. according to Rocha and Lennartz, and -0.64 v. according to our data (Fig. 6), the average value of which is -0.63 v. This is equivalent to a standard free energy change of 58,100 cal. for reaction 2. From ΔG^0 of formation of $H_2O(l)$ and H^+, equal to $-56,690$ and 0 cal./mole, respectively, ΔG^0 of formation for O_2M is equal to $-55,100$ cal./mole. This is significantly different from the corresponding values of ΔG^0/mole O_2 for Fe_2O_3 or Fe_3O_4 equal to $-118,000$ or $-121,200$ cal., respectively.[25]

On the other hand, looking at O_2M as oxygen chemisorbed on Fe, the heat of adsorption measured by Tompkins[26] is

$$O_2 + \text{Fe surface} \longrightarrow O_2\text{(adsb. on Fe)} \qquad \Delta H^0 = -75{,}000 \text{ cal.} \quad (3)$$

Assuming that the entropy of adsorption is not far different from that for N_2 chemisorbed on Fe (-46.2 e.u./mole O_2, standard state equals $^1/_2$ coverage), and noting that ΔH is not sensitive to surface coverage,[27] it follows that at 25° from the relation: $\Delta G^0 = \Delta H^0 - T\Delta S^0$, the free energy change for reaction 3 equals $-61,250$ cal. This is more nearly in accord with the value $-55,100$ cal./mole O_2 calculated from the activation potential and supports the premise that the passive film is essentially chemisorbed O_2. Thicker passive films corresponding to potentials more noble than the activation potential probably consist of an adsorbed oxygen complex made up of O, OH, H_2O or various solute ions.[8] Furthermore the difference between calculated and observed values can be accounted for by considering the free energy of adsorption of H_2O on Fe. Since a film of adsorbed H_2O must be displaced by adsorbed O_2 in aqueous solutions when iron is passivated, but not when O_2 is adsorbed from the gas, the corresponding free energy change measured by the activation potential is actually

$$2H_2O + n H_2O\text{(adsb. on Fe)} \longrightarrow n H_2O{\cdot}O_2\text{(adsb. on Fe)} + 4H^+ + 4e^- \qquad \Delta G^0 = 58{,}100 \text{ cal.} \quad (4)$$

where $nH_2O{\cdot}O_2$(adsb. on Fe) represents nH_2O adsorbed on layers of oxygen, which in turn are adsorbed on Fe. Also, ΔG^0 for the reaction

$$2H_2O + \text{Fe surface} \longrightarrow O_2\text{(adsb. on Fe)} + 4H^+ + 4e^- \quad (5)$$

as calculated from the free energy of adsorption of O_2 on Fe $= -61,250 + 2(56,690) = +52,100$ cal. Subtracting (4) from (5) yields the reaction

(25) W. M. Latimer, "Oxidation Potentials," Prentice-Hall, Inc., New York, N. Y., 1952, p. 221.

(26) B. Trapnell, "Chemisorption," Academic Press, Inc., New York, N. Y., p. 215.

(27) Ref. 26, p. 213–216.

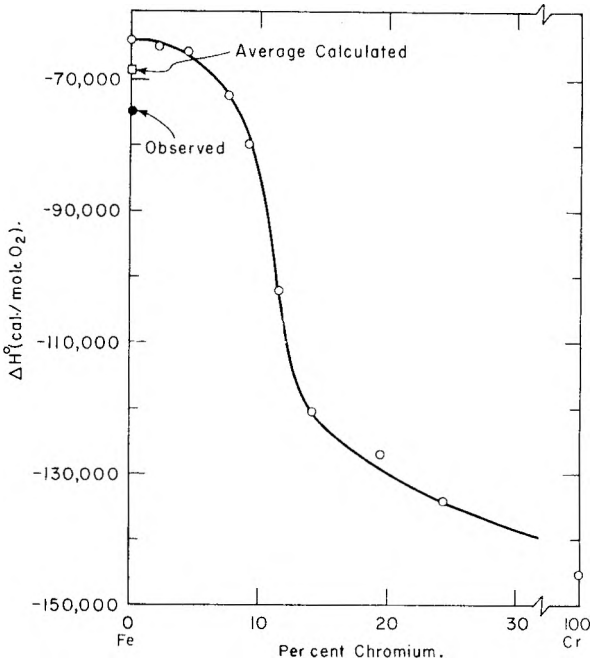

Fig. 8.—Heats of adsorption per mole O_2 on Fe, Cr–Fe alloys and Cr calculated from activation (Flade) potentials (25°).

$$\text{Fe surface} + nH_2O{\cdot}O_2\text{(adsb. on Fe)} \longrightarrow O_2\text{(adsb. on Fe)} + nH_2O\text{(adsb. on Fe)} \qquad \Delta G^0 = -6{,}000 \text{ cal.} \quad (6)$$

If we assume that the free energy of adsorption of water on the passive film is negligible compared to the free energy of adsorption of H_2O on Fe, this equation simplifies to

$$\text{Fe surface} + nH_2O \longrightarrow nH_2O\text{(adsb. on Fe)} \qquad \Delta G^0 = -6{,}000 \text{ cal.} \quad (7)$$

where n is probably equal to 1 or 2 ($^1/_2$ to 1 molecule H_2O displaced on the surface for every O atom adsorbed). This value for ΔG^0 is reasonable for physical adsorption of H_2O on Fe; it would be larger if corrected for the adsorption of H_2O on the passive film.

The value for E_F^0 for Cr according to Rocha and Lennartz is $+0.2$ volt, which similarly provides a free energy for O_2 adsorbing on Cr (in water) of $-131,800$ cal./mole O_2. The absolute value would be slightly higher taking into account H_2O adsorbed on Cr. The corresponding value for free energy of formation of Cr_2O_3 per mole O_2 is $-167,000$ cal./mole O_2[28] which value is more negative than for adsorption, as should be expected from the fact that the adsorbed oxygen film is an intermediate metastable state preceding formation of metal oxide of lower free energy. On Cr, the reported equivalents of passive film substance varies from 0.002 to 0.006 coulomb/cm.^{2} [13,14] as measured in sulfuric acid, the smaller values corresponding to times of passivation related to an arbitrary passive potential, and the larger values corresponding to potentials at or just below the value at which CrO_4^{--} is formed. A passive film of thickness corresponding to this order of chemical equivalents, therefore, is also in accord

(28) Ref. 25, p. 246.

with a chemisorbed film. Since a chemisorbed oxygen film appears to make up the passive film on iron, as the foregoing thermodynamic calculation indicates, it is reasonable that the passive film on Cr–Fe alloys, amounting similarly to about 0.01 coulomb/cm.^{2}, is chemisorbed. Additional evidence points in the same direction.[4,29,30] Snavely and Hackerman[20] also concluded that a passive film composed of sorbed ions and dipoles is reasonable. On this basis, heats of adsorption of O_2 on the Cr–Fe alloys can be calculated from activation potentials. These values plotted in Fig. 8 assume that the entropy contribution to oxygen adsorption throughout the alloy series is constant and is the same as was assumed for Fe; if corrected for adsorption of H_2O the values would be somewhat higher. Activation potentials are taken from Rocha and Lennartz' data, and the average of the three reported potentials for Fe is used for the point labelled "Average Calculated." Since $-\Delta H^0$ undergoes a sharp change around 10–12% Cr, it follows from the reasoning outlined above that the alloys have greater affinity for oxygen, beginning particularly at this composition range, leading to the more stable passive film characteristic of stainless steels.

Acknowledgment.—The authors are grateful for support of this research by the Office of Naval Research and to Jörg Osterwald for helpful discussions.

(29) H. H. Uhlig, "Metal Interfaces," Am. Soc. for Metals, Cleveland, 1952, p. 312–335.

(30) Th. Heumann and W. Rösener, *Z. Elektrochem.*, **59**, 722 (1955).

PROPERTIES OF THE ELECTRICAL DOUBLE LAYER IN CONCENTRATED POTASSIUM CHLORIDE SOLUTIONS[1]

BY J. R. SAMS, JR.,[2] C. W. LEES AND D. C. GRAHAME[3]

Contribution from the Department of Chemistry, Amherst College, Amherst, Mass.

Received June 15, 1959

The rational values of the potential of the electrocapillary maximum of mercury in contact with 2, 3 and 4 *N* aqueous solutions of potassium chloride at 25° have been determined. Differential capacity data for 2 and 3 *N* potassium chloride are presented. Values for the rate of change of capacity attributable to the anions with respect to potential between 2 and 3 *N* potassium chloride have been compared with values calculated from the theory of the diffuse double layer. Values for the components of charge in the double layer for 2.449 *N* potassium chloride have also been computed from the data. All results are found to be in agreement with the predictions of the theory at large values of cathodic polarization. At lesser values of the polarization, rather large discrepancies from the values predicted by the theory are found if specific adsorption is neglected. The anomalous results of Iofa and Frumkin concerning the nature of the double layer in concentrated solutions of acids are not observed in concentrated potassium chloride solutions.

Introduction

Electrocapillary measurements at high concentrations have not been reported in the literature, except in the case of such acids as HBr, HCl and H_2SO_4, on which work has been done by Iofa and Frumkin.[4] The results of these investigators appear to be anomalous and have been interpreted[5] as indicating repulsion of the cations from the interface at highly cathodic potentials. Such results are contradictory to the currently accepted theory of the diffuse double layer, and the question arises as to whether this represents a breakdown of the theory in concentrated solutions or some anomaly attributable to the hydronium ion.

Thus, it is of considerable interest to investigate the properties of the electrical double layer between mercury and concentrated salt solutions. First, such a study will provide a check on the validity of the current theory of the diffuse double layer, at high concentrations and, secondly, it will give an indication of the extent of the anomalous behavior observed by Iofa and Frumkin.[4,5]

(1) Requests for reprints should be addressed to the Department of Chemistry, Amherst College, Amherst, Massachusetts.

(2) Department of Chemistry, University of Washington, Seattle, Washington.

(3) Late Professor of Chemistry, Amherst College.

(4) S. Iofa and A. Frumkin, *Acta Physicochim. U.R.S.S.*, **10**, 473 (1939).

(5) A. Frumkin, private communication to D.C.G.

Experimental Details and Methods of Calculation

Potassium chloride was chosen for this study and all solutions were made up in conductivity water from once recrystallized Baker C.P. reagent. Measurements at 25° of the differential capacity of mercury in contact with 2 and 3 *N* aqueous solutions of KCl were made, using techniques which have been described previously.[6,7] Measurements of potential were made relative to a normal calomel electrode and no correction for liquid junction potentials was or should have been made. Rather, the potential relative to a hypothetical electrode reversible to the potassium ion and kept always at the concentration of the salt in question was computed. The details of this computation may be found elsewhere.[8]

The potential of the electrocapillary maximum (e.c. max.) was determined for 2, 3 and 4 *N* KCl solutions, using a streaming mercury electrode technique (ref. 9, method VI). Despite the fact that all possible precautions were taken to exclude oxygen from the system, ideal conditions were not adequately realized using this method. Therefore, Δ e.c. max. values were determined by difference in the observed values, measured by switching back and forth between two concentrations of KCl, since even though the observed values may be slightly in error, the Δ values should be more nearly correct. Rational values for 2, 3 and 4 *N* KCl were then calculated on the basis of the previously reported value for the e.c. max. of 1 *N* KCl.[9] These values, along with a value for 2.449 *N* KCl, appear in Table I. This last value was determined by interpolation from a plot of e.c. max. *vs.* concentration, including not only the present

(6) D. C. Grahame, *J. Am. Chem. Soc.*, **71**, 2975 (1949).

(7) D. C. Grahame, *Z. Elektrochem.*, **59**, 740 (1955).

(8) C. W. Lees and J. R. Sams, Jr., Thesis, Amherst College, 1958.

(9) D. C. Grahame, E. M. Coffin, J. I. Cummings and M. A. Poth, *J. Am. Chem. Soc.*, **74**, 1207 (1952).

data, but also those presented in ref. 9 for lesser concentrations of KCl. The need for the 2.449 N value is discussed below.

TABLE I

POTENTIAL OF THE ELECTROCAPILLARY MAXIMUM OF MERCURY IN KCl, 25°

Concn., moles/l.	Potentia.,[a] v.
2.0	0.5802
2.449	.5890
3.0	.5989
4.0	.6153

[a] Potentials measured relative to a normal calomel electrode.

The differential capacity curves for 2 and 3 N KCl appear in Fig. 1. Due to the methods of calculation employed (as described below) it was necessary to know accurately the position of the 3 N curve relative to the 2 N one. This was ensured by making several rapid measurements of C values at potentials ranging from −0.60 to −1.80 v. in steps of 0.20 v. at each concentration, switching back and forth between solutions as rapidly as possible. This minimized errors arising from variations in the condition of the dropping mercury electrode. Subtraction then gave ΔC values between these two concentrations at these potentials. Several ΔC values were determined at each potential and their median values calculated. A smoothed plot of ΔC *vs.* E^+ was then constructed and this curve was used to draw a 3 N curve relative to the 2 N one. This 3 N curve coincided sufficiently with the 3 N curve determined in the usual way so that we could safely assume that we had fixed the position and shape of the complete 3 N curve relative to the 2 N one.

The equations employed in the calculations have been presented elsewhere,[10-12] but it will be convenient to restate some of them here. From a purely thermodynamic argument it is possible to derive the equations

$$\nu_+ (\partial q/\partial \mu)_{E^-} = (\partial \Gamma_+/\partial E^-)_\mu \text{ and}$$
$$\nu_- (\partial q/\partial \mu)_{E^+} = (\partial \Gamma_-/\partial E^+)_\mu \quad (1)$$

(ref. 10, eq. 26), where ν_+ and ν_- are the number of cations and anions formed by dissociation of one molecule of salt, q is the surface charge density of electricity on the metallic phase, μ is the chemical potential of the salt, $\Gamma_+(\Gamma_-)$ is the superficial density of cations (anions) and $E^+(E^-)$ is the potential relative to an electrode reversible to the cation (anion). These two equations may be differentiated with respect to potential to give

$$\nu_+(\partial C/\partial \mu)_{E^-} = (\partial C_+/\partial E^-)_\mu \text{ and}$$
$$\nu_-(\partial C/\partial \mu)_{E^+} = (\partial C_-/\partial E^+)_\mu \quad (2)$$

where C_+ and C_- represent that part of the capacity of the double layer attributable to cations and anions, respectively, and are defined as

$$C_+ = \partial \Gamma_+/\partial E^- \text{ and } C_- = \partial \Gamma_-/\partial E^+ \quad (3)$$

After rearrangement, the second of equations 2 gives (for a 1:1 electrolyte)

$$\Delta C_{E^+} = (dC_-/dE^+)_\mu \Delta\mu \quad (4)$$

If specific adsorption is assumed absent, no ions will populate the region between the interface and the outer Helmholtz plane and equation 4 may be rewritten as

$$\Delta C_{E^+}{}^{de} = (dC_-{}^{de}/dE^+)_\mu \Delta\mu \quad (5)$$

where the superscript de refers to the diffuse region of the double layer and indicates that the variation is with respect to the applied potential E^+ and not some other potential.[13] Equation 5 enables us to compare the experimental results

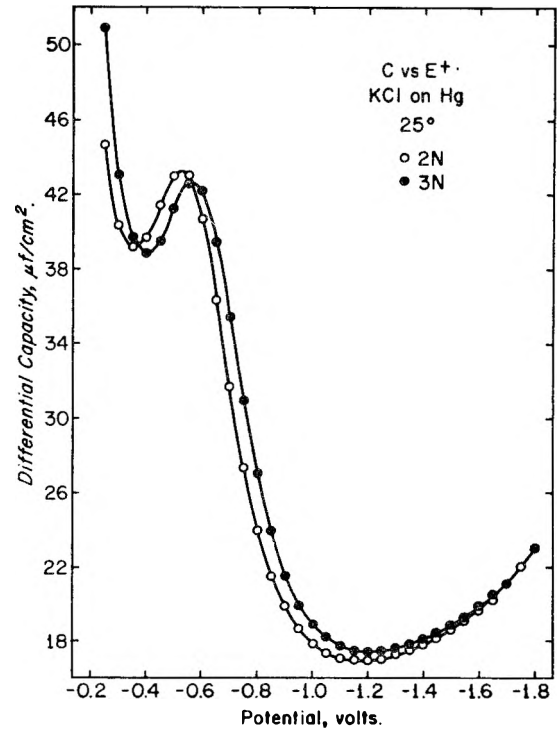

Fig. 1.—Differential capacity of the electrical double layer at a mercury–potassium chloride solution interface C as a function of potential E^+.

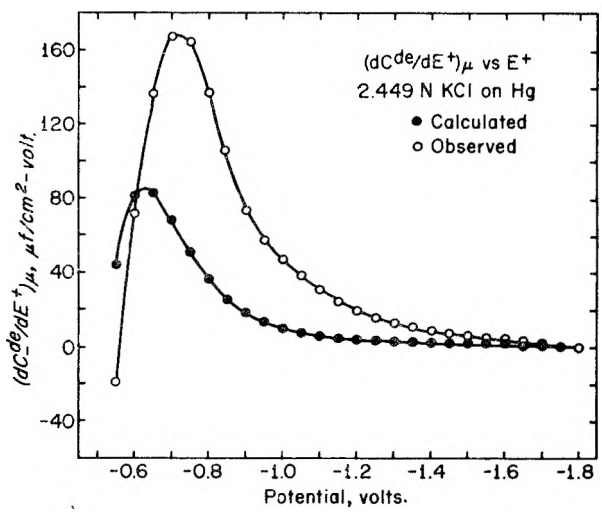

Fig. 2.—Observed and calculated values of the rate of change of capacity attributable to the anions with respect to potential $(dC^{de}/dE^+)_\mu$ as a function of potential E^+.

with the predictions of the theory as follows. $(dC^{de}/dE^+)_\mu$ is given by diffuse double layer theory as

$$(dC_-{}^{de}/dE^+)_\mu = \frac{1}{2(1+v^2)^{1/2}} \left[([1+v^2]^{1/2} - v) \frac{dC^{de}}{dE} + \frac{(C^{de})^2}{2A(1+v^2)} \right] \quad (7)$$

(ref. 12, eq. 25). In this equation, $v = \eta^d/2A$, and A is a constant, equal to 5.8716 $c^{1/2}$ for aqueous solutions at 25°, where c is the molar concentration of the solution. In calculating v, η^d was taken as being equal to $-q$ (as a consequence of assuming no specific adsorption), which in turn may be determined as a function of E^+ by numerical integration of a differential capacity curve for 2.449 N KCl, this concentration being one whose activity is equal to the geometric mean of the activities of 2 and 3 N KCl. This 2.449 N curve was drawn between the two observed curves

(10) D. C. Grahame, *Chem. Revs.*, **41**, 441 (1947).
(11) D. C. Grahame, *J. Chem. Phys.*, **21**, 1054 (1953).
(12) D. C. Grahame and B. A. Soderberg, *ibid.*, **22**, 449 (1954).
(13) There is another differential capacity C^d of the diffuse double layer defined as $C^d = -d\eta^d/d\psi^0$ where η^d is the surface charge density of the diffuse region and ψ^0 is the potential of the outer Helmholtz plane. The potential ψ^0 is very different from the applied potential; and moreover $d\psi^0 \neq dE^+$, so that these two capacities are quite different.

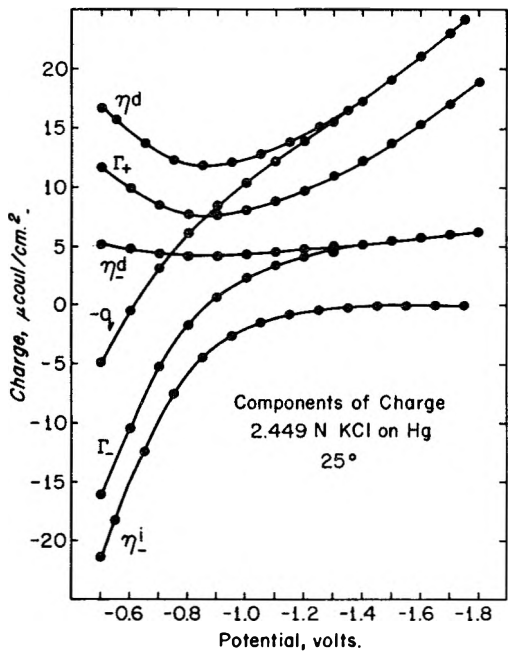

Fig. 3.—Components of charge in the double layer between mercury and 2.449 N potassium chloride solution as a function of potential. $-q$ is total charge; η^d is total charge in the diffuse double layer; Γ_+ is charge attributable to cations in the double layer. η^d is charge attributable to anions in the diffuse double layer; η^i is charge attributable to anions adsorbed on the mercury surface; Γ_- is the sum of these two.

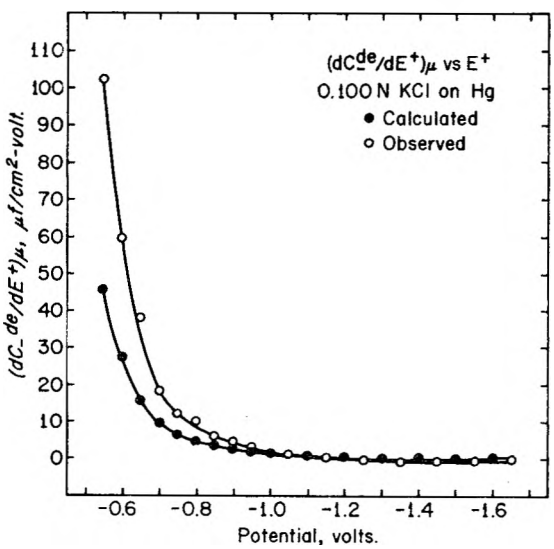

Fig. 4.—Observed and calculated values of the rate of change of capacity attributable to the anions with respect to potential $(dC^{de}/dE^+)_\mu$ as a function of potential E^+ calculated from data of Grahame and Soderberg.[12]

by plotting average values of the 2 and 3 N curves. The integration was carried out starting at the e.c. max., thus setting the constant of integration equal to zero. Values of C and dC/dE were also obtained from the 2.449 N curve by direct reading and by graphical tangential slope measurements, respectively, it being assumed that $C = C^{de}$ and $dC/dE = dC^{de}/dE$ (again as a consequence of our assumption of no specific adsorption). Experimental values for $(dC^{de}/dE^+)_\mu$ were obtained from ΔC values through equation 5. Figure 2 shows observed and calculated values of this quantity.

From the data it is also possible to calculate the components of charge in the double layer. A numerical integration of the observed $(dC_-/dE^+)_\mu$ curve with respect to potential gives C_- as a function of E^+. The constant of integration is obtained by calculating the value of C_- at -1.805 v. by use of equation 62 of ref. 11. This potential is selected because the convergence of the two curves in Fig. 2 indicates that the diffuse double layer theory upon which the calculation is based holds best in the highly cathodic region. An integration of the C_- *vs.* E^+ curve gives Γ_-. Again it is necessary to determine the constant of integration, this time by calculating Γ_- at a potential of -1.81 v. (the most cathodic value obtainable without extrapolation), from equations 43 and 72 of ref. 10. Γ_+ is otained by difference from q and Γ_-. The surface excess of *specifically adsorbed* anions η^i is found by subtracting from Γ_- the surface excess of anions in the *diffuse* part of the double layer η^d. The latter is found from Γ_+ using equations 72 and 73 of ref. 10. The validity of these calculations rests on the requirement that cations be present solely in the diffuse part of the double layer. Summing Γ_+ and η^d_- gives η^d. This quantity can also be obtained from the relation

$$\eta^d = -2A \sinh(ze\psi^0/2kT) \qquad (8)$$

and this was used as a check on the numerical accuracy of the results. All the components of charge are shown in Fig. 3.

Discussion of Results

The differential capacity curves for 2 and 3 N KCl (Fig. 1) exhibit the same general shape characteristic of lower concentrations of the same salt, and the 2 N curve agrees quite well with independent data obtained at this concentration.[14] The good agreement between the points calculated from ΔC values and those obtained directly for 3 N KCl indicates that the shape and position of this curve relative to the 2 N curve have been closely established.

It is clear that the discrepancy between the two curves in Fig. 2 is due to specific adsorption of the chloride ion on the mercury surface. It will be remembered that in the calculation of $(dC^{de}/dE^+)_\mu$ by equation 7 it was assumed that specific adsorption was absent. However, if anions are present in the inner region in the cathodic branch of the curve, this causes an increase in the negative charge on the metallic phase and hence an increase in the capacity of the double layer. This accounts for the fact that the observed values are greater than the calculated ones.

The curves converge as the potential becomes more cathodic, due to the fact that the bonds between the adsorbed anions and the mercury are weakened by the increasingly negative charge on the mercury and anions are repelled from the interface. Thus, the discrepancy due to specific adsorption decreases.

It may finally be noted that both curves approach zero as the potential becomes more cathodic. What is actually observed is that $(\partial C/\partial\mu)_{E^+}$ equals zero at some highly cathodic E^+ (see Fig. 1). But by equation 2, this is equivalent to observing that $(\partial C_-/\partial E^+)_\mu$ equals zero. Since the quantity C_- is the differential of Γ_- with respect to E^+, one observes that $(\partial^2\Gamma_-/\partial E^{+2})_\mu$ approaches zero. This phenomenon is also predicted by the theory of the diffuse double layer. From equation 73 of ref. 10 it may be seen that

$$(d^2\eta_-{}^d/dy^2) = -(A/4)\exp(y/2) \qquad (9)$$

where y is a monotonic function of E^+. Hence as y approaches a large negative value, $d^2\eta_-{}^d/dE^{+2}$

(14) D. C. Grahame, unpublished results.

approaches zero. This precise mathematical picture may be expressed qualitatively by saying that as E^+ approaches large negative values, the negative charge on the double layer approaches a limit. Hence $(\partial C_-^{de}/\partial E^+)_\mu$, the second derivative of this charge, approaches zero.

It is instructive to compare Fig. 2 with Fig. 4, in which observed and calculated values of $(dC_-^{de}/dE^+)_\mu$ for 0.1 N KCl calculated from the data of Grahame and Soderberg[12] are plotted against E^+. A discrepancy of the type found at 2.449 N is observed but does not become apparent until relatively more anodic potentials are reached. If one again attributes the discrepancy to specific adsorption, this behavior is entirely expected.

The components of charge (Fig. 3) behave as one would expect from the theory, and the curves are qualitatively very similar to those presented previously for more dilute solutions.[10] At large values of negative polarization, the surface excess of specifically adsorbed anions goes to zero, as all the anions are expelled from the inner region of the double layer. At these same potentials η^d becomes identical with $-q$, and η_-^d becomes identical with Γ_-, as must be the case when specific adsorption is absent. It is to be noted that Γ_+ is positive even on positive polarization, since as a result of specific adsorption, more anions are held to the mercury surface than corresponds to the positive charge on the mercury. Hence, the net charge is negative, and cations are attracted. Iofa and Frumkin[4] report that Γ_+ decreases as E approaches large negative values in solutions containing high concentrations of HCl, HBr and H_2SO_4. Such anomalies are not found in concentrated solutions of potassium chloride and may possibly be caused by the nature of the hydronium ion.

Conclusions

The agreement obtained between observed and calculated values for the rate of change of capacity attributable to the anions with respect to potential for 2.449 N potassium chloride at large values of cathodic polarization indicates that the theory of the diffuse double layer remains valid in this concentration range as well as in more dilute solutions. The discrepancies observed at lesser values of the cathodic polarization are evidently due to specific adsorption of the chloride ion on the mercury surface, and if this adsorption were taken into account, good agreement between theory and experiment should be obtained over the entire range of potentials. The values calculated for the components of charge likewise show no anomalies due to increasing the concentration range of the measurements. The results of Iofa and Frumkin,[4] which indicate repulsion of the cations from the interface at high values of cathodic polarization in concentrated acid solutions, are not observed in concentrated solutions of potassium chloride.

A STUDY OF THE ZIRCONIUM–HYDROGEN AND ZIRCONIUM–HYDROGEN–URANIUM SYSTEMS BETWEEN 600 AND 800°

BY LEE D. LA GRANGE, L. J. DYKSTRA, JOHN M. DIXON AND ULRICH MERTEN

John Jay Hopkins Laboratory for Pure and Applied Science, General Atomic Division of General Dynamics Corporation, San Diego, Cal.

Received June 22, 1959

The zirconium–hydrogen and zirconium–uranium–hydrogen systems have been investigated at various temperatures between 600 and 800° by means of hydrogen-dissociation-pressure measurements in conjunction with high-temperature X-ray diffraction techniques. Phase diagrams deduced from the data are presented. The results on the binary zirconium–hydrogen diagram are in good agreement with earlier work. A ternary zirconium–uranium–hydrogen diagram is proposed which must be considered tentative in several respects. No new phases were encountered that are not already known to exist in the related binary systems. The miscibility gap appearing in the body-centered-cubic solid-solution field of the zirconium–uranium diagram rapidly expands with the addition of hydrogen. The solubility of uranium in the face-centered zirconium–hydride phase is very limited.

Introduction

In recent years a considerable amount of work on the binary zirconium–hydrogen system has been reported in the literature. Ells and McQuillan[1] published a fairly complete phase diagram based on the results of several investigators who all used the hydrogen-dissociation-pressure technique. The diagram of Ells and McQuillan, which differs but little from that given in Fig. 1, shows a eutectoid at 547° at a composition of 32 at.-% hydrogen.

A more or less complete diagram based entirely on X-ray diffraction work was published by Vaughan and Bridge.[2] Their diagram deviates from the previously cited one in a few respects. First, the $\alpha + \beta$ phase region extends much farther to the hydrogen-rich side; second, the eutectoid composition is shown near 42 at.-% hydrogen. On the basis of heat-capacity measurements, Douglas and Victor[3] concluded that the diagram given by Vaughan and Bridge is essentially correct.

In view of these discrepancies, it was considered worthwhile to redetermine parts of the zirconium–hydrogen diagram by dissociation-pressure measurements. In addition, it was found possible to extend the measurements into a few regions not investigated by other workers.

Little effort had been made previously to investi-

(1) C. E. Ells and A. D. McQuillan, *J. Inst. Metals*, **85**, 89 (1956).
(2) D. A. Vaughan and J. R. Bridge, *J. Metals*, **8**, 528 (1956).
(3) T. B. Douglas and A. C. Victor, *J. Research Natl. Bur. Standards*, **61**, 13 (1958).

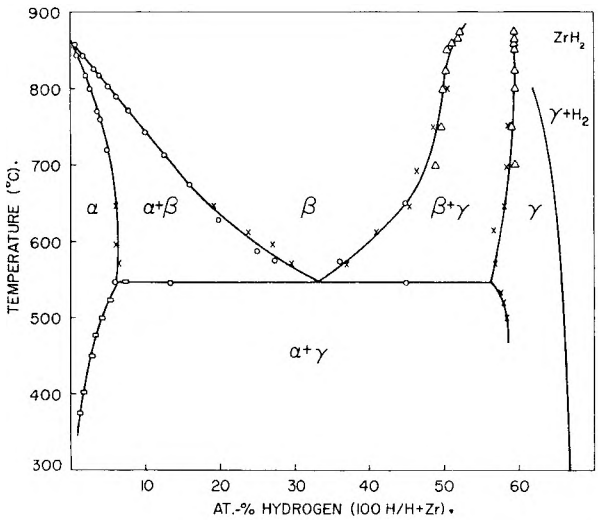

Fig. 1.—Zirconium–hydrogen phase diagram derived from various sources (see ref. 1): △, Edwards, Levesque and Cubicciotti; □, Gulbransen and Andrew; O, Ells and McQuillan; ×, present authors.

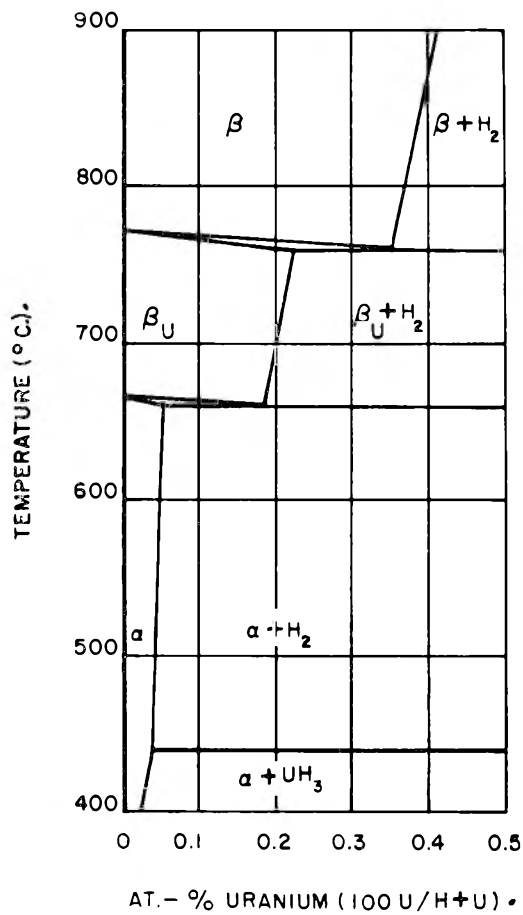

Fig. 2.—Uranium–hydrogen phase diagram at 1 atm. (based on ref. 5).

gate the ternary system. The only work reported is by Singleton, *et al.*,[4] who studied in detail the phase transformations occurring when a 28 at.-% uranium alloy was hydrided at temperatures between 540 and 800°. Both dissociation-pressure and X-ray techniques were employed. The X-ray data were obtained on quenched specimens.

(4) J. H. Singleton, R. Ruka and E. A. Gulbransen, "The Reaction of Hydrogen with a 50 Weight Percent Alloy of Uranium and Zirconium Between 542 and 798°," Westinghouse Electric Corporation Report AECU-3630, November 16, 1956.

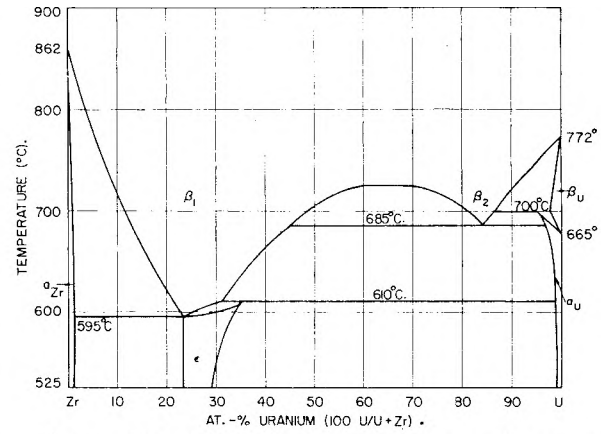

Fig. 3.—Zirconium–uranium phase diagram (based on A. A. Bauer, S. Kass and K. M. Goldman, "Proceedings of the Second United Nations International Conference on the Peaceful Uses of Atomic Energy," United Nations, Geneva, 1958, Paper UN/P/1785).

The determination of the ternary phase diagram is greatly facilitated by the fact that the three related binary diagrams are reasonably well established. These binary diagrams are shown in Figs. 1, 2 and 3. The zirconium–hydrogen diagram is based on data taken from previous studies as well as from the present work. The zirconium–uranium diagram also contains contributions by various other investigators and is tentative in several respects.

In the present work, the experimental approach was as follows: the phase boundaries were determined by measuring the hydrogen-dissociation pressure during hydriding of several zirconium–uranium alloys at various temperatures. From these measurements and the known binary diagrams, tentative isothermal sections of the ternary diagram could be deduced without serious difficulty.

In addition to these measurements, X-ray diffraction patterns were taken on alloys of selected compositions as a check of the validity of this diagram. Since the high-temperature phases usually are not retained during quenching of the alloy, all X-ray data were taken at temperature.

The excellent dissociation-pressure data by Singleton, *et al.*,[4] were of great benefit to us and have been used in constructing the diagrams which are presented here.

Preparation of the Alloys and Experimental Technique

Reactor-grade, crystal-bar zirconium made by the Foote Mineral Company was used for the study of the zirconium–hydrogen system and for preparing the zirconium–uranium alloys, and uranium metal, analytical reagent-grade, made by the Mallinckrodt Chemical Works was used in the alloys. The oxygen content of the zirconium and uranium stock was not known. The zirconium–uranium alloys were made by arc-melting in a water-cooled copper crucible in a carefully purified inert-gas atmosphere. Atmosphere purity during melting was maintained by a hot zirconium "getter" foil inside the arc furnace. The homogeneity of the alloys was checked and found to be excellent. Chemical analysis

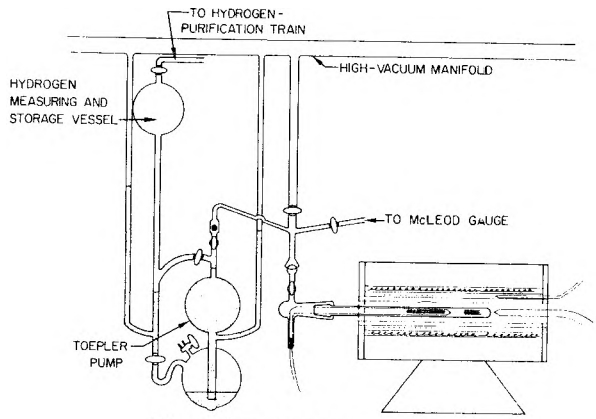

Fig. 4.—Hydriding apparatus.

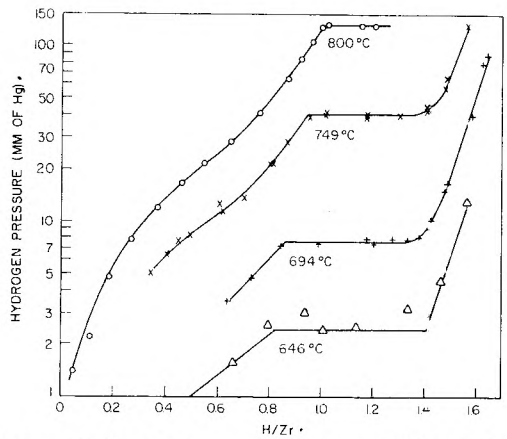

Fig. 5.—Hydrogen pressure *versus* composition isotherms for zirconium-hydrogen system between 650 and 800°.

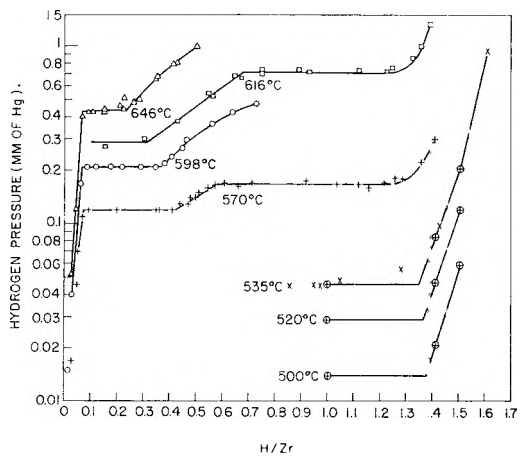

Fig. 6.—Hydrogen pressure *versus* composition isotherms for zirconium-hydrogen system between 500 and 650°.

showed that the uranium content of different sections of a sample were constant within the experimental error. The zirconium-uranium alloys investigated were 1.69, 3.26, 5.05, 15.0 and 54.0 at.-% uranium. A 28.0 at.-% uranium alloy was studied by Singleton, *et al.*[4]

The hydriding apparatus is shown schematically in Fig. 4. Small known increments of hydrogen that had been purified by passing it over activated charcoal at liquid-nitrogen temperature were taken from the storage and measuring vessel through a Toepler pump into the reaction tube. The hydrogen pressure in the reaction tube was measured with a McLeod gauge (for pressures below 2 mm.) or with a mercury manometer.

At 800°, hydriding of massive samples weighing a few grams occurred very rapidly. At lower temperatures, where

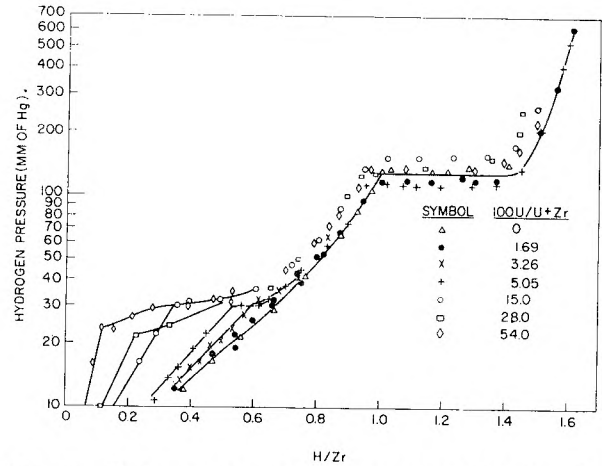

Fig. 7.—Hydrogen pressure *versus* composition for zirconium-uranium-hydrogen system at 795°.

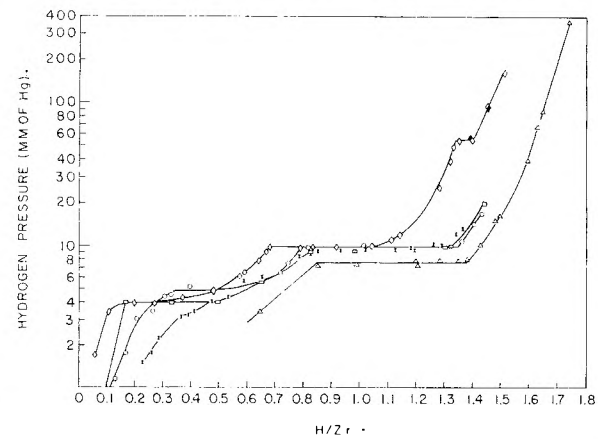

Fig. 8.—Hydrogen pressure *versus* composition for zirconium-uranium-hydrogen system at 687°.

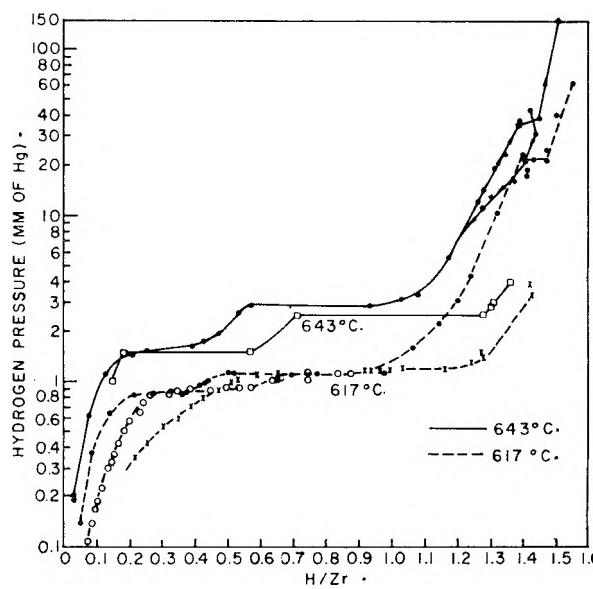

Fig. 9.—Hydrogen pressure *versus* composition for zirconium-uranium-hydrogen system at 643 and 617°. The symbol ● indicates (100 U/U + Zr) = 54.0 rather than 1.69 as in Fig. 7.

the reaction became sluggish, the time to reach equilibrium was reduced materially by the use of samples consisting of very coarse filings. Even then, at 625° several hours were

required and the time increased with increasing uranium and hydrogen content.

No chemical analysis was made of the samples after hydriding. The ready reproducibility of the dissociation-pressure curves for different samples of a given alloy composition and also during dehydriding was taken as evidence that even if a slight pick-up of oxygen or other impurity occurred during handling and hydriding, this did not seriously affect the results.

X-Ray diffraction patterns were recorded by a Norelco diffractometer using molybdenum Kα radiation. Powder samples sealed in evacuated, thin-walled quartz capillaries were mounted inside a furnace provided with a slit for the X-rays. This simple setup proved adequate for phase identification, although precise lattice-spacing determinations were not possible. To prevent thermal diffusion of the hydrogen along the length of the specimen (2 to 3 mm.) three separate furnace windings were employed to minimize the thermal gradient.

The 54 at.-% alloys yielded extremely weak patterns and were not further investigated. During exposure of the alloys of high uranium content at 800°, there was sometimes evidence of a reaction occurring between the quartz and the alloy. In such an event the run was disregarded.

Results and Discussion

The phases that occur in the binary systems are designated as shown in Figs. 1, 2 and 3. As a rule, the conventional nomenclature has been adopted except where this would lead to confusion in discussing the ternary system.

The high-temperature body-centered-cubic phase, which is common to all binary systems, has been called β. This phase is designated β_1 if it appears on the zirconium-rich side and β_2 if it appears on the uranium-rich side of the miscibility gap.

In Figs. 5 through 9 the logarithm of the isothermal dissociation pressure is plotted against the atomic composition ratio H/Zr. The binary as well as the ternary diagrams are drawn for a pressure on the system of 1 atm.

The Zirconium–Hydrogen System.—Pressure *versus* composition isotherms for several temperatures are presented in Figs. 5 and 6. Where the pressure is composition-dependent, a single solid phase exists. On the plateaus where the pressure is independent of composition, two solid phases in equilibrium are present, in accordance with the phase rule. The discontinuities in slope locate phase boundaries. There is some uncertainty in locating the hydrogen-poor boundary of the γ-phase field because of the absence of a sharp break in the curve. The points on the boundary are best determined from a log pressure *versus* $1/(2 - \mathrm{H/Zr})$ plot. Below 550°, hydriding proceeded very slowly and data were most easily obtained by measuring the dissociation pressure as a function of temperature at constant composition. The points plotted on the 500, 520, and 535° isotherms in Fig. 6 were found by interpolating plots of log p *versus* $1/T$ for the three compositions. The fragment of an isotherm at 535° (marked by x's in Fig. 6) was measured as a check on the validity of this procedure.

The zirconium–hydrogen diagram in Fig. 1 is based on data from a number of sources, all obtained by dissociation-pressure measurements. The agreement between these data is indeed satisfactory. The eutectoid is found at 33 at.-% hydrogen.

It follows from thermodynamic considerations that the initial slopes of the phase boundaries meeting at the α-β transition point of pure zirconium differ by $\Delta H/RT^2$, where ΔH is the latent heat of transformation of pure zirconium and T is the absolute temperature of transformation, 1149°K. From Fig. 1 we calculate $\Delta H = 1050$ cal./mole, which is in reasonable agreement with the value of 900 cal./mole derived from heat-capacity measurements of pure zirconium.[3] Evidently the direction of the $(\alpha + \beta)$-β boundary as drawn by Vaughan and Bridge[2] in their phase diagram cannot be correct.

The Zirconium–Uranium–Hydrogen System.—The pressure *versus* hydrogen composition isotherms for several temperatures are shown in Figs. 7, 8 and 9. For comparison with the previously discussed curves, the atomic ratio H/Zr is again plotted as the abscissa. The key in Fig. 7 identifies the hydriding curves for the various alloys in all three figures.

In interpreting the curves, one is guided by the known related binary diagrams and the following rules. In any single-solid-phase field the pressure shows a rapid and steady increase with increasing hydrogen content. In general, when a boundary of a single-phase field is crossed, a two-phase field is entered. The appearance of a two-solid-phase region will manifest itself by a sudden decrease in slope. The slope in a two-phase field can be very small but must remain finite, since the phase rule requires that the pressure can only be constant for a series of compositions if these all fall on a single tie line, so that the phases in equilibrium do not change their composition. In the presence of three solid phases in equilibrium, the pressure is independent of over-all composition.

The 795° isotherms in Fig. 7 seem to offer the least difficulty in interpretation. The early, steeply rising portion of each curve indicates the solid solution of hydrogen in a single phase, β. The following sharp break onto a plateau-like region indicates the start of a two-phase field. The near coincidence of the curves for all alloys and for pure zirconium beyond H/Zr = 0.7 is conspicuous and suggests that the reaction occurring along these plateaus is the rejection of a uranium-rich β_2 phase. This rejection is completed at the upward bend in the curves at about H/Zr = 0.7, at which point β_2 is nearly pure uranium and β_1 is largely depleted of uranium. Beyond this H/Zr ratio the behavior of the system closely resembles that of the zirconium–hydrogen system, with the uranium-rich phase participating only slightly in further hydriding. Therefore, the three solid phases in equilibrium along the true pressure plateaus between H/Zr = 1 and H/Zr = 1.4 must be β_1, β_2, and the γ-hydride. Apparently, the solubility of uranium in the γ-hydride at this temperature is very small. The final, steeply rising portion of the curves represents the hydriding of the γ-hydride.

The 800° section of the ternary phase diagram is shown in Fig. 10. (The key in Fig. 10 identifies the symbols in the following three figures.) The solid lines across the diagram, ending in the

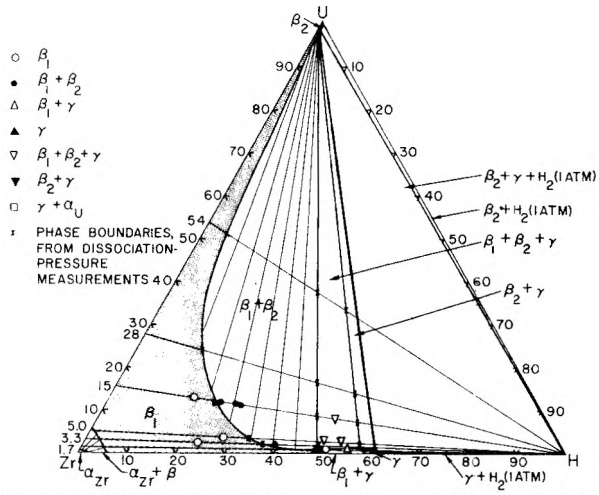

Fig. 10.—795° section of the zirconium–uranium–hydrogen phase diagram.

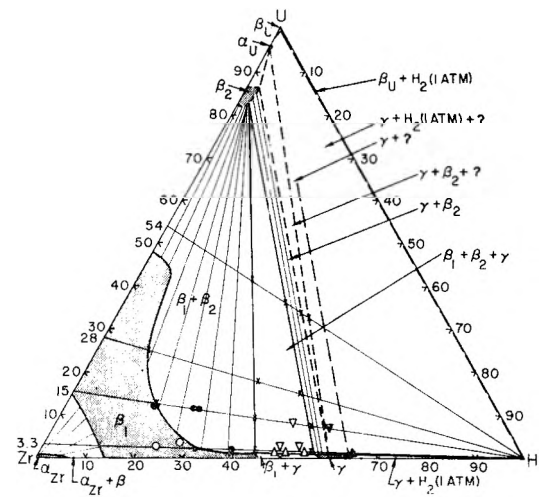

Fig. 11.—687° section of the zirconium–uranium–hydrogen phase diagram (tentative).

hydrogen corner, indicate the hydriding paths of the various alloys. Though the number of available data fixing the boundaries of the phase fields is rather limited, the position of the boundaries is fairly well determined. The two long boundaries of the $\beta_1 + \beta_2 + \gamma$ region clearly intersect near the uranium corner of the diagram. X-Ray data showed that the lattice spacing of β_2 was slightly larger than that of body-centered-cubic uranium at 800°. Since the hydriding curve for the 1.69 at.-% uranium alloy shows no break, whereas the 3.26 at.-% alloy does, the β_1 corner of the $\beta_1 + \beta_2 + \gamma$ triangle lies slightly above the hydriding path of the 1.69 at.-% alloy. The accuracy of the pressure measurements is inadequate to determine the tie lines from the data in Fig. 7. The directions of the tie lines drawn in the two-phase fields are believed to be approximately correct.

The solubility of hydrogen in uranium is extremely small in comparison with its solubility in zirconium. The standard heat of solution of hydrogen in body-centered-cubic uranium, calculated from data in ref. 5, is 1000 cal./mole, as compared with a value of −38,000 cal./mole in body-centered-cubic zirconium derived from the dissociation-pressure measurements. The large difference between these values explains thermodynamically the rejection of the uranium-rich phase during hydriding.

The hydriding curves and the isothermal section of the ternary diagram at 687° are shown in Figs. 8 and 11. The initial composition-sensitive portion of the curves for alloys of 28 at.-% uranium or less is in the β_1 region and the break onto the first plateau is again interpreted as the appearance of a uranium-rich β_2 phase. The 54 at.-% alloy is peculiar in that according to the zirconium–uranium diagram this alloy is already in the $\beta_1 + \beta_2$ field without the addition of hydrogen. Here, the initial steep rise reflects the hydriding of β_1 and to a lesser degree of β_2, with little change in the Zr/U ratio of either phase. At a critical hydrogen composition, $H/Zr \approx 0.12$, the sharp break in the hydriding curve onto a plateau indicates a further rejection of uranium from the β_1 phase.

There is some question as to whether the uranium-rich phase in this portion of the diagram is really

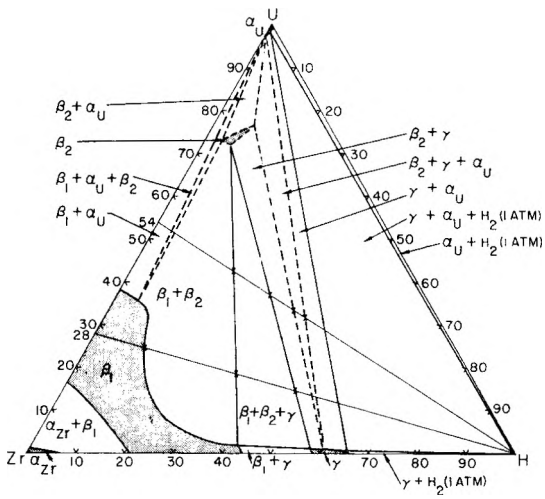

Fig. 12.—643° section of the zirconium–uranium–hydrogen phase diagram (tentative).

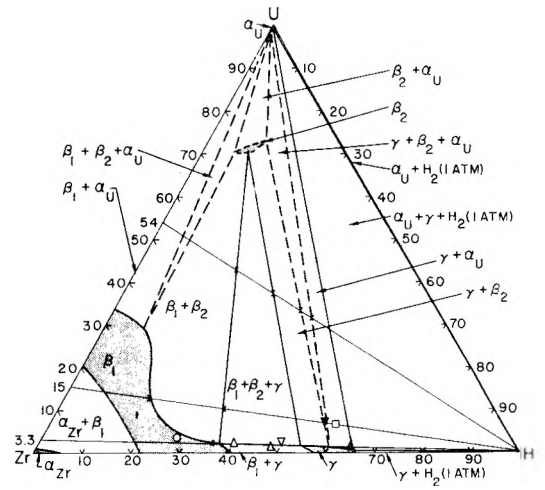

Fig. 13.—617° section of the zirconium–uranium–hydrogen phase diagram.

(5) H. A. Saller and F. A. Rough, "Compilation of U.S. and U.K. Uranium and Thorium Constitutional Diagrams," Battelle Memorial Institute Report BMI-1000, June 1, 1955.

Table I

Phases Determined by X-Ray Diffraction

Sample no.	Compn. (atom ratio) U/U + Zr	H/H + Zr	Phases at 625°	Phases at 700°	Phases at 800°
1	0.017	0.49	γ + tr β_1	β_1 + tr γ	β_1 + tr β_2
2	.017	.51		γ + β_1	β_1
3	.017	.55		γ + β_1	γ + β_1
4	.033	.24		β_1	β_1
5	.033	.40	γ + β_1	β_1 + tr β_2	β_1 + β_2
6	.033	.65	γ	γ + tr α_U(?)[a]	γ + tr β_2
7	.050	.29	β_1	β_1	β_1
8	.050	.50		β_1 + β_2 + tr γ	β_1 + β_2 + tr γ
9	.050	.51	β_1 + γ + β_2(?)[a]		
10	.050	.54		γ + tr β_1 + tr β_2	β_1 + β_2 + γ
11	.050	.66			γ + tr β_2
12	.15	.20		β_1 + β_2	β_1
13	.15	.30	β[b]	β_1 + β_2	β_1 + β_2
14	.15	.31		β_1 + β_2	β_1 + β_2
15	.15	.32		β_1 + β_2	
16	.15	.32	β_1 + β_2(?)[a]		
17	.15	.45	β_1 + γ + β_2(?)[a]		
18	.15	.53		β_1 + β_2 + γ	β_1 + β_2 + tr γ
19	.15	.61	β_2 + γ	β_2 + γ	
20	.15	.63	γ + α_U		

[a] Doubtful if β_2 or α_U. [b] Single body-centered-cubic phase with broadened lines.

β_2, since in the binary zirconium–uranium system at 687°, at least two uranium-rich phases—β_2 and β_U and possibly a third one, α_U—appear. However, according to Figs. 2 and 3, both β_U and α_U have a relatively small solubility for zirconium as well as for hydrogen, and the top of the three-phase triangle in Fig. 11 is clearly located near the β_2 region. The extent of the β_2 field was not precisely determined. The break in the hydriding curve for the 3.26 at.-% alloy is not clearly discernible and the β_1 corner of the $\beta_1 + \beta_2 + \gamma$ three-phase triangle is therefore drawn just below the hydriding path of this alloy.

Beyond the $\beta_1 + \beta_2$ field the interpretation is much the same as at 795°, except that the 54 at.-% alloy breaks into a narrow second three-phase plateau. Two of the three phases in equilibrium have to be β_2 and γ, but the third phase may be either α_U or β_U. The curves for the low-uranium alloys either were not extended far enough to intercept this plateau or the region is too narrow to be seen on these curves. The dissociation pressure of the alloy beyond this three-phase region is considerably higher than for pure zirconium of equal H/Zr ratio. This indicates some solubility of uranium in the γ-hydride at this temperature.

The hydriding curves at 643 and 617° differ but slightly from those at 687° and are shown in Fig. 9. The corresponding isothermal sections of the ternary diagram are shown in Figs. 12 and 13.

These temperatures are well below the β_2-eutectoid temperature of 685° in the zirconium–uranium system, and the β_2 phase appears as an island at the top of the $\beta_1 + \beta_2 + \gamma$ three-phase triangle. The extent and precise location of this island are not well defined. The narrow $\beta_1 + \beta_2 + \alpha_U$ three-phase region which necessarily exists between the $\beta_1 + \alpha_U$ and $\beta_1 + \beta_2$ phase fields is beyond detection. The final, narrow, three-phase plateau, which appears at 687° on the 54 at.-% alloy curve, is again unmistakably present on the curves for this alloy both at 643 and 617°. It is here believed to be a $\beta_2 + \gamma + \alpha_U$ region since the existence of β_U at these temperatures is not likely.

The hydriding and dehydriding curves around this final plateau did not coincide as they did in Fig. 9. This hysteresis phenomenon, which was not observed at the higher temperatures, is apparently caused by nucleation difficulties in the β_2 phase.

X-Ray Diffraction Data.—X-Ray data were obtained on only a limited number of samples, the compositions of which were chosen in those phase fields which were considered to be of most interest. Identification of the phases was often difficult because of the weak diffraction patterns and the close overlap of several of the principal diffraction lines of some of the phases. Sometimes, especially in the higher-uranium samples, traces of UO_2 were detected.

The results are shown in Table I and the points obtained are plotted in the isothermal sections in Figs. 11, 12 and 13. The temperatures at which the X-ray data were taken for each isothermal section are slightly higher than those for the dissociation-pressure measurements. In general, the X-ray data confirm our other results, although a number of uncertainties remain, mainly at 625°. In particular, the diffraction pattern of sample 13 at 625° showed only the lines of a single β-phase with a lattice parameter intermediate between those for β_1 and β_2. The line-broadening was considerable, however, and suggested that segregation of a second phase, presumably β_2, had occurred, though on a very small scale. Sample 16, similar to sample 13, therefore was annealed for thirty days at 625°, and this treatment resulted indeed in a complete splitting of the (110)-reflection. Unfortunately, because of high background

scattering, the other lines were too weak for one to decide conclusively whether the second phase was β_2 or α_U.

Acknowledgment.—We are indebted to F. D. Carpenter for preparing the zirconium–uranium alloys.

SOME ASPECTS OF THE RADIATION CHEMISTRY OF LIQUID ALIPHATIC CARBOXYLIC ACIDS[1]

BY RUSSELL H. JOHNSEN

Contribution from the Chemistry Department, Florida State University, Tallahassee, Florida

Received June 29, 1959

The decomposition of ten aliphatic carboxylic acids by γ-radiation has been studied with particular reference to their relative rates of decarboxylation. The effects of structural variation, added iodine and temperature have been investigated as well as the distribution of free radicals for one of the acids as determined by radio-iodine trapping techniques. It is suggested that the mechanism of decarboxylation involves the intermediate formation of free alkyl and carboxyl radicals.

Introduction

The radiolysis of carboxylic acids in the pure state has been studied previously by Whitehead,[2] Newton[3] and Burr.[4]

Aqueous solutions of varying concentration of acetic acid up to 16 *M* have been investigated by Garrison.[5]

With the exception of the work by Burr, all investigations have involved the use of heavy particle radiation, either alphas from naturally radioactive materials or cyclotron beams.

The volatile products of radiolysis of compounds of this class are generally agreed to be carbon dioxide, the saturated hydrocarbon of one carbon less than the parent acid, smaller amounts of hydrogen, carbon monoxide, water, methane (for compounds of higher molecular weight than acetic acid) and traces of other hydrocarbons of chain length both greater and smaller than that of the parent acid. In addition unsaturated acids and unsaturated hydrocarbons are observed. However, no detailed mechanism has been developed and it was felt, therefore, that an investigation of the γ-ray induced decomposition would be of value in providing further information leading to a clarification of the mechanism of decomposition.

Experimental

Ten carboxylic acids were irradiated. These were acetic, propionic, *n*-butyric, isobutyric, *n*-valeric, isovaleric, trimethylacetic, α-methylbutyric, *n*-caproic and isocaproic acids. The acetic acid was analytical grade. The others were Eastman Kodak "white label" grade. All were distilled through a 30-cm. spinning band or equivalent column and center cuts having boiling range of less than 0.2° were collected. The center fraction was redistilled after drying for 24 hr. by stirring with "Drierite." The acids were distilled from "Drierite" into the irradiation vessels, which were Pyrex ampoules, on a vacuum line. Samples were thoroughly degassed by repeated freezing, pumping and thawing. Samples were irradiated in the FSU Cobalt-60 irradiator, which is of the type described by Burton, Hochanadel and Ghormley.[6]

The mixture of gaseous decomposition products was analyzed either by a modification of the technique of Saunders and Taylor,[7] employing differential vapor pressure and chemical absorption techniques for the separation of the reported constituent, or by vapor phase chromatography. Reproducibility with duplicate samples by these means was of the order of ±5% of the "*G*"-value.

Dose rates were calculated from atomic density and absorption coefficients of the solution referred to a standard absorption in 0.8 *N* sulfuric acid of 3.0×10^{20} e.v./l.-min. This calibration was obtained by use of the aqueous ferrous sulfate dosimeter, with a specific yield of 15.6 ferric ions per 100 e.v. The radical trapping experiments were carried out using the technique of McCauley and Schuler.[8]

Results and Discussion

1. The Effect of Temperature during Irradiation.—The range of temperatures studied was limited by the desire to consider irradiation effects only in the liquid state. The yield of carbon dioxide from acetic acid was studied for the temperature range 0° (super cooled) to + 105°. For propionic acid the temperature range was −20° to 88°. The yields of other gaseous decomposition products from acetic acid and propionic acid were also studied. The data are presented in Table I. Carbon dioxide yields from the other eight acids are shown in Table II

Above room temperature the effect of temperature in the case of both acids is slight and the yield of all products shows a linear increase with temperature. The yield of CO_2 at 0° for both acetic and propionic acid is anomalous. In both cases a rather sharp increase in $G(CO_2)$ over the value at 27° is seen. This is in accord with the observation of Whitehead, *et al.*,[2] who observed in their study on behenic acid (C_{22}) the same unexpected rise in yields at 0°.

If one postulates that the combined yields of carbon dioxide and carbon monoxide represents a measure of the total decomposition of acetic acid *leading to the formation of methyl radicals*, then the ratio $[G(CH_4) + 2G(C_2H_6)]/[G(CO_2) + G(CO)]$ will have a value of one if *all* of the methyl radicals produced by the decomposition react to form methane or ethane. It is of interest to consider the value of this ratio and its variation with temperature. At 27° the value of this ratio is

(1) This work was supported in part by the USAEC under contract AT-(40-1)-2001 and in part by the FSU Research Council.

(2) W. L. Whitehead, C. Goodman and I. A. Breger, *J. Chem. Phys.*, **48**, 184–189 (1951).

(3) A. Newton, *ibid.*, **26**, 1764 (1957).

(4) J. Burr, THIS JOURNAL, **61**, 1481 (1955).

(5) W. Garrison, *J. Am. Chem. Soc.*, **77**, 2720 (1955).

(6) M. Burton, J. A. Ghormley and C. J. Hochanadel, *Nucleonics*, **13**, 10 (1955).

(7) K. W. Saunders and H. A. Taylor, *J. Chem. Phys.*, **9**, 616 (1941).

(8) C. E. McCauley and R. H. Schuler, *J. Am. Chem. Soc.*, **79**, 4008 (1957).

TABLE I

LIQUID PHASE RADIOLYSIS OF ACETIC AND PROPIONIC ACIDS

Acid	$n^{20}D$	Scavenger	T, °C.	G (molecules/100 e.v.)[a] CO_2	CO	CH_4	C_2H_6	H_2	C_2H_4
CH_3COOH	1.37192		0	6.7					
CH_3COOH	1.37192		27	6.0	0.73	3.34	0.62	0.35	Trace
CH_3COOH	1.37192	$I_2(1 \times 10^{-2} M)$	27	6.2	.44	0.69	.65		
CH_3COOH	1.37192		88	7.1	.85	4.25	.72	0.42	
CH_3COOH	1.37192		105	7.4					
CH_3CH_2COOH	1.38686		−20	5.5					
CH_3CH_2COOH	1.38686		0	5.7					
CH_3CH_2COOH	1.38686		27	4.4	.46	0.01	3.3		0.76
CH_3CH_2COOH	1.38686		88	6.2					

[a] Average value for three runs.

TABLE II

CARBON DIOXIDE YIELDS FROM HIGHER ACIDS

Acid	$n^{20}D$	Scavenger	T, °C.	G-(CO_2)[a]
$CH_3CH_2CH_2COOH$	1.39713		27	5.0
$CH_3CH(CH_3)COOH$	1.39265		27	14.4
$CH_3CH_2CH_2CH_2COOH$	1.40804		27	5.4
$CH_3CH(CH_3)CH_2COOH$	1.20292		27	5.9
$CH_3CH_2CH(CH_3)COOH$	1.40353		27	6.3
$(CH_3)_3CCOOH$	.....		83	6.3
$CH_3CH_2CH_2CH_2CH_2COOH$	1.41633		27	4.4
$CH_3CH_2CH_2CH_2CH_2COOH$	1.41633	$I_2(1 \times 10^{-2} M)$	27	4.5
$CH_3CH(CH_3)CH_2CH_2COOH$	1.41460		27	6.7

[a] Average values for at least three runs.

0.68 and at 88° it is virtually unchanged (0.70). This suggests that something less than one-third of the methyl radicals produced by carbon–carbon bond scission escape to form higher hydrocarbons and in the liquid phase this number is independent of temperature. Alternatively, if CO_2 is produced by some other reaction, such as suggested by Garrison[5] ($2CH_3COOH \rightarrow CH_3COCH_3 + CO_2 + H_2O$), the relative rates of these two reactions must be independent of temperature.

2. **The Effect of Iodine.**—(i) The effect of irradiating acetic acid at 27° in the presence of $1 \times 10^{-2} M$ iodine is threefold. First it is found that the yield of carbon dioxide is virtually unaffected. Secondly, the yield of methane is sharply diminished (from 3.34 to 0.69 molecules/100 e.v.); and finally, the yield of ethane is essentially independent of the presence of iodine. These latter observations strongly suggest that ethane is formed independent of a process involving thermal methyl radicals while about 80% of the methane arises from thermal radical reactions. This latter figure is in fair agreement with J. Burr's[3] estimate of about 15% for methane produced by a molecular process. The effect of added iodine on $G(CO_2)$ for *n*-caproic acid also was studied and found to be negligible. (ii) Results of the determination of the distribution of thermal free radicals from valeric acid, using a radio-iodine technique show that approximately 80% of the radicals detected were those resulting from the loss of a carboxyl group by the parent acid. This suggests that C–C scission at the carboxyl group is the predominant reaction even in acids of moderate chain length.

3. **Structural Effects.** (i) **Straight Chain Acids.**—The most exhaustive study on the effect of ionizing radiation on straight chain acids was carried on by Whitehead, *et al.*,[2] using α-particles. Their studies were carried out in the solid phase and were concentrated mainly on the acids of longer chain length. Only acetic and propionic acids, of the lower members of the series, were studied. On the basis of these data it was concluded that the yield of carbon dioxide decreased linearly with increasing chain length. While this seems to be generally true for the acids of chain length greater than eight, or perhaps generally true for the acids containing an even number of carbon atoms we have observed deviations from this generalization deemed to be significant. From an examination of Tables I and II it can be seen that while acetic, *n*-butyric and *n*-caproic acids show the expected linear decrease, propionic and *n*-valeric acids, a careful examination of the earlier data reveals that the disproportionately low yield of CO_2 in the case of propionic acid also was observed. A value of 2.75 for $G(CO_2)$ is predicted on the basis of the linear relationship while experimentally a value of 2.4 was obtained. This is a deviation of 12% from the expected value, while in this work a deviation of about 25% has been observed.

No ready explanation for these anomalies presents itself. It can be conjectured that these deviations arise from differences in the magnitude of short-range ordering effects in the liquid state when even-numbered and odd-numbered acids are compared. This would lead to different "caging" efficiencies for the various acids. Such speculation is supported by the fact that at higher temperatures these differences in $G(CO_2)$ are smaller than at the lower temperature. That differences in the nature of aggregation in the liquid state exist for the odd numbered acids is attested to by anomalous viscosities, heats of vaporization and melting points of the odd numbered compounds. Similar anomalies have been observed in this Laboratory for the odd-numbered acids in the case of the recoil-tritium labeling of these compounds.

(ii) **Branched Acids.**—The most striking effect of structural variation is to be seen in the case of the two butyric acids. The yield of carbon dioxide is almost three times as great from the branched as from the straight-chain compound. This is in agreement with the observations of Dewhurst,[9] who found that the preferred site of scission in hydrocarbons was at the point of branching.

In the case of the isomers of *n*-valeric acid it is seen that when the carboxyl group is at the point of

(9) H. A. Dewhurst, *J. Am. Chem. Soc.*, **80**, 5607 (1958).

branching (pivalic acid and α-methylbutyric) the yields are higher than for the other two isomers, although the difference is not so great as in the case of the four carbon acids.

4. Linear Energy Transfer Effects.—In Table III the experimental data from this Laboratory on acetic acid using γ-radiation are compared with those of other workers using various other types of radiation.

TABLE III

LINEAR ENERGY TRANSFER EFFECTS

Radiation	dx/dE, Å./e.v.	G_{CO_2}	G_{CO}	G_{CH_4}	$G_{C_2H_6}$	G_{H_2}	Ref.
27 Mev He^{++}	0.3	4.0	0.31	1.20	0.77	0.5	5
18 Mev H^2	1.9	4.0	..	1.35	.63	.4	5
γ	40–50	6.0	0.73	3.34	.62	.35	This Laboratory

An examination of Table III indicates that linear energy transfer has a marked effect on the yields of the products of radiolysis. Thus the yield of CO_2 is increased 50% in going from helium ions to cobalt-60 γ-rays, and the yield of methane is almost tripled. In a like manner, the yield of hydrogen is substantially less in the γ-case. The absolute yield of ethane is, however, only slightly diminished as one goes to lower ionization densities. This fact requires further consideration.

The consequences of high L.E.T. are generally considered to be the production of high local concentrations of the primary and secondary products of radiation. Very low L.E.T. radiations, in contrast, produce an essentially homogeneous distribution of activity throughout the bulk of the system under irradiation. Thus, high L.E.T. radiation will result in enhanced participation of those reactions involving the interaction of two or more activated species such as two radicals, or two excited molecules while low L.E.T. radiation produces systems in which reactions of an activated species with the substrate predominate. An example is to be found in the high peroxide and hydrogen yield produced by alpha radiation in water.

It is of interest to compare the effect of an L.E.T. difference on the ratio of methyl radicals (observed as methane and ethane) to carboxyl radicals which are observed as carbon dioxide plus carbon monoxide. The results of irradiation of acetic acid with 27 Mev. helium ions and with cobalt-60 γ-rays are compared. Here the yield of methyl radicals is taken to be equal to $G(CH_4) + 2G(C_2H_6)$. The yield of carboxyl radicals is assumed to be equal to $G(CO_2) + G(CO)$. For helium ions the ratio $G(CH_3\cdot)/G(COOH\cdot)$ is found to be 0.63,[10] and for γ-rays the ratio is 0.68.

The fact that the ratios are nearly equal despite the *over-all* difference in total decomposition [based on $G(CO_2) + G(CO)$] suggests that the over-all mechanism is the same for both cases and in both cases about $^1/_3$ of the methyl radicals produced initially go to form something other than methane or ethane.

It is also instructive to consider the ratio $G(CH_4)/G(CH_3\cdot)$ for the two cases. For the 27 Mev. He^{+2} case the value is 0.44 and for the γ-ray case it is 0.73. Furthermore, if one compares the ratios of methane yield to carboxyl yield for the two cases, we obtain values of 0.27 and 0.50 for the high and low L.E.T. cases, respectively. Thus, per molecule of acetic acid attacked about twice as many events result in the formation of methane in the γ-ray case, whether one considers the number of methyl radicals produced or the total number of molecules of acetic acid decomposed. Since these "missing" methyl radicals appear as the dimer (C_2H_6), it is tentatively concluded that a distinct L.E.T. effect is observed in the case of ethane formation even though comparison of the absolute yields shows them to be very nearly the same for both high and low L.E.T. radiation.

The mechanism for the radiolytic decomposition of carboxylic acids has been discussed by a number of authors.[1-4] The photolysis of acetic acid in the vapor phase has been studied by Burton[11] and Ausloos and Steacie.[12]

The latter authors have concluded that 10% or less of the reaction is due to direct decomposition to methane and carbon dioxide but rather that the bulk of the decomposition involves free radical intermediates. This is in qualitative agreement with the conclusions of Burr on the formation of methane from liquid acetic acid and our results using iodine as a free radical scavenger. It is thus concluded that a substantial part of the radiolysis involves alkyl and carboxyl free-radical intermediates.

Acknowledgments.—The author wishes to acknowledge the technical assistance of Messrs. Wayne Westmark and Kenneth Chellis and to thank Dr. C. J. Hochanadel of the Oak Ridge National Laboratory for the use of his radiation facilities during the early phases of this work.

(10) These are extrapolated yields based on the work of Garrison on aqueous solutions of acetic acid.

(11) M. Burton, *J. Am. Chem. Soc.*, **58**, 692 (1936).

(12) P. Ausloos and E. W. R. Steacie, *Can. J. Chem.*, **33**, 1530 (1955).

THE PREPARATION AND PROPERTIES OF SOME SYNTHETIC INORGANIC ANION EXCHANGERS

BY E. J. DUWELL AND J. W. SHEPARD

Contribution from the Central Research Department, Minnesota Mining and Manufacturing Company, St. Paul 9, Minnesota

Received July 6, 1959

Inorganic anion exchangers have been prepared by coprecipitating cations of higher valence with aluminum and zinc hydroxide in slightly acidic solutions. The gels are dried to form white finely divided amorphous powders of Al(OH)- and $Zn(OH)_2$. We have postulated that the higher valent cations are in lattice positions ordinarily occupied by the cation of the base structure, the charge unbalance being made up by loosely adsorbed exchangeable anions. If an alumina base exchanger is prepared with aluminum chloride precipitated with sodium hydroxide in which is dissolved some silica, the chloride form of the exchanger is obtained. Analysis of the dried and washed product gives the stoichiometric formula $Al_{0.86}Si_{0.14}(OH)_3Cl_{0.13}$. The slight deficiency of chloride ion to compensate for all the charge unbalance caused by silicon is probably made up by hydroxide ions. Only a trace of sodium is found in the product, which may be due to incomplete washing.

Introduction

Many naturally occurring alumina-silicates such as orthoclase ($K_2O \cdot Al_2O_3 \cdot 6SiO_2$), albite ($Na_2O \cdot Al_2O_3 \cdot 6SiO_2$), analcite ($NaAlSi_2O_6 \cdot H_2O$) or heulandite ($CaO \cdot Al_2O_3 \cdot 6SiO_2 \cdot 5H_2O$) are cation exchangers. These structures contain silicate chains in which are substituted aluminum atoms in tetrahedral coordination with oxygen atoms. Because the aluminum atom has a charge of three, a cation deficiency arises which is balanced by the exchangeable alkaline or alkaline earth cation.

We have prepared $Al(OH)_3$ with substitutional silicon atoms. The resulting solids have an anion exchange capacity equivalent to the number of silicon atoms in the solid. The silicon atoms are postulated to have replaced aluminum atoms in their octahedrally coördinated positions. The lattice therefore has a positive charge excess, and this is balanced by exchangeable anions. In a sense, these materials may be considered the anion exchange counterparts of the natural and synthetic zeolites, and other cation exchanging alumina-silicates which consist of chains of tetrahedrally coördinated aluminum and silicon atoms.

Al^{+3} has been introduced into the $Zn(OH)_2$ lattice also. Again, an anion-exchange capacity equivalent to the positive charge excess is observed.

Unlike the exchangers just described, which are primarily cation or anion exchangers, some exchangers exhibit both an anion and cation-exchange capacity depending on the *p*H. This behavior results from the amphoteric nature of surface hydroxyl groups

$$XOH \rightleftharpoons XO^- + H^+ \text{ (basic solution)}$$

$$XOH \rightleftharpoons X^+ + OH^- \text{ (acid solution)}$$

Kaolinite ($Al_2O_3 \cdot 2SiO_2 \cdot 2SiO_2 \cdot 2H_2O$) and some other naturally occurring clays are ion exchangers because of amphoteric hydroxyl ligands.[1-3] Recently, the hydrous oxides of zirconium, thorium, titanium and tungsten, also have been shown to have ion-exchange capacity that can be explained by the amphoteric nature of surface hydroxyl groups.[4,5] To a small degree, the exchangers that will be described also exhibit this type of behavior.

Compound Preparation

The $Zn(OH)_2$ exchanger was prepared by adding NaOH to a 0.25*M* solution of $ZnCl_2$ containing $AlCl_3$ in the molar ratio of 8:1 until a mixed colloid in a slightly acidic solution was obtained. This gel was dehydrated at 130° and the resulting white powder, $Zn_{0.89}Al_{0.11}(OH)_2Cl_{0.11}$, was repeatedly washed to remove NaCl.

The $Al(OH)_3$ exchangers were prepared similarly except that the minor constituent was tetravalent silicon, titanium or zirconium. The exchangers containing zirconium or titanium were prepared using solutions of $TiCl_2(OAc)_2$ or $ZrOCl_2$ in 0.25 *M* $AlCl_3$ solutions. The $TiCl_2(OAc)_2$ was obtained from the Titanium Pigment Corporation.[6] The procedure for preparation was the same as that described for the $Zn(OH)_2$ base exchanger.

Silicon was added to the colloidal alumina by hydrolyzing $(C_2H_5)_4SiO_4$ over a slightly acidic solution containing the alumina gel. The mixed acidic colloid could also be prepared by introducing the silica in the last third of the NaOH used to precipitate the $AlCl_3$ solution, or by adding HCl to a solution of aluminum and silicon in NaOH. In any case, the mixed colloid must be in a slightly acidic solution before dehydrating and washing as previously described. It is significant that anion-exchange properties are only obtained if colloids from acidic solutions are dehydrated. This will be discussed later.

The white powders produced in this way are easily separated from solutions by filtering or centrifuging. Although column experiments have been performed, all of the experiments reported in this paper were the batch-type. This involved shaking one gram of the exchanger with 200 ml. of solution that was 0.015 *M* with respect to the potentially adsorbed anion. The *p*H was adjusted by use of the acids or sodium salts of the particular anion investigated. After mixing the exchanger and solution sufficiently long for equilibrium to be established, the exchanger was separated by centrifuging, and the supernatant liquid was analyzed and compared with the original solution to determine the number of adsorbed or released ions.

Analysis of The Exchanger

A total analysis for H_2O and all elements except oxygen in the alumina-silicate exchanger yielded the stoichiometric formula

$$Na_{0.015}Cl_{0.254}[Al_{1.716}Si_{0.284}O_3] \cdot 3.02H_2O$$

The sodium content may have resulted from incomplete removal of NaCl by washing. It was assumed that all the anion-exchange sites were filled by chloride ions, whereas some hydrolysis probably occurred during washing

(1) P. P. Stout, *Soil Sci. Soc. Am. Proc.*, **4**, 177 (1939).

(2) S. Mattson, *Soil Sci.*, **49**, 109 (1940).

(3) R. P. Graham and A. E. Horning, *J. Am. Chem. Soc.*, **69**, 1214 (1947).

(4) C. B. Amphlett, L. A. McDonald and M. J. Redman, *J. Inorg. & Nuclear Chem.*, **6**, No. 3, 236 (1958).

(5) K. A. Kraus and H. O. Phillips, *J. Am. Chem. Soc.*, **78**, 249 (1956).

(6) U. S. Patent 2,670,363, J. P. Wadington, Feb. 23, 1954 (National Lead Co.).

$$Cl_n[Al_{2-n}Si_nO_3]\cdot 3H_2O + HOH = (OH)_x[Al_{2-n}Si_nO_3]\cdot 3H_2O + (H^+ + Cl^-)_x$$

For this reason the chloride ion content may not equal the silicon content. Also, there is not an exact charge balance, the error being an excess on the positive side by about 1%. This also would be compensated for by any hydroxide ions on the exchange sites, although the accumulation of analytical errors prohibits drawing any further conclusions on this basis. The theoretical capacity for this exchanger is 1.52 meq./g. on the basis of chloride ion content.

Analysis of the other exchangers for Na^+ and Cl^- yielded the same result: the Na^+ content was negligibly small, and the Cl^- content was equal to the quantity of the higher valent cation and the exchange capacity. The formula for the exchangers can be written

$$Cl_n\ [Al_{2-n}C_n^{+4}O_3]\cdot 3H_2O$$

and

$$Cl_n\ [Zn_{1-n}Al_nO]\cdot H_2O$$

where C^{+4} can be Ti^{+4}, Zr^{+4} or Si^{+4}.

It should be noted that the formula for the alumina base exchanger can be written $Al_2O_3\cdot 3H_2O$, whereas the equivalent formula $Al(OH)_3$ more accurately describes the structure, which contains hydroxyl bonds.[7] This also holds true for $ZnO\cdot H_2O$, the structure of which is more accurately described by the formula $Zn(OH)_2$.

Dehydration of each of these exchangers at 150° results in the loss of water and loss of anion exchanger capacity. With the alumina–silicate exchanger in the chloride form, the loss of HCl was noted. The reaction is postulated to occur at an anion-exchange site as

$$Cl^- + [Si(OH)_3^+] \xrightarrow{150^\circ} SiO_2 + HCl\uparrow + H_2O\uparrow$$

Similar reactions occur with the other exchangers, with loss of anion-exchange capacity.

X-Ray diffraction analysis indicated that the exchangers were all amorphous. This could be due to short range order in the structures resulting from the method of preparation. Using X-ray diffraction, it was noted that TiO_2 was formed on heating the alumina exchanger containing titanium to 150°. The material also lost its anion-exchange capacity under these conditions.

Ion-Exchange Reactions

The preparations we have described yield the anion exchangers in the chloride form. Several washings of the dehydrated colloid with distilled water readily removes the NaCl formed by neutralization of the starting materials. Subsequent washes continue to leach small traces of chloride ion from the exchanger, as is evidenced by a slight turbidity of AgCl when a qualitative test with $AgNO_3$ is performed. This leaching may involve hydrolysis as described earlier. A wash with dilute NaOH solution serves to remove most of the chloride ion from the exchanger, as is noted readily by neutralizing the NaOH solution with HNO_3, and again testing for chloride ion with $AgNO_3$. A copious amount of AgCl is precipitated. This process converts the exchanger to the hydroxide form.

The exchanger also can be tested qualitatively by shaking it in a solution of $KMnO_4$. Adsorption of MnO_4^- by ion exchange turns the white exchanger to a dark purple color. The permanganate ion is retained, and only a small degree of leaching is evident with distilled water washes. However, a single wash with saturated NaCl solution serves to decolorize the exchanger by converting it to the chloride form, the supernatant solution becoming purple from the released MnO_4^- ions.

(7) A. F. Wells, "Structural Inorganic Chemistry," Oxford University Press, New York, N. Y., 1950, p. 417.

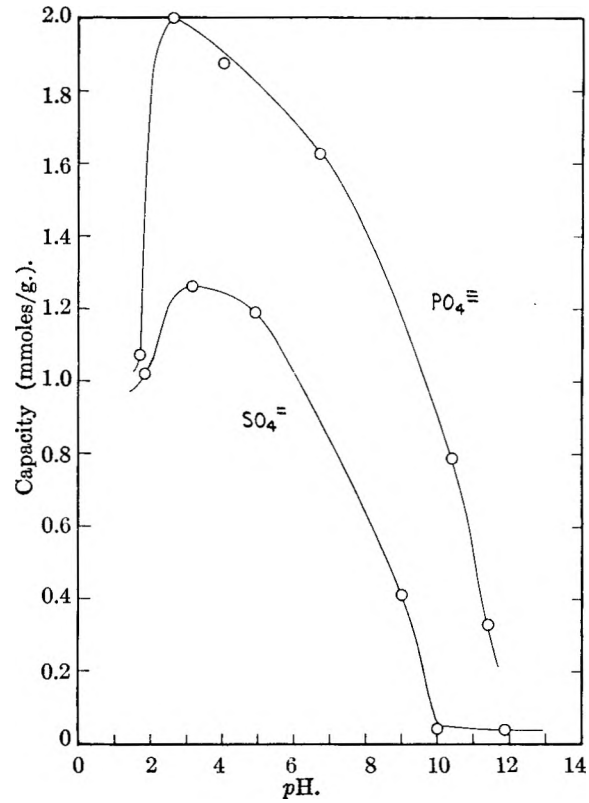

Fig. 1.—Anion-exchange capacity of alumina titanate exchanger (chloride form) for sulfate and phosphate ion as a function of *p*H.

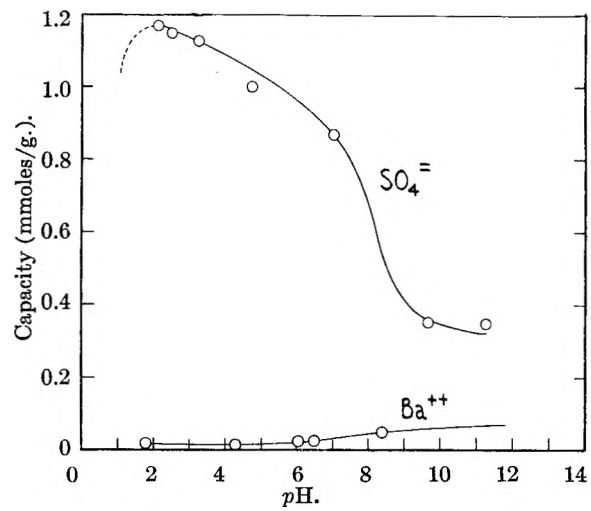

Fig. 2.—Capacity of alumina silicate exchanger (chloride form) for sulfate and barium ion as a function of *p*H.

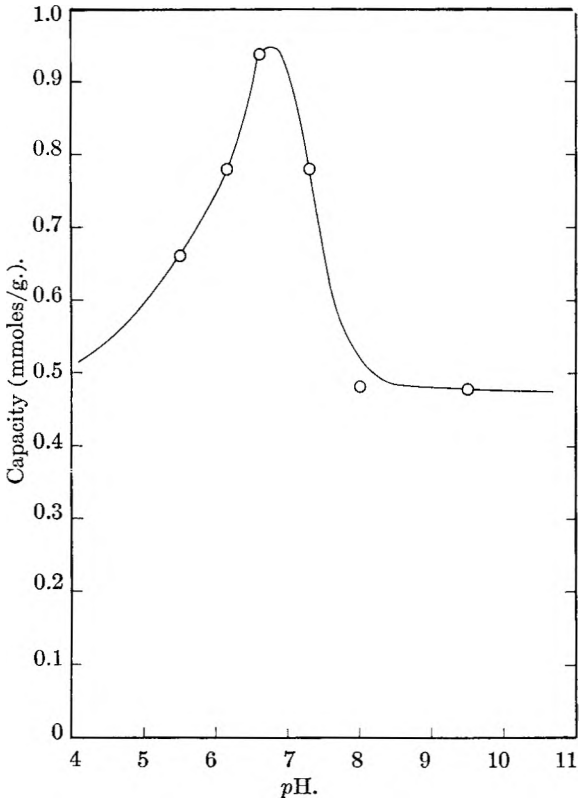

Fig. 3.—Capacity of the zincate aluminate exchanger (chloride form) for sulfate ion as a function of pH.

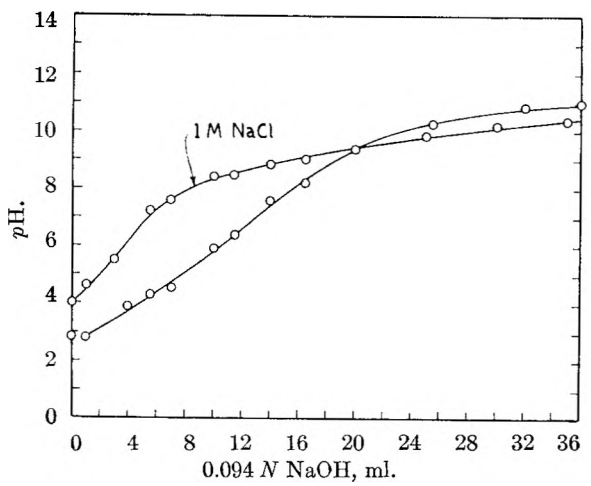

Fig. 4.—Titration of the chloride form of the alumina silicate anion exchanger with NaOH in distilled water and 1 M NaCl solution.

The capacity of the exchanger $Al_{0.89}Ti_{0.11}(OH)_3Cl_{0.11}$ for sulfate and phosphate ion was determined as a function of pH (Fig. 1). In basic solutions the capacity decreases because hydroxide ions begin to occupy the exchange sites. The capacity also tends to decrease in acid solutions because these anions are largely present in the lower valence acid forms, which are less strongly adsorbed than the higher valence forms simply because of the lesser degree of coulombic attraction to the exchange site.

The exchange capacity of the alumina-silicate exchanger for sulfate ion (Fig. 2) closely parallels that of the titanium analog (Fig. 1). The capacity of the alumina–silicate exchanger for Ba^{++} also was noted as a function of pH. A small amount of exchange capacity for Ba^{++} in basic solutions was noted. This may arise from some degree of amphoteric character in the exchanger.

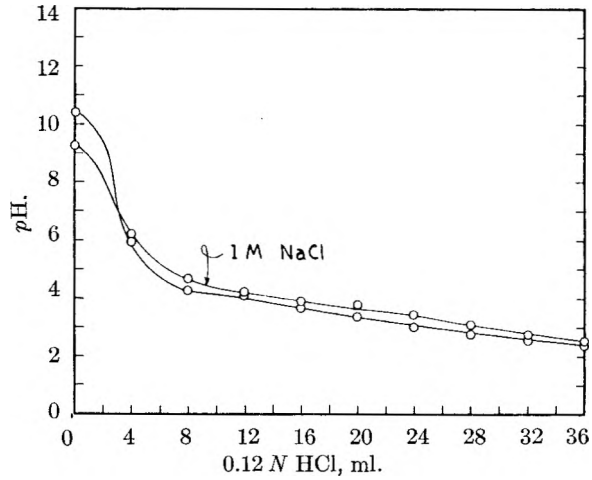

Fig. 5.—Titration of the hydroxide form of the alumina silicate anion exchanger with HCl in water and 1 M NaCl solution.

Adsorption of sulfate ion by the $Zn(OH)_2$ structure containing aluminum (Fig. 3) was similar to that observed for the alumina base exchangers, except that the capacity decreased more rapidly in acid solutions.

The alumina-silicate exchangers were titrated in the chloride form with NaOH (Fig. 4) and in the hydroxide form with HCl (Fig. 5). The hydroxide form was prepared by shaking one gram of the chloride form with 200 ml. of 0.1 N NaOH for two hours. When the titrations are carried out in 1 M NaCl solution, the titration curves tend toward neutral from either the basic or acid side, *i.e.*, the solutions containing NaCl are less acid in acid solutions and less basic in basic solutions. This is a result of the amphoteric character of hydroxyl groups at the edges or surfaces of the exchanger. The reactions are

$$XOH + Na^+ = XONa + H^+ \text{ (basic solution)}$$
$$XOH + Cl^- = XCl + OH^- \text{ (acid solution)}$$

Exchange capacity on these sites is small compared with sites arising from isostructural substitution of a foreign cation of higher valence. The small amount of barium adsorption in basic solution (Fig. 2) may result from these exchange sites.

Exchange of sulfate for chloride ion also has been performed at 100° under reflux with both the zinc and aluminum base exchangers. No appreciable change in capacity was noted for any of the exchangers.

Thickening agents, such as those formed by adsorbing quaternary ammonium salts by cation exchange on clays, can be formed by adsorbing high molecular weight organic anions (sodium stearate) by anion exchange. The resulting solids are hydrophobic and can be used to increase the viscosity of hydrocarbon solutions.

Discussion

It is significant that exchangers with anion-exchange capacities as large as those observed are only obtained from the dehydration of acidic gels

containing the proper higher valent cation. In the presence of excess hydroxide ions, the higher valent cations probably coördinate with their usual number and arrangement of hydroxyl bonds and therefore do not contribute to the anion exchange capacity. When the hydroxide concentration is low, the cation in excess may determine the arrangement and number of hydroxyl groups around the occluded impurity cation, if this cation is capable of coördinating in the same manner as the excess cation.

Although the exchangers do not give diffraction patterns, the $Al(OH)_3$ base exchangers probably have short range order corresponding to the hydrargillite structure (octahedral arrangement of hydroxide groups around aluminum). Ti^{+4} and Zr^{+4} commonly coördinate in this manner. Si^{+4} does not, however, ordinarily coördinate octahedrally, but is found tetrahedrally coördinated in all the common silicates. This may be due to the small size of the silicon ion, around which six ligands are not accommodated easily. Since octahedral coördination is observed with the small fluoride ion (K_2SiF_6) and also in SiP_2O_7, the assumption that Si^{+4} has coördinated octahedrally in the hydrargillite structure is not unreasonable.

Zinc is tetrahedrally coördinated in $Zn(OH)_2$, and although aluminum ordinarily coördinates octahedrally in aqueous systems, it does coördinate tetrahedrally in the zeolites, $AlBr_3$, and other structures. Again, isostructural substitution of the foreign atom in the base structure may occur, although in both cases this may consist of imperfectly coördinated atoms at the surfaces.

Acknowledgment.—We wish to thank A. Duncan and J. J. Gavenda for carrying out the chemical analyses and W. E. Thatcher for making the X-ray diffraction analyses.

CORRELATION OF SOLUBILITY DATA FOR LONG CHAIN COMPOUNDS. II. THE ISOPLETH METHOD OF PREDICTING SOLUBILITIES OF MISSING MEMBERS OF HOMOLOGOUS SERIES

BY EVALD L. SKAU AND AUGUST V. BAILEY

Southern Regional Research Laboratory,[1] *New Orleans, Louisiana*

Received July 6, 1959

A new graphical method of correlating solubility data for homologous series of compounds and for predicting the solubilities of missing members of the series is described. It supplements the "isotherm method" so that solubility prediction can be extended over a wider range of temperatures and concentrations and applied to additional homologous series. It is based upon the linear relationship $1/T = a(1/n) + b$, derived from the approximate freezing point depression equation and empirical relationships between the number of carbon atoms n and the heats and entropies of fusion of the members of a homologous series. T represents the absolute temperature at which the saturated solutions of the various homologs in a given solvent contain the same mole fraction of solute. The coefficients a and b are constants. The validity of the isopleth method was established by the fact that the $1/T$ *vs.* $1/n$ "isopleth" plots based upon accurate literature data for a number of systems consisted of a family of straight or only slightly curved lines. The isopleth method can be used (1) to smooth out experimental solubility data, (2) to locate discrepancies and (3) by graphical interpolation or extrapolation to predict the solubilities of missing members of a series. The published solubility data for the normal hydrocarbons containing 8, 12, 16 and 32 carbon atoms were used to predict the solubilities of those containing 10, 14, 18, 20, 22, 24, 26, 28, 30 and 34 carbon atoms at a number of temperatures in 9 solvents. Similar predictions were made for the solubilities of the normal alkyl methyl ketones containing 11, 15, 17 and 21 carbon atoms in 13 solvents and for the following compounds in *n*-hexane: the symmetrical normal alkyl ketones containing 27 and 39 carbon atoms; the symmetrical normal secondary amines containing 18, 20, 22, 26, 30, 32, 34 and 38 carbon atoms; the symmetrical normal tertiary amines containing 30, 42, 48 and 60 carbon atoms; the normal fatty acids containing 11, 13 and 19 carbon atoms; and the fatty acid methyl esters containing 11 and 21 carbon atoms. The combined use of the isopleth and isotherm methods of correlation makes it possible to obtain similar complete solubility data for other solvents and other homologous series on the basis of a minimum of experimental measurements.

In a recent publication[2] from this Laboratory, an interpolative method was developed for predicting the solubilities of the missing members of a homologous series. This was based upon the observation that a smooth curve is obtained by plotting the logarithm of the molar solubilities of the higher members of a homologous series in a given solvent and at a given temperature against the total number of carbon atoms in the molecule. It was shown that these isotherms can be drawn accurately on the basis of the experimentally determined solubilities of a few members of a series and used to determine the solubilities of the missing intermediate members by interpolation. Though this method of prediction is applicable to a large number of homologous series in a large variety of solvents,[3] its use is limited to temperature ranges and to systems for which sufficient experimental data are available to establish the isotherms. The present paper deals with a second method of correlation on the basis of which solubility prediction can be extended over a wider range of temperatures and concentrations and applied to additional homologous series.

It was shown by Garner and co-workers[4,5] that

(1) One of the laboratories of the Southern Utilization Research and Development Division, Agricultural Research Service, U. S. Department of Agriculture.

(2) E. L. Skau and R. E. Boucher, THIS JOURNAL, **53**, 460 (1954).

(3) R. E. Boucher and Evald L. Skau, "Solubility Charts for Homologous Long-Chain Organic Compounds," U. S. Dept. Agr., ARS-72-1, 1954.

(4) W. E. Garner, F. C. Madden and J. E. Rushbrooke, *J. Chem. Soc.*, 2491 (1926).

(5) W. E. Garner and A. M. King, *ibid.*, 1849 (1929).

the heats and entropies of fusion of the higher members of a homologous series are essentially linear functions of the number of carbon atoms in the molecule. That is

$$\Delta H_f = b'n + a' \quad (1)$$

and

$$\frac{\Delta H_f}{T_0} = b''n + a'' \quad (2)$$

where ΔH_f is the molar heat of fusion, T_0 is the freezing point of the pure compound in degrees absolute, n is the total number of carbon atoms in the molecule, and a', a'', b', and b'' are constants. These constants may have one set of values when n is even and another when n is odd.

Equations 1 and 2 can be combined to give

$$\frac{1}{T_0} = \frac{(b''n + a'')}{(b'n + a')} \quad (3)$$

Huggins[6,7] concluded from this equation that for large values of n a linear relation exists between $1/T_0$ and $1/n$. That is, by expanding the right-hand member of equation 3 into a series and neglecting terms containing higher powers of $1/n$

$$\frac{1}{T_0} = \frac{b''}{b'} + \left(\frac{a''}{b'} - \frac{a'b''}{b'^2}\right)\frac{1}{n} \quad (4)$$

Huggins pointed out that, as expected, the $1/T_0$ *vs.* $1/n$ plot for the normal paraffins was an approximately straight line. Data for other homologous series indicate the generality of this relationship.

Since the solubility of a compound is also a function of its heat of fusion it should be possible, if the solutions are ideal, to show a similar correlation between the solubility temperatures (primary freezing points) of members of a homologous series and the number of carbon atoms in their chains, all at the same concentration in a given solvent. The approximate equation for the lowering of the freezing point, assuming ideal solutions, may be written as

$$2.303 \log N = \frac{\Delta H_f}{R}\left(\frac{1}{T_0} - \frac{1}{T}\right) \quad (5)$$

where N is the mole fraction of the compound with which the solution is saturated, T is the solubility absolute temperature in degrees for the given composition and R is the gas constant. By substitution from equations 1 and 2

$$2.303R \log N = -(b'n + a')\left(\frac{1}{T}\right) + (b''n + a'') \quad (6)$$

At a given concentration in a given solvent $2.303R \log N$ is a negative constant k and

$$\frac{1}{T} = \frac{b''n + (a'' - k)}{b'n + a'} \quad (7)$$

By expansion and elimination of terms containing higher powers of $1/n$ this becomes

$$\frac{1}{T} = \left(\frac{b''}{b'}\right) + \left(\frac{a'' - k}{b'} - \frac{a'b''}{b'^2}\right)\frac{1}{n} \quad (8)$$

This is the same as equation 4 when $N = 1.0$, that is, when $k = 0$. For any given value of N, equation 8 reduces to the linear relation

$$\frac{1}{T} = a\left(\frac{1}{n}\right) + b \quad (9)$$

in which a and b are constants.

If the basic equations and the assumptions involved in this derivation were valid over the range considered, a straight line would therefore be obtained for any given concentration N by plotting the reciprocal of the solubility temperatures of the members of a homologous series in a given solvent against the reciprocal of the total number of carbon atoms. The slope of the line would depend upon the homologous series and the concentration being considered.

The equations and assumptions are of course not strictly valid and therefore the experimental values would not be expected to conform exactly to the linear relationship of equation 9. However, since the deviations in a homologous series of compounds would in all probability vary regularly with the chain length, the $1/T$ *vs.* $1/n$ plot for each value of N would at least be expected to be a smooth curve.

Since these plots represent the relation between two variables at constant concentration, they will be called *isopleths*, using the terminology suggested by Hill,[8] and this method of correlating the solubilities of homologs will be referred to as the *isopleth method* to distinguish it from the *isotherm method* previously described.[2]

Procedure for Constructing Isopleth Plots.—In order to construct the isopleth plots for the solubilities of a homologous series of compounds in a given solvent, large-scale log N *vs.* $1/T$ plots are first made for all the members of the series for which experimental data are available. The values of $1/T$ at various selected values of N then are read from these curves for each of the homologs and plotted on a large scale against $1/n$.

The validity of the isopleth method of correlation was established by applying it to published solubility data for various series of long chain homologous compounds. Isopleth plots were constructed for a number of systems for which there were sufficient data to establish the contour of the log N *vs.* $1/T$ plots.[9] This resulted in a family of straight or slightly curved lines as expected. Figure 1 shows such a family of isopleths representing various concentrations in mole fraction based upon the published solubility data for the even members of the saturated fatty acid series in chloroform.[10]

Prediction of Solubilities of Missing Members of Homologous Series.—Since they can be expected to be straight lines or smooth curves the $1/T$ *vs.* $1/n$ isopleth plots can be used to predict the solubilities of missing members of a homologous series, the precision depending upon the accuracy and consistency of the experimental data available, and upon the amount of curvature of the isopleths. Thus, the solubility data for the homologous sym-

(6) M. L. Huggins, THIS JOURNAL, **43**, 1083 (1939).

(7) M. L. Huggins, *Record Chem. Progr. Kresge-Hooker Sci. Lib.*, **11**, 85 (1950).

(8) A. E. Hill, *J. Am. Chem. Soc.*, **45**, 1144 and footnote 4 (1923).

(9) The data as published are generally limited to the solubilities at ten-degree intervals only, obtained by interpolation in the smooth curves drawn through a large number of experimental points. Thus, the available data are often inadequate to establish the exact contour of the log N *vs.* $1/T$ plots.

(10) C. W. Hoerr and A. W. Ralston, *J. Org. Chem.*, **9**, 329 (1944).

TABLE I

PREDICTED SOLUBILITY TEMPERATURES IN DEGREES CENTIGRADE OF SOME *n*-ALIPHATIC COMPOUNDS IN *n*-HEXANE

Mole % → No. carbon atoms	80	60	40	20	10	6	4	2	1	0.5
					Symmetrical secondary amines					
38	73.2	71.4	68.8	64.3	60.2	56.9	54.6			
34	68.4	66.5	63.8	59.1	54.5	51.3	48.8			
32	65.4	63.5	60.8	55.9	51.2	47.8	45.2			
30	62.4	60.4	57.5	52.6	47.7	44.3	41.8			
26	54.8	52.6	49.3	43.9	38.9	35.3	32.7			
22	45.1	42.5	38.8	33.0	27.6	23.8	21.0			
20	39.1	36.3	32.4	26.4	21.0	17.0	14.0			
18	32.0	29.0	24.7	18.6	13.0	8.8	5.7			
					Symmetrical tertiary amines					
60	61.6	60.4	58.0	53.2						
48	42.6	41.0	38.5	32.8						
42	29.9	28.0	25.1	19.0						
30	−5.6	−7.8	−11.4	−18.7						
					Odd saturated fatty acids					
19	65.3	60.6	55.8	49.0						
13	35.8	31.0	25.9	19.2						
11	22.7	17.4	11.9	4.5						
					Methyl esters of even saturated fatty acids					
21	42.6	40.0	36.3	29.2	23.4	19.7				
11	−11.7	−15.0	−19.4	−25.6	−31.5	−35.6				
					Symmetrical ketones					
39						68.0	65.0	59.2	55.4	51.4
27				58.3[a]	54.9	50.4	47.0	41.1	35.1	29.9
					Methy lketones					
21	57.0	53.4	49.2	42.5	36.6	32.6				
17	44.1	40.5	35.8	29.5	23.4	19.2				
15	34.5	31.0	26.2	19.8	13.7	9.3				
11	8.3	4.0	−0.5	−7.3	−13.7	−18.5				

[a] Solubility temperature for 15 mole %.

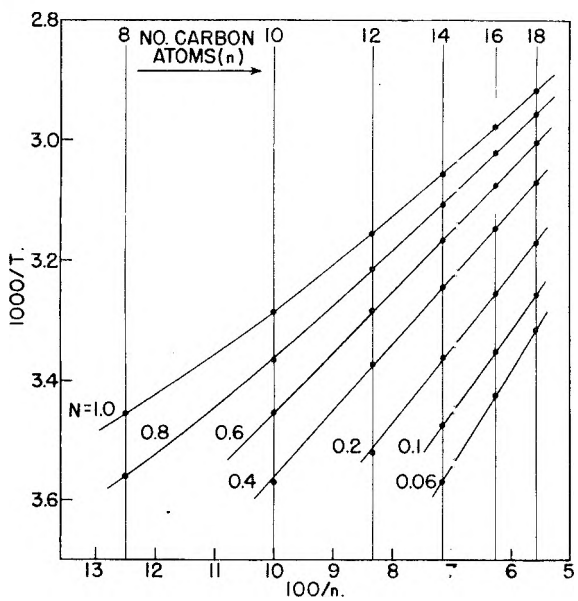

Fig. 1.—Solubility isopleths showing relation between carbon chain length and the reciprocal of the solubility temperature at selected concentrations of the normal saturated fatty acids in chloroform (N = mole fraction).

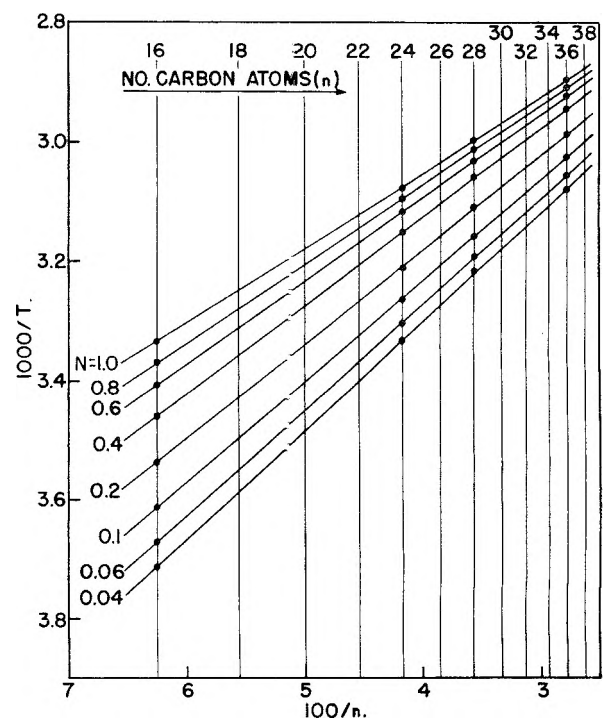

Fig. 2.—Solubility isopleths showing relation between carbon chain length and the reciprocal of the solubility temperature at selected concentrations of the symmetrical normal secondary amines in *n*-hexane (N = mole fraction).

metrical normal aliphatic secondary amines in *n*-hexane included only the members containing 16, 24, 28 and 36 carbon atoms.[11] From the isopleth plots (Fig. 2) it was possible by graphical interpola-

(11) C. W. Hoerr and H. J. Harwood, *J. Org. Chem.*, **16**, 779 (1951).

TABLE II

PREDICTED SOLUBILITY TEMPERATURES IN DEGREES CENTIGRADE OF SOME *n*-ALIPHATIC HYDROCARBONS IN VARIOUS ORGANIC SOLVENTS

No. carbon atoms Mole %	10	14	18	20	22	24	26	28	30	34
					In butanone					
80	−31.7	3.2	25.6	34.2	41.0	47.4	53.0	57.9	62.5	69.9
60	−32.6	2.2	24.3	32.6	39.3	45.8	51.3	56.1	60.5	67.7
40	−33.3	1.2	23.2	31.5	38.5	44.6	50.1	54.8	59.2	66.2
20	−34.0	0.4	22.3	30.4	37.2	43.5	48.8	53.4	57.6	64.6
10	−36.3	−0.9	21.1	29.3	36.2	42.5	47.8	52.3	56.6	63.4
6	−38.7	−2.7	20.1	28.2	35.0	41.4	46.6	51.1	55.4	62.4
4	−41.6	−4.6	18.8	27.3	34.3	40.7	46.0	50.6	54.9	61.7
2		−8.5	15.7	24.6	31.9	38.5	44.2	48.9	53.4	60.5
1		−13.1	12.4	21.4	38.2	35.5	41.5	46.3	50.9	58.4
0.6		−16.1	9.5	18.6	35.3	32.8	38.8	43.7	48.3	56.1
					In ethyl acetate					
80	−32.7	2.5	25.4	33.8	41.0	47.2	52.7	57.6	61.9	69.2
60	−33.6	1.2	23.5	31.9	39.1	45.2	50.7	55.6	59.8	67.0
40	−34.3	−0.1	22.0	30.3	37.5	43.6	49.1	53.9	58.0	65.1
20	−35.2	−1.5	20.5	28.7	35.9	41.9	47.4	52.2	56.3	63.3
10	−37.4	−2.8	19.2	27.4	34.5	40.6	46.0	50.7	54.9	62.0
6	−40.0	−5.0	17.6	25.9	33.1	39.2	44.8	49.6	54.0	61.1
4		−6.9	16.3	24.8	32.1	38.4	44.0	48.9	53.2	60.6
2		−10.3	13.7	22.5	30.2	36.5	42.2	47.1	51.6	59.3
1		−14.0	10.6	19.7	27.3	33.9	39.7	44.7	49.1	56.7
					In butyl acetate					
80	−33.0	2.1	24.6	33.2	40.5	46.9	52.6	57.4	61.9	69.1
60	−34.7	−0.1	22.1	30.6	37.8	44.1	49.7	54.7	59.1	66.3
40	−35.9	−2.1	19.6	28.2	35.3	41.7	47.2	52.3	56.9	64.3
20	−39.5	−4.6	17.7	26.2	33.4	39.6	45.1	50.2	54.7	62.1
10		−8.5	14.6	23.3	30.8	37.2	42.9	48.0	52.6	59.8
6		−11.6	12.2	21.1	28.6	35.2	41.0	46.2	50.7	58.6
4		−14.5	9.9	19.0	26.6	33.2	39.1	44.3	48.9	56.7
2		−19.4	6.1	15.5	23.4	30.2	36.2	41.4	46.0	54.0
1		−23.8	2.6	11.9	19.8	26.6	32.6	37.8	42.5	50.3
					In 1-butanol					
80	−30.4	5.3	27.8	36.0	43.1	49.6	54.6	59.3	63.7	70.7
60	−31.0	5.0	27.2	35.4	42.3	48.7	53.7	58.4	62.6	69.3
40	−31.8	4.5	27.0	35.0	41.9	48.5	53.5	58.2	62.4	69.0
20	−33.4	3.5	26.2	34.4	41.4	47.9	52.8	57.5	62.0	68.6
10	−38.6	1.6	24.9	33.4	40.4	47.3	52.4	57.0	61.4	68.1
6		−2.2	22.0	31.4	38.7	45.5	50.8	56.0	60.6	67.9
4		−5.1	19.7	28.9	36.6	43.9	49.4	54.7	59.5	67.3
2		−10.7	15.2	24.8	32.9	40.5	46.3	51.8	56.9	65.1
1		−17.1	10.3	20.3	28.8	36.8	42.9	48.6	53.9	62.4
0.6		−21.8	6.6	16.9	25.8	34.0	40.1	46.1	51.4	60.4
					In isopropyl alcohol					
80	−30.2	5.4								
60	−30.6	5.1								
40	−31.2	4.8								
20	−31.7	4.5								
10	−35.3	2.9								
6	−38.3	1.3								
1.5		−6.1	19.9	29.9	38.2	45.2	51.4	56.9	61.7	
1.0		−9.3	17.5	27.9	36.4	43.7	50.1	55.8	61.0	
0.6		−13.4	14.2	24.6	33.3	40.8	47.4	53.0	58.4	
0.4		−16.6	11.5	21.9	30.8	38.5	45.3	51.2	56.9	
					In chloroform					
80	−33.2	1.9								
60	−36.1	−1.5								
40	−40.3	−5.5								
20		−10.8	12.0	20.6	27.9	34.3	39.5	44.5	48.8	56.1
10		−15.6	6.7	15.2	22.2	28.4	33.6	38.4	42.7	49.8
6		−19.2	3.2	11.5	18.6	25.0	30.2	34.9	39.1	46.3
4		−22.8	−0.2	8.4	15.6	22.0	27.1	32.0	36.4	43.9

TABLE II (*Continued*)

2		−28.2	−5.4	3.2	10.4	16.9	22.3	27.3	31.9	39.3
1		−33.3	−10.2	−1.4	6.1	12.6	18.0	22.9	27.4	34.8
				In carbon tetrachloride						
90	−30.8	4.0	26.4	34.9	42.3	48.9	54.7	59.8	64.7	72.1
80	−32.3	1.7	24.2	32.8	40.3	47.0	53.0	58.3	63.2	70.8
70	−34.5	−0.6	22.2	31.0	38.6	45.4	51.4	56.8	61.7	69.5
60	−36.8	−3.1	19.9	28.8	36.4	43.4	49.4	54.8	59.8	67.8
50	−39.7	−5.9	17.3	26.2	34.0	41.0	47.0	52.6	57.7	65.8
40		−8.7	14.6	23.6	31.2	38.3	44.3	49.7	55.0	63.0
30		−11.9	10.6	20.3	27.6	34.9	40.9	46.5	51.5	59.5
				In cyclohexane						
80	−33.2	2.1	24.6	33.2	40.7	47.3	53.2	58.3	63.1	70.6
60	−37.3	−2.6	20.6	29.1	36.7	43.3	49.4	54.6	59.5	67.4
40	−42.7	−8.5	14.7	23.4	31.3	38.1	44.3	49.9	55.0	63.0
20		−16.8	6.3	15.4	23.3	30.3	36.5	42.2	47.3	55.5
				In benzene						
90		3.9	26.5	35.3	42.6	49.2	54.7	59.8	64.4	71.9
80		2.0	24.6	33.5	41.0	47.6	53.3	58.4	63.1	70.6
70		0.4	22.6	31.5	39.1	45.7	51.5	56.9	61.5	69.2
60		−1.5	20.8	29.7	37.1	43.9	49.7	54.9	59.7	67.6
				In diethyl ether						
80	−32.5	2.6								
60	−36.2	−0.9								
40	−41.0	−5.3								

tion or extrapolation to determine the values of $1/T$ at various molar concentrations down to $N = 0.04$ for each of the missing members of the series; *i.e.*, for the homologs containing 18, 20, 26, 30, 32, 34 and 38 carbon atoms.[12] The results in centigrade degrees are shown in Table I. Because the basic equation involves the assumption that n is large, predicted data obtained by extrapolation to lower values of n would be less reliable and have therefore not been included in any of the tables.

Table I also gives predicted solubilities in *n*-hexane based upon the experimental data[11] for the methyl esters of the normal fatty acids containing a total of 9, 13, 15, 17 and 19 carbon atoms; for the normal fatty acids containing 9, 15 and 17 carbon atoms; for the symmetrical normal aliphatic ketones containing 19, 23, 31 and 35 carbon

(12) The authors are indebted to H. J. Harwood and C. W. Hoerr, Research Division, Armour and Co., for supplying the complete original experimental solubility data upon which their published data and the predicted data of Tables I, II and III are based.

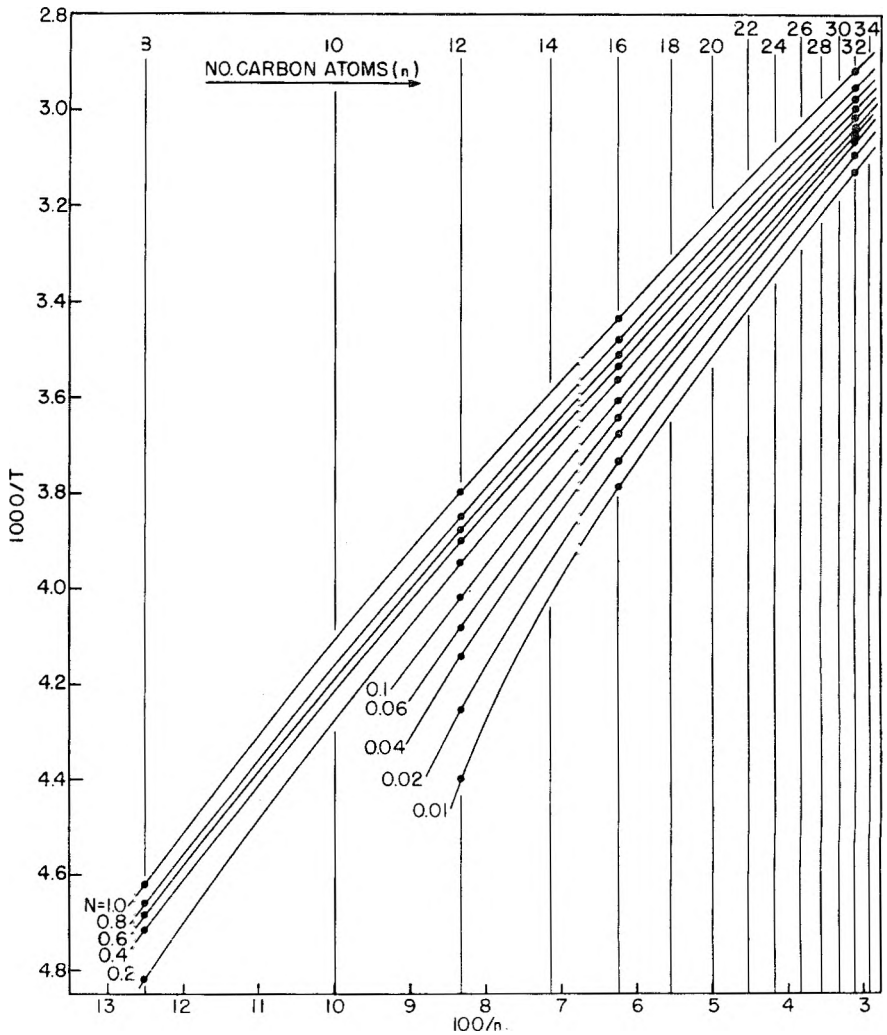

Fig. 3.—Solubility isopleths showing relation between carbon chain length and the reciprocal of the solubility temperature at selected concentrations of the normal hydrocarbons in butyl acetate (N = mole fraction).

TABLE III

PREDICTED SOLUBILITY TEMPERATURES IN DEGREES CENTIGRADE OF SOME *n*-ALIPHATIC METHYL KETONES IN VARIOUS ORGANIC SOLVENTS

No. carbon atoms Mole %	11	15	17	21	11	15	17	21	11	15	17	21
		In 1,4-dioxane				In benzene				In chloroform		
90	10.3	37.0	45.9	58.9	10.5	37.1	46.0	58.9	10.1	36.4	45.6	58.5
80	8.5	35.2	44.3	57.2	8.6	35.2	44.1	56.9	7.1	34.2	43.4	56.4
70	6.3	33.2	42.5	55.6	6.5	32.8	41.8	54.7	3.9	31.3	40.8	54.4
60	4.2	31.5	41.0	54.2	3.5	30.6	39.3	52.3	−0.8	27.9	37.7	51.6
50					0.0	27.6	36.6	49.4	−7.2	23.8	33.8	48.4
		In toluene				In carbon tetrachloride				In cyclohexane		
90	10.5	36.9	46.0	58.9	9.5	35.7	44.9	58.2	10.5	36.9	46.0	59.2
80	7.9	34.7	44.0	57.2	6.6	32.7	42.0	55.9	8.6	35.4	44.5	57.4
70	4.9	32.6	41.9	55.3	3.6	29.7	39.3	53.4	6.4	33.3	42.4	55.7
60	1.7	30.2	39.7	53.0	0.3	26.7	36.3	51.0	4.2	30.9	40.0	53.6
50	−2.2	27.6	37.4	50.5	−3.3	23.5	33.4	48.4	1.6	28.4	37.7	51.1
40	−8.1	24.5	34.5	47.7	−7.6	19.8	30.0	45.3	−1.0	25.5	34.8	48.6
30					−12.4	15.9	26.2	41.5	−3.2	22.2	31.4	45.1
20					−18.1	10.3	21.0	36.7				
		In ethyl acetate				In methanol				In 95% ethanol		
90	10.5	37.0	46.1	59.1	11.3	37.7	47.2	60.0	11.2	37.7	46.8	60.0
80	8.4	35.2	44.5	57.6	10.1	37.1	46.3	59.4	10.1	36.9	46.2	59.4
70	6.0	33.2	42.7	56.2	8.9	36.2	45.5	58.7	8.9	36.0	45.3	58.9
60	3.6	31.0	40.6	54.7	7.7	35.3	44.8	58.2	7.5	34.8	44.4	58.2
50	1.2	29.0	38.7	52.9	6.2	34.3	43.9	57.6	5.9	33.5	43.2	57.5
40	−1.9	26.4	36.3	51.0	4.9	33.1	42.9	56.9	4.8	32.6	42.3	56.4
30	−5.3	24.2	34.1	48.8	3.3	31.7	41.7	55.8	2.9	31.0	40.9	55.6
20	−10.2	21.0	31.1	45.8	1.5	30.3	40.5	55.0	0.8	29.3	39.5	54.5
10					−1.8	28.2	38.8	53.7	−2.5	26.4	36.8	52.2
6					−5.0	26.9	37.6	52.9	−5.5	23.9	34.6	50.0
4					−8.0	25.2	36.3	52.2	−8.3	21.7	32.6	48.6
		In isopropyl alcohol				In acetone				In acetonitrile		
90	10.9	37.3	46.3	59.6	10.5	37.2	46.5	59.3	10.1	36.7	46.3	59.8
80	9.7	36.1	45.3	58.6	8.8	35.9	45.3	58.4	8.2	35.1	44.9	59.1
70	8.2	34.7	44.1	57.8	6.6	34.3	44.0	57.4	6.5	33.8	43.8	58.4
60	7.0	33.5	42.9	56.7	4.6	32.5	42.3	56.4	4.9	32.7	42.7	57.6
50	5.6	32.4	41.8	55.8	1.9	30.6	40.8	55.5	3.2	31.6	41.8	56.8
40	4.4	31.4	40.8	54.8	−1.4	28.3	38.9	54.3	1.5	30.5	40.8	56.1
30	2.3	29.6	39.1	53.7	−4.5	26.0	36.9	53.0	−0.5	29.2	39.8	55.5
20	0.0	27.5	37.4	52.3	−9.0	23.1	34.7	51.7	−2.2	28.4	39.3	54.8
10	−4.7	23.5	33.9	49.5	−15.9	18.6	31.4	50.4	−4.3	27.8	38.7	54.6
6	−7.8	20.1	30.6	46.8					−6.1	27.0	38.2	54.5
4	−10.1	17.8	28.2	44.5					−8.1	25.5	37.5	54.4

atoms; and for the symmetrical normal aliphatic tertiary amines containing 24, 36 and 54 carbon atoms.

The experimental data for the normal alkyl methyl ketones containing 9, 13 and 19 carbon atoms[13] and for the normal paraffin hydrocarbons containing 8, 12, 16 and 32 carbon atoms[14] in a large variety of solvents were treated in the same way. The predicted solubilities of the missing members of each of these series are given in Tables II and III, respectively. They are based only on isopleths established by at least three points without resorting to extrapolation of the experimental solubility curves.

In general the isotherms and isopleths for the odd members of a homologous series do not coincide with those for the even members. They would not be expected to, since the constants in equations 1 and 2 have different values for the odd and even members. In a sense the symmetrical normal secondary amines $(C_mH_{2m+1})_2NH$ may be considered as belonging to an even or odd series depending upon whether m is even or odd. Actually, however, solubility data are available for members of both these series in a variety of solvents and in each case the isotherms[2,3] and the isopleths coincide. Thus, the hexane solubilities of the missing members of both the odd and even series can be predicted with confidence from the data for even members and they have been included in Table I. It seems reasonable to assume that the corresponding odd and even members of the homologous symmetrical ketones, $(C_mH_{2m+1})_2CO$, would show similar agreement and, therefore, that the solubilities in *n*-hexane of the (even) members containing a total of 21, 25, 29, 33 and 37 carbon atoms could be predicted from the data for the (odd) members containing 19, 23, 31 and 35 carbons.

(13) C. W. Hoerr, R. A. Reck, G. B. Corcoran and H. J. Harwood, THIS JOURNAL, **59**, 457 (1955).

(14) A. W. Ralston, C. W. Hoerr and L. T. Crews, *J. Org. Chem.*, **9**, 319 (1944).

However, since there are no solubility data for any of the even members to confirm this assumption, predictions have been made for the missing members of the odd series only.

The isopleth plots for many of the systems for which predictions were made consisted of straight or almost straight lines. In no case was the deviation from linearity very great. The isopleth plot for the normal hydrocarbons in butyl acetate (Fig. 3) is typical of the systems in which the greatest curvature was observed. Here the isopleth for $N = 1$, which coincides with that obtained by plotting the reciprocal of the melting points of all the members of the series,[15] is almost straight. The deviation from linearity is greatest at the lower values of n, as might be expected since the derivation of equation 9 involves the assumption that n is large.

Relative Applicability of Isotherm and Isopleth Methods.—The relative applicability of the isotherm and isopleth methods for correlating or predicting solubilities of homologous series depends upon the nature of the experimental data. Three points are required to establish the contour of a log N *vs.* n isotherm or a $1/T$ *vs.* $1/n$ isopleth. If a non-linear relationship is involved, additional points will usually be necessary, especially when marked degrees of curvature or large gaps in the data are involved.

Most of the experimental data from which the solubilities in Tables I, II and III were predicted are such that only the isopleth method is applicable. This is apparent from Fig. 4, representing the solubility curves for the normal hydrocarbons in butyl acetate, which can be considered more or less typical of these systems. Since fewer than three solubilities are known at any given temperature, isotherms cannot be drawn. Three or more points, however, are available for plotting isopleths representing the whole range of concentrations from $N = 1.0$ to $N = 0.01$ (Fig. 3).

Generally, however, the isopleth and isotherm methods are both applicable, each over a different range of concentration and temperature. Since the two ranges overlap, more extensive predicted data usually can be obtained by applying both methods. Consider, for example, the prediction of the solubilities of the normal fatty acids containing 14 and 20 carbon atoms in chloroform on the basis of the solubility curves for those containing 10, 12, 16 and 18 carbon atoms, represented by Fig. 5. At least three points are available for plotting isotherms for all temperatures below 43.9°. Similarly, three or more points are available for plotting isopleths for all concentrations between 19 and 100 mole %. Since these isotherms and isopleths are straight or only slightly curved lines they can be used to predict the solubilities of the C_{14} and C_{20} acids within these respective overlapping ranges. Thus, that portion of the C_{14} and C_{20} solubility curves which falls in the rectangular area representing temperatures below 43.9° and compositions above 19 mole % can be predicted by both methods. The portion of these

(15) National Bureau of Standards–American Petroleum Institute Research Project 44, Table 20a, Pts. 1–2.

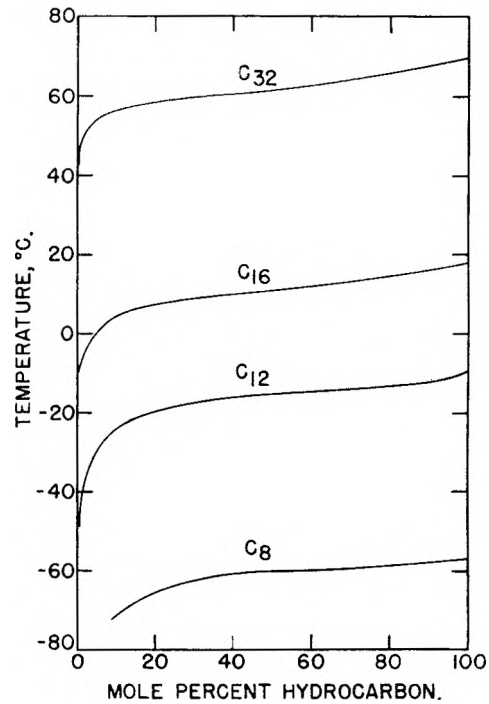

Fig. 4.—Solubility curves for normal hydrocarbons in butyl acetate used for predictions, illustrating the inapplicability of the isotherm method of prediction.

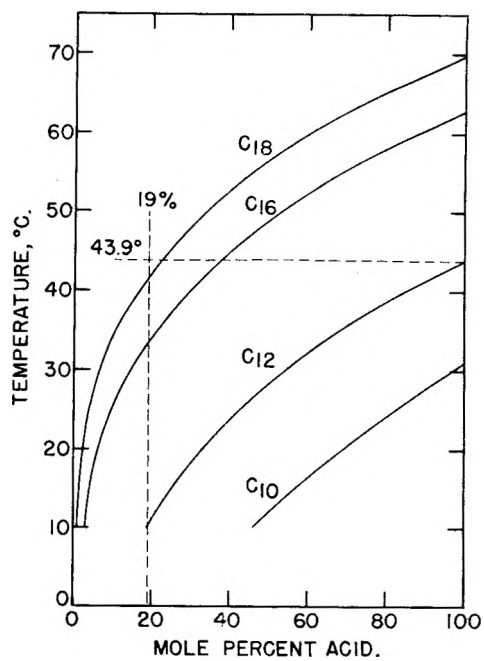

Fig. 5.—Solubility curves for capric, lauric, palmitic and stearic acids in chloroform, illustrating the overlapping of the isotherm and isopleth methods of prediction.

two curves representing solubilities above 43.9° can be predicted by the isopleth method only and that portion representing solubilities of less than 19 mole % can be predicted by the isotherm method only. In the range where both methods are applicable, that method should be used which gives the more linear relationship in the given range.

Having predicted the solubilities of the missing homologs listed in Tables I, II and III, it was now possible in most instances to apply the isotherm

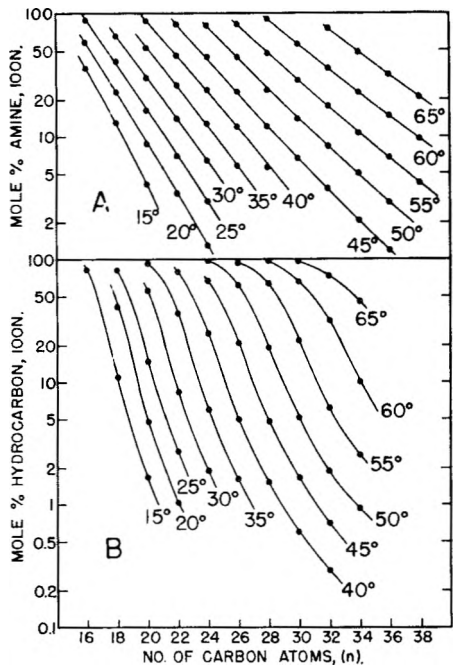

Fig. 6.—Log N *vs.* n isotherm plots based on the original and predicted solubility data for (A) the symmetrical normal secondary amines in n-hexane, and (B) the normal hydrocarbons in butyl acetate.

method of correlation to the combined data for each homologous series in each solvent. Smooth isotherms were obtained in all cases.

Comparison of the isopleth and isotherm plots for these systems over a given range of n values indicates that the isopleths are less likely to show marked curvature. Often neither method involved much curvature, *e.g.*, see Figs. 2 and 6A. At the other extreme, when the isopleth plots showed considerable curvature, the isotherms sometimes showed sigmoid curvature. Illustrative of this behavior are the solubilities of the normal hydrocarbons in butyl acetate (Figs. 3 and 6), ethyl acetate or butanone. Sigmoid curvature of isotherms has been shown previously[2,3] to be a fairly common occurrence.

The curvature of the isotherms can be attributed in part to the fact that the solubility data do not obey the laws of ideal solutions and therefore deviate from the requirements of equation 5.[2] The same is true of isopleths. In either case, the least curvature would be anticipated when the correlation curve represents solubility data all of which deviate from ideality most nearly to the same extent. A lesser tendency toward curvature can therefore be expected in the isopleth plots since they represent a correlation of the solubilities of the different homologs at the same mole per cent. concentration rather than at widely different concentrations.

Though the derivation of equation 9 involves the assumption that the solubilities follow the laws of ideal solutions, it was found that the isopleth method may still be applicable to markedly non-ideal systems. For example, the complete binary freezing point diagrams for lauric, myristic, palmitic and stearic acids with 2-aminopyridine show that two molecular compounds form in each of these systems.[16] Thus, in each case specific portions of the diagram represent the solubilities of the acid, the 1:1 acid–amine compound, and the 4:1 acid–amine compound, respectively, in the amine as solvent. The isopleth plots for these three systems proved to be almost straight lines and therefore permitted prediction of the corresponding portions of the binary freezing point diagram for arachidic acid with 2-aminopyridine. The predicted primary freezing points t in degrees centigrade for various binary compositions expressed as mole fraction of arachidic acid, N, are

N	t	N	t
1.00	74.7	0.70	70.0
0.90	73.3	...	...
.85	72.1	.50	70.0
...	...	.40	68.6
.80	72.3	.30	66.2

The freezing points for values of N between 0.85 and 0.80, between 0.70 and 0.50, and between 0.30 and 0.00 could not be predicted.

Isopleth plots also can be employed to smooth out experimental solubility data for a given homologous series of long chain compounds in a given solvent and to locate discrepancies in such data. The procedure used is essentially the same as that described in connection with the isotherm method of correlation.[2] By taking advantage of the two methods of prediction complete solubility data for additional solvents and other homologous series can be obtained with the minimum of experimental work.

Acknowledgments.—The authors express appreciation to H. J. Harwood and C. W. Hoerr for making their original experimental solubility data available and to G. I. Pittman for assistance in constructing the figures.

(16) R. R. Mod and E. L. Skau, THIS JOURNAL, **60**, 963 (1956).

SOME METAL CHELATES OF MERCAPTOSUCCINIC ACID[1]

BY GRAEME E. CHENEY, QUINTUS FERNANDO AND HENRY FREISER

Department of Chemistry, University of Pittsburgh, Pittsburgh 13, Pennsylvania

Received July 13, 1959

The acid dissociation constants of mercaptosuccinic acid and the stability constants of its chelates with zinc(II), cobalt(II) and nickel(II) have been determined. The zinc(II) chelate is more stable than the nickel(II) chelate; this is usually the case when a sulfur–metal bond is present in a metal chelate. Mercaptosuccinic acid, like most mercaptans, reduces copper(II) to copper(I).

This investigation was undertaken in order to obtain more information on the manner in which the mercaptide sulfur complexes with divalent metal ions. The Calvin[2]–Bjerrum[3] potentiometric titration technique has been used to study the behavior of cobalt(II), nickel(II), copper(II), manganese(II) and zinc(II) with mercaptosuccinic acid. Previous work on the chelate stabilities of mercaptoacetic acid,[4] β-mercaptopropionic acid[5] and 6-mercaptopurine[6] have shown that zinc(II) is more stable than the corresponding nickel(II) complex; in addition, these mercaptans tend to reduce copper(II) to copper(I). As revealed by this study, mercaptosuccinic acid behaves in a similar manner toward these three metal ions.

Experimental

Apparatus and Materials.—The titration apparatus, and standardization of sodium hydroxide and metal perchlorate solutions have been described previously.[7]

Potentiometric measurements of *p*H values were made with a Beckman Model "G" *p*H meter equipped with an external glass-saturated calomel electrode pair and standardized with Beckman buffers at *p*H 4.00 and 7.00 at 25°.

Mercaptosuccinic acid, kindly supplied by Evans Chemetics Inc., New York, was purified by extraction with ether, and dried in a vacuum desiccator. The equivalent weight found by titrating the two carboxylic acid protons was 75.2 (theoretical 75.1).

Neocuproine was obtained from G. F. Smith Chemical Co. and used without further purification.

Procedure.—The general procedure employed for the determination of the chelate formation constants in this work was to add 105.0 ml. of water and 5.0 ml. of metal perchlorate to a weighed amount of mercaptosuccinic acid in the titration vessel, degas the solution with prepurified nitrogen, and then titrate with standard sodium hydroxide (0.1 *N*) maintaining an atmosphere of nitrogen in the titration vessel throughout the titration. The ratio of reagent to metal ion was varied from 1:1 to 6:1 and the reported values of chelate formation constants are an average of four determinations for zinc(II) and nickel(II) and two for cobalt(II).

In the determination of the acid dissociation constants of mercaptosuccinic acid, 110 ml. of water was added to a weighed amount of reagent and the titration carried out with 0.1 *N* sodium hydroxide in a nitrogen atmosphere.

Calculation of Acid Dissociation Constants.—The acid dissociation constants of mercaptosuccinic acid were calculated from the potentiometric titration data as described. The equilibria involved are

$$H_3R \rightleftharpoons H^+ + H_2R^-, \quad K_1 = [H^+][H_2R^-]/[H_3R] \quad (1)$$

$$H_2R^- \rightleftharpoons H^+ + HR^=, \quad K_2 = [H^+][HR^=]/[H_2R^-] \quad (2)$$

$$HR^= \rightleftharpoons H^+ + R^\equiv, \quad K_3 = [H^+][R^\equiv]/[HR^=] \quad (3)$$

where H_3R represents mercaptosuccinic acid and parentheses denote molar concentrations.

In the titration of mercaptosuccinic acid with sodium hydroxide, the first two buffer regions overlap; the third buffer region occurs at a sufficiently high *p*H so that the equilibrium involving K_3 may be considered independently of K_1 and K_2.

Considering the equilibria involving only K_1 and K_2 it can be shown that

$$\frac{H^+ + Na^+ - OH^-}{T_{H_3R}} = \frac{K_1(H^+ + 2K_2)}{(H^+)^2 + H^+K_1 + K_1K_2}$$

where T_{H_3R} is the total concentration of mercaptosuccinic acid and if

$$\frac{(H^+ + Na^+ - OH^-)}{T_{H_3R}} = S, \text{ then}$$

$$\frac{(H^+)^2S}{(S-2)} + H^+K_1\left(\frac{S-1}{S-2}\right) + K_1/K_2 = 0$$

a plot of $(H^+)^2S/(S-2)$ against $H^+[(S-1)(S-2)]$ will give a straight line of slope equal to K_1 and intercept equal to K_1K_2. K_3 was evaluated from the part of the neutralization curve pertaining to the species $HR^=$ in the usual manner.[8]

Calculation of Stepwise Formation Constants.—If K_1 and K_2 are the acid dissociation constants of the carboxylic acid functionalities and K_3 is that pertaining to the mercaptan dissociation in mercaptosuccinic acid, it can be shown that $\bar{n}$, the average number of anions $(O_2C\text{–}CHS\text{–}CH_2\text{–}CO_2)^{-3}$ bound to a divalent metal ion is given by

$$\bar{n} = \frac{1}{T_M}\left[3T_{H_3R} - Q\left(\frac{H^+(3[H^+]^2 + 2H^+K_1 + K_1K_2) + [H^+]^2K_1 + 2H^+K_1K_2 + 3K_1K_2K_3}{H^+(3[H^+]^2 + 2H^+K_1 + K_1K_2}\right)\right]$$

where T_M = total metal ion concentration, T'_{H_3R} = total mercaptosuccinic acid concentration, $Q = 3T_{H_3R} - H^+ - Na^+ + OH^-$. The stepwise formation constants for the chelates of zinc(II), nickel(II) and cobalt(II) were obtained by plotting $\bar{n}$ against $-\log R$ where

$$R = (O_2C\text{–}CHS\text{–}CH_2\text{–}CO_2)^{-3} = \frac{QK_1K_2K_3}{H^+(3[H^+]^2 + 2H^+K_1 + K_1K_2)}$$

The values of $-\log R$ at $\bar{n} = 0.5$ and 1.0 gave the first stepwise formation constant as $\log K_1$ and the useful comparative constant $\log K_{av}$, respectively. The second stepwise formation constant, $\log K_2$, was evaluated from the relation

$$2 \log K_{av} = \log K_1 + \log K_2$$

since the maximum value of $\bar{n}$ obtainable below the metal hydrolysis region was 1.3.

Results and Discussion

Titration Curves.—The titration curve of mercaptosuccinic acid against sodium hydroxide indicates that the two carboxylic acid groups have "overlapping" dissociation constants since there are only two buffer regions, one between *p*H 3 and 5, and the other beyond *p*H 10. Further, a strong

(1) Abstracted from the thesis submitted by G. E. Cheney in partial fulfillment of the requirements for the Ph.D. degree at the University of Pittsburgh, June, 1959.

(2) M. Calvin and K. Wilson, *J. Am. Chem. Soc.*, **67**, 2003 (1945).

(3) J. Bjerrum, "Metal Ammine Formation in Aqueous Solution," P. Haase and Son, Copenhagen, 1941.

(4) D. L. Leussing, *J. Am. Chem. Soc.*, **80**, 4180 (1958).

(5) Q. Fernando and H. Freiser, *ibid.*, **80**, 4929 (1958).

(6) G. Cheney, H. Freiser and Q. Fernando, *ibid.*, **81**, 2011 (1959).

(7) H. Freiser, R. G. Charles and W. D. Johnston, *ibid.*, **74**, 1383 (1952).

(8) A. E. Martell and M. Calvin, "Chemistry of the Metal Chelate Compounds," Prentice-Hall Inc., New York, N. Y., 1952.

inflection point, between pH 6 and 9 corresponds to the formation of the disodium salt of mercaptosuccinic acid. Thus, the first buffer region is attributed to the two carboxylic acid groups and the second to the sulfhydryl group. The acid dissociation constants determined on this basis are given in Table I together with values for similar carboxylic acids for purposes of comparison; pK_{a1} and pK_{a2} refer to carboxylic acid group dissociations, pK_{a3} refers to the mercaptan group dissociation.

A comparison of the dissociation constants of the sulfhydryl groups in mercaptosuccinic, mercaptoacetic and β-mercaptopropionic acids reveals that pK_{a3} of mercaptosuccinic acid is somewhat lower than might be expected on the basis that the dissociation involved is from a dinegatively charged anion.

TABLE I

ACID DISSOCIATION CONSTANTS OF SOME CARBOXYLIC ACIDS AT 25.0° IN WATER

	pK_{a1}	pK_{a2}	pK_{a3}
Mercaptoacetic acid[4]	3.60	..	10.55
β-Mercaptopropionic acid[5]	4.38	..	10.38
Mercaptosuccinic acid	3.30	4.94	10.64
Aminosuccinic acid[9]	1.94	3.70	9.62[a]
Malic acid[10]	3.26	4.68	...
Succinic acid[10]	4.07	5.28	...

[a] Refers to amino group.

The titration curves in the presence of metal ions reveal the over-all stoichiometry of the reactions between these ions and mercaptosuccinic acid. In order to neutralize the protons released by the two carboxylic acid groups of the reagent, 6.4 ml. of 0.1 N sodium hydroxide are required; consequently, the displacement of the reagent ion curve at 6.4 ml. of base and pH 8.5 from the reagent curve must be due to proton release, which in the absence of metal hydrolysis must depend on the reaction between the mercaptan group and the metal ion. Since nickel(II) and zinc(II) show an equivalent weight corresponding to one-half the atomic weight at this pH, whereas cobalt(II) shows an equivalent weight corresponding to its atomic weight, it may be concluded that the nickel and zinc chelates are 2:1, mercaptosuccinic acid to metal ion, while the cobalt chelate is 1:1.

The titration curve of mercaptosuccinic acid in the presence of manganese(II) does not correspond to a stoichiometry of either 1:1 or 2:1 mercaptosuccinic acid to manganese(II). Further, the displacement from the mercaptosuccinic acid curve occurred in the metal hydrolysis region; thus, this reaction was not further considered.

The titration curve with copper(II) and mercaptosuccinic acid shows the same displacement from the reagent curve as that of the similar curves for nickel(II) and zinc(II) at pH 8.5, however, this is misleading and the reaction is discussed below.

Chelate Formation Constants.—Table II gives the stepwise formation constants for zinc(II) and nickel(II) with mercaptosuccinic acid, and log K_1 for cobalt(II). Values of log K_2 are calculated from the values of log K_1 and log K_{av} since the maximum value of $\bar{n}$ obtainable below the metal hydrolysis region was 1.3. Formation constants of structurally similar compounds have been added for comparison.

As would be expected if mercaptosuccinic acid is tridentate, there is a large difference, Δ, between log K_1 and log K_2 (Table II) for the nickel(II) and zinc(II) chelates. This value is much larger than the corresponding values for the mercaptoacetic and β-mercaptopropionic acid chelates. Further log K_1 for mercaptosuccinic acid is larger than the corresponding values for the other carboxylic acids, and since Chaberek and Martell[11] have suggested that aminosuccinic acid is tridentate by comparing formation constant values of it and other amino carboxylic acids with various transition metal ions, it seems probable that mercaptosuccinic acid behaves as a tridentate ligand with nickel(II) and zinc(II). In this connection it is noteworthy that Sidgwick[12] has compared the relative donor properties of oxygen and sulfur and in general showed that the donor properties of sulfur are dependent to a greater extent on the acceptor properties of the metal; on the other hand, according to Sidgwick, oxygen and nitrogen may be considered quite similar with respect to their tendency to complex with metal ions. Therefore, it is not surprising that the mercaptosuccinic acid–zinc(II) chelate is more stable than the aminosuccinic acid–zinc(II) chelate, nor is the fact that there is a reversal in order of stabilities between the corresponding nickel(II) and zinc(II) chelates of mercapto- and aminosuccinic acids, since zinc(II) would appear to accept sulfur as the donor atom

TABLE II

CHELATE FORMATION CONSTANTS AT 25.0° IN WATER FOR MERCAPTOSUCCINIC AND STRUCTURALLY RELATED CARBOXYLIC ACIDS

Metal ion	Mercaptoacetic acid[4]	β-Mercaptopropionic acid[5]	Mercaptosuccinic acid	Aminosuccinic acid[12]
Co(II)				
log K_1	5.84	...	6.31	5.90
log K_2	...	...	...	4.28
2 log K_{av}	12.15	...	...	10.18
Ni(II)				
log K_1	6.98	5.21	7.97	7.12
log K_2	6.55	4.39	4.90	5.27
2 log K_{av}	13.51	9.60	12.87	12.39
Zn(II)				
log K_1	7.86	6.75	8.47	5.84
log K_2	7.18	6.05	5.28	4.31
2 log K_{av}	15.04	12.80	13.75	10.15
Δ = log K_1 − log K_2				
Ni(II)	0.43	0.82	3.07	1.85
Zn(II)	0.68	0.70	3.19	1.53

[a] At 30° in water.

(9) R. F. Lumb and A. E. Martell, THIS JOURNAL, **57**, 690 (1953).

(10) R. K. Cannan and A. Kibrick, *J. Am. Chem. Soc.*, **60**, 2314 (1938).

(11) S. Chaberek and A. E. Martell, *J. Am. Chem. Soc.*, **74**, 6021 (1952).

(12) N. V. Sidgwick, *J. Chem. Soc.*, 433 (1941).

(13) S. Chaberek and A. E. Martell, *J. Am. Chem. Soc.*, **74**, 6021 (1952).

in its coördination sphere more readily than would nickel(II). It is suggested that this may be attributed to a steric effect since sulfur is larger than nitrogen.

It is interesting to note that values of 2 log K_{av} for mercaptosuccinic acid with nickel(II) and zinc(II) are less than the corresponding values for mercaptoacetic acid (Table II). This is readily understandable in view of the fact that the 2:1 chelate with mercaptosuccinic acid requires that there be four negative charges on it; consequently, it would be expected to be less stable, over-all, than a dinegatively charged chelate; further, the values of 2 log K_{av} for mercaptosuccinic acid are greater than those of β-mercaptopropionic acid. This is understandable since it has been shown[5] that six-membered sulfur-containinge helate rings are much less stable than five-membered sulfur-containing chelate rings.

The Copper(II) Reaction.—When copper(II) was added rapidly to a solution of mercaptosuccinic acid previously degassed with nitrogen, a transient blue-purple color was observed initially, and the solution developed a yellow color when the addition of the copper(II) was completed. The development of the yellow color indicated that copper(II) was reduced to copper(I) and the presence of the latter in solution was confirmed by reaction with neocuproine and subsequent extraction into chloroform.[14]

A consideration of the titration curve of copper(II) and mercaptosuccinic acid with sodium hydroxide shows that two protons are released from the mercaptan functionality per mole of copper(II) present. These data would fit the over-all stoichiometry represented by these equations postulated by Klotz, *et al.*[15]

$$2RSH^- + 2Cu^{++} = RSSR^{-4} + 2Cu^+ + 2H^+ \quad (4)$$

$$RSH^- + Cu^+ = RSCu^{-2} + H^+ \quad (5)$$

Over-all

$$4RSH^- + 2Cu^{++} = RSSR^{-4} + 2RSCu^{-2} + 4H^+ \quad (6)$$

where RSH represents mercaptosuccinic acid and RSSR represents the corresponding disulfide.

Acknowledgment.—The authors gratefully acknowledge the financial assistance of the U. S. Public Health Service.

(14) G. H. Morrison and H. Freiser, "Solvent Extraction in Analytical Chemistry," John Wiley and Sons, Inc., New York, N. Y., 1957.

(15) I. M. Klotz, G. H. Czerlinski and H. A. Fiess, *J. Am. Chem. Soc.*, **80**, 2920 (1958).

NOTES

SEPARATION OF BORON ISOTOPES BY ION EXCHANGE

By Yukio Yoneda, Toshio Uchijima[1] and Shoji Makishima

Department of Applied Chemistry, Faculty of Engineering, University of Tokyo, Tokyo, Japan

Received January 14, 1959

Various methods have been tried for separating boron isotopes,[2] some of which are used industrially. In this work we determined the separation factor of boron isotopes in the exchange reaction between an aqueous solution of boric acid and an anion-exchange resin. Such an ion-exchange method has been used for the separation of nitrogen isotopes.[3]

Experimental

Two ion-exchange columns (about 120 cm. in height) were prepared from 100–200 mesh spheres of Amberlite CG-400-I (polystyrene-quaternary amine type, strong base for chromatographic use); the capacities of the columns were about 650 and 900 meq. of $H_2BO_3^-$, respectively. After the usual pretreatment, the bed was restored to the OH^--cycle. Experimental procedures and the method of analysis have been described by Spedding, *et al.*[3]

An aqueous 0.03 *M* H_3BO_3 solution (I) or an aqueous 0.1 *M* H_3BO_3 solution containing 8 wt. % purified glycerol (II) was passed through a resin column at a flow rate of 0.5–0.7 ml./min. at room temperature. The OH^- ion is completely replaced by a certain form of borate ion due to the large reaction constant. When all the OH^- ion on the resin has been replaced by borate ion, boric acid solution begins to flow from the resin bed. The front boundary is somewhat diffuse because of the weak acidity of boric acid solution, even in the presence of glycerol. The amount of boric acid and the isotopic ratio of boron in each fraction of the effluent were analyzed. Isotopic analyses of boron isotopes were carried out by the usual method; B_2O_3, prepared from the sample, was fluorinated with CoF_3[4] to give BF_3 and the ratio of boron isotopes was measured with a mass spectrometer designed for isotopic analysis.[5]

In Fig. 1 the atomic fraction of ^{10}B (N%) in successive fractions of the effluent is plotted against the sum of the milliequivalents of $H_2BO_3^-$ in the effluent expressed as percentage of the column capacity. The form of the adsorbed

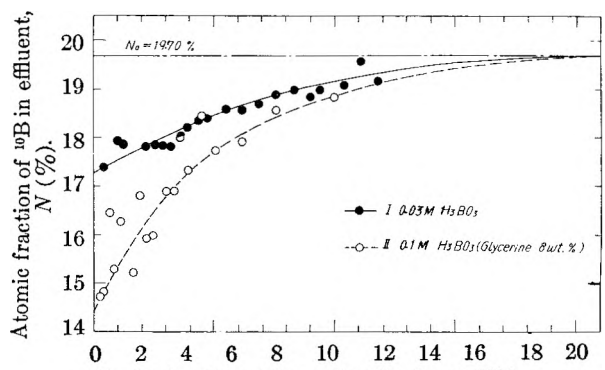

Fig. 1.—Atomic fraction of ^{10}B in effluent *vs.* equivalents in effluent.

(1) Tokai Laboratory, Japan Atomic Energy Research Institute, Tokai-mura, near Mito, Japan.

(2) See, S. Makishima, Y. Yoneda and T. Tajima, This Journal, **61**, 1618 (1957); or "Proc. of the Intern. Symposium on Isotope Separation," North-Holland Publ. Co., Amsterdam, 1958.

(3) F. H. Spedding, J. E. Powell and H. J. Svec, *J. Am. Chem. Soc.*, **77**, 6125 (1955).

(4) I. Kirschenbaum, U. S. Patent 2,622,014 (Dec. 16, 1952).

(5) A report of this mass spectrometer will appear soon.

ions was assumed to be $H_2BO_3^-$, as boric acid is a very weak acid. The natural abundance of ^{10}B in our boric acid sample was 19.70%.[6] In both runs, the lighter isotope was enriched in the resin phase. The exchange capacity of the resin used with these solutions was measured as follows; as the boric acid on a resin bed was eluted with rinsing water in an ordinary column method, resin after being filtered off with dry filter paper was equilibrated with a solution of a certain concentration. The exchange capacity at a specific concentration of boric acid was obtained by interpolation between the values at known concentration, as it *varies* with concentration. The exchange capacities of the resin when used with solutions I and II were 4.36 and 4.65 meq. ($H_2BO_3^-$)/g. resin (dry), respectively; the capacity with OH^- was 2.65 meq./g.

Discussion

From the exchange capacity of the resin and the data in Fig. 1, the separation factor α for the exchange reaction

$$R\text{-}H_2{}^{11}BO_3^- + H_3{}^{10}BO_3 \rightleftarrows R\text{-}H_2{}^{10}BO_3^- + H_3{}^{11}BO_3$$

was calculated according to Spedding, *et al.*[3]; the curves in Fig. 1 were extrapolated to the point where the atomic fraction N becomes equal to the atomic fraction of the original boron sample N_0. The following values were obtained for $\alpha = (^{10}B/^{11}B)_R/(^{10}B/^{11}B)_S$, where R and S denote the resin and solution phases, respectively. α (I, 0.03 M H_3BO_3) = 1.010_0, and α (II, 0.1 M H_3BO_3 with glycerine (8 wt. %)) = 1.016_6.

As a preliminary experiment has shown, α in simple aqueous boric acid solutions increases with decreasing concentration, the difference between the α-values of I and II is probably related to the presence of glycerol which is known to increase the acidity of boric acid solutions; the pK_a values of I and II were 10.2 and 7.6, respectively. This effect on acidity has been attributed to a difference in the ionization of boric acid which would also account for the difference in α-values.

Further experiments are in progress concerning the effect of concentration and acidity on α, and the separation of boron isotopes from other ions in various solvents and from the borate complex.

Acknowledgment.—The authors are indebted to Dr. Shun Araki for his help with the isotopic analysis, to Mr. Fujio Mochizuki for technical assistance and to Mr. Tetsuya Miyake for the measurement of exchange capacity. Ion-exchange resin and cobalt trifluoride were supplied by Nippon Organo Co., Ltd., and Osaka Kinzoku Kogyo Co., Ltd., respectively. The expense of this research was defrayed by a Grant in Aid from the Ministry of Education, Japan.

(6) The natural abundance of boron varies somewhat widely according to the origin of the reagent.

THE HIGH-TEMPERATURE TRANSFORMATION OF $MoGe_2$

BY ROBERT J. PEAVLER AND C. GERARD BECK, JR.

Contribution from the Materials Engineering Departments, Westinghouse Electric Corporation, East Pittsburgh, Pa.

Received April 20, 1959

During an X-ray diffraction study of the molybdenum–germanium system, Searcy and Peavler[1] found two forms of $MoGe_2$: α-$MoGe_2$, which constituted the whole of specimens prepared at 980°, and β-$MoGe_2$, always found mixed with α-$MoGe_2$ in specimens prepared at 1350°. These facts were first explained by assuming β-$MoGe_2$ to be the high-temperature form, which did not transform completely on rapid cooling to room temperature. Later, Searcy and Carpenter,[2] from studies of specimens quenched from high temperatures, concluded that α-$MoGe_2$ decomposed above 1095 ± 20°, forming Mo_2Ge_3 and liquid. They therefore held that β-$MoGe_2$ was not a stable phase of the system but a metastable phase formed during rapid cooling of the Mo_2Ge_3–liquid mixture.

The behavior of $MoGe_2$, if confirmed, would be of great interest, for β-$MoGe_2$ is isostructural with $MoSi_2$, a stable phase of the molybdenum–silicon system. This fact suggests that β-$MoGe_2$ will be stable under the proper conditions of temperature and pressure. A study of $MoGe_2$ at high temperature was therefore desirable to test the results of quenching experiments.

Experiments

A specimen of α-$MoGe_2$ was prepared by the reaction of the necessary quantities of thoroughly mixed molybdenum and germanium powders at 1000° in an evacuated sealed Vycor tube. A specimen for X-ray diffraction analysis was placed in a thin-wall capillary and sealed to prevent loss of germanium by evaporation. Diffraction patterns at temperatures from 970 to 1155° were made by use of a Unicam high-temperature diffraction camera of 19 cm. diameter. Copper radiation was used.

Results and Conclusions

The study showed that α-$MoGe_2$ is stable up to 1080 ± 15°, decomposing above this temperature to a mixture of Mo_2Ge_3 and liquid. In all diffraction patterns made up to 1065°, α-$MoGe_2$ was the only phase observed. In patterns made at 1095° or above, α-$MoGe_2$ had disappeared and was replaced by Mo_2Ge_3. The liquid phase could not be detected by X-ray diffraction methods, but liquid must have been present to meet phase rule requirements. The conclusions of Searcy and Carpenter are therefore fully confirmed by this study.

From the results of this work and the results of Searcy and Carpenter, it seems assured that β-$MoGe_2$ cannot appear in equilibrium diagrams of the Mo–Ge system at low pressure. In work done by Searcy and Peavler, by Searcy and Carpenter, and in these experiments, pressure was low, never exceeding the vapor pressure of germanium.

While the place of β-$MoGe_2$ in the Mo–Ge system is not yet established, we believe that it will be stable at high pressures. Searcy and Peavler found the pycnometric density of a mixture of α-$MoGe_2$ and β-$MoGe_2$ to be 6.9 g. cc., and found the X-ray density of β-$MoGe_2$ to be 8.91 g. cc. Although pycnometric densities of powders tend to be lower than X-ray densities, the difference between these values indicates that β-$MoGe_2$ is more dense than α-$MoGe_2$ and high pressures would promote the stability of β-$MoGe_2$. The presence of

(1) A. W. Searcy and R. J. Peavler, *J. Am. Chem. Soc.*, **75**, 5657 (1953).

(2) A. W. Searcy and J. H. Carpenter, unpublished work.

β-$MoGe_2$ in quenched specimens may therefore be explained by the formation of small high-pressure regions, in which β-$MoGe_2$ is stable, in rapidly cooling alloys.

SELF DIFFUSION IN LIQUIDS. II. COMPARISON BETWEEN MUTUAL AND SELF-DIFFUSION COEFFICIENTS[1]

By A. P. Hardt, D. K. Anderson, R. Ratcbun, B. W. Mar and A. L. Babb

Department of Chemical Engineering, University of Washington, Seattle Washington

Received March 28, 1959

The study of self and mutual diffusion in ideal and non-ideal systems has received much attention in recent years.[2-7] Attempts to account for the differences observed between the various diffusivities have been made by several authors.[8,9] The following generalizations concerning the behavior of self and mutual diffusivities may be made. Self and mutual diffusivities are equal in dilute solutions only. In ideal systems both self and mutual diffusivities are practically linear with mole fraction, while in non-ideal systems the curves show various degrees of curvature. It was shown previously[3] that in systems containing one associated and one unassociated component, the non-ideal characteristics are exhibited chiefly by the self diffusivity of the associated component.

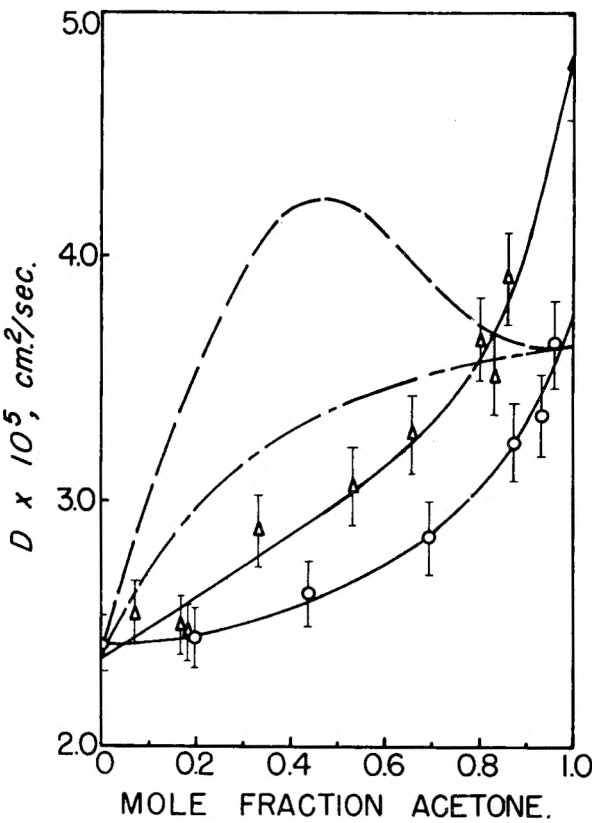

Fig. 1.—Diffusion in the acetone-chloroform system at 25°: — — —, mutual diffusion (ref. 7); ——, $(D_1X_2 + D_2X_1)(\mathrm{d} \ln a_1/\mathrm{d} \ln X_1)$; △, self diffusion of acetone; ○, self diffusion of chloroform; ▲, self diffusion of pure acetone (ref. 11).

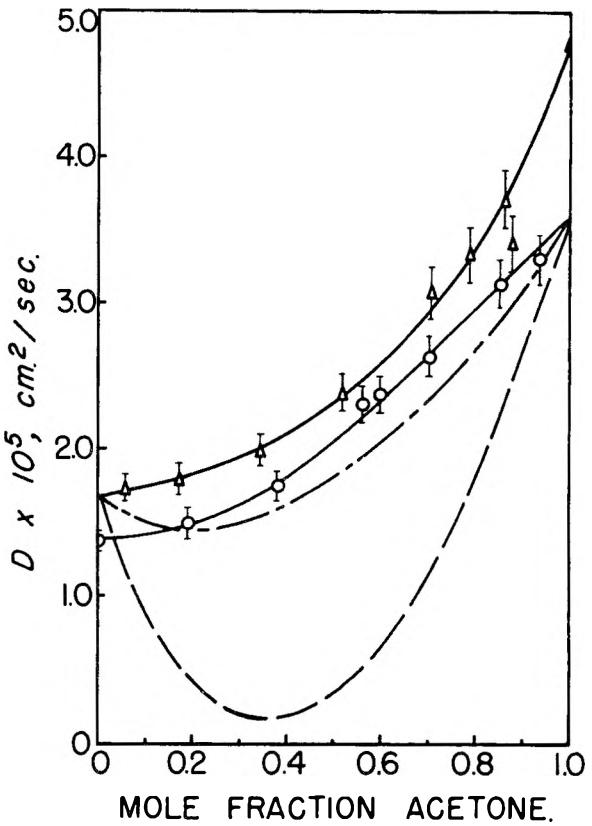

Fig. 2.—Diffusion in the acetone–carbon tetrachloride system at 25°: — — —, mutual diffusion (ref. 7); ——, $(D_1X_2 + D_2X_1)(\mathrm{d} \ln a_1/\mathrm{d} \ln X_1)$; △, self diffusion of acetone; ○, self diffusion of carbon tetrachloride; ▲, self diffusion of pure acetone (ref. 11).

Self diffusion coefficients at 25° for four binary liquid systems are reported together with a comparison with mutual diffusivities reported previously.[4,6,7] At present no attempt will be made to interpret the results theoretically.

Experimental

A capillary cell technique which has been described elsewhere[2] was used to obtain the experimental data. The solvents were the highest grades commercially available and in most cases were used without further purification. Benzene was stored over metallic sodium. Carbon-14 tracers were purchased from Volk Radio-Chemical Company. The counting cell used previously was replaced by a brass cell with a bottom tray of 0.0025 mm. aluminum foil, eliminating the use of glue or cement.

Results and Discussion

Self diffusion coefficients for the several systems are given in Table I: acetone–chloroform (Fig. 1), acetone–carbon tetrachloride (Fig. 2), benzene–carbon tetrachloride (Fig. 3) and ethanol–carbon tetrachloride (Fig. 4). The results are

(1) This work was supported by the Office of Ordnance Research, U. S. Army.

(2) P. A. Johnson and A. L. Babb, This Journal, **60**, 14 (1956).

(3) P. C. Carman and L. H. Stein, *Trans. Faraday Soc.*, **52**, 619 (1956).

(4) C. S. Caldwell and A. L. Babb, This Journal, **60**, 51 (1956).

(5) C. S. Caldwell and A. L. Babb, *ibid.*, **59**, 1113 (1955).

(6) R. H. Stokes and B. R. Hammond, *Trans. Faraday Soc.*, **52**, 781 (1956).

(7) D. K. Anderson, J. R. Hall and A. L. Babb, This Journal, **62**, 404 (1958).

(8) O. Lamm, *Acta Chem. Scand.*, **6**, 1331 (1952).

(9) L. S. Darken, *Am. Inst. Mining Met. Engrs., Inst. Met. Div., Metals Technol., Tech. Publ.*, 2311 (1948).

TABLE I

SUMMARY OF EXPERIMENTAL SELF DIFFUSION DATA

Acetone (1)–Chloroform (2)										
Mole fraction (1)	0.071	0.169	0.187	0.338	0.531	0.660	0.807	0.833	0.865	
$D_1 \times 10^5$, cm.²/sec.	2.55	2.49	2.47	2.89	3.05	3.27	3.66	3.52	3.91	
Mole fraction (2)	0.034	0.063	0.126	0.302	0.563	0.809	1.000			
$D_2 \times 10^5$, cm.²/sec.	3.64	3.35	3.24	2.85	2.64	2.45	2.42			
Acetone (1)–Carbon tetrachloride (2)										
Mole fraction (1)	0.060	0.175	0.343	0.520	0.710	0.790	0.865	0.881		
$D_1 \times 10^5$, cm.²/sec.	1.75	1.80	2.00	2.41	3.07	3.32	3.74	3.42		
Mole fraction (2)	0.059	0.146	0.294	0.402	0.435	0.615	0.804	1.000		
$D_2 \times 10^5$, cm.²/sec.	3.29	3.14	2.61	2.37	2.33	1.73	1.50	1.37		
Ethanol (1)–Carbon tetrachloride (2)										
Mole fraction (1)	0.012	0.020	0.121	0.147	0.216	0.337	0.487	0.888	1.000	
$D_1 \times 10^5$, cm.²/sec.	2.78	2.45	1.60	1.47	1.24	1.10	1.11	1.00	1.00	
Mole fraction (2)	0.069	0.224	0.363	0.636	0.764	0.960	1.000			
$D_2 \times 10^5$, cm.²/sec.	1.54	1.65	1.75	1.86	1.76	1.44	1.37			
Carbon tetrachloride (1)–Benzene (2)										
Mole fraction (1)	0.072	0.130	0.215	0.303	0.396	0.500	0.600	0.687	0.844	1.000
$D_1 \times 10^5$, cm.²/sec.	1.90	1.83	1.83	1.74	1.61	1.59	1.48	1.50	1.46	1.37

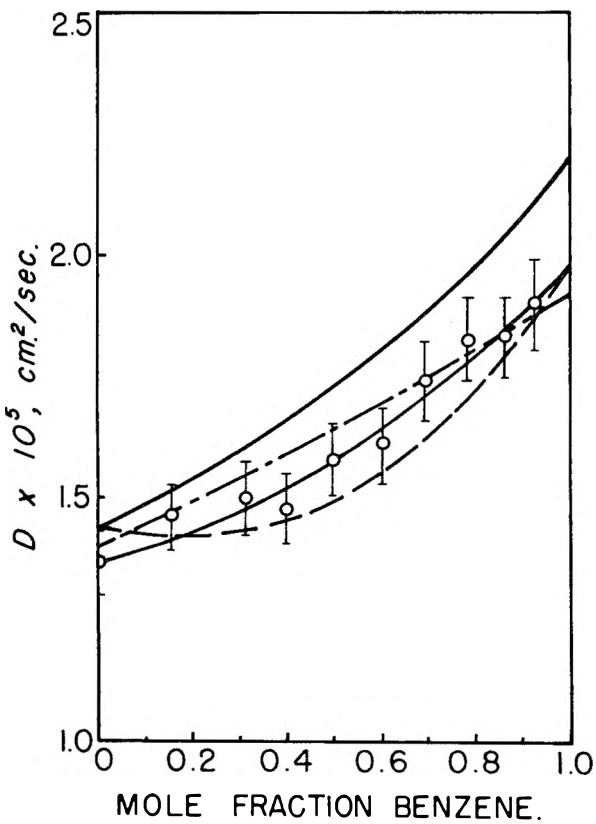

Fig. 3.—Diffusion in the benzene-carbon tetrachloride system at 25°: — — —, mutual diffusion (ref. 7); — —, $(D_1X_2 + D_2X_1)(\mathrm{d} \ln a_1/\mathrm{d} \ln X_1)$; ——, self diffusion of benzene (ref. 2); ○, self diffusion of carbon tetrachloride.

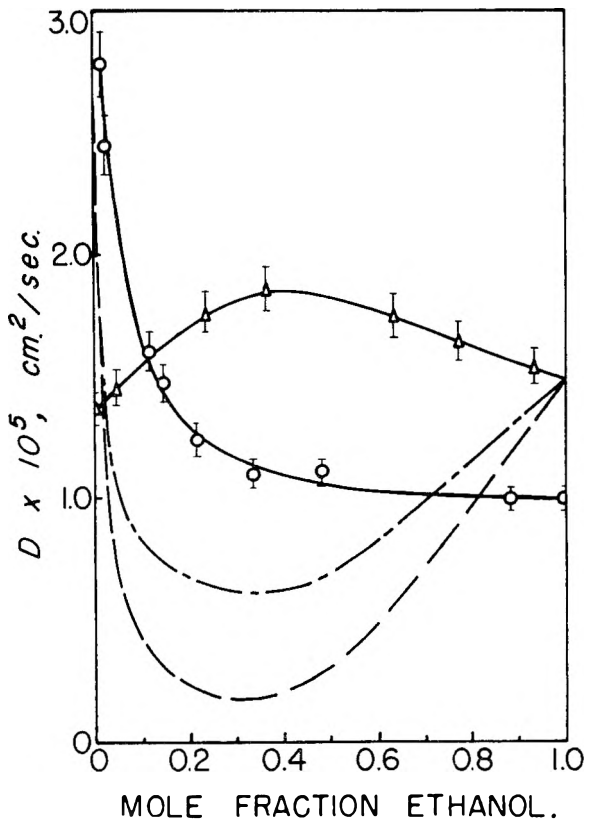

Fig. 4.—Diffusion in the ethanol–carbon tetrachloride system at 25°: — — —, mutual diffusion (ref. 6); — —, $(D_1X_2 + D_2X_1)(\mathrm{d} \ln a_1/\mathrm{d} \ln X_1)$; Δ, self diffusion of carbon tetrachloride; ○, self diffusion of ethanol.

considered to be accurate to within 5%. Considerable difficulty was encountered in obtaining the self diffusion coefficients of acetone in concentrated solutions. The amount of scatter for pure acetone was as large as 20%. For this reason, none of the authors' values for acetone are reported for mixtures greater than 90 mole % acetone. However, McCall and Douglas[11] of Bell Telephone Laboratories have measured the self diffusion coefficients of pure acetone at a series of temperatures using a nuclear magnetic resonance technique. Their data were interpolated to give a value of 4.8×10^{-5} cm.²/sec. at 25°.

Values of $(D_1X_2 + D_2X_1)(\mathrm{d} \ln a_1/\mathrm{d} \ln X_1)$ where D_i, X_i and a_i are the self diffusivity, mole fraction and solution activity, respectively, are plotted with the mutual diffusivity for the purposes of comparison. The activity term was calculated from ther-

(11) D. W. McCall and D. C. Douglas, Bell Telephone Laboratories, personal communication.

modynamic data available in the literature.[12-15] For acetone–carbon tetrachloride isobaric boiling point–composition data were used. For the remaining systems, isothermal data were available at the temperature required.

At the present time, the belief is generally held that the gradient of the chemical potential constitutes the effective driving force for diffusion. The process of self diffusion, however, is visualized as the movement of molecules in a thermodynamically homogeneous environment such that the chemical potential gradient for the diffusion process is unity. From this it follows that self diffusivities are related to mutual diffusivities through this gradient, a principle first announced by Darken[9] and recently reiterated by Carman and Stein.[3]

The experimental data obtained in this study were applied to Darken's proposed relationship between self and mutual diffusivities

$$D_{12} = (D_1X_2 + D_2X_1)(\mathrm{d} \ln a_1/\mathrm{d} \ln X_1)$$

It is apparent that, although the shape of the curve and the location of the minima are predicted correctly for non-ideal systems, the over-all effect of the activity term is to over-correct the predicted values. This is true for both positive and negative deviations from Raoult's law since both cases are exhibited here. One would expect better agreement between theory and experiment for ideal systems. It is surprising to note, however, that for the nearly ideal system, benzene–carbon tetrachloride, theory predicts a non-linear diffusion curve, while the experimental data are linear.

It seems certain from these results that the relationship between diffusion and chemical potential is not as simple as previous investigators have believed. These discrepancies between theory and experiment probably are due in part to association of the diffusing molecules. However, the difficulties in describing the diffusion mechanism for associated systems are many since one must obtain quantitative results as to the degree of association and relate these results to diffusion phenomena. At present the authors are working on this problem with encouraging results and will submit a report on it later.

(12) H. Röck and W. Schröder, *Z. physik. Chem. N. F.*, **11**, 41 (1957).

(13) K. C. Bachman and E. L. Simmons, *Ind. Eng. Chem.*, **44**, 203 (1952).

(14) A. L. Edwards, B.S. Thesis, University of Washington, 1954.

(15) F. Ishikawa and T. Yamaguchi, *Bull. Inst. Phys. and Chem. Res. (Tokyo)*, **17**, 246 (1938).

PROTON RESONANCE SHIFTS OF ACIDS IN LIQUID SULFUR DIOXIDE

BY S. BROWNSTEIN[1] AND A. E. STILLMAN

Department of Chemistry, Cornell University, Ithaca, New York

Received May 2, 1959

It is desirable to have a simple means for determining the dissociation constants of strong acids. A correlation between the change in frequency of the proton resonance signal of an acidic hydrogen and the dissociation constant of that acid has been obtained for several strong acids in aqueous solution.[2,3] Since there is rapid exchange between the protons of the acid and those of the solvent only a single resonance line is observed for both these species. By measuring the chemical shift of this line at a variety of acid concentrations the dissociation constant for the acid may be estimated. This method is especially useful for strong acids, where most other methods are not too good.

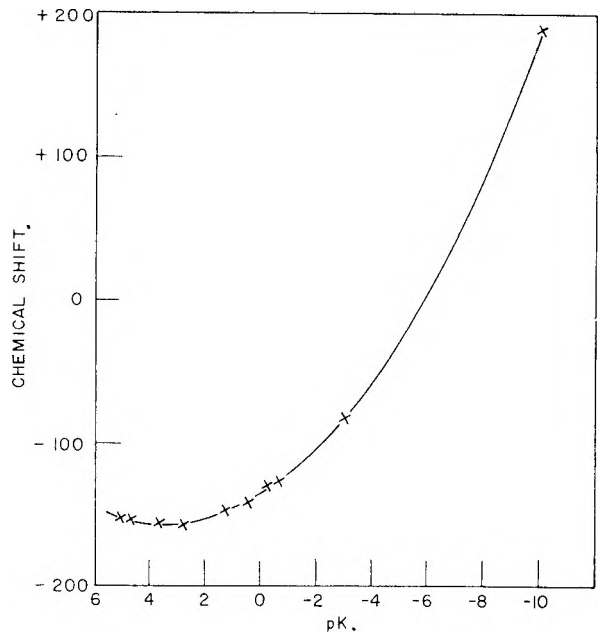

Fig. 1.—Dependence of chemical shift upon acid strength: The chemical shift is in cycles per second at a resonance frequency of 40 megacycles.

It was thought that if a solvent not containing exchangeable protons was used, a single measurement might suffice to determine an approximate acid dissociation constant. Liquid sulfur dioxide was chosen as solvent since a wide variety of compounds is soluble in it. Although relative acid strengths in liquid sulfur dioxide need not be in the same order as in water nevertheless it was found that an excellent correlation exists between the dissociation constant of an acid in water and its proton resonance shift when dissolved in liquid sulfur dioxide.

Experimental

The proton resonance spectra were obtained in a manner described previously.[4] The side band modulation[5] was generated by a Heathkit Square Wave Generator, Model SQ1. After the frequency was adjusted for superposition of the side band with the peak due to the acid proton the pulses from the square wave generator were counted on an Instrument Development Laboratories Model 161 Scaling Unit. The modulating frequency could be adjusted to within one cycle per second and its value determined within one tenth of a cycle per second.

The sample cell was the inner tube of a precision bore concentric tubing assembly[6] to which was attached a male

(1) Division of Applied Chemistry, National Research Council, Ottawa, Canada.

(2) H. S. Gutowsky and A. Saika, *J. Chem. Phys.*, **21**, 1688 (1953).

(3) G. C. Hood, A. C. Jones and C. A. Reilly, THIS JOURNAL, **63**, 101 (1959), contains earlier references.

(4) S. Brownstein, *J. Am. Chem. Soc.*, **80**, 2300 (1958).

(5) J. T. Arnold and M. E. Packard, *J. Chem. Phys.*, **19**, 1608 (1951).

(6) J. R. Zimmerman and M. R. Foster, THIS JOURNAL, **61**, 282 (1957).

6/20 standard taper joint. With a known weight of acid in it, the cell was placed on a vacuum line and sulfur dioxide condensed into it at −60°. The cell was capped quickly and the weight of sulfur dioxide determined.

The reference for the chemical shifts was benzene in the annular space between the concentric tubes. The shifts are in cycles per second with the more positive values at higher field. Diamagnetic susceptibility corrections were made in the usual manner.[7] The volume magnetic susceptibilities of the solutions were calculated from those of the pure components assuming ideal behavior. Even if the diamagnetic susceptibilities are not exactly additive only a small error would be introduced.

Results

The correlation between chemical shifts of the acidic proton and the pK of the acid in aqueous solution are shown in Fig. 1 and in Table I. The chemical shift for acetic acid was found to be constant up to a concentration of at least 7.40 molal. None of the determinations listed were made for concentration higher than 4.70 molal to assure the absence of concentration effects on the chemical shift.

TABLE I

RESONANCE POSITION OF ACIDIC PROTONS IN LIQUID SULFUR DIOXIDE

Acid	pK	Molality	Obsd. shift	Cor. shift
$(CH_3)_3C$–COOH	5.1	1.46	−139.8	−152.1
CH_3COOH	4.75	2.15	−132.3	−154.2
HCOOH	3.68	4.05	−134.9	−156.2
$CH_2ClCOOH$	2.81	0.98	−135.6	−156.7
$CHCl_2COOH$	1.30	2.16	−129.5	−147.3
CCl_3COOH	0.52	2.19	−127.5	−143.6
CF_3COOH	−0.26	4.70	−114.6	−128.9
CH_3SO_3H	−0.6	1.71	−117.5	−126.6
H_2SO_4	−3	1.03	− 59.0	− 83.2
$HClO_4$ (70%)	−10	2.12	+207	+189
HBr	−9	18.4	+380	+375
HI	−10		+203	+202

Spectra of 51, 60, 65 and 70% aqueous perchloric acid dissolved in liquid sulfur dioxide were obtained. A single line, due to rapid exchange of the acid and water hydrogens, was observed at the lowest concentration. At higher concentrations two lines are observed with the one at highest field attributed to perchloric acid because of its lesser intensity. The data are given in Table II. It is assumed that the chemical shift of 100% $HClO_4$ dissolved in liquid sulfur dioxide would be that shown by the 70% acid since the rate of exchange of acid and water protons is no longer affecting the observed chemical shift.

TABLE II

PROTON RESONANCE OF AQUEOUS PERCHLORIC ACID IN LIQUID SULFUR DIOXIDE

Aq. acid, % concn.	Molality in SO_2 soln.	Cord. shift	
51	2.33	H_2O	− 15.0
		$HClO_4$	− 15.0
60	2.13	H_2O	+ 15.8
		$HClO_4$	+ 18.7
65	2.51	H_2O	+ 28.7
		$HClO_4$	+189
70	2.12	H_2O	+ 45
		$HClO_4$	+189

A general treatment of shifts in line positions due to proton exchange has been presented.[8] Simplifying assumptions were made and an equation obtained that related displacement of the lines of two species in equal concentration with the rate of exchange of the two species. For the case where the mole fractions of the exchanging species are not equal, but the line widths are small compared with the distance between them, one obtains

$$\Delta\omega[4\tau^2(\Delta\omega)^2 - \tau^2(\delta\omega)^2 + 2] = \delta\omega(p_B - p_A)$$

The symbols have the same meaning as in ref. 8. From this one may calculate that a 2.13 molal solution of 60% perchloric acid in liquid sulfur dioxide has the proton exchange rates

$$k_{H_2O} = 2.05 \text{ sec.}^{-1}$$
$$k_{HClO_4} = 15.0 \text{ sec.}^{-1}$$

These exchange rates are in a convenient region for measurement by proton resonance spectroscopy. It is likely that they would depend upon the molality of the aqueous acid in sulfur dioxide and upon the concentration of the aqueous acid. The exchange rates might be related to the concentration of ion pairs in the solution.

All the acids shown in the figure have the acidic proton attached to oxygen. If the proton is bonded directly to another element different magnetic anisotropy effects would overshadow the change in shielding of the proton due to its different acidity. One such example is hydrogen bromide. An 18.4 molal solution in liquid sulfur dioxide has a corrected chemical shift of +375 cycles. This is much higher than would be expected from its acid strength alone and is considerably higher than that for the pure liquid.[9] There is evidence for 1:1 complexes of SO_2 and hydrogen halides in aqueous solution and such a complex if present in liquid sulfur dioxide could easily give unusual shielding effects.[10] It was necessary to keep the sample in a Dry Ice-bath until shortly before running the spectra since at room temperature it reacted fairly quickly to give bromine, sulfur and water. Hydrogen iodide in liquid sulfur dioxide had a corrected chemical shift of +202 cycles, in agreement with its acid strength. This is much lower than the value observed for the pure liquid.[9] In this case no chemical reaction is observed for the solution in sulfur dioxide.

Discussion

It appears that there may be a correlation between the chemical shift of an acidic proton in liquid sulfur dioxide solution and the dissociation constant of the corresponding acid in aqueous solution. Therefore this method might be useful as an easy way to get approximate dissociation constants of strong acids. If concentrated aqueous solutions of strong acids are dissolved in sulfur dioxide, one may determine the exchange rates between the water and the acidic protons.

(7) A. A. Bothner-By and R. E. Glick, *J. Chem. Phys.*, **26**, 1651 (1957).

(8) H. S. Gutowsky and C. H. Holm, *ibid.*, **25**, 1228 (1956).

(9) W. G. Schneider, H. J. Bernstein and J. A. Pople, *ibid.*, **28**, 601 (1958).

(10) S. Witekowa, T. Paryjczak and T. Witek, *Zeszty Nauk Politech. Lodz., No. 22, Chem.*, **7**, 17 (1958); *C.A.*, **53**, 1975e (1959).

THE HEAT OF FORMATION OF FORMIC ACID

BY G. C. SINKE

Thermal Laboratory, The Dow Chemical Company, Midland, Michigan

Received April 24, 1959

The heat of formation of formic acid derived by Waring[1] from equilibrium studies is not in agreement with the heat of combustion (determined prior to 1900). The disagreement is unusual in that the equilibrium data indicate the heat of combustion to be too high, while most of the older heat of combustion values tend to be too low. A new determination of the heat of combustion is in agreement with the equilibrium values.

Experimental

Commercial formic acid was purified by fractional crystallization until freezing curve analysis indicated a purity of better than 99.8 mole %. Analysis of the combustion gases indicated the sample had a carbon content of 99.9 ± 0.1% of theoretical.

The calorimetric system and technique was the same as that used previously[2] except that the sample was enclosed in a small bag of Mylar film. The film had a heat of combustion of $\Delta U_R/M$ = 5461.7 ± 1.8 cal. g.$^{-1}$ and analyzed 62.12% carbon and 4.18% hydrogen. The remainder was assumed to be oxygen. Washburn corrections were calculated by the method of Prosen.[3] Results are given in Table I. The sample mass is based on the mass of carbon dioxide produced, after correction for the carbon dioxide calculated from the weighed Mylar bag. Results based on sample weight were slightly lower which would be expected if the impurity was water.

TABLE I

q_{Total}	q_{Mylar}	q_{HNO_3}	$q_{Washburn}$	Sample mass, g.	$-\Delta U_R/M$, cal. g.$^{-1}$
6224.36	905.22	0.16	14.40	3.99148	1329.0
6313.54	950.12	.00	14.43	4.02558	1328.8
6168.03	907.30	.32	13.81	3.95442	1326.8
6008.06	947.82	.16	13.04	3.79585	1329.6
				AV.	1328.6
				Stand. dev.	0.6

Results and Discussion

Employing a molecular weight of 46.027 and calculating to constant pressure gives ΔH^0_{c298} (l) = −60.86 ± 0.06 kcal. mole^{-1}. From heats of formation of liquid water and gaseous carbon dioxide[2] the heat of formation is calculated as $\Delta H^0_{f\ 298}$ (l) = −101.52 ± 0.06 kcal. mole^{-1}. The entropy of liquid formic acid at 298°K. is given by Stout and Fisher[4] and of carbon, hydrogen and oxygen by Stull and Sinke,[5] from which the free energy of liquid formic acid is −86.38 ± 0.06 kcal. mole^{-1}. Waring derived −86.45 and −86.39 kcal. mole^{-1} from two different dissociation equilibria. The excellent agreement is evidence against the existence of residual entropy in formic acid and supports recent spectroscopic and X-ray studies.[6] The most likely explanation for the high previous combustion data is that the formic acid contained some acetic acid, a common impurity which has a considerably higher heat of combustion.

(1) W. Waring, *Chem. Revs.*, **51**, 171 (1952).

(2) G. C. Sinke, D. L. Hildenbrand, R. A. McDonald, W. R. Kramer and D. R. Stull, THIS JOURNAL, **62**, 1461 (1958).

(3) E. J. Prosen, Chapter 6 in "Experimental Thermochemistry," edited by F. D. Rossini, Interscience Publishers, New York, N. Y., 1956.

(4) J. W. Stout and L. H. Fisher, *J. Chem. Phys.*, **9**, 163 (1941).

(5) D. R. Stull and G. C. Sinke, "Thermodynamic Properties of the Elements, No. 18 of the Advances in Chemistry Series, Edited by the Staff of Industrial and Engineering Chemistry," American Chemical Society, Washington, D. C.

(6) R. C. Millikan and K. S. Pitzer, *J. Chem. Phys.*, **27**, 1305 (1957).

A PARTIAL PHASE STUDY OF THE SYSTEM NaF–HF

BY ROBERT L. ADAMCZAK,[1] J. ARTHUR MATTERN AND HOWARD TIECKELMANN

Contribution from the Department of Chemistry, University of Buffalo, Buffalo, N. Y.

Received May 4, 1959

Although phase studies have been performed for the binary systems KF–HF,[2] RbF–HF[3] and CsF–HF,[4] little work has been done on the system NaF–HF. Several investigators[5–7] have studied the ternary system NaF–HF–H_2O in part. Tananaev,[8] studied this system more completely. He found that the solubility curves in the system showed an analogy to the KF–HF–H_2O system.[9] His 0° isotherm consisted of five branches corresponding to the solid phases NaF, NaF·HF, NaF·2HF, NaF·3HF and NaF·4HF. Unlike the acid fluorides of potassium, those of sodium had no congruent melting points but decomposed into HF and NaF·HF. The latter was stable up to 90° but decomposed completely at 150°. Jache and Cady[10] reported the solubility of NaF in liquid HF as follows: 30.1 ± 0.1 g. of NaF per 100 g. of HF at 11.0°, 25.1 ± 0.1 g. at −9.8° and 22.1 ± 0.1 g. at −24.3°. Wartenberg and Bosse[11] reported the decomposition temperature of NaF·HF to be approximately 270° while Froning, *et al.*,[12] reported 278°. In this Laboratory, phase studies of the system NaF–HF were made in the range of mole fraction 0.75 to 0.87 HF.

Experimental

The sodium fluoride was Mallinckrodt reagent grade (99.4%). The anhydrous hydrogen fluoride (99.9%) was obtained from Harshaw Chemical Company and was distilled before addition to the sodium fluoride.

A known amount of sodium fluoride was weighed into a reaction vessel of 200 to 250-ml. capacity. The reaction vessels were constructed of monel with needle valves machined from solid monel stock. Teflon gaskets were used to ensure air-tight seals. The hydrogen fluoride was distilled into the reaction vessel using a multipurpose manifold constructed of 1/4 in. copper tubing and brass needle valves. The vessels weighed about 700 g. when empty and usually held about a 300 g. charge of NaF and HF.

(1) From the M.A. thesis of Robert L. Adamczak, University of Buffalo, 1955.

(2) G. H. Cady, *J. Am. Chem. Soc.*, **56**, 1431 (1934).

(3) K. R. Webb and E. B. R. Prideaux, *J. Chem. Soc.*, 111 (1939).

(4) R. V. Winsor and G. H. Cady, *J. Am. Chem. Soc.*, **70**, 1500 (1948).

(5) A. Ditte, *Ann. chim. phys.*, [7] **10**, 556 (1897).

(6) D. B. Jehu and L. J. Hudleston, *J. Chem. Soc.*, **125**, 1451 (1924).

(7) N. D. Nagorskaya and A. V. Novoselova, *J. Gen. Chem.* (*U.S.S.R.*), **5**, 182 (1935).

(8) I. V. Tananaev, *ibid.*, **11**, 267 (1941).

(9) I. V. Tananaev, *J. Appl. Chem.* (*U.S.S.R.*), **11**, 214 (1938).

(10) A. W. Jache and G. H. Cady, THIS JOURNAL, **56**, 1106 (1952).

(11) V. H. N. Wartenberg and O. Bosse, *Z. Elektrochem.*, **28**, 386 (1922).

(12) J. F. Froning, M. K. Richards, T. W. Stricklin and S. G. Turnbull, *Ind. Eng. Chem.*, **39**, 275 (1947).

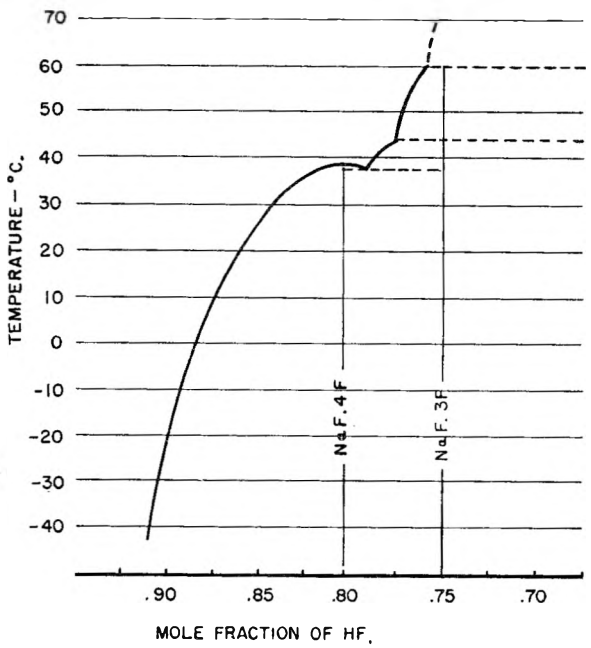

Fig. 1.—The system NaF–HF.

The reaction vessel and contents were heated to a temperature high enough to melt all the material and were maintained at this temperature for at least 24 hours with intermittent shaking. The establishment of homogeneity was verified by taking a weighed portion of the solution and evaporating the hydrogen fluoride. Thus, the ratio of the constituents could be checked against the original value. The heated reaction vessel was placed in an insulated apparatus mounted on a Fisher–Kahn shaker which produced about 280 vibrations per minute. Alternately, cooling and heating curves were obtained. Temperatures were measured using two calibrated copper–constantan thermocouples connected to a Leeds and Northrup Type K potentiometer and a modified Leeds and Northrup Micromax recorder.

After a sufficient number of curves had been obtained at the one mole fraction, the composition was changed by replacing the reaction vessel on the manifold and removing some hydrogen fluoride by distillation. Prior to recording further values, the vessel was heated to at least 50° above the expected temperature of the thermal effect and maintained at this temperature for at least ten hours with intermittent shaking. In this manner equilibrium was attained and results of heating and cooling curves were reproducible to within 0.2°. When a series of curves were completed the reaction vessel was opened and the contents examined. The melts were found to be completely homogeneous.

In cases where it was necessary to measure the pressure of this system an Ames strain gauge attached to a Be–Cu diaphragm was used.

Discussion

The average temperatures of the observed significant breaks in the curves are shown in Table I and illustrated in Fig. 1. The solubility results of Jache and Cady[10] were converted to mole fraction of HF in solution and are included in these data.

No freezing points were obtained from cooling and heating curves below a mole fraction of 0.75. Attempts were made to record pressure readings in this region but no significant results were obtained. At temperatures of 200° and above, pressures from ten to fifteen atmospheres were recorded. Even if freezing points had been obtained in this region the results would be of questionable accuracy because of the change in composition of the liquid phase by the vaporization of the hydrogen fluoride.

TABLE I

Mole fraction of HF in soln.	F.p., °C.	Eutectics 1	2	3	Solid phase
0.870[a]	13.3	...	...	...	NaF·4HF
0.860[a]	22.1	...	...	...	NaF·4HF
0.835[a]	34.2	...	...	...	NaF·4HF
0.830	35.4	...	...	...	NaF·4HF
0.821	37.1	...	...	...	NaF·4HF
0.815	37.5	...	...	...	NaF·4HF
0.810	38.6	...	...	...	NaF·4HF
0.806	39.1	...	...	...	NaF·4HF
0.801	39.7	...	...	...	NaF·4HF
(0.800)	39.8	...	...	...	F.P. of NaF·4HF
0.798	39.6	...	...	...	NaF·4HF
0.798	39.7	39.1	...	...	NaF·4HF
0.796	39.7	...	...	...	NaF·4HF
0.794	39.4	...	...	...	NaF·4HF
(0.792)	39.1	...	...	...	Eutectic
0.790	39.0	...	...	...	αNaF·3HF
0.790	39.3	39.1	...	...	αNaF·3HF
0.795	41.1	39.0	...	...	αNaF·3HF
0.784	41.5	38.9	...	...	αNaF·3HF
(0.776)	43.4	39.1	...	...	Transition
0.773	49.0	...	43.1	...	βNaF·3HF
0.772	51.2	...	43.1	...	βNaF·3HF
0.768	55.2	...	42.9	...	βNaF·3HF
(0.762)	62.5	...	43.0	...	βNaF·3HF
(0.762)	63.6	...	43.1	...	βNaF·3HF
(0.762)	...	...	43.1	...	βNaF·3HF
(0.762)	64.6	...	[b]	...	βNaF·3HF
0.757	62.6	...	[b]	...	βNaF·3HF
0.755	61.9	...	[b]	...	βNaF·3HF
0.754	...	...	42.9	61.6	βNaF·3HF
0.741	...	...	[b]	60.5	βNaF·3HF
0.731	...	...	[b]	60.4	βNaF·3HF
0.731	...	...	[b]	60.5	βNaF·3HF
0.724	...	...	[b]	60.3	βNaF·3HF
0.720	...	...	[b]	60.8	βNaF·3HF
0.712	...	...	[b]	60.3	βNaF·3HF
0.702	...	...	43.0	60.3	βNaF·3HF

[a] Calculated from solubility data of Jache and Cady.[10] [b] Indicates cooling was stopped before these temperatures were reached.

Thermal data in the region studied showed that the compound NaF·4HF had a congruent melting point at 39.8°. This work also indicated that the compound NaF·3HF had an incongruent melting point at 60.5° and that it existed in two forms. The form stable below 43.1° was called αNaF·3HF and the form stable above that temperature was called βNaF·3HF. It seems unlikely that any compounds richer in HF than NaF·4HF are formed. Table II lists significant points for the portion of the system studied.

Windsor and Cady[4] have observed several trends among alkali metal compounds MF·XHF as the atomic number of M increases: (1) corresponding compounds show decreasing melting points, (2) corresponding compounds show increasing stability, (3) the maximum value of X increases. In the present work, the melting point of NaF·4HF (39.8°) does not follow the general trend since the melting point of KF·4HF is 72.0°.[2] The melting point of Na·3HF (60.5°) is lower than that of KF·3HF (65.8°)[2] but the former compound has

TABLE II

Mole fraction HF in soln.	Temp., °C.	Type of point	Solid phases present
0.800	39.8	Freezing	NaF·4HF
0.792	39.1	Eutectic	NaF·4HF and αNaF·3HF
.776	43.1	Transition	αNaF·3HF and βNaF·3HF
.762	60.5	Peritectic	βNaF·3HF and (NaF·2HF)

an incongruent melting point. The "actual" melting point would be much higher. It appears from this work that the trend in stability is as expected with NaF·3HF less stable than KF·3HF. That NaF·4HF seems to be the highest acid fluoride of the NaF–HF system does not contradict the general trend of increasing maximum values for $\bar{X}$.

Summary.—In the range of mole fraction of HF 0.75 to 0.87, sodium fluoride and hydrogen fluoride form the compounds NaF·4HF, αNaF·3HF and βNaF·3HF.

DIFFUSION COEFFICIENTS OF ZIRCONIUM(IV) IN HYDROCHLORIC ACID SOLUTION AT 25°

BY D. A. WILLIAMS-WYNN

Leather Industries Research Institute, Rhodes University Grahamstown, South Africa

Received May 6, 1959

Diffusion coefficients of zirconium in nitric and perchloric acid solutions have been reported by previous workers using a somewhat limited range of time, concentration and acidity.[2,3] In the present work, diffusion coefficients of zirconium oxychloride have been determined over a wide range, using the porous glass diaphragm method previously developed.[4–7] In order to nullify the effect of the electric charge on the movement of the zirconium ion, a relatively high concentration of electrolyte was used as "swamping agent."[6,8] Sodium nitrate was used as supporting electrolyte because no complex nitrates of zirconium are known.[9]

Experimental

Reagents.—The solutions of zirconium oxychloride and supporting electrolyte (swamping agent) were made up in de-ionized distilled water. Purified zirconium oxychloride octahydrate was prepared from commercial salt by repeated recrystallizations from 9 *N* hydrochloric acid and was found by analysis to be more than 99.5% pure. All other reagents used for the supporting electrolyte or for *p*H adjustment were of C.P. grade.

Apparatus.—The magnetically-stirred diffusion cell employed in this work was similar to that described by Stokes[7] except that the pore size of the sintered-glass disc was 30–40 μ. All measurements were made in a thermostat at 25 ± 0.025°.

Procedure.—For the first series of measurements, 0.5 and 0.1 *M* solutions were prepared in 1.0 *M* sodium nitrate solution. Diffusion measurements were made at the natural *p*H of the oxychloride after storage at 21 ± 1° for varying periods up to 12 weeks. The second series was an investigation of the effect of concentration on the rate of diffusion. The solutions were all aged for 5 to 6 weeks before diffusion measurements were made.

The effect of acidity on the diffusion coefficient was investigated in the third series of measurements. In this case, acid was used as supporting electrolyte. When the concentration of the acid was <1 *M*, additional supporting electrolyte was added.

In all determinations the de-aerated zirconium solution was introduced into the lower cell compartment while the upper compartment was filled with supporting electrolyte of the same concentration and *p*H. Diffusion was permitted to proceed until 8 to 10% of the diffusing material had entered the upper compartment. The solutions were then removed and analyzed for zirconium by the Alizarin-S spectrophotometric method modified by the writer.[10] The diffusion coefficient was calculated in accordance with the equation given by Stokes.[11] The cell was calibrated using 0.1 *N* potassium chloride solution, the diffusion coefficient of which is 1.873×10^{-5} cm.^{2} sec.$^{-1}$.[12]

Results and Discussion

Diffusion Coefficient as a Function of Time.—The diffusion coefficient is relatively large initially (Table I) but rapidly decreases with increasing time. Within a period of 4 to 5 weeks the diffusion coefficient reaches a limiting value which changes only slightly with further aging up to 12 weeks. For the more concentrated solution (0.5 *M*), the decrease of the diffusion coefficient and the attainment of equilibrium is more rapid than with the 0.1 *M* solution. The effect of concentration on rate of diffusion is given in detail below.

TABLE I

VARIATIONS IN THE DIFFUSION COEFFICIENT OF ZIRCONIUM OXYCHLORIDE WITH AGE OF SOLUTION

Supporting electrolyte 1.0 *M* sodium nitrate; $\bar{D}$ in cm.^{2} sec.$^{-1}$.

0.5 *M* Zr solution		0.1 *M* Zr solution	
Age of soln., days	$\bar{D} \times 10^6$	Age of soln., days	$\bar{D} \times 10^6$
1.5	4.30	1.5	4.70
4	3.96	4	4.39
8	3.86	6	4.11
16	3.85	14	3.65
24	3.85	21	3.54
28	3.84	28	3.47
40	3.78	42	3.40
56	3.81	56	3.40
84	3.80	84	3.40

Diffusion Coefficient as a Function of Concentration.—The effect of zirconium concentration on the diffusion coefficient is given in Table II. Dilute solutions aged for 5 to 6 weeks were shown to have a lower diffusion coefficient than the more concentrated solutions aged for the same period, when measured at the natural *p*H. This indicates that the particles were less mobile in dilute solution than in concentrated solution. When the solu-

(1) Part of a thesis to be submitted to the Faculty of Science, Rhodes University, Grahamstown, in partial fulfillment of the requirements for the degree of Master of Science.

(2) G. Jander and K. F. Jahr, *Kolloid-Beih.*, **43**, 295 (1936).

(3) B. A. J. Lister and L. A. McDonald, *J. Chem. Soc.*, 4315 (1952).

(4) J. H. Northrop and M. L. Anson, *J. Gen. Physiol.*, **12**, 543 (1929).

(5) J. W. McBain and T. H. Liu, *J. Am. Chem. Soc.*, **53**, 59 (1931).

(6) G. S. Hartley and D. F. Runnicles, *Proc. Roy. Soc.* (*London*) **A168**, 420 (1938).

(7) R. H. Stokes, *J. Am. Chem. Soc.*, **72**, 763 (1950).

(8) A. Doyle Abbott and H. V. Tartar, THIS JOURNAL, **59**, 1193 (1955).

(9) W. B. Blumenthal, "The Chemical Behavior of Zirconium," D. Van Nostrand Co., Inc., New York, N. Y., 1958, p. 288.

(10) D. A. Williams-Wynn, *J. Soc. Leather Trades' Chemists*, **42**, 360 (1958).

(11) R. H. Stokes, *J. Am. Chem. Soc.*, **72**, 2243 (1950).

(12) R. H. Stokes, *ibid.*, **73**, 3527 (1951).

tions were diluted while maintaining the *p*H at the original value of the 0.8 *M* solution by addition of hydrochloric acid, and then aged, diffusion was much more rapid. The rate of diffusion is dependent less on the zirconium concentration than on acidity.

TABLE II

VARIATIONS IN THE DIFFUSION COEFFICIENT OF ZIRCONIUM OXYCHLORIDE WITH CONCENTRATION OF SOLUTION

Supporting electrolyte 1.0 *M* sodium nitrate; solutions aged 5–6 weeks; *c* in moles/l., $\bar{D}$ in cm.^{2} sec.$^{-1}$.

No *p*H adjustment			*p*H adjusted to 0.38		
c	*p*H	$\bar{D} \times 10^6$	*c*	*p*H	$\bar{D} \times 10^6$
0.856	0.38	3.86	0.856	0.38	3.86
.558	.47	3.84			
.494	.50	3.84			
.281	.65	3.71			
.280	.65	3.71			
.236	.72	3.65	.200	.38	4.01
.185	.86	3.69			
.110	1.00	3.47	.110	.38	4.17
.097	1.08	3.48			
.052	1.32	3.27	.055	.38	4.49

Diffusion Coefficient as a Function of Acidity.—Diffusion coefficients obtained in hydrochloric acid solutions are given in Table III together with coefficients for zirconium particles in solutions to which alkali had been added. The presence of acid increases the diffusion coefficient of zirconium but a limiting value is reached quickly. This value is attained when the acid concentration is 1 *M* or greater. By comparison, the results found by Lister and McDonald[3] in nitric acid solution show no limiting value. The addition of alkali on the other hand rapidly reduces the rate of diffusion. These results are probably in agreement with the formation of highly aggregated hydrolysis products. The highly basic solutions, particularly those that are faintly opalescent, contain particles that are probably markedly asymmetric and of high molecular weight, in which case the calibration of the cell by low molecular weight substances is not necessarily valid.[13]

TABLE III

VARIATIONS IN THE DIFFUSION COEFFICIENT OF 0.05 *M* ZIRCONIUM OXYCHLORIDE WITH ACIDITY OF SOLUTION

Solutions aged 8 weeks; *c* in moles/l., $\bar{D}$ in cm.^{2} sec.$^{-1}$

Added supporting electrolyte $NaNO_3$, *M*	Acid *c*	$\bar{D} \times 10^6$
...	5.00	4.63
...	2.00	4.63
...	1.00	4.59
0.5	0.50	4.57
.63	.37	4.49
.8	.20	4.46
.9	.10	4.30
1.0	.00	3.27
	Alkali *c*	
1.0	0.02	2.75
1.0	.04	2.44
1.0	.05	2.21

(13) A. E. Alexander and P. Johnson, "Colloid Science," Oxford University Press, Oxford, 1950, p. 242.

General Discussion.—A complete theoretical treatment of the relation between diffusion coefficient in liquid systems and ionic or molecular weight is lacking.[3] Approximate values of particle weight can be calculated from the Sutherland–Einstein equation and the equation expressing radius in terms of particle weight and partial specific volume.[14] Although these values are no more than approximate, it is interesting to examine the effect of various solution conditions on the particle size of zirconium, even if the results are regarded as only qualitatively correct. The particle weight of 730, calculated from the diffusion coefficients of 0.5 *M* zirconium in acid solutions of 1.0 to 5.0 *M*, indicate a degree of polymerization in the region of 3.7 (particle weight of the monomer[15] is taken to be 196). This is in close agreement with the values of 3 to 4 obtained by other methods.[16–18] In connection with the above, aggregation of zirconium particles by oxygen bridges[19] to give asymmetric linear polymers imposes severe limitations on the validity of particle weights calculated from diffusion data, particularly when the diffusion coefficients are small.

Acknowledgment.—The author wishes to thank Dr. R. L. Sykes for useful suggestions and constructive criticism during the course of this work.

(14) Ref. 13, p. 259.
(15) Ref. 9, p. 124.
(16) K. A. Kraus and J. S. Johnson, *J. Am. Chem. Soc.*, **75**, 5769 (1953).
(17) J. S. Johnson and K. A. Kraus, *ibid.*, **78**, 3937 (1956).
(18) A. J. Zielen and R. E. Connick, *ibid.*, **78**, 5785 (1956).
(19) W. B. Blumenthal, *Ind. Eng. Chem.*, **46**, 528 (1954).

THE SLOW EVOLUTION OF HEAT IN HEAT OF IMMERSION CALORIMETRY[1]

BY C. A. GUDERJAHN, D. A. PAYNTER, P. E. BERGHAUSEN AND R. J. GOOD[2]

University of Cincinnati, Department of Applied Science, Cincinnati Ohio

Received May 22, 1959

Since the time of Pouillet[3] thermal data in studies of heats of immersion have been analyzed assuming that the "heat of immersion" is released all at once, and that effects of appreciable duration are due to thermal transients of the system.[4,5]

During measurements of the heat of immersion of alumina in water, heat release was observed for a period of several hours—a time far greater than that required for thermal transients to die out. This note reports our efforts to analyze this phenomenon.

Experimental

Our twin calorimeter has been described elsewhere[5]; it was run adiabatically. All runs stretched over periods of several hours. Results are reported for immersion at 20°.

The solids were extracted with distilled water and acti-

(1) From the Ph.D. theses of C. A. Guderjahn (1955) and D. A. Paynter (1954).
(2) Convair Scientific Research Laboratory, 5001 Kearney Villa Road, San Diego 11, California.
(3) M. Pouillet, *Ann. chim. phys.*, **10**, 141 (1822).
(4) G. E. Boyd and W. D. Harkins, *J. Am. Chem. Soc.*, **64**, 1190, 1195 (1942).
(5) P. E. Berghausen, in "Adhesion and Adhesives," F. Clark, J. E. Rutzler and R. L. Savage, editors, John Wiley and Sons, Inc., New York, N. Y., 1954, p. 225.

vated under vacuum. Fifteen-ml. sample bulbs were used. Correction for heat of bulb breaking was made [6] Heat of stirring was measured separately for each run. Areas were measured by N_2 adsorption.[7]

J. T. Baker and Co. Al_2O_3 was activated at 150 to 300°, commercial Davidson Co. SiO_2 was activated at 250°, du Pont "Ti-Pure" anatase and rutile were activated at 150 to 350° and Godfrey L. Cabot Co. Graphon was activated at 300°. Of the five solids, only the SiO_2 was porous as indicated by a Type 4 adsorption isotherm.[7]

Analysis of Data.—To facilitate estimation of slow heat from time–temperature curves, we assumed the rate of release of slow heat decayed exponentially with time. With this hypothesis, the expression for total heat evolved up to time t takes the form

$$r = h_i + h_s(1 - e^{-\lambda t}) + \int_0^t m\,\Delta T\,dt \qquad (1)$$

h_s = total slow heat
h_i = total immediate heat
$r(t)$ = total heat released up to time t
m = heat leakage coefficient (measured separately, as a function of differential temp.). The last term on the right is the cumulative heat leakage
ΔT = absolute temp. difference between flask and bath
λ = time constant for the process

A typical graph of raw data for alumina (a sample activated at 150°) is given in Fig. 1; also shown are the raw data corrected for heat leakage. (In the absence of slow heat, the curve for the open circles would approach a straight line after about 5 minutes.) Figure 2 shows result of the treatment eq. 1, rearranged to the form

$$(h_i + h_s) - r + \int_0^t m\,\Delta T\,dt = h_s e^{-\lambda t} \qquad (2)$$

Extrapolation to $t = 0$ yields 105 ergs/cm.^{2} for h_s, and the half-life for the slow heat $t_{1/2}$ is 67 minutes. The satisfactory fit to a straight line is evident, indicating that over the intervals employed the analysis is valid.

When the slow heat is known as a function of time, its contribution to the temperature rise may be deducted. The resulting curve resembles temperature traces obtained when there is no slow heat, and the usual extrapolation to zero time can be made accurately.

Results.—Table I summarizes our results. Probable errors (50% confidence limits for mean values) are reported where five or more runs under constant experimental conditions were made.

TABLE I

HEATS OF IMMERSION IN WATER

Substance	Act. temp., °C.	Surface area, m.^{2}/g.	Immed. heat, erg/cm.^{2}	Slow heat, erg/cm.^{2}	Half-life of slow heat, min.
Al_2O_3	150	7.16	427	86	70
	250	7.94	582	319	51
	300	8.3	679 ± 7	332 ± 39	139 ± 27
SiO_2	250	701	165 ± 0.3	6.3 ± 0.1	34 ± 4
TiO_2					
Anatase	300	11.06	441 ± 14	<5	<8
Rutile	300	7.59	406 ± 2	<7	<8
Graphon	300	95.0	31.2	7.5	(60–120)

(6) C. A. Guderjahn, D. A. Paynter, P. E. Berghausen and R. J. Good, *J. Chem. Phys.*, **28**, 520 (1958).

(7) S. Brunauer, "The Adsorption of Gases and Vapors," Princeton University Press, Princeton, N. J., 1945.

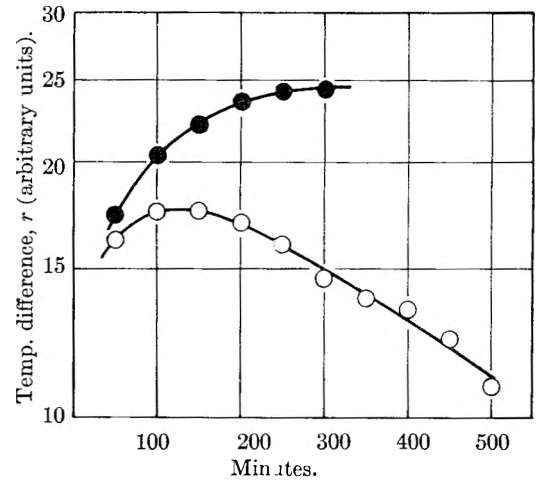

Fig. 1.—Calorimeter differential temperature *vs.* time for immersion of alumina in water: ○, raw data; ●, data corrected for heat leakage; Al_2O_3 activated at 150°.

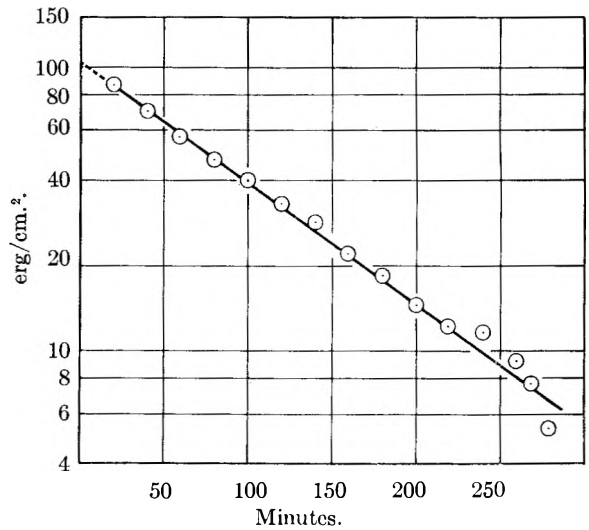

Fig. 2.—Semilog plot of total heat minus heat evolved up to time t *vs.* time; Al_2O_3 activated at 150°.

It may be seen that for alumina, the slow heat was very appreciable, of long duration, and increased with activation temperature. There was no sensible dependence of slow heat, or of its half-life, on immersion temperature. For a series of Al_2O_3 samples activated simultaneously at 300°, it appeared that $t_{1/2}$ increased linearly with h_s.

For silica gel, slow heat also was evolved over a long period of time, but the magnitude of the heat, per cm.^{2}, was much smaller than with alumina. (Since the area was very large, a small heat per cm.^{2} represented a large total heat.) $t_{1/2}$ appeared to be independent of the magnitude of the slow heat.

With rutile and anatase, no slow heat was observed. If any was present, its time constant was less than the time for thermal transients to die out, and its magnitude was too small (less than 2% of the fast heat) to be detected.

With Graphon, slow heat was observed both with oxygen-saturated and oxygen-free water. The uncertainty in $t_{1/2}$ (60 or 120 minutes) was caused at least in part by the small absolute magnitude of h_s: the total slow heat, in joules, was less than

$^1/_{50}$ that observed with alumina or silica; hence the analysis of the recorded data was more uncertain.

No data of heats of immersion of alumina in water were found in the literature, for comparison with our results. For silica, the immediate heat was of the same order as that previously reported[8,9] for high-area silica. Immediate heat values for TiO_2 and Graphon are in satisfactory agreement with published results.[10,11]

Discussion.—The very small relative magnitude of the slow heat, *e.g.* as reported above for silica, explains why this effect has not been noticed before. A run ordinarily lasts about 20 minutes (Boyd and Harkins[4] ran 16 minutes). For a first-order process, one must run two half-lives to get the reaction 75% to completion.[12] For our silica, with h_s = 6.3 erg/cm.^{2} and $t_{1/2}$ = 34 minutes, only 2.2 erg/cm.^{2} of slow heat would be evolved in a 20-minute run. This is 1.3% of the total heat, a magnitude that would ordinarily be laid to experimental error. When a twin calorimeter is not used, it is difficult to attain sufficient stability and low noise level to be confident of an effect of this size.

A possible mechanism for slow evolution of heat for Al_2O_3 and SiO_2 is rehydration of surface aluminoxane or siloxane groups to aluminol or silanol groups. Young[13] has showed that silica dehydrates reversibly above 150° and (in part) irreversibly above 400°, but complete dehydration does not occur until above the sintering range (>900°). Young discussed mechanisms but not energetics. Probably the hydrolysis of unstrained surface siloxanes should be endothermic. But at sites of surface strain[14] (*e.g.*, highly strained siloxane groups) hydrolysis could be highly exothermic. Makrides and Hackerman[9] discuss hydrolysis of surface siloxane groups and comment on their heats of immersion of SiO_2, "An undetermined, but probably small, heat evolution from rehydration is included in the apparent heat of wetting of powders evacuated at temperatures above 200–300°."

Thus it seems reasonable to attribute the slow heat for Al_2O_3 and SiO_2 to this hydrolysis. This mechanism agrees with the trend of increase of slow heat, and of $t_{1/2}$, with activation temperature for alumina. The rather large probable errors in h_s and $t_{1/2}$ are not surprising, since it might be hard to reproduce the exact concentration of strained groups, let alone the distribution of strain energies, in independent activations. Very probably the number of sites taking part in the processes leading to slow heat is much smaller than the number of sites responsible for the immediate heat.

It is not clear why TiO_2 produced effectively no slow heat. If the rehydration mechanism is correct for Al_2O_3 and SiO_2, then the absence of slow heat for anatase and rutile may be due to the fact that they are formed as crystals from solution, and not by dehydration of a gelatinous hydrous oxide. Or perhaps if surface titanol groups exist, they can be dehydrated without leaving a strained group susceptible to hydrolysis.

For graphite, the mechanism is probably quite different. Oxidation of surface carbons by water was suggested by McBain, *et al.*,[15] and was more recently studied by Pierce, *et al.*[16] The reaction was slow, and the products were H_2, CO and no doubt chemisorbed oxygen.

Presumably only carbons located at edges of basal planes would react with water. (Attack on carbon atoms in the interior of a plane would be endothermic, having a very large activation energy.) An estimate using bond energies, for possible reactions of *edge* carbons, gives a heat of 5 to 20 kcal./mole. Combining this range for the heat with the estimate[10] that about 1/1500 of the sites for Graphon are hydrophilic, a value of about 1 to 4 erg/cm.^{2} is obtained. This is of the same order of magnitude as the observed values, which ranged from 5 to 13 erg/cm.^{2}

Support of the U. S. Air Force, under contracts AF 33(616)231 and AF 33(616)2824, is acknowledged. This work forms part of WADC reports 55–44 and 56–188. We thank L. A. Girifalco and J. A. McAndrews for the surface area measurements.

(8) F. E. Bartell and R. M. Suggitt, THIS JOURNAL, **58**, 36 (1954).

(9) A. C. Makrides and N. Hackerman, *ibid.*, **63**, 594 (1959).

(10) J. J. Chessick, F. H. Healey, A. C. Zettlemoyer and G. J. Young, *ibid.*, **58**, 887 (1954).

(11) P. Basford, C. Anderson, F. Murphy and G. Jura, "Proc. 2nd Int. Cong. Surf. Act.," Vol. 2, Academic Press, Inc., New York, N. Y., 1957, p. 90.

(12) J. M. Sturtevant, in Weissberger's "Technique of Organic Chemistry," Vol. 1, 2nd ed., Interscience Pub. Co., New York, N. Y., 1949, pp. 731–845.

(13) G. J. Young, *J. Coll. Sci.*, **13**, 67 (1958).

(14) E. B. Cornelius, T. H. Milliken, G. A. Mills and A. G. Oblad, THIS JOURNAL, **59**, 809 (1955).

(15) J. W. McBain, J. L. Porter and R. F. Sessions, *J. Am. Chem. Soc.*, **55**, 2294 (1933).

(16) C. Pierce, R. N. Smith, J. W. Wiley and H. Cordes, *ibid.*, **73**, 4451 (1951).

TRACER-DIFFUSION COEFFICIENTS OF CESIUM ION IN AQUEOUS ALKALI CHLORIDE SOLUTIONS AT 25°

BY REGINALD MILLS AND L. A. WOOLF[1]

Department of Radiochemistry, Research School of Physical Sciences, The Australian National University, Canberra, A.C.T.

Received June 5, 1959

Considerable data have now accumulated for the tracer-diffusion of several monovalent ions, in the three supporting electrolytes KCl, NaCl and LiCl, over the general concentration range 0.1–4 *M*. The ions, the coefficients of which have been measured under these conditions, are the anions Cl^- [2] and I^- [3] and the cations Na^+, [4–6] Rb^+ [6] and H^+.[7] All these measurements have been made by the reliable magnetically-stirred diaphragm cell method, which, however, sets a lower limit on the concentration, at which measurements are valid, of about 0.1 *M*. This limitation precludes the use of these

(1) Department of Chemistry, University of Wisconsin, Madison, Wisconsin.

(2) R. Mills, THIS JOURNAL, **61**, 1631 (1957).

(3) R. H. Stokes, L. A. Woolf and R. Mills, *ibid.*, **61**, 1634 (1957).

(4) R. Mills, *ibid.*, **61**, 1258 (1957).

(5) R. Mills, *J. Am. Chem. Soc.*, **77**, 6116 (1955).

(6) R. Mills, THIS JOURNAL, **63**, 1873 (1959).

(7) L. A. Woolf, Ph.D. Thesis, University of New England, Armidale, N.S.W., 1959.

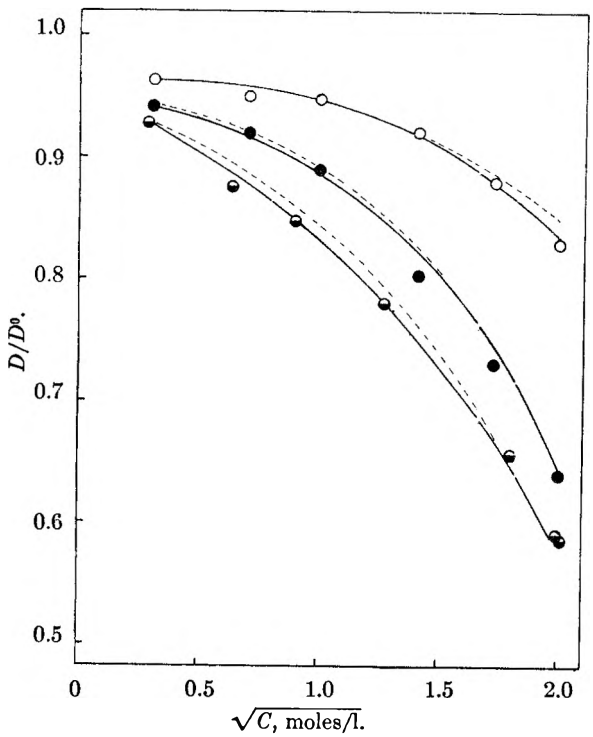

Fig. 1.—Cs^+ ion diffusion in KCl, NaCl and LiCl: O, KCl; ●, NaCl; ⊖, LiCl; – – – –, Rb^+ ion diffusion curves.

data for the testing of the Onsager limiting law.[8] Measurements in the very dilute region are, however, now being made with the continual monitoring capillary method[9,10] and data in the concentration range up to 0.1 *M* for the above ions should soon be forthcoming. Such complementary data ought to allow formulation of theoretical and empirical extensions to the limiting law covering both dilute and concentrated solutions as in the analogous conductivity case.[11] In the meantime, accumulation of data such as are reported in this paper is justified for the intercomparison of cations and anions in the same supporting medium. In particular, the testing of semi-empirical viscosity corrections should prove very useful when the limiting laws can be extended.

Experimental

The potassium chloride and sodium chloride solutions were prepared by weighing calculated amounts of the analytical quality reagent and diluting to volume. Lithium chloride was prepared by a similar method to that of Stokes and Stokes.[12] The concentration of the initial lithium chloride stock solution was determined by conductance measurements after appropriate weight dilution and this then was diluted by volume to give solutions covering the concentration range studied. These procedures were checked by conductance measurements with a Leeds and Northrup Jones bridge and shown to give an accuracy in concentration of better than 0.1%. Diaphragm cell manipulation has been adequately described in previous papers.[3,5]

The radiotracer was Cs^{134} which was obtained in the form of aqueous cesium chloride from the Radiochemical Centre, Amersham, England. As in previous studies,[3,4] scintillation counting techniques were used.

(8) L. Onsager, *Ann. N. Y. Acad. Sci.*, **46**, 241 (1945).
(9) R. Mills and E. W. Godbole, *Aust. J. Chem.*, **11**, 1 (1958).
(10) R. Mills and E. W. Godbole, *ibid.*, **12**, 102 (1959).
(11) R. A. Robinson and R. H. Stokes, "Electrolyte Solutions," Butterworth's Scientific Publications, London, England, 1955, p. 153.
(12) J. M. Stokes and R. H. Stokes, THIS JOURNAL, **60**, 217 (1956).

Results

The results of the work are given in Table I. The estimated accuracy in D is 0.4%. $D^0_{Cs^+}$ has been calculated to be 2.057×10^{-5} cm.^{2}/sec., taking $\lambda^0_{Cs^+} = 77.26$/ohm/cm.[13]

(13) Ref. 11, p. 452.

TABLE I

TRACER-DIFFUSION COEFFICIENTS OF Cs^+ IN AQUEOUS ALKALI CHLORIDE SOLUTIONS AT 25°

c, moles/l.	$D \times 10^5$, cm.^{2}/sec.	D/D^0
	KCl	
0.1	1.981	0.963
0.5	1.957	.951
1.0	1.951	.948
2.0	1.897	.922
3.0	1.810	.880
4.0	1.707	.830
	NaCl	
0.1	1.936	0.941
0.5	1.892	.920
1.0	1.828	.889
2.0	1.651	.803
3.0	1.504	.731
4.0	1.315	.639
	LiCl	
0.0805	1.890	0.919
0.4025	1.801	.876
0.805	1.744	.848
1.610	1.607	.781
3.221	1.351	.657
3.990	1.216	.591
4.025	1.208	.587

Discussion

In Fig. 1, the present data for Cs^+ are compared with tracer-diffusion results for Rb^+ taken from a previous publication.[6] The concentration dependence of the two ions is seen to be very similar and the values of the coefficients are in fact the same within the stated limits of error at all points of the curves. This might have been expected since both ions are probably unhydrated and of comparable size. This similarity means that D/D^0 (Cs^+) can be compared to D/D^0 (Na^+) in similar terms to D/D^0 (Rb^+). The reader is therefore advised to consult the discussion of reference (6) for this comparison.

Acknowledgments.—L.A.W. wishes to express his gratitude to the Australian National University for permission to use their facilities and also to the University of New England for leave to undertake the work.

AN X-RAY DIFFRACTION INVESTIGATION OF SODIUM HYALURONATE[1]

BY FREDERICK A. BETTELHEIM

Chemistry Department, Adelphi College, Garden City, N. Y.

Received June 16, 1959

The purpose of this note is to elucidate the structure of crystalline sodium hyaluronate. Dif-

(1) Supported in part by a grant (C-3984 BBC) of the National Cancer Institute, Public Health Service.

ferent preparations of sodium hyaluronate show different degrees of crystallinity depending on the isolation techniques. To obtain crystalline samples one has to remove completely the complexed proteins.[2] However, hyaluronic acid samples of different origin (umbilical cord, Streptococci and liposarcoma) free of proteins and having molecular weights of millions were found to be amorphous.[3] These same preparations once subjected to an acidic pepsin digestion (*p*H 2 at 37°) showed different degrees of crystallinity depending on the length of the acidic treatment. Meyer[4] suggested that high molecular weight hyaluronates may contain a few non-glycosidic linkages acting as branching points. The removal of these branches by acidic treatment may cause depolymerization and at the same time enable crystalline organization.

Experimental

Crystalline sodium hyaluronate was isolated from umbilical cords. The procedure and the analytical data were given earlier.[2] Partial orientation of the sample was achieved by stretching the hyaluronate film in a swollen condition in a 82:18 mixture of ethanol and water. The stretched film was clamped in a jig, dried and humidified to 9.55% water content. X-Ray diffraction pattern was taken by Cu Kα radiation. The density of the highly crystalline powder and that of the oriented film was determined by the flotation method using carbon tetrachloride and iodobenzene. Both had a density of 1.66 ± 0.01 g./cm.^{3}. The density of the amorphous hyaluronates provided by Prof. Meyer[3] was 1.51 ± 0.01 g./cm.^{3}. Hyaluronate preparations having different degrees of crystallinity had densities which fall between these two values.

The analysis of crystal symmetry indicated a hexagonal unit cell. The partial orientation was insufficient to resolve adequately the layer lines, hence a direct determination of the fiber identity period was not possible. One assumes, however, that the long axis of the polyuronide chain is orienting in the direction of stretch. Two reflections corresponding to interplanar spacings of 5.99 and 2.99 Å. had definite meridional orientation, hence they were tentatively assigned as 001 reflections.

In Table I, the X-ray data are summarized. In the first column the interplanar spacings are given as calculated from observed reflections. Column 2 lists the $(2 \sin \theta/\lambda)^2$ values obtained from the photographs, while column 5 gives the estimated intensities of the reflections. Considering the chemical structure of hyaluronates and especially the 1–3 and 1–4 β-glycosidic linkages, the meridional interplanar spacing of 5.99 Å. was assigned as a possible 002 reflection. An identity period of 11.98 Å. is in good agreement with the atomic scale projection of a N-acetyl sodium hyalobiuronate moiety along the chain axis. Indexing the powder photographs with the aid of reciprocal lattice was done the usual way.[5] The strongest equatorial reflection was assumed to be 200. The hexagonal unit cell calculated on this basis, therefore, has the dimensions a = 12.66 Å., c = 11.98 Å. (fiber axis), volume = 1662.84 Å.^{3} The calculated $(2 \sin \theta/\lambda)^2$ based on such an hexagonal unit cell is in good agreement with the observed values. This is given in column 3 of Table I, while column 4 indicates the indexing of the obtained reflections in the hexagonal unit cell.

TABLE I

X-RAY DIFFRACTION DATA OF SODIUM HYALURONATE

d (obsd.), Å.	$(2 \sin \theta/\lambda)^2 \times 10^3$ Obsd.	Calcd.	hkl (hexag.)	I^a (est.)
6.33	24.9	24.9	200	S
7.20	19.3	18.7	110	W
4.83	42.8	43.6	210	W
3.48	82.6	81.1	310	W
3.17	99.6	99.8	400	W
8.82	12.8	13.2	101	M
3.99	62.8	63.1	301	W
3.09	104	106	401	S
2.83	125	125	321	W
1.78	315	314	531	VW
5.99	27.8	27.8	002	S
3.72	72.3	71.5	212	MS
2.61	147	146	322	VW
2.22	202	202	422	VW
2.35	181	181	323	VW
2.99	111	111	004	S
2.42	170	168	304	VW
2.18	210	210	404	VW
2.09	229	230	324	VW
1.94	266	267	504	VW
1.90	277	276	405	W
1.74	330	330	505	VW

[a] M, medium, S, strong, VW, very weak, W, weak.

Discussion

The number of hyaluronate chains per hexagonal unit cell is 3.75 calculated on the basis of the experimental density, 1.66 g./cm.^{3}. However, it is well known that even highly crystalline natural polymers contain a certain amount of amorphous material. Hence the density of the crystalline portion of the polymer may be higher than that found experimentally. Therefore, one may assume that the hexagonal unit cell contains four hyaluronate chains. The calculated density of such a unit cell is 1.77 g./cm.^{3}. Using this value and the 1.51 g./cm.^{3} found experimentally for the amorphous hyaluronate the estimated degree of crystallinity of the partially oriented film was 58%.

The fiber axis identity period of 11.98 Å. is considerably longer than, for instance, a corresponding two glucose period (10.30 Å.) would be in the case of cellulose. This means that the hyaluronate chain is more stretched out, hence more rigid, than cellulose, probably due to the steric hindrance caused by the bulky N-acetylamine groups. The position occupied by the sodium ions in the 001 planes cannot be determined because of lack of sufficient $hk0$ reflections. However, the intense 002 and 004 reflections suggest that the carboxyl groups and their associated sodium ions lie in planes which halve the fiber identity period. This indicates that the repeating unit in the identity period is a N-acetyl sodium hyalobiuronate moiety.

The stiffness of the hyaluronate chain can partly explain the absence of crystallinity in the presence of a few branches. It also can account for the difficulty one encounters in stretching crystalline hyaluronate films. The unusually high anisotropy one observes in birefringence measurements,[6] viscometry[7] and electron microscopic observation[8]

(2) F. A. Bettelheim, *Nature*, **182**, 1301 (1958).

(3) These samples were generously provided by Dr. K. Meyer of Columbia University.

(4) K. Meyer, *Federation Proc.*, **17**, 1075 (1958).

(5) L. V. Azaroff and M. J. Buerger, "The Powder Method in X-ray Crystallography," McGraw-Hill Book Co., Inc., New York, N. Y., 1958, pp. 106–122.

(6) B. Sylven and E. J. Ambrose, *Biochim. Biophys. Acta*, **18**, 587 (1955).

(7) T. C. Laurent, *J. Biol. Chem.*, **216**, 263 (1955).

substantiates the great rigidity of the hyaluronate chain deduced from the X-ray diffraction data.

The relative orientation of the pyranose rings in adjacent chains of sodium hyaluronate cannot be established definitely at the present time. Nevertheless these tentative conclusions can be made. The width of the sodium glucuronide unit is calculated to be about 10 Å. while that of the N-acetylglucosamine moiety is 12 Å. Since the stiff hyaluronate chain forms a ribbon-like structure of an average thickness of 4 Å. the only way to pack four chains in the hexagonal unit cell is to allow the residues of the adjacent chains to lie with the plane of their ring parallel to the line connecting the adjacent chains.

Acknowledgment.—The author wishes to thank Prof. I. Fankuchen of the Polytechnic Institute of Brooklyn for the X-ray diffraction facilities and for the valuable criticism of the manuscript; Mr. V. DerSarkissian for the technical help in the isolation of the sodium hyaluronate.

(8) F. A. Bettelheim and D. Philpott, *Biochim. Biophys. Acta*, **34**, 124 (1959).

ON THE MECHANISM OF OZONE PRODUCTION IN THE PHOTOÖXIDATION OF ALKYL NITRITES

By Philip L. Hanst[1] and Jack G. Calvert

The Ohio State University, Columbus 10, Ohio

Received June 10, 1959

The formation of ozone when organic nitrites are photolyzed in air with near ultraviolet light has been demonstrated by Haagen-Smit, *et al.*,[2] Stephens, *et al.*,[3] and others. Other substances reported to produce ozone on photoöxidation include NO_2–hydrocarbon mixtures,[2,4] diacetyl[2,3] and azomethane.[5]

It has been proposed by Stephens, *et al.*, that in the photoöxidation of the NO_2–hydrocarbon mixtures the reaction $NO_2 + h\nu \rightarrow NO + O$ precedes the ozone forming reaction $O_2 + O \rightarrow O_3$. The diacetyl and azomethane, however, must produce the ozone by a mechanism not involving NO_2. It seemed to us worthwhile to attempt to establish which type of mechanism is involved in ozone production from nitrites.

If the nitrites followed the mechanism of the NO_2–hydrocarbon mixtures, they would either have to yield NO_2 on photolysis at least part of the time

$$\begin{aligned} RONO + h\nu &\longrightarrow R + NO_2 \\ NO_2 + h\nu &\longrightarrow NO + O \\ O + O_2 &\longrightarrow O_3 \end{aligned}$$

or they would have to yield oxygen atoms on photolysis

$$\left.\begin{aligned} RONO + h\nu &\longrightarrow R + NO + O \\ RONO + h\nu &\longrightarrow RON + O \end{aligned}\right\}$$
$$O + O_2 \longrightarrow O_3$$

If this were the case, it would account for the fact that the nitrites and the NO_2–hydrocarbon mixtures can be classed together as fast ozone producers while the other compounds are slower.

If the nitrites do not yield NO_2 or oxygen atoms on photolysis, then it seems to us reasonable to assume that the ozone is produced in free radical reactions similar to those which occur in the photoöxidation of the diacetyl and azomethane.

$$\begin{aligned} RONO + h\nu &\longrightarrow RO + NO \\ RO + RH &\longrightarrow ROH + R \\ R + O_2 &\longrightarrow RO_2 \\ RO_2 + O_2 &\longrightarrow RO + O_3, \text{ etc.} \end{aligned}$$

Our method of attempting to choose between these alternatives is to analyze the products obtained when methyl nitrite is photolyzed both in the presence and absence of oxygen and in the presence of excess NO, to see what reactions must be assumed to explain these products, and to compare these products with the products of the reaction of methyl radicals and nitric oxide.

The photolyses were conducted at room temperature in a 5-liter Pyrex flask. The flask was immersed in water, and in its center was located a 550-watt medium pressure Hanovia mercury arc surrounded by a water cooling jacket. This jacket was made of Pyrex glass which absorbed practically all of the light of wave length shorter than 3130 Å., thus minimizing photolyses of reaction products.

Pressures of reactants in the range of a few millimeters of mercury were measured on a manometer containing silicone vacuum pump oil. Higher pressures were measured on a mercury manometer. A reaction was started when the lighted arc was lowered into its place at the center of the 5 liter chamber and was ended when the arc was raised.

Analyses were made by means of infrared absorption spectroscopy using ten centimeter and one meter gas absorption cells on a Perkin-Elmer Model 21 double beam spectrophotometer.

Measurements of concentrations of products were made by comparisons to reference spectra run on pure compounds under conditions of resolution, pressure broadening, per cent. absorption, etc., as near as possible to those existing during the analysis. No major infrared bands remained unidentified.

Methyl nitrite was prepared by dropping sulfuric acid into a mixture of methanol, water and sodium nitrite. The evolved gas was collected in a Dry Ice trap and then distilled into the storage bulb.

Azomethane was prepared by the reduction of dimethylhydrazine with mercuric oxide according to the method of Renaud and Leitch.[6]

The nitric oxide, oxygen and nitrogen were taken directly from commercial tanks.

The methyl nitrite was photolyzed both in the absence and presence of oxygen and also in the presence of excess nitric oxide. The results of the infrared analyses are shown in Table I.

When azomethane was photolyzed in the presence of a small amount of nitric oxide with no oxygen present, the resulting spectra indicated that nitrosomethane and its isomer formaldoxime were formed.

$$\begin{aligned} CH_3{-}N{=}N{-}CH_3 + h\nu &\longrightarrow 2CH_3 + N_2 \\ CH_3 + NO &\longrightarrow CH_3NO \longrightarrow H_2CNOH \end{aligned}$$

These spectra were similar to those recently reported for CH_3NO and its isomerization product by Lüttke.[7] He observed that the characteristic infra-

(1) Physics Department, AVCO Research and Advanced Development, Wilmington, Mass.

(2) A. J. Haagen-Smit, C. E. Bradley and M. M. Fox, *Ind. Eng. Chem.*, **45**, 2086 (1953).

(3) E. R. Stephens, W. E. Scott, P. L. Hanst and R. C. Doerr, *Proc. Am. Petrol. Inst.*, Sec. III, **36**, 288 (1956).

(4) E. R. Stephens, P. L. Hanst, R. C. Doerr and W. E. Scott, *Ind. Eng. Chem.*, **48**, 1498 (1956).

(5) P. L. Hanst and J. G. Calvert, This Journal **63**, 71 (1959).

(6) R. Renaud and L. C. Leitch, *Can. J. Chem.*, **32**, 545 (1954).

(7) W. Lüttke, *Z. Elektrochem.*, **61**, 302 (1957).

TABLE I

PRODUCTS OF THE PHOTOLYSIS OF METHYL NITRITE

Exposure time, 5 min.; pressures in mm.

	Reactants			
	8 mm. CH_3ONO, 1 atm. N_2	8 mm. CH_3ONO, 8 mm. NO, 1 atm. N_2	8 mm. CH_3ONO, 8 mm. O_2, 1 atm. N_2	8 mm. CH_3ONO, 1 atm. O_2
Formaldehyde	3.6	4.0	3.0	1.0
Methanol	0.6	0.15	0.3	0.0
Carbon monoxide	0.0	0.0	0.0	1.7
Nitrous oxide	1.1	1.4	0.9	0.0
Nitric oxide	1.7	10.0	1.8	0.0
Nitrogen dioxide	0.0	0.0	0.0	2.6
Methyl nitrate	0.0	0.0	0.0	4.0
Methyl nitrite	4.1	4.6	4.1	1.3
Total C	8.3	8.7	7.4	8.0
Total N	8.0	17.4	7.7	7.9

red band of the monomer of nitrosomethane (1564 cm.$^{-1}$) formed when nitrosomethane dimer was heated at 160°, but quickly disappeared as the absorption bands due to formaldoxime appeared. In our case similar phenomena were observed. The nitroso band at 6.4 μ was large when the gases were first admitted to the absorption cell, but it decreased with time (a few minutes), while the OH band at 2.8 μ and a characteristic structure between 10 and 12 μ increased. If even a small amount of oxygen was present (*e.g.*, 2.4 mm. of azomethane, 4.8 mm. of nitric oxide and 4.8 mm. of oxygen), no nitrosomethane or formaldoxime was formed and the products were methyl nitrite and its photolysis products, primarily methyl nitrate, formaldehyde, and nitrous oxide.

The observed products of the photolysis of methyl nitrite can be explained by the mechanisms

(1) In the absence of large amounts of oxygen:

$$CH_3ONO + h\nu \longrightarrow CH_3O + NO$$
$$CH_3O + NO \longrightarrow CH_3ONO$$
$$CH_3O + NO \longrightarrow H_2CO + HNO$$
$$2HNO \longrightarrow N_2O + H_2O$$
$$2CH_3O \longrightarrow H_2CO + CH_3OH$$
$$CH_3O + HNO \longrightarrow CH_3OH + NO$$

(2) In the presence of one atmosphere of oxygen:

$$CH_3ONO + h\nu \longrightarrow CH_3O + NO$$
$$2NO + O_2 \longrightarrow 2NO_2$$
$$CH_3O + NO_2 \longrightarrow CH_3ONO_2$$

In mechanism 1 most of the CH_3O radicals recombine with NO but, in some cases, NO abstracts a hydrogen from CH_3O to yield H_2CO and HNO. N_2O and H_2O then are formed by reaction of HNO radicals. The methanol and a small part of the formaldehyde result from interaction of pairs of CH_3O radicals. This is a reaction indicated by the results of the photooxidation of methyl radicals.[5] The observation that added NO does not significantly change the yield of H_2CO and N_2O supports this nitrite photolysis mechanism on the basis of the following reasoning. Newly-formed CH_3O radicals can react in two ways; they can disproportionate to yield H_2CO and CH_3OH, or they can react with NO to yield usually CH_3ONO, but sometimes H_2CO and HNO. The disproportionation is only important in the experiments without added NO, and then only during the very first stages of the photolysis. The only effect of added NO ought to be a nearly complete suppression of CH_3OH formation and a shortening of the lifetime of the CH_3O radicals. This is in fact the observed result, as is shown in Table I.

The formation of methyl nitrate in the photolysis of methyl nitrite in one atmosphere of oxygen is explained by the second mechanism above. The greater decomposition of methyl nitrite when oxygen is present supports our contention that in the absence of oxygen there was a good deal of recombination of methoxy and NO to regenerate the methyl nitrite. The lack of formation of methyl nitrate when the oxygen pressure was low was undoubtedly due to the fact that under these conditions the NO was not oxidized appreciably to NO_2 during the course of the experiment.

The complete absence of nitrosomethane and formaldoxime from the products of the no-oxygen photolysis of methyl nitrite indicates that there is no significant amount of cleavage at the carbon-oxygen bond. In other words, methyl nitrite is photolyzed only into CH_3O and NO and not into CH_3 and NO_2, CH_3, NO and O, nor CH_3OH and O.

Since the C–O and O–N bond strengths are not greatly affected by the length of the hydrocarbon chain, and since the light absorption process will be essentially the same for all the members of the homologous series, we feel that what is indicated here for the photolysis of methyl nitrite also applies to *n*-butyl nitrite. We conclude, then, that the relatively large yield of ozone obtained on photolysis of *n*-butyl nitrite in air is not due to NO_2 formation and its subsequent photolysis (remembering that $2NO + O_2 \rightarrow 2NO_2$ is very slow at low NO pressure), but is due to free radical reactions started by the butoxy radicals.

$$CH_3CH_2CH_2CH_2ONO + h\nu \longrightarrow CH_3CH_2CH_2CH_2O + NO$$
$$CH_3CH_2CH_2CH_2O + RH \longrightarrow CH_3CH_2CH_2CH_2OH + R$$
$$R + O_2 \longrightarrow RO_2$$
$$RO_2 + O_2 \longrightarrow RO + O_3$$
$$RO + RH \longrightarrow ROH + R$$

continue chain reaction

In the above mechanism, the molecule RH might be the starting material, the alcohol product, the butoxy radicals, aldehydes formed by the interaction of butoxy radicals, or any other organic molecule formed in the variety of reactions which could follow the initial photolysis.

One possible explanation of the fact that the ozone is easier to observe in the photooxidation of

a nitrite than in the photooxidations of diacetyl and azomethane may be that the nitrites have a higher absorption coefficient in the near ultraviolet. This will result in a fast photolysis with a copious production of free radicals.

The authors greatfully acknowledge the financial support of the National Institutes of Health, Bethesda, Maryland.

POLYMORPHISM OF RARE EARTH DISILICIDES[1]

BY J. A. PERRI, E. BANKS AND B. POST

Department of Chemistry, Polytechnic Institute of Brooklyn, New York

Received June 15, 1959

An X-ray diffraction investigation by Brauer and Haag[2] established that the disilicides of some of the rare earth metals crystallize with the tetragonal, $ThSi_2$ type, structure. More recent work[3] indicates that the disilicides of the smaller rare earth metal atoms are actually orthorhombic and that their structures are slightly distorted versions of the "normal" tetragonal structure; of the rare earth metals only La, Ce, Pr and Eu were found to form tetragonal disilicides. $YbSi_2$ was not prepared but it is probably tetragonal like $EuSi_2$. The degree of distortion from the tetragonal structure appears to increase monotonically with decrease in the size of the metal atom.

In this paper we describe the results of an X-ray diffraction study of the ranges of stability of the two polymorphic forms of this phase. Reversible transformations have been observed; the temperatures of these transformations appear to be simply related to the atomic radii of the metals.

Experimental

A Norelco diffractometer adapted for studies at both low and high temperatures (−160 to 1,200°) was used for the X-ray diffraction studies. The high temperature camera has been described previously.[4] A helium atmosphere was maintained in the camera at elevated temperatures to prevent oxidation of the specimens. For work below room temperature, the powdered samples were dusted onto glass slides coated with thin layers of Vaseline; cooling was accomplished by blowing cold nitrogen gas (cooled by bubbling through liquid nitrogen) over the specimens. The temperature was controlled by mixing the cold gas with warm, dry nitrogen gas.

The preparation and some of the properties of the disilicides have been described previously.[3] The X-ray diffraction patterns obtained were generally of poor quality; high angle peaks, on which attention would normally have been focussed, were broad and weak and difficult to measure with precision. It was found most convenient to concentrate on measurements of the (004), (101), (001), (013) and (103) reflections of the orthorhombic phases and the corresponding peaks of the tetragonal phases. Although these reflections occur at relatively low Bragg angles when Cu radiation is used, they were relatively sharp and free from interference from neighboring peaks; in general their angular locations were relatively easy to measure.

The progress of the structure transformations was followed by observing the variations of the reflection angles of these peaks over suitable ranges of temperature. When these measurements indicated that a transformation had been completed, a trace of the entire X-ray diffraction pattern of the new phase was obtained. To check on the reversibility of the transformations, patterns were re-recorded at room temperature after each high or low temperature run. All the transformations observed were reversible.

Specimens were prepared in finely powdered form. Ni filtered Cu K radiation was used; peaks were scanned at a speed of $1/4°$ (2θ) per minute. Dimensions of the "*c*" axes of the unit cells were obtained generally from measurements of (004); "*a*" and "*b*" dimensions were obtained from (101), (011), (103) and (013); the latter also furnished independent checks on the values of "*c*."

Although the transitions probably occur within relatively narrow temperature ranges, the X-ray diffraction data did not permit precise determination of these ranges. The onset of the transformations was obscured by several factors: in most instances the (101), (011) and the (103), (013) orthorhombic pairs of peaks merged gradually into single broad peaks as the transition temperature was approached, as the temperature was raised further, the peaks sharpened and acquired shapes characteristic of "single" reflections, indicating that the transition had taken place.

The (004) peak which was expected to serve as a sensitive indicator of the transformations did not prove to be one. Even at room temperature (004) was generally weak; at the elevated temperatures at which most of the transformations occurred, it was even weaker and changes in its reflection angle were very difficult to measure. As a result only relatively broad temperature ranges, within which the transformations were known to take place, are reported here.

The atomic radii of the metal atoms and the transition temperature ranges are shown in Table I. The orthorhombic form is stable below the indicated temperatures. The approximate transition temperatures clearly increase with decreasing atomic radius of the parent metal.

TABLE I

TRANSITION TEMPERATURES OF RARE EARTH "DISILICIDES"

Meta	Atomic no.	Average metallic radius (Å.)	Transition temp. of disilicide, °C.
Eu	63	1.99	−150[a]
Pr	59	1.83	−120 ± 15
Nd	60	1.82	[b]
Sm	62	1.81	380 ± 40
Gd	64	1.81	400 ± 25
Y	39	1.80	450 ± 50
Dy	66	1.77	540 ± 40

[a] (200) peak broadened indicating beginning of transition. [b] Transformation occurs somewhere between room temperature and 150°.

It was not possible to determine the transition temperature of neodymium disilicide. It appears to be orthorhombic at room temperature but the distortion from tetragonal is very slight and the point at which complete conversion to tetragonal occurred could not be established though it is apparent that the transformation occurs somewhere between room temperature and 150°.

The (101) and (103) reflections of tetragonal $PrSi_2$ broaden as the temperature is lowered and are resolved into two peaks below −120°, indicating a transformation to the orthorhombic form.

In the case of $EuSi_2$, the (200) reflection of the tetragonal form was most convenient to study. It was observed that the peak began to broaden noticeably at −150°. Little additional broadening occurred between that temperature and −160°. Our experimental procedure did not permit investigations at still lower temperatures. It was evident, though, that the onset of the orthorhombic distortion was responsible for the broadening of the peak. At that temperature the (200) and (020) reflections were separating but were not completely resolved. Unfortunately reflections at higher angles were too broad to be useful.

No comparable broadening of any peaks was detected in the cases of $LaSi_2$ or $CeSi_2$ at −160°. Presumably a

(1) Supported by Air Force Office of Scientific Research.

(2) V. G. Brauer and H. Haag, *Z. anorg. allgem. Chem.*, **267**, 198 (1952).

(3) J. A. Perri, I. Binder and B. Post, THIS JOURNAL, **63**, 616 (1959).

(4) J. A. Perri, E. Banks and B. Post, *J. Appl. Phys.*, **28**, 1272 (1957).

TABLE II

UNIT CELL DIMENSIONS OF RARE EARTH DISILICIDE POLYMORPHS[a]

Compound	Temp., °C.	Low temp. form[a] a (Å.)	b (Å.)	c (Å.)	High temp. form[a] a (Å.)	c (Å.)
$PrSi_2$	−130	4.23	4.20	13.68	(4.20)	(13.76)
$SmSi_2$	470	(4.105)	(4.035)	(13.46)	4.08	13.51
$GdSi_2$	460	(4.09)	(4.01)	(13.44)	4.10	13.61
$DySi_2$	585	(4.04)	(3.95)	(13.33)	4.03	13.38
YSi_2	545	(4.04)	(3.95)	(13.33)	4.04	13.42

[a] Parentheses indicate room temperature form.

transformation similar to that noted above occurs in the cases of these compounds at still lower temperatures. Lattice dimensions of the polymorphs which could be measured with reasonable precision are shown in Table II.

THE REACTION OF PERFLUORO-*n*-PROPYL RADICALS WITH CYCLOHEXANE IN THE GAS PHASE[1]

BY GLYN O. PRITCHARD AND GLENN H. MILLER

Department of Chemistry, University of California, Santa Barbara, Goleta, California

Received June 22, 1959

Recently Giacometti and Steacie[2] have measured the rates of reaction of C_3F_7 radicals with methane and ethane. They obtained $k_1/k_2^{1/2} = 9.7 \times 10^3 \exp[-(9.5 \pm 0.5) \times 10^3/RT]$ (mole/cc.)$^{-1/2}$ sec.$^{-1/2}$ for methane, and $k_1/k_2^{1/2} = 1.7 \times 10^5 \exp[-(9.2 \pm 0.5) \times 10^3/RT]$ (mole/cc.)$^{-1/2}$ sec.$^{-1/2}$ for ethane, where subscript 1 refers to the hydrogen abstraction reaction and subscript 2 to the radical recombination reaction.

It is seen that these results are in contradistinction to similar CH_3 and CF_3 radical systems where the difference in rate constants is reflected almost entirely in the activation energies of the processes, the pre-exponential factors being approximately constant for either series. Further, in methyl radical systems the activation energies of the hydrogen abstraction reactions exhibit a stepwise decrease along the series methane, ethane, compounds containing secondary hydrogen atoms, and compounds containing tertiary hydrogen atoms, which demonstrates that the activation energy is dependent on the nature of the hydrogen atom which is abstracted.[3,4]

In view of this discrepancy we have studied the reaction between C_3F_7 radicals and a compound, here cyclohexane, containing secondary hydrogen atoms. The rates of abstraction from cyclohexane, where there is little strain in the ring, will be almost exactly the same as that for a secondary hydrogen in a paraffin.

Perfluoro-*n*-propyl ketone was used as a photolytic source of C_3F_7 radicals. Its preparation and purification, the apparatus and procedure were identical to that described previously[5] except that the reaction cell was 174 ml. The cyclohexane was Phillips research grade, and was purified and outgassed before use. CO and C_3F_7H were the only products which were collected and measured. Mass spectrographic analysis showed that there was no carry over of any other products or reactants in the respective samples at the temperatures at which they were collected. It is not possible to separate and measure the C_6F_{14} under the conditions of our experiment.[6]

The results of the experiments are summarized in Table I.

The reaction mechanism for the temperature range 25 to 290° is assumed to be

$$C_3H_7COC_3H_7 + h\nu \longrightarrow 2C_3H_7 + CO$$
$$C_3F_7 + RH \longrightarrow C_3F_7H + R \quad (1)$$
$$C_3F_7 + C_3F_7 \longrightarrow C_6F_{14} \quad (2)$$
$$C_3F_7 + R \longrightarrow C_3F_7R \quad (3)$$
$$R + R \longrightarrow R_2 \quad (4)$$

where RH is cyclohexane and R is cyclohexyl radical.

For steady-state conditions, that is constant light intensity and small percentage decomposition of the ketone (in these experiments less than 3%), $k_1/k_2^{1/2} = R_{C_3F_7H}/R^{1/2}_{C_6F_{14}}[RH]$ where the rate of formation of perfluorohexane $R_{C_6F_{14}} = R_{CO} - {}^1/_2 \cdot (R_{C_3F_7H} + R_{C_3F_7R})$ from radical balance. We were unable to measure the C_3F_7R formed, so it has been assumed that $R_{C_3F_7R} = 0$. The amounts of C_6F_{14} given in Table I have been calculated in this manner. A least squares plot of the data is shown in Fig. 1. The rate expression is $k_1/k_2^{1/2} = 1.2 \times 10^4 \exp[-(5.2 \pm 0.1) \times 10^3/RT]$ (mole/cc.)$^{-1/2}$ sec.$^{-1/2}$.

There is good agreement between the pre-exponential factors for the methane and cyclohexane systems, 9.7×10^3 and 1.2×10^4 (mole/cc.)$^{1/2}$ sec.$^{-1/2}$, respectively. Giacometti and Steacie found in their experiments with methane that the quantities of $C_3F_7CH_3$ formed were too small for accurate analysis and putting $R_{C_3F_7CH_3} = 0$ did not affect the $k_1/k_2^{1/2}$ values by more than 1%.

However, their treatment for ethane is more complex due to radical–radical disproportionation reactions which can occur in higher hydrocarbon radical systems. In addition to reactions 1′, 2′, 3′ and 4′ (identical to reactions 1, 2, 3 and 4, except that RH is ethane and R is ethyl radical).

$$C_3F_7 + C_2H_5 \longrightarrow C_2H_4 + C_3F_7H \quad (5')$$

and

$$C_2H_5 + C_2H_5 \longrightarrow C_2H_4 + C_2H_6 \quad (6')$$

must be considered. They analyzed for $C_5F_7H_5$ (from reaction 3′) and for butane (from 4′), and

(1) This work was supported by a grant from the National Science Foundation.

(2) G. Giacometti and E. W. R. Steacie, *Can. J. Chem.*, **36**, 1493 (1958).

(3) E. W. R. Steacie, *J. Chem. Soc.*, 3986 (1956).

(4) G. O. Pritchard, H. O. Pritchard, H. I. Schiff and A. F. Trotman-Dickenson, *Trans. Faraday Soc.*, **52**, 849 (1956).

(5) G. H. Miller and E. W. R. Steacie, *J. Am. Chem. Soc.*, **80**, 6486 (1958).

(6) G. H. Miller, G. O. Pritchard and E. W. R. Steacie, *Z. physik. Chem.*, **15**, 262 (1958).

TABLE I

Temp., °C.	Cyclohexane, moles/cc. × 10⁶	Ketone, moles/cc. × 10⁶	Products: CO, moles/cc. × 10⁹	Products: C_3F_7H, moles/cc. × 10⁹	Products: (CO − ½C_3F_7H) or C_6F_{14}, moles/cc. × 10⁹	Time, sec.	$k_1/k_2^{1/2}$, (mole/cc.)$^{-1/2}$ sec.$^{-1/2}$
23.5	1.33	1.92	5.79	3.36	4.11	540	1.69
77.5	2.77	3.27	39.6	43.1	18.0	360	6.12
152.5	1.29	2.61	71.2	97.3	22.5	180	37.6
172.0	1.32	2.77	50.8	72.7	14.4	120	41.9
208.8	1.74	3.11	46.3	75.1	8.82	120	41.9
250.0	1.67	3.69	52.0	92.2	5.88	120	65.9
293.0	0.702	2.47	46.8	70.3	11.7	120	84.6

knowing that k_6'/k_4' is 0.12, independent of temperature and pressure, correction for the C_3F_7H formed in reaction 5′ can be made. The justification for this procedure is demonstrated by the constancy of the ratio $k_5'/k_3' = 0.40$ over the whole temperature range. $R_{C_6F_{14}}$ was obtained from the radical balance $R_{CO} - {}^1/_2(R_{C_3F_7H} + R_{C_6F_7H_5})$.

The methane and ethane systems are unique in that it is possible to separate out easily the products of the type 3 reaction and measure them. In the cyclohexane system, the C_3F_7–cyclohexyl is lost and masked in the vast excess of unused reactants. To assess the accuracy of our result we must consider first any error introduced by assuming that reaction 3 is negligible, and second the effect of additional C_3F_7H formed in reaction 5, if reactions 5 and 6 are operative in the system

$$C_3F_7 + R \longrightarrow R(-H) + C_3F_7H \qquad (5)$$
$$R + R \longrightarrow R(-H) + RH \qquad (6)$$

Whether reaction 5 occurs or not, the $R_{C_6F_{14}}$ is given by $R_{CO} - {}^1/_2(R_{C_3F_7H} + R_{C_3F_7R})$. As reaction 1 is temperature dependent, higher temperatures will lead to greater R radical concentrations, and hence, for the competitive removal of C_3F_7 radicals from the system, $R_{C_3F_7R}$ will gain over $R_{C_6F_{14}}$. So the assumption that $R_{C_3F_7R} = 0$ leads to an increasing error in $R_{C_6F_{14}}$ with temperature. Recalculating Giacometti and Steacie's results for the C_3F_7 + ethane system on the basis that $R_{C_6F_7H_5} = 0$ gives an activation energy for reaction 1′ of about 8.0 kcal./mole, an error of 1.2 kcal. in their result, which means our result is low if reaction 3 is important.

Not correcting the rate expression for the C_3F_7H contribution from reaction 5 seems to have little effect on the activation energy for reaction 1. A consideration of this correction to the C_3F_7 + ethane system involves a subtraction of 21.5 ± 0.5% from the total C_3F_7H formed in the reaction. (This is for 6 of the 10 runs reported; the other runs involve subtractions of 14, 19, 19 and 30%.) In a logarithmic plot this shows up as virtually a constant increment, which does not alter the slope of the line, so that the activation energy for reaction 1′ is unaltered, whether the correction is made or not. On this basis we can assume that no appreciable error is introduced by equating the C_3F_7H total to that formed in reaction 1, due to the similarity in the two systems. From a steady-state treatment it is not obvious why the ratio of C_3F_7H by (5)/C_3F_7H by (1) should be a constant, unless at very high C_3F_7 radical concentrations (conditions which do not hold in these experiments) we assume that reactions 3 and 5 swamp reactions 4 and 6 for the removal of R radicals. Then the ratio reduces to $k_5/(k_3 + k_5)$.

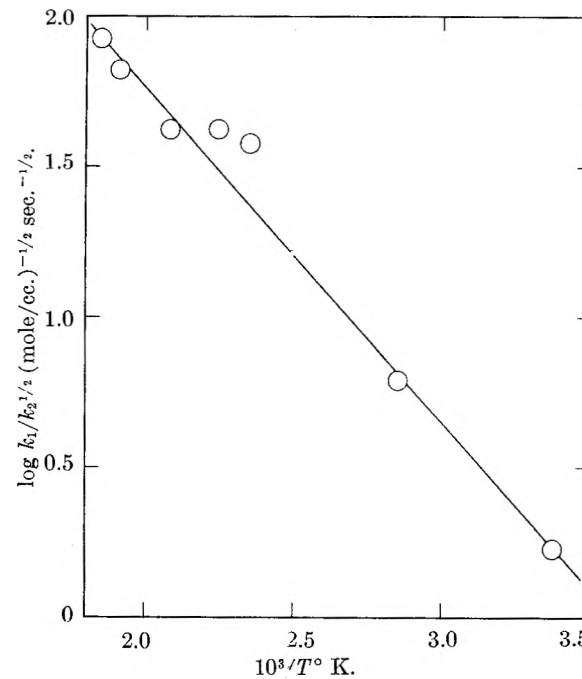

Fig. 1.—Arrhenius plot for the reaction of C_3F_7 radicals with cyclohexane.

Hence, any error in our result is reflected almost entirely in the assumption that reaction 3 does not make a significant contribution to the reaction scheme. For C_2H_5 and C_3F_7 radicals $k_5'/k_3' = 0.40$. It is probable that the ratio k_5/k_3 for cyclohexyl and C_3F_7 radicals is the same or even bigger, which implies a reduction in $R_{C_3F_7R}$ and also to the correction to $R_{C_6F_{14}}$. We consider therefore that our result of 5.2 kcal./mole for C_3F_7 + cyclohexane is in error, but at the most is low by about 1.0 kcal., so that we can estimate that in general C_3F_7 radicals abstract a secondary H-atom from a hydrocarbon with an activation energy of about 6 kcal./mole.

Thus it appears that there is a discrepancy in the results for C_3F_7 with CH_4 and C_3F_7 with C_2H_6, but further work along the lines of these experiments is unjustified until some more precise method of determining $R_{C_6F_{14}}$ is found, other than radical balance.

A STRUCTURE PROPOSAL FOR $Na_7Zr_6F_{31}$

By P. A. Agron and R. D. Ellison

Chemistry Division, Oak Ridge National Laboratory,[1] Oak Ridge, Tennessee

Received June 18, 1959

A structure for one of the binary phase compounds occurring in the NaF–ZrF_4 system[2] is proposed. Powder diffraction[3] data of samples crystallized from melts of the composition 50 mole % NaF–50 mole % ZrF_4 have indicated that these crystals are isomorphous with crystals of $NaUF_5$. The latter were found by Zachariasen and reported by Katz and Rabinowitch[4] to be rhombohedral with space group $R\bar{3}$–(C^2_{3i}) and 6 molecules per unit cell. The metal ions are in the sixfold general positions (f): ± (*XYZ*); (*ZXY*); (*YZX*) with the parameters

	X	*Y*	*Z*
U	3/13	1/13	9/13
Na	6/13	2/13	5/13

Density measurements made on the single solid phase produced from large melts of slightly different compositions, namely, 52 mole % NaF–48 mole % ZrF_4 and 53 mole % NaF–47 mole % ZrF_4, indicate the existence of a stoichiometry different from $NaZrF_5$. The densities observed are

52 mole % NaF: 4.14 ± 0.03 g./cc.
53 mole % NaF: 4.11 ± 0.01 g./cc.[5]

while the calculated density for $NaZrF_5$ is 4.01 g./cc. The unit cell volumes of the solids crystallized from melts of compositions in the region 50 mole % NaF to 53.8 mole % NaF differ by less than 0.5%. In order to satisfy the requirements of a greater density with a greater amount of the lighter component in a substantially constant volume, it is necessary to assume the addition of an NaF molecule to the unit cell, rather than the substitution of a lighter sodium for a zirconium ion with the accompanying fluorine vacancies even further reducing the density. It is significant that the additional Na^+ cation could fit into the vacant special position, (000), without changing the space group. This would yield a unit cell of the stoichiometric composition $Na_7Zr_6F_{31}$ ($7NaF \cdot 6ZrF_4$) with a calculated density of 4.16 g./cc., in reasonable agreement with the above measured values.

Single crystals obtained from melts of the 53 mole % NaF composition have become available. Diffraction patterns obtained by using film techniques on the Buerger precession and the Weissenberg cameras have confirmed that the space group $R\bar{3}$ is still possible for this composition. It is hoped that further measurements of the diffracted intensities using counting techniques will yield the fluorine positions, as well as confirm the suggested position (000) for the added Na^+.

(1) Work performed for the U. S. Atomic Energy Commission at the Oak Ridge National Laboratory, operated by the Union Carbide Corporation, Oak Ridge, Tennessee.

(2) C. J. Barton, W. R. Grimes, H. Insley, R. E. Moore and R. E. Thoma, This Journal, **62**, 665 (1958).

(3) P. A. Agron and M. A. Bredig, ORNL-1729, 47, 1954.

(4) J. J. Katz and E. Rabinowitch, "The Chemistry of Uranium," McGraw-Hill Book Co., Inc., New York, N. Y., 1951, p. 379.

(5) S. I. Cohen, Oak Ridge National Laboratory, personal communication.

In the course of this study, an accurate cell size for this compound was obtained. To refine the accuracy of the cell size measurement, two Debye–Scherrer patterns were taken, using Cr-K_α radiation. The samples were prepared by grinding several of the above mentioned single crystals. These patterns were measured with a steel scale and vernier and corrections were made for film shrinkage and sample absorption. All clearly resolved and unambiguously indexed reflections in the range $18° < 2\theta < 142°$ were used to obtain a least squares fit of the cell size to the data by a method described elsewhere.[6] The refined hexagonal cell size was found to be

$a = 13.802 \pm 0.002$ Å.
$c = 9.420 \pm 0.001$ Å.

The corresponding rhombohedral unit cell is

$a = 8.565$ Å., $\alpha = 107°21'$

(6) W. R. Busing and H. A. Levy, *Acta Cryst.*, **11**, 798 (1958).

THE TIN(II) REDUCTION OF METHYL ORANGE[1]

By F. R. Duke and N. C. Peterson

Institute for Atomic Research and Department of Chemistry, Iowa State University, Ames, Iowa

Received June 22, 1959

The possibility that one particular Sn(II) chloride complex might have high reactivity relative to others led to this kinetic study of the reduction of an azo compound to the amine

$$8Cl^- + 4H^+ + Ar{-}N{=}N{-}Ar + 2Sn(II) \longrightarrow 2ArNH_2 + 2SnCl_4$$

The rates of reduction of a number of such compounds were measured by Goldschmidt and Braanaas,[2] who reported a variable order in chloride ion, first order in azo compound and first order in Sn(II). The recent equilibrium data for the Sn(II) chloride complexes[3] allow a more precise interpretation of the mechanism of the reaction relative to the role played by the chloride. The reduction of methyl orange was found to proceed at a convenient rate and, thus, was selected for study.

Experimental

Sn(II) perchlorate was prepared by dissolving A.C.S. reagent grade Sn(II) chloride in 2 *N* $HClO_4$ and passing the solution through a column of Dowex 50 exchange resin in the acid form, followed by an elution with 2.0 *m* perchloric acid. Chloride ion was shown to be absent from the solution.

Commercial methyl orange was recrystallized twice from water and dried in a desiccator over anhydrous calcium sulfate. Perchloric and hydrochloric acid solutions were prepared by diluting the concentrated reagents to 2.00 *M* with water distilled from alkaline permanganate.

A model 6A Coleman Junior Spectrophotometer was used to follow absorbancy for all rate measurements, with Pyrex 1 cm. cells.

(1) Contribution No. 768. Work was performed in the Ames Laboratory of the U. S. Atomic Energy Commission and Department of Chemistry at Iowa State University.

(2) H. Goldschmidt and A. Braanaas, *Z. physik. Chem.*, **96**, 180 (1920).

(3) C. E. Vanderzee and D. E. Rhodes, *J. Am. Chem. Soc.*, **74**, 3552 (1952).

Results and Discussion

The reaction between Sn(II) and methyl orange was found not to proceed in the absence of chloride. In the presence of chloride at all concentrations, the reaction was found to be first order in Sn(II) and first order in methyl orange.

The chloride effect was studied by using very low methyl orange concentrations and relatively high Sn(II) and chloride ion concentrations. Under these conditions, the reaction is pseudo-first order in methyl orange.

Since Sn(II) forms the complexes $SnCl^+$, $SnCl_2$ and $SnCl_3^-$ in appreciable concentrations under the conditions of these experiments, a general rate equation would be

$$-\frac{dM}{dt} = M\{k_1[Sn^{++}] + k_2[SnCl^+] + k_3[SnCl_2] + k_4[SnCl_3^-]\}$$

where M is the methyl orange concentration. If the stepwise formation constants for the Sn(II) complexes are K_1, K_2 and K_3 for the formation of complexes containing 1, 2 and 3 chlorides, respectively, and Sn(II) = $[Sn^{++}]$ + $[SnCl^+]$ + $[SnCl_2]$ + $[SnCl_3^-]$, then

$$\frac{-dM}{dt} = \left(\frac{k_1 + k_2K_1[Cl^-] + k_3K_1K_2[Cl^-]^2 + k_4K_1K_2K_3[Cl^-]^3}{1 + K_1[Cl^-] + K_1K_2[Cl^-]^2 + K_1K_2K_3[Cl^-]^3}\right) M\text{Sn(II)}$$

Since Sn(II) and Cl^- are large compared with M, $k' = A_{Sn(II)}$, where k' is the slope of the log M *vs.* time and A is the bracketed term in the above equation. If P is the denominator of the bracketed term, then we define a parameter $F(Cl^-) = k'P/Sn(II)$ where $F(Cl^-)$ is the numerator of the bracketed term, such that $F(Cl^-)/P = A$.

The term P was evaluated from the literature values for K_1, K_2 and K_3.[2] It was first assumed that $Cl^- = T_c$, where T_c is the total chloride. Since $T_c = Cl^- + SnCl^+ + 2SnCl_2 + 3SnCl_3^-$, a series of approximations allowed calculation of Cl^-, the uncomplexed chloride. This was used to make a final calculation of P. The data and calculated values of $[Cl^-]$, P and $F(Cl^-)$ are given in Table I.

TABLE I

METHYL ORANGE REDUCTION RATES[a]

Expt. no.	T_c, M	T_s, M	$[Cl^-]$, M	P	$k' \times 10^3$, min.$^{-1}$	$F(Cl)$
1	0.190	0.00217	0.187	5.21	11.5	27.6
2	.472	.00217	.468	21.3	83.5	820
3	.0950	.00217	.0930	2.56	5.69	6.71
4	.187	.00429	.181	5.01	27.0	31.5
5	.0188	.00939	.0169	1.21	0.371	0.0478
6	.0574	.00939	.0522	1.74	3.76	0.697
7	.0960	.00939	.0881	2.43	12.45	3.22
8	.1356	.00939	.1255	3.34	28.3	10.2
9	.1732	.00939	.1620	4.38	49.3	23.1
10	.2026	.00469	.1965	5.54	40.4	47.4

[a] T_c and T_s are total concentrations in Cl^- and in Sn(II), respectively, $[Cl^-]$ is uncomplexed chloride; P, k' and $F(Cl^-)$ are defined in the text.

A plot of log $F(Cl^-)$ *vs.* log $[Cl^-]$ was prepared. It might be expected that at low $[Cl^-]$, a small slope would be observed, the slope increasing as Cl^- increases; however, a straight line, with slope = 3 resulted. Thus we reach the conclusion that the appropriate rate equation is

$$-\frac{dM}{dt} = \frac{k_4K_1K_2K_3[Cl^-]^3\, M\text{Sn(II)}}{1 + K_1[Cl^-] + K_1K_2[Cl^-]^2 + K_1K_2K_3[Cl^-]^3} = k_4[SnCl_3^-]M$$

Thus, it appears that $SnCl_3^-$ reacts much more rapidly than any other tin species. It is not unlikely that the tin is tetracoördinated in the activated complex, the fourth position being occupied by the methyl orange.

SILICA–ALUMINA-CATALYZED OXIDATION OF ANTHRACENE BY OXYGEN

BY RICHARD M. ROBERTS, CYRIL BARTER AND HENRY STONE

Shell Development Company, Emeryville, California

Received June 25, 1959

We have found that silica–alumina catalyzes the oxidation of anthracene by molecular oxygen at room temperature.

Before describing this reaction, it is necessary to give an account of the behavior of anthracene and silica–alumina in the absence of oxygen. Silica–alumina, anthracene and *n*-heptane (solvent) were separately outgassed and were mixed under strictly anaerobic and anhydrous conditions, employing all-glass apparatus, break-seals and high vacuum technique. The silica–alumina had been evacuated at 500°, the anthracene at room temperature and the anhydrous *n*-heptane by repeated freezing, evacuation and thawing. When the three components were mixed under the above conditions, the silica–alumina turned green. (Anthracene solutions do not absorb visible light.) The green color is characteristic of anthracene adsorbed on acidic solids under anaerobic and anhydrous conditions; anthracene adsorbed on pure silica gel, an extremely weak acid, is colorless. The green color of anthracene adsorbed on silica–alumina may be due to a carbonium ion formed by transfer of a proton from the silica–alumina to the anthracene molecule, probably on the 9-carbon atom.[1]

The adsorption of anthracene on silica–alumina under the above conditions, producing the green color on the solid, is reversible. When a little outgassed *n*-butylamine was added through a break-seal to the anaerobic mixture of silica–alumina, anthracene and *n*-heptane, the green color disappeared and the silica–alumina became perfectly white. The *n*-butylamine is evidently more basic than anthracene and displaces the latter from the silica–alumina surface. It may be

(1) G. Dallinga, E. L. Mackor and A. A. Verrijn Stuart, *Molecular Phys.*, **1**, 133 (1958). We have examined the absorption spectrum of anthracene adsorbed on silica–alumina from decahydronaphthalene solution under anaerobic and anhydrous conditions, with a Cary spectrophotometer. Decahydronaphthalene was employed as solvent to reduce the scattering of light. Absorption bands not present in the spectrum of anthracene in solution were noted at 4200 and 7500 Å. with two possible very weak bands at 5850 and 6400 Å. A publication on the absorption spectra of adsorbed molecules, including anthracene, is planned by one of us (C.B.).

remarked that water also displaces anthracene from silica–alumina.

Now when oxygen was admitted at room temperature to the anaerobic system containing green silica–alumina, the color of the solid rapidly changed from green to very dark brown. On addition of *n*-butylamine to this mixture, the solid did not revert to its original white appearance, but remained brown, suggesting that in this case the adsorbed material may have been more basic than the amine. Anthracene adsorbed on pure silica gel is not oxidized by oxygen under the present conditions.

A quantitative oxidation experiment was made in a static system consisting of a glass reaction vessel connected through a Kovar seal to a metal packless valve, and then to an all-metal pressure gage through a stainless steel line. Silica–alumina (1.03 g.) was evacuated at 550° for 1.5 hr.; 10 ml. of *n*-heptane and 20 mg. of anthracene were separately thoroughly outgassed; the three components then were mixed by break-seal technique. Oxygen was admitted to the reaction vessel at room temperature at a pressure of 540 mm. and the vessel was shaken. A gradual decrease in pressure was observed, the green silica–alumina began to darken and in three minutes was almost black. After one hour there was no further decrease in pressure. The remaining oxygen was removed and measured, and the solution was analyzed for anthracene by ultraviolet spectroscopy before and after treatment of the silica–alumina with *n*-butylamine. There was 73% conversion of anthracene, and 1.6 moles of O_2 was consumed per mole of anthracene converted. The absorption spectrum of the brown silica–alumina was not obtained. However, at the conclusion of an experiment similar to that described above, the brown catalyst was eluted with methanol (all the adsorbed material was not removed by this treatment), giving a red solution with an absorption maximum at 5550 Å. This solution turned yellow on standing in air for a few hours.

It should be emphasized that anthracene in *n*-heptane solution is completely unreactive with oxygen at room temperature in the absence of a catalyst.

Eastman Kodak Company "blue-violet fluorescent" anthracene was employed in the above experiments. The *n*-heptane was treated with an excess of NO_2–N_2O_4 to remove traces of olefins and then was chromatographed on silica gel. The silica–alumina was American Cyanamid Company Aerocat cracking catalyst, with the following properties: 22.1% Al_2O_3, 0.92% SO_4, 0.032% Fe, 0.009% Na and B.E.T. surface area of 526 $m.^2/g.$ Before use, this catalyst was heated in air for five hours and was perfectly white after this treatment.

The reaction reported above appears at first sight to be anomalous because there seems to be agreement that hydrocarbon reactions catalyzed by silica–alumina involve ionic or polar intermediates,[2] while hydrocarbon autoxidations are generally believed to proceed by homolytic mechanisms.[3] As far as is known, hydrocarbon oxidations catalyzed by the solid acid, silica–alumina, have not been reported.

We find two reports in the literature which appear to demonstrate acid-catalyzed oxidation of hydrocarbons. Friedel and Crafts found that phenol was formed when air was bubbled through a refluxing mixture of benzene and aluminum chloride.[4] Dallinga, Mackor and Verrijn Stuart reported that the spectra of solutions of perylene, pyrene and naphthacene in hydrogen fluoride were greatly altered by the presence of oxygen and suggested that oxidation to a free radical positive ion was responsible for the alteration in spectrum in the case of perylene.[5]

Matsumoto and Funakubo observed a small amount of oxidation of anthracene to anthraquinone during chromatography of a benzene solution of anthracene on activated alumina.[6] This observation may be an example of the reaction reported here, although alumina is considered a very weak solid acid.

The present experiments raise a warning that oxidation may interfere with the chromatographic separation of aromatic hydrocarbons. By the same token studies of hydrocarbon catalysis by acidic solids may involve errors due to an attenuation of catalytic activity by products of oxidation or other basic molecules such as water. The latter may be especially true when catalysts are "regenerated" by contact with air immediately before use.

The experimental assistance of R. M. Ross is gratefully acknowledged.

(2) H. H. Voge in "Catalysis," Vol. VI, P. H. Emmett, Editor, Reinhold Publ. Corp., New York, N. Y., 1958, pp. 407–493.

(3) G. A. Russell, *J. Chem. Ed.*, **36**, 111 (1959).

(4) C. Friedel and J. M. Crafts, *Compt. rend.*, **86**, 885 (1878). The conversion of benzene and the yield of phenol were not reported.

(5) G. Dallinga, E. L. Mackor and A. A. Verrijn Stuart, *Molecular Phys.*, **1**, 125, 137 (1958).

(6) Y. Matsumoto and E. Funakubo, *J. Chem. Soc. Japan, Pure Chem. Sect.*, 731 (1951); Y. Matsumoto, *ibid.*, 733 (1951).

A GLASS CONDUCTANCE CELL FOR THE MEASUREMENT OF DIFFUSION COEFFICIENTS

BY HERBERT S. HARNED AND MILTON BLANDER

Contribution No. 1556 from the Department of Chemistry of Yale University, New Haven, Conn.

Received June 25, 1959

The determination of diffusion coefficients of electrolytes by the conductance method has been carried out in Lucite cells of types described by Harned and Nuttall.[1] To avoid the disadvantages of the use of Lucite and of grease in the region of the electrodes, the glass cell, the cross section of which is shown in Fig. 1, was constructed.

The cell is of soft glass tubing of 8 mm. internal diameter. The electrodes at positions C are platinum tubes about 2 cm. in length and 3 mm. in diameter. The ends of these tubes were closed and made flat by spinning. They are sealed at positions C at a distance from the top and bottom of the cell of one sixth its depth. The top of the tube was flanged at B. A glass plate A ground to this flange serves when clamped to seal off the top of the cell. The bottom of the cell is attached to a special stopcock E with a hole only half way through it. This hole or cup D in the stopcock can be turned to any position and serves to introduce salt solution into the cell. The cell, with lead wires from the conductance bridge attached to electrodes, is mounted on a brass block in a Lucite box which is covered and submerged in a water-bath. A cork was sealed to the stopcock handle and Nylon cord was attached to the cork so that the stopcock could be turned from outside the Lucite box.

The sequence of manipulation of the glass cell is similar to that previously used with the cells made of Lucite. After the electrodes were platinized, the cell was repeatedly washed with distilled water until the resistance between any pair of electrodes after standing overnight was over 500,000 ohms. The cell in the upright position was filled with fresh distilled water. The flange was greased lightly. A mound of water above the surface of the flange was built up so that by sliding the glass plate along the ground surface of the flange, the liquid could be sheared off completely. Care was exer-

(1) H. S. Harned and R. L. Nuttall, *J. Am. Chem. Soc.*, **69**, 736 (1947).

cised to eliminate all bubbles. The glass plate then was clamped to the flanged surface. The salt is introduced as follows:

(1) The cell is turned upside down to position I (Fig. 1) with the salt cup D aligned with the filling tube F.

(2) Salt solution is introduced into D through F and all bubbles forced out with a sharpened rod.

(3) The salt cup is turned to position II, the lead wires are attached and the cell in the upright position III is placed in the Lucite box which then is submerged in the water-bath.

(4) When the system has come to temperature equilibrium after 48 hours, the salt cup is turned to position IV for a suitable time and then turned to position III. With 0.15 M potassium chloride in D, it took 70 minutes for sufficient salt to diffuse into the cell to yield a final concentration of 0.00255 M.

Following the former procedure with Lucite cells, five conductance measurements were made each day at approximately two hour intervals. The ratio of the cell constants at the bottom pair and top pair of electrodes, k_B/k_T, was determined before the diffusion experiment was made. If then K_B and K_T are the specific conductances between the bottom and top electrodes, respectively, at a time, t

$$(k_B K_B - k_T K_T) = Ae^{-t/\tau} \qquad (1)$$

and

$$\ln\left(\frac{k_B}{k_T} K_B - K_T\right) = -\frac{t}{\tau} + \text{constant} \qquad (2)$$

where

$$\frac{1}{\tau} = \frac{\pi^2 \mathfrak{D}}{a^2} \qquad (3)$$

$\mathfrak{D}$ is the diffusion coefficient of the salt and a is the depth of the cell. The quantity $1/\tau$ was evaluated by the usual method as described by Harned and Nuttall.[1]

Table I contains the results obtained over a five day period. The first column are the values of the diffusion coefficient of potassium chloride from measurements on the first and second days, the second column values obtained for the second to third day and so on.

TABLE I

DETERMINATION OF THE DIFFUSION COEFFICIENT OF POTASSIUM CHLORIDE AT 25° BY THE GLASS CONDUCTANCE CELL

1–2 Values are determined from measurements made on first and second days, 2–3 from second to third day conductances, etc.

c = 0.00255 mole/l., a = 8.214 cm., k_B/k_T = 0.93

$\mathfrak{D} \times 10^5$			
1–2	2–3	3–4	4–5[a]
1.908	1.948	1.941	1.943
1.910	1.942	1.953	1.942
1.913	1.944	1.956	1.934
1.903	1.955	1.953	1.950
1.915	1.939	1.956	1.942

[a] Mean for three day runs from second to fifth day: $\mathfrak{D} = 1.946 \times 10^{-5}$; theoretical = 1.949×10^{-5}.

It is apparent from these results that the diffusion was steady after the second day of the run. The mean result of the last three days is 1.946×10^{-5} at 0.00255 molar concentration which agrees well with the value of 1.949×10^{-5} which was obtained by means of the theory of Onsager and Fuoss.[2]

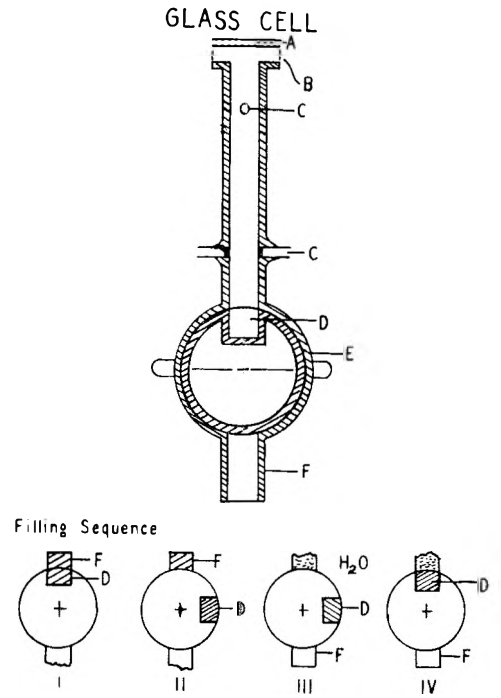

Fig. 1.—A glass cell for determining diffusion coefficients.

This result proves that a glass cell of the type described can be used to determine diffusion coefficients of salts in dilute solutions. However, attempts to determine the diffusion coefficient of the more mobile electrolyte, hydrochloric acid, in this cell were not successful.

This contribution was supported in part by The Atomic Energy Commission under Contract AT (30–1) 1375.

(2) H. S. Harned and B. B. Owen, "The Physical Chemistry of Electrolytic Solutions," 3rd Edition, Reinhold Publ. Corp., New York, N. Y., 1958, pp. 119–122, 143–144.

THE ACTIVITY COEFFICIENT OF HYDROCHLORIC ACID IN THORIUM CHLORIDE SOLUTIONS AT 25°

BY HERBERT S. HARNED AND ALAN B. GANCY

Contribution No. 1560 from the Department of Chemistry of Yale University, New Haven, Conn.

Received June 25, 1959

From measurements of the electromotive force of the cell

$$H_2 | HCl(m_1), ThCl_4(m_2) | AgCl\text{-}Ag$$

at 25°, the activity coefficient of the acid has been computed by the equation

$$E = E^0 - 0.1183 \log \gamma_\pm \sqrt{m_1(m_1 + 4m_2)} \qquad (1)$$

The results were obtained at constant total ionic strengths $\mu = (m_1 + 10m_2)$ of 0.1, 0.5, 1, 3 and 5. The experimental electromotive forces and the derived activity coefficients are given in Table I.

The solutions were prepared by weight from carefully analyzed thorium chloride and hydrochloric acid solutions. Uncrystallized thorium chloride by "Lindsay, Code 130" was used. Although no difficulty was encountered in reproducing the electromotive forces, the results should

TABLE I

ELECTROMOTIVE FORCES OF THE CELL H_2/HCl (m_1), $ThCl_4$ (m_2)/AgCl–Ag AND ACTIVITY COEFFICIENTS OF HYDROCHLORIC ACID IN SOLUTIONS OF VARIOUS TOTAL IONIC STRENGTHS

$\mu = 0.1$			$\mu = 0.5$		
m_1	E	γ_{HCl}	m_1	E	γ_{HCl}
0.1	0.35261	0.795	0.5	0.27227	0.759
.07	.36707	.792	.3	.29517	.720
.05	.38053	.781	.1	.33804	.655
.03	.39978	.761	.01	.43319	.365
.01	.44039	.672	...	...	...
$\mu = 1$					
m_1	E	γ_{HCl}	m_1	E	γ_{HCl}
1.0	0.23321	0.811	0.3	0.28572	0.700
.7	.24989	.774	.1	.32909	.586
.5	.26455	.745	.01	.41581	.365
$\mu = 3$			$\mu = 5$		
m_1	E	γ_{HCl}	m_1	E	γ_{HCl}
3.0	0.15183	1.318	5.0	0.09519	2.380
2.7	.15779	1.275	4.5	.10427	2.167
2.4	.16440	1.229	4.0	.11434	1.953
2.1	.17166	1.182	3.5	.12469	1.769
1.8	.18000	1.128	3.0	.13613	1.598
1.5	.18956	1.069	2.5	.14879	1.427
1.2	.20086	1.003	2.0	.16261	1.266
0.9	.21529	0.919	1.5	.17995	1.096
.6	.23370	.831	1.0	.20202	0.923
.3	.26433	.688	0.5	.23325	.756
.1	.34054	.283	0.2	.30179	.328

be regarded as preliminary until repeated with other preparations of thorium chloride.

Plots of log γ_{HCl} *versus* m_1, the acid concentration at these constant stoichiometrical ionic strengths, all tend to decrease rapidly as the acid concentration decreases. This behavior indicates that the "true" ionic concentration product, $m_H m_{Cl}$, is reduced.[1] This behavior is consistent with recent investigations of thorium chloride solutions.[2,3]

This contribution was supported in part by the Atomic Energy Commission under Contract AT (30–1) 1375.

(1) See Fig. (14-13-2), p. 631, H. S. Harned and B. B. Owen, "The Physical Chemistry of Electrolytic Solutions," 3rd Edition, Reinhold Publ. Corp., New York, N. Y., 1957.

(2) W. C. Waggener and R. W. Stoughton, THIS JOURNAL, **56**, 1 (1952).

(3) K. A. Kraus and R. W. Holmberg, *ibid.*, **58**, 325 (1954).

HEATS OF SOLUTION FROM THE TEMPERATURE DEPENDENCE OF THE DISTRIBUTION COEFFICIENT[1]

BY F. A. TRUMBORE AND C. D. THURMOND

Bell Telephone Laboratories, Incorporated, Murray Hill, New Jersey

Received June 29, 1959

The temperature dependence of the distribution coefficient k of a given component of a binary alloy system is determined by the relative amounts of that component in the alloys lying along the solidus and liquidus curves. In recent years, a number of papers have appeared[2–5] in which the temperature dependence of the distribution coefficient (specifically, the slope of a log k *vs.* $1/T$ plot, where T is the absolute temperature) of the minority component of the solid solutions has been interpreted to give heats of solid solution of the minority component in alloy systems for which the major component is germanium or silicon. In certain cases emphasis has been placed on the form of the temperature dependence of k near the melting point of the major component. Recently, for example, Weiser[6] has suggested that such data near the melting points of Ge or Si could be used to obtain heats and entropies of solution in the very dilute solution range and would constitute a sensitive test of his theory on the magnitude of k. In interpreting distribution coefficient data in this manner it has been assumed that the effects of non-ideal solution behavior in the liquid phase can be neglected. Recently, however, it has been shown[7] that in certain systems the non-ideality of the liquid phase appears to play a major role in determining the temperature dependence of the distribution coefficient. In this note we shall consider in greater detail the effects due to non-ideal solution behavior in both solid and liquid phases. From these considerations it will be evident that the interpretation of distribution coefficient data is complex and that serious errors can be made in calculating heats of solution from such data.

General Equation for the Temperature Dependence of k.—From the usual definitions of activity coefficients, namely

$$\mu_2^S = \mu_2^{0S} + RT \ln \gamma_2^S x_2^S \quad (1)$$

$$\mu_2^L = \mu_2^{0L} + RT \ln \gamma_2^L x_2^L \quad (2)$$

and the fact that, at equilibrium between solid and liquid phases, $\mu_2^S = \mu_2^L$ it follows that the distribution coefficient k can be written

$$k \equiv x_2^S/x_2^L = (\gamma_2^L/\gamma_2^S) \exp(\Delta F_2'/RT) \quad (3)$$

In these equations R is the gas constant, T is the absolute temperature while x_2^S and x_2^L, γ_2^S and γ_2^L, and μ_2^S and μ_2^L are the atom fractions, activity coefficients and chemical potentials of component 2 (the minor component of the solid solution) in the solidus and liquidus alloys, respectively. The quantities μ_2^{0S} and μ_2^{0L} are the chemical potentials of pure solid and liquid component 2 while $\Delta F_2'$ is the free energy of fusion of component 2, equal to $(\mu_2^{0L} - \mu_2^{0S})$. Equation 3 is a modified form of an equation developed previously by Thurmond and Struthers.[2]

Since we are concerned here with the interpretation of the slope of a log k *vs.* $1/T$ plot we may write the relation

$$\frac{d \ln k}{d\, 1/T} = \frac{\dfrac{\bar{H}_2^L - \bar{H}_2^S}{R} + \left[\left(\dfrac{\partial \ln \gamma_2^L}{\partial x_2^L}\right)_T - k\left(\dfrac{\partial \ln \gamma_2^S}{\partial x_2^S}\right)_T\right]\left(\dfrac{dx_2^L}{d\, 1/T}\right)}{1 + kx_2^L\left(\dfrac{\partial \ln \gamma_2^S}{\partial x_2^S}\right)_T} \quad (4)$$

(1) Presented at the American Chemical Society Meeting, Boston, Massachusetts, April 7, 1959.

(2) C. D. Thurmond and J. D. Struthers, THIS JOURNAL, **57**, 831 (1953).

(3) F. Van der Maesen and J. A. Brenkman, *Philips Research Repts.*, **9**, 225 (1954).

(4) R. N. Hall, *J. Phys. Chem. Solids* **3**, 63 (1957).

which follows from equation 3 and standard thermodynamic equations relating activity coefficients to heats of solution. Here $\bar{H}_2^L$ and $\bar{H}_2^S$ are the partial molar heat contents of component 2 in the liquidus and solidus alloys, respectively. Equation 4 is the general equation defining the temperature dependence of k in terms of a heat of solution and the departures from ideal solution behavior in the liquid and solid phases. In this paper an *ideal* solution is defined as one in which γ_2^S or γ_2^L is unity (Raoult's law). An *ideal dilute* solution is defined as one in which γ_2^S or γ_2^L is a constant, other than unity, at a given temperature and is independent of concentration (Henry's law).

Interpretation of Distribution Coefficient Data to Give Heats of Solution.—It is evident from equation 4 that the slope of a log k *vs.* $1/T$ plot is directly proportional to a heat of solution only in special cases where the terms other than $(\bar{H}_2^L - \bar{H}_2^S)/R$ are zero. An obvious case where this is true is the case where both liquid and solid solutions are ideal and

$$\frac{\mathrm{d} \ln k}{\mathrm{d}\, 1/T} = \frac{\Delta H_2^f}{R} \qquad (5)$$

where ΔH_2^f is the heat of fusion of component 2. A situation more likely to be encountered experimentally is the case where the liquid solutions are ideal and the solid solutions are ideal dilute solutions in which case

$$\frac{\mathrm{d} \ln k}{\mathrm{d}\, 1/T} = \frac{H_2^{0L} - (\bar{H}_2^S)^*}{R} \qquad (6)$$

where H_2^{0L} is the heat content of pure liquid component 2 and the asterisk denotes that the partial molar heat content is independent of composition. Equation 6 appears to be valid for systems such as the Sn–Si system[7] where, at low temperatures, the liquidus alloys are nearly pure component 2.

Let us now consider the interpretation of log k *vs.* $1/T$ plots in the region of the melting point of the major component T_1 where both x_2^S and x_2^L tend to zero. In previous work[2-5] it has been assumed that the solid alloys were ideal dilute solutions and that the liquid alloys were either ideal solutions or the non-ideality in the liquid phase could be neglected. Another possible assumption would be that the liquid alloys were also ideal dilute solutions. If either ideal or ideal dilute solution behavior is assumed to hold strictly (*i.e.*, $\gamma_2^L = 1$ or γ_2^L is absolutely constant at a given temperature) all terms involving a variation of the activity coefficient with composition would vanish and

$$\left[\frac{\mathrm{d} \ln k}{\mathrm{d}\, 1/T}\right]_{T_1} = \frac{(\bar{H}_2^L)^* - (\bar{H}_2^S)^*}{R} \qquad (7)$$

While the assumptions made in the derivation of equation 7 seem quite reasonable, consideration of the possible behavior to be expected experimentally leads to a quite different result.

To illustrate this point let us retain the assumption that the dilute solid solutions obey Henry's law and consider how closely we would expect Henry's law to be obeyed by the liquid alloys for a real system where there are significant departures from Raoult's law. Specifically, let us assume that the liquid alloys are "regular" solutions in the sense that

$$\ln \gamma_2^L = \frac{\alpha}{RT}(1 - x_2^L)^2 \qquad (8)$$

where α is a constant, independent of temperature and composition. Evidence has been presented that equation 8 may be a useful first approximation to the activity coefficients in Ge and Si binary alloy systems.[8] With these assumptions, near the melting point of the major component T_1 equation 4 becomes

$$\left[\frac{\mathrm{d} \ln k}{\mathrm{d}\, 1/T}\right]_{T_1} = \frac{1}{R}\left[(\bar{H}_2^L)^* - (\bar{H}_2^S)^* - \frac{2\alpha \Delta H_1^f}{(1 - k^0)RT_1}\right] \qquad (9)$$

where ΔH_1^f is the heat of fusion of component 1 and k^0 is the value of k at T_1. From equation 9 it is evident that if the slope of the log k *vs.* $1/T$ plot is interpreted directly to give a heat of solution, this heat will be in error by an amount equal to $2\alpha \cdot \Delta H_1^f/(1 - k^0)RT_1$. This term may be particularly large for alloy systems with major components such as Ge or Si where the heats of fusion are especially large, 8 and 12 kcal./g.-atom, respectively. For Ge and Si systems k^0 is usually negligible compared with unity and estimated values of α range from about -3.5 to $+11.5$ kcal. so that the term $2\alpha\Delta H_1^f/(1 - k^0)RT$ can amount to as much as $\sim$80 kcal. for certain systems.

Even greater errors are possible at intermediate temperatures for systems showing large positive departures from ideality in the liquid phase. For such systems the $(\mathrm{d}x_2^L/\mathrm{d}\, 1/T)$ term in equation 4 may become even larger than its value of $\Delta H_1^f/(1 - k^0)RT_1$ at T_1. For example, for the Sn–Si system,[7] interpreting the slope of the high temperature log k *vs.* $1/T$ data directly to give a heat of solution yields a value of $\sim$ 100–200 kcal. whereas the actual heat of solution estimated from the low temperature data (see equation 6) is an order of magnitude smaller.

In view of the possible errors which might result from the assumption of ideal or ideal dilute solution behavior for the liquid alloys, the question arises as to whether or not similar complications might result from the assumption of Henry's law for the solid solutions. Experimentally, for the systems involving electrically neutral impurities in Ge and Si, this does not seem to be the case[9] although experimental data are not now sufficiently precise or extensive to permit any definite conclusions. In equation 4 it is seen that any departures from Henry's law as expressed by the $(\partial \ln \gamma_2^S/\partial x_2^S)_T$ terms are multiplied by k, which is usually appreciably less than unity, thus reducing the importance of these terms. If these terms were roughly of the same order of magnitude as the $(\partial \ln \gamma_2^L/\partial x_2^L)_T$ term, the assumption of Henry's

(5) R. A. Oriani and R. N. Hall, *ibid.*, **6**, 97 (1958)

(6) K. Weiser, *ibid.*, **7**, 118 (1958).

(7) F. A. Trumbore, C. R. Isenberg and E. M. Porbansky, *ibid.*, **9**, 60 (1959).

(8) C. D. Thurmond, THIS JOURNAL, **57**, 827 (1953).

(9) For donor or acceptor impurity elements in semiconductors departures from Henry's law are to be expected in quite dilute solid solutions. These interactions influence the distribution coefficient even though the distribution coefficient may be rather small.[10]

(10) F. Trumbore, E. M. Porbansky and A. A. Tartaglia, *J. Phys. Chem. Solids*, to be published.

law would be an appreciably better approximation for the solid solutions than for the liquid solutions. Some estimates have been made, assuming the regular solution model for the solid solutions, which indicate that as k becomes smaller the $(\partial \ln \gamma_2^s/\partial x_2^s)_T$ term becomes larger. However, the k term tends to dominate the activity coefficient term thus reducing the latter's importance.

Summary.—A general equation for the temperature dependence of the distribution coefficient has been given which indicates the complications inherent in the interpretation of log k *vs.* $1/T$ plots to give heats of solution. A simple solution model has been used to indicate the magnitude of the errors which might result if the experimental data are not properly interpreted.

QUENCHING OF EXCITED $Hg(^3P_1)$ BY NO[1]

By Robert J. Fallon, Joseph T. Vanderslice and Edward A. Mason

Institute for Molecular Physics, University of Maryland, College Park, Maryland

Received July 6, 1959

Noyes[2] has studied the mercury photosensitized reaction of NO and, after a careful analysis of the experimental data, has concluded that the overall process corresponds to the reaction

$$2Hg + 2NO \longrightarrow 2HgO + N_2 \qquad (1)$$

and that the rate-determining step is

$$Hg^* + NO \longrightarrow Hg + NO^* \qquad (2)$$

Bates[3] has measured the cross section for the quenching of excited $Hg(^3P_1)$ by NO and found the extremely large value of 24.7 Å.^{2}, which indicates a resonant process. On the basis of the then known potential curves for NO, both Bates and Noyes were forced to conclude that the NO* formed in reaction 2 was most likely in a highly excited vibrational level of the ground $X^2\Pi$ state. In order to explain the kinetics, Noyes postulated that the lifetime of the NO* was appreciably longer than the average time between collisions, even at the low pressures used in the experiments. A highly vibrationally excited molecule in the $X^2\Pi$ electronic state would have a long lifetime. Noyes stated, however, that one would expect the formation of such a highly excited (about $v = 26$) state by collision to be rare in the absence of some special resonant effect.

Recently, a large number of potential curves for the different states of NO have been calculated from spectroscopic data and quantum-mechanical theory.[4] Two of these, the $X^2\Pi$ and the $^4\Pi$, are shown in Fig. 1. These are the only ones which will be of importance in the subsequent discussion. The lowest vibrational level of the $^4\Pi$ state is estimated to lie 4.64 ± 0.10 e.v. above the lowest vibrational level of the $X^2\Pi$ state. Since 4.88 e.v. is transferred from the Hg* to the NO in reaction 2,

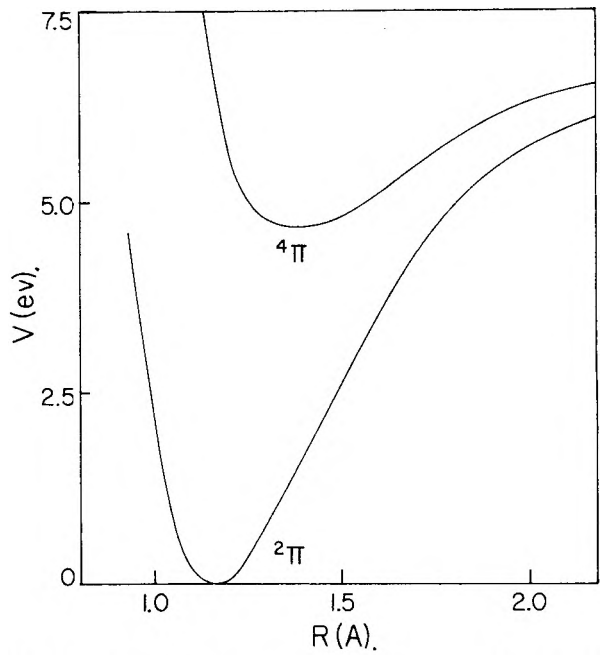

Fig. 1.—Potential energy curves for the lower states of NO.

it is quite possible from an energy point of view for the NO to end up in one of the lower vibrational levels of this $^4\Pi$ state. This transition from the $^2\Pi$ to the $^4\Pi$ also satisfies the correlation rules for such processes.[5] Furthermore, a transition to the $^4\Pi$ state would result in an excited molecule with a long lifetime, since the radiative transition back to the $^2\Pi$ state has an exceptionally low transition probability.[6] This is in agreement with Noyes' suggestion regarding the lifetime of the NO*. A transition to this state also agrees with Laidler's suggestion[7] that a process involving the least net change in electronic energy is the most likely. Finally, a transition to one of the lower vibrational levels of the $^4\Pi$ state is in accord with the Franck–Condon principle, since there would be a very small change in internuclear distance. Because the quenching cross section is so large, the transition must occur readily and one would expect that this would not happen if a large change in internuclear distance had to occur during the process. In short, a transition between the $^2\Pi$ and $^4\Pi$ states of NO by collision with $Hg(^3P_1)$ would be essentially a resonant process.

In conclusion, we should like to propose that the NO* formed in reaction 2 might be in the $^4\Pi$ state rather than in the vibrationally excited $X^2\Pi$ state, the one suggested by Noyes on the basis of the then known potential curves of NO. If our suggestion can be verified, it would be added experimental confirmation that the $^4\Pi$ state lies in the region first proposed by Mulliken,[8] later tentatively confirmed by Ogawa[9] on the basis of his experimental data and recently reconfirmed[4] on

(1) This research was supported in part by the National Aeronautics and Space Administration.

(2) W. A. Noyes, Jr., *J. Am. Chem. Soc.*, **53**, 514 (1931).

(3) J. R. Bates, *ibid.*, **54**, 569 (1932).

(4) J. T. Vanderslice, E. A. Mason and W. G. Maisch, *J. Chem. Phys.*, **31**, 738 (1959).

(5) K. E. Shuler, *ibid.*, **21**, 624 (1953).

(6) R. S. Mulliken, "The Threshold of Space," Pergamon Press, Ltd., New York, N. Y., 1957, p. 123.

(7) K. J. Laidler, "The Chemical Kinetics of Excited States," Oxford University Press, London, England, 1955, p. 101.

(8) R. S. Mulliken, *Revs. Modern Phys.*, **4**, 1 (1932).

(9) M. Ogawa, *Science of Light (Tokyo)*, **3**, 39 (1954).

the basis of additional theoretical and experimental information.

Acknowledgment.—The authors wish to thank Professor B. de B. Darwent for helpful discussions and comments.

THE HYDRODYNAMIC VOLUME OF THE HETEROPOLY HEXAMOLYBDOCOBALTATE(III) ANION FROM VISCOSITY MEASUREMENTS

BY MICHAEL T. POPE[1] AND LOUIS C. W. BAKER[2]

Contribution from the Department of Chemistry, Boston University, Boston 15, Massachusetts

Received July 6, 1959

In a recent paper, Kurucsev, Sargeson and West[3] demonstrated that the Einstein viscosity equation is valid for various large spherical inorganic ions. They were able to show that the 12-tungstosilicate ion has a hydrodynamic radius of 5.6 Å., in good agreement with that calculated from the molar volume[4] and consistent with the crystallographic unit cell dimensions of $H_4[SiW_{12}O_{40}]\cdot 5H_2O$.[5,6]

Application of this method to the investigation of other heteropoly anions is limited by the solubilities of the salts available. In general, for most heteropoly anions, those salts which are readily purifiable are only soluble to an extent of up to about 20 g. per 100 ml. Therefore even saturated solutions usually have low molarity (less than 0.1 *M*) because of the high molecular weights of the solutes. The viscosities of such solutions are not sufficiently greater than that of water to make possible a series of reasonably accurate measurements. The free acids of these anions are generally much more soluble, but in many cases are unstable, especially in concentrated (>0.2 *M*) solutions.

In the course of an investigation of the solution chemistry of the isomorphous 6-molybdo anions of trivalent Co, Cr, Fe and Al, it was found that the free 6-molybdocobaltic acid can be concentrated without decomposition. We have discussed the chemistry of these anions in a previous paper[7] and recently have shown that they are of high thermodynamic stability and are monomeric in solution.[8]

The 6-molybdocobaltic acid was prepared by passing an aqueous solution of the purified ammonium salt through an Amberlite IR-120 (Rohm and Haas Co.) ion-exchange column in the hydrogen cycle.[7,9] The effluent acid was concentrated at just below room temperature by placing it in a cellophane sac and blowing a current of warm air over the outside of the sac. The molarity of the resulting solution was determined by analysis of aliquots. A portion of the effluent acid, concentrated at 40° by aspirating dry air through the solution for 48 hours, gave the same viscosity results as the acid concentrated by the cellophane sac method. Viscosity measurements were made in an Ostwald viscometer at 25°.

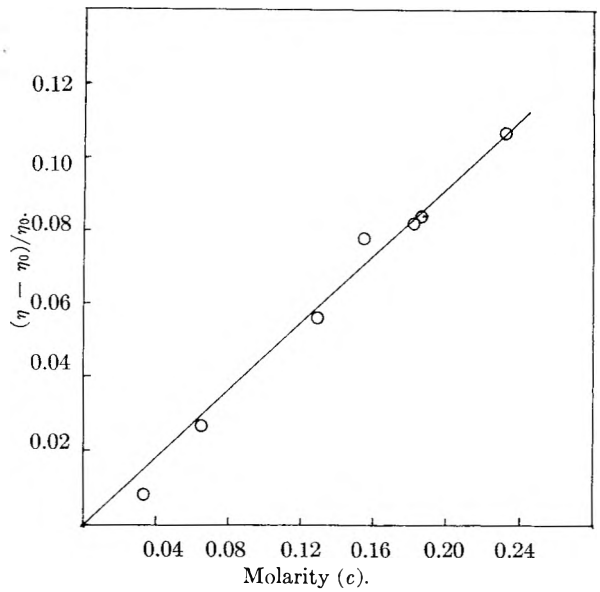

Fig. 1.—Viscosity values for aqueous solutions of $H_3[CoMo_6O_{21}]$ at 25°. The line shown was drawn from the origin by the method of least squares.

The results of the viscosity determinations are recorded in Fig. 1. They can be expressed by the Jones–Dole[10] equation

$$\frac{\eta - \eta_0}{\eta_0} = A\sqrt{c} + Bc$$

where $A = 0$ and $B = 0.46$, over the concentration range 0.035 to 0.23 *M*.

The acid has the formula $H_3[CoMo_6O_{21}]$, and its three dissociation constants all lie close together, having *pK*'s within the range 2–3.[7,8] Assuming that the *pK*'s merely lie close to this range and assuming Gurney's[11] value of +0.07 for the *B*-coefficient of the solvated proton, the *B*-coefficient of the heteropoly particles was calculated to lie between +0.40 and +0.45. Whence, according to the Einstein equation, the apparent hydrodynamic volume of the $[CoMo_6O_{21}]^{-3}$ ion falls between 265 and 300 Å.^{3}, within the concentration region investigated. This corresponds to an hypothetical sphere with radius between 4.0 and 4.2 Å.

Since the structure of this series of isomorphous 6-molybdo anions has not yet been determined, there are no independent data for direct comparison with the above results. However, there is some evidence[12] that these anions may have very similar structure to that of a 6-heteropoly tungstonickelate of similar formula and known crystal structure.[12] That tungsto complex is essentially isostructural with the 6-molybdotellurate(VI) anion, the structure of which was suggested by Anderson[13] and

(1) Monsanto Research Fellow at Boston University.

(2) Addressee for reprints.

(3) T. Kurucsev, A. M. Sargeson and B. O. West THIS JOURNAL, **61**, 1567 (1957).

(4) M. C. Baker, P. A. Lyons and S. J. Singer, *J. Am. Chem. Soc.*, **77**, 2011 (1955).

(5) R. Signer and H. Gross, *Helv. Chim. Acta*, **17**, 1076 (1934).

(6) O. Kraus, *Z. Krist.*, **100**, 394 (1939).

(7) L. C. W. Baker, G. Foster, W. Tan, F. Schelnick and T. P. McCutcheon, *J. Am. Chem. Soc.*, **77**, 2136 (1955).

(8) G. A. Tsigdinos, M. T. Pope and L. C. W. Baker, Abstracts of papers presented before the Division of Inorganic Chemistry, American Chemical Society National Meeting, Boston, Mass., April, 1959.

(9) L. C. W. Baker, B. Loev and T. P. McCutcheon, *J. Am. Chem. Soc.*, **72**, 2374 (1950).

(10) G. Jones and M. Dole, *ibid.*, **51**, 2950 (1929).

(11) R. W. Gurney, "Ionic Processes in Solution," McGraw-Hill Book Co., Inc., New York, N. Y., 1953, p. 159.

(12) U. C. Agarwala, Doctoral Dissertation, Boston University, 1959.

(13) J. S. Anderson, *Nature*, **140**, 850 (1937).

proved by Evans.[14-16] In the crystals, these similar ions are both thick hexagonal discs, approximating oblate spheroids. From the crystallographic data, the effective minor radius (half-thickness) of each may be estimated as 2.7–3.0 Å. and the effective major radius averages about 6.0 Å. The volume of each of these two disc anions is about 600 Å.^{3}. In arriving at these estimates, the possible closeness of approach of water molecules to the irregular surface of the polyanion was considered. While the nickelate and tellurate complexes each contain twenty-four oxygen atoms, the 6-molybdocobaltate(III) anion and its Cr, Fe and Al isomorphs might contain as few as twenty-one oxygen atoms apiece (their proportion of "constitutional water" being uncertain at present).[7,8,12] The discrepancy between the effective hydrodynamic volume determined above and the probable range of the total crystallographic volume of the anion is easily understood in view of the size and probable disc shape of the anion. The size is below that for which good applicability of the Einstein equation should be assumed for polyions. Factors involving the fit of solvent molecules to the irregular surface of the solute particle are proportionately more important the smaller a polyanion becomes. These 6-molybdo ions are presumably far from spherical; and, if they have the probable disc-like structure, it is likely that their planes would become oriented parallel to the direction of liquid flow. In view of the dimensions cited, it is most reasonable that such anions would have an apparent hydrodynamic volume close to that observed. The results also indicate that the degree of solvation of the anion is negligible. This is consistent with the low charge density on the surface of heteropoly anions and with the negligible solvation observed for 12-tungstosilicate ion.[3]

An attempt to measure the viscosity of solutions of the free acid of 6-molybdoiodate(VII), which is presumably isomorphous with the 6-molybdotellurate(VI),[16] was unsuccessful owing, apparently, to decomposition of the acid in concentrated solution. For the same reason, analogous measurements could not be made upon the heteropoly 6-molybdo anions of Cr(III), Fe(III) or Al(III).

Acknowledgments.—This research was supported in part by a grant from Monsanto Chemical Company and in part by the U. S. Atomic Energy Commission, through Contract AT(30-1)-1853.

(14) H. T. Evans, Jr., *J. Am. Chem. Soc.*, **70**, 1291 (1948).

(15) H. T. Evans, Jr., Abstracts of papers presented before the American Crystallographic Association, Cambridge, Mass., 1954.

(16) H. J. Emeléus and J. S. Anderson, "Modern Aspects of Inorganic Chemistry," Second Edition, D. Van Nostrand Co., Inc., New York, N. Y., 1952, pp. 225–226.

THE PYROLYSIS OF ACETYLACETONE

By Robert G. Charles, W. M. Hickam and Joan von Hoene

Westinghouse Research Laboratories, Pittsburgh 35, Pennsylvania

Received July 16, 1959

In previous work concerning the pyrolysis of the metal acetylacetonates (I), acetylacetone itself was observed in several instances as one of the major degradation products.[1] These results suggested that acetylacetone may be more heat stable than

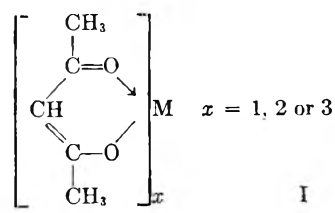

I

the metal chelates derived from it. The present work on the pyrolysis of acetylacetone permits a more direct comparison of the heat stabilities and also permits a comparison of the degradation products from acetylacetone with those of the metal acetylacetonates. There appears to have been no previous comparison of the pyrolysis of a chelating agent with the pyrolyses of the metal chelates derived from it.

Table I gives the gaseous products obtained by heating acetylacetone in sealed evacuated glass tubes for 4 hours at the temperatures indicated. At the lowest temperature employed, 266°, little decomposition has occurred. This is in contrast to the Cu(II), Ni(II), Co(II), Co(III), Al(III), Cr(III), Fe(III) and Mn(III) acetylacetonates, all of which decompose to a significant extent at this temperature.[1] The introduction of a metal atom into the acetylacetone molecule results, therefore, in a decrease of thermal stability, at least for these metals.[2]

Table I

Thermal Degradation of Acetylacetone

Samples heated 4.0 hours at the temperature indicated

Components of gas	Moles gas per mole of acetylacetone taken 266°	346°	462°
Acetylacetone	0.99	0.78	0.00
Acetic acid	.01	.08	.08
Acetone	.00	.12	.88
CO_2	.00	.01	.34
CO	.00	.00	.39
CH_4	.00	.00	.28

The principal gaseous products of pyrolysis for acetylacetone given in Table I are also major decomposition products for the metal acetylacetonates.[1] This fact suggests that at least one possible route for the decomposition of the metal acetylacetonates involves first the formation of acetylacetone followed by decomposition of the latter to the products given in Table I. That acetylacetone is actually found as nearly the sole decomposition product, at the lower temperatures, for the Mn(III) and Cu(II) chelates supports this view.[1] The fact that only small amounts of acetylacetone were found among the decomposition products of the other metal acetylacetonates studied may indicate that, in these instances, the decomposition of the initially formed acetylacetone is catalyzed by the

(1) J. von Hoene, R. G. Charles and W. M. Hickam, This Journal, **62**, 1098 (1958).

(2) On the basis of volatile decomposition products, sodium acetylacetonate appears to be more stable than acetylacetone. The decomposition of the former compound may, however, involve non-volatile pyrolysis products which cannot be detected by the mass spectrometer (ref. 1).

presence of undecomposed metal acetylacetonate or by metal-containing decomposition products.

The principal pyrolysis products of acetylacetone at 346° are acetic acid and acetone At 462° appreciable quantities of CO_2, CO and methane are also present. The latter products may very well result from the pyrolysis of the initially formed acetone or acetic acid rather than from acetylacetone directly.

The only previous study of the pyrolysis of acetylacetone is that of Hurd and Tallyn.[3,4] These workers determined the formation of ketene from acetylacetone, using a flow system and much higher temperatures than those employed here. The production of ketene is not inconsistent with the present results since ketene is, under the proper experimental conditions, a product of the pyrolysis of acetone.[5]

Experimental

A Consolidated mass spectrometer was used to identify and to determine the pyrolysis products. The apparatus and procedure were essentially the same as those previously employed.[1] Ten-mg. samples of high purity acetylacetone[6] were weighed into Pyrex glass tubes having break-tips and the tubes were evacuated and sealed. The acetylacetone was cooled with liquid nitrogen during the evacuation and sealing procedures. The tubes were heated for 4 hours in a constant temperature tube furnace with the sealed portions entirely within the hot zone. The heated tubes were cooled to room temperature, sealed to the inlet system of the mass spectrometer and the gas expanded, before analysis to 3000 ml. by breaking the break-tip with a magnetic bar.

Acknowledgments.—The authors wish to acknowledge the work of Mr. J. F. Zamaria, Miss I. Laminack and Mrs. M. H. Loeffler, all of whom assisted in the experimental portion of this study.

(3) C. D. Hurd and W. H. Tallyn, *J. Am. Chem. Soc.*, **47**, 1427 (1925).

(4) C. D. Hurd, "The Pyrolysis of Carbon Compounds," A.C.S. Monograph No. 50 (Chemical Catalog Co.), Reinhold Publ. Corp., New York, N. Y., 1929, p. 264.

(5) C. D. Hurd, ref. 4, p. 248.

(6) R. G. Charles and S. Barnartt, THIS JOURNAL, **62**, 315 (1958).

THE SYSTEM GALLIUM TRIOXIDE—SILICA (Ga_2O_3–SiO_2)

BY F. P. GLASSER[1]

Contribution No. 58-130, College of Mineral Industries, The Pennsylvania State University, University Park, Penna.

Received August 13, 1959

Although no previous studies have been reported, the system Ga_2O_3–SiO_2 is of interest. The ionic radius of Ga^{+3} (0.62 Å.)[2] is intermediate between that of Al^{+3} (0.57 Å.) and Fe^{+3} (0.67 Å.). The structure of the stable (β) modification of Ga_2O_3 is related to that of α-Al_2O_3 and α-Fe_2O_3. It is of interest, therefore, to examine the melting relations of Ga_2O_3 with other common oxides and compare the behavior of Ga_2O_3 with that of Al_2O_3 and Fe_2O_3. For this purpose, phase relations in the system Ga_2O_3–SiO_2 have been determined.

Experimental

Starting materials were prepared by blending Ga_2O_3 and SiO_2. One gram batches were prepared from electronic grade Ga_2O_3 (Eagle Pitcher Co.), and ignited SiO_2 gel (Baker Analyzed Reagent Grade). The calculated proportions of Ga_2O_3 and SiO_2 were weighed out and ground under alcohol in an agate mortar. The alcohol was evaporated off and the dried powder blended thoroughly. It was returned to the mortar, moistened with alcohol, reground and redried. This resulted in a starting material of satisfactory homogeneity, as later proved by replicate runs on small portions of the original preparation.

Equilibrium determinations were made as follows. A small portion of the starting preparation was wrapped in platinum foil and suspended in a controlled temperature furnace. At the conclusion of the equilibration, the sample was quenched by dropping it into a dish of mercury. The phases present at the high temperature were determined by petrographic examination and powder X-ray diffraction techniques.

Furnaces were of a vertical tube model suited for quenching work. They were heated by a platinum–20% rhodium resistance element and the temperature regulated by a Weston-Tagliabue "Celectray" controller. The furnace temperature could be regulated to ±2°. Temperatures inside the furnace were read by a platinum–platinum 10% rhodium thermoelement suspended next to the sample. The thermoelement was calibrated frequently at the melting point of $CaMg(SiO_3)_2$ (1391.5°) and $CaSiO_3$ (1544°). The thermocouple error was of the order of ±2°, making the temperatures reported here accurate to about ±4°.

Results

The experimental results are shown diagramatically in Fig. 1. From the melting point of SiO_2 at 1723°, liquidus temperatures fall to a eutectic at about 7 mole % Ga_2O_3 and 1642°. Phases in equilibrium at this eutectic are β-Ga_2O_3, liquid and silica (cristobalite). Liquidus temperatures rise slightly from this eutectic to a point located at about 8 mole % Ga_2O_3 and 1652°, marking one end of an extensive region of liquid immiscibility. The range of compositions melting to two liquids extends to ~65 mole % Ga_2O_3. From 65–100 mole % Ga_2O_3 liquidus temperatures rise from 1652° to the melting point of Ga_2O_3 (1725°).[3] This is shown as a dashed line in Fig. 1, as no runs were made on compositions between 70 mole % Ga_2O_3 and Ga_2O_3.

Discussion of Results

Recognition of the high temperature liquid immiscibility in the system Ga_2O_3–SiO_2 is comparatively simple. Quenched charges of appropriate compositions heated above 1652° contain two glassy phases. One is a clear isotropic glass, having N = 1.504 (sodium light). The other is a partly devitrified brownish glass of high index. The index of this gallium oxide-rich liquid could not be determined, on account of its partial devitrification upon quenching. The relative proportions of the two glasses varies with the bulk composition of the mixture. The liquids have a relatively low viscosity, and separate fairly well in runs of a few minutes' duration: however, the high silica liquid frequently traps droplets of the Ga_2O_3-rich liquid.

Although gallium oxide is essentially non-volatile,[2] possible losses of Ga_2O_3 from the mixtures were checked by duplicating runs on the 10 mole % and 70 mole % Ga_2O_3 compositions using samples sealed in platinum tubes. The tubes were welded shut at one end, a sample inserted and the open end welded shut. Using a micro-welder, it was possible to weld tubes shut without sensible heating of the

(1) Department of Chemistry, University of Aberdeen, Old Aberdeen, Scotland.

(2) Goldschmidt radii are used throughout.

(3) V. G. Hill, R. Roy and E. F. Osborn, *J. Am. Ceram. Soc.*, **35** [6], 135 (1952).

sample. The sealed tube runs on the 10 and 70% gallium oxide mixtures gave results identical with those obtained in open foil envelopes.

No compounds of gallium oxide and SiO_2 were encountered in this study. The 50, 60 and 70% Ga_2O_3 compositions were heated at solidus temperatures, and also at 1550 and 1450° for 24 and 48 hours, respectively. Only β-Ga_2O_3 and cristobalite were present in the runs. Thus no gallium analogs of mullite ($3Al_2O_3 \cdot 2SiO_2$) or the Al_2SiO_5 polymorphs are stable at high temperatures. The high temperature liquid immiscibility in the Ga_2O_3–SiO_2 system is another feature not found in Al_2O_3–SiO_2.[4]

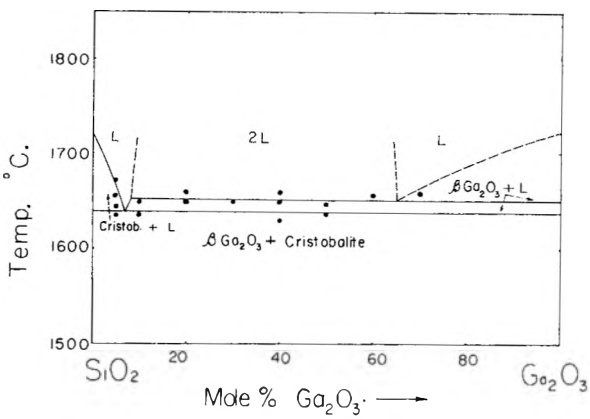

Fig. 1.—Phase relations in the system Ga_2O_3–SiO_2. Solid dots represent the temperature of critical quench runs.

Phase relations in the Fe_2O_3–SiO_2 systems are not known at liquidus temperatures because of the difficulty of maintaining the iron in the ferric state, so that no direct comparisons can be made with other M_2O_3–SiO_2 systems. An extrapolation of data obtained at oxygen pressures of 1 atmosphere and less[5] indicates that extensive liquid immiscibility exists in the Fe_2O_3–SiO_2 system. It may be suggested, therefore, that melting relations are similar in the systems Ga_2O_3–SiO_2 and Fe_2O_3–SiO_2.

(4) N. L. Bowen and J. W. Greig, *ibid.*, **7** [4], 242 (1924); with corrections by J. F. Schairer, *ibid.*, **25**, 243 (1942); further revision suggested by N. A. Toropov and F. Ya. Galakhov, *Doklady Akad. Nauk S.S.S.R.*, **78** [2], 301 (1951).

(5) A. Muan, *J. Metals*, **7** [9], 965 (1955).

THE ACTIVITY COEFFICIENT OF HYDROCHLORIC ACID IN CADMIUM CHLORIDE SOLUTIONS AT 5 *M* TOTAL IONIC STRENGTH

BY HERBERT S. HARNED AND ROBERT GARY

Contribution No. 1559 from the Department of Chemistry of Yale University, New Haven, Conn.

Received June 25, 1959

As a further contribution to the study of the systems containing two electrolytes in water, the activity coefficient of hydrochloric acid in cadmium chloride solutions at 5 *M* total stoichiometric ionic strength has been determined at 25° from measurements of the cells

$$H_2 | HCl\ (m_1),\ CdCl_2\ (m_2) | AgCl\text{–}Ag$$

The observed electromative forces and values of the activity coefficients are recorded in Table I.

TABLE I

THE ACTIVITY COEFFICIENT OF HYDROCHLORIC ACID IN CADMIUM CHLORIDE SOLUTIONS

$T = 25°$; $\mu_T = \mu_1 + \mu_2 = m_1 + 3m_2 = 5$

m_1	E	log γ_1
5.0	0.09519	0.3766
4.5	.10906	.2896
4.0	.12359	.2001
3.5	.13859	.1102
3.0	.15390	.0224
2.5	.16935	− .0600
2.0	.18529	− .1574
1.5	.20253	− .2114
1.0	.22245	− .2822
0.5	.25009	− .3550

This contribution was supported in part by The Atomic Energy Commission under Contract AT (30-1) 1375

ELECTRON PARAMAGNETIC RESONANCE STUDIES ON CARBON DISULFIDE—INSOLUBLE SULFUR

BY A. G. PINKUS AND L. H. PIETTE[1]

Department of Chemistry, Baylor University, Waco, Texas, and Varian Associates, Palo Alto, California

Received July 14, 1959

Recently,[2] a close-packed helical structure was uggested for crystalline polymeric carbon disulfide —insoluble sulfur obtained from the slow cooling of a purified sulfur melt in order to explain the similarity of its X-ray diffraction pattern to that of orthorhombic sulfur.[3] A more extended helical structure also had been suggested recently for the fibrous constituent of stretched plastic sulfur,[4,5] Das's white sulfur,[5,6] and for "supersublimation" sulfur.[6,7] It was pointed out[2] that stereochemical considerations exclude a macrocyclic[8] structure for the close-packed helical configuration and suggested that electron paramagnetic resonance determinations on the insoluble sulfur would distinguish between the biradical (I) or three-electron bond (II)[9] structures on the one hand and the ionic structure (III) on the other. In their classical paper,[10] Gardner and Fraenkel previously had re-

(1) Varian Associates.

(2) A. G. Pinkus, J. S. Kim, J. L. McAtee, Jr., and C. B. Concilio, to be published.

(3) A. G. Pinkus, J. S. Kim, J. L. McAtee, Jr., and C. B. Concilio, *J. Am. Chem. Soc.*, **79**, 4566 (1957).

(4) L. Pauling, *Proc. Nat. Acad. Sci., U. S.*, **35**, 495 (1949); J. A. Prins, J. Schenk and P. A. M. Hospel, *Physica*, **22**, 770 (1956); A. Ripamonti and C. Vacca, *Ricerca Sci.*, **28**, 1880 (1958).

(5) S. R. Das, *Indian J. Phys.*, **12**, 163 (1938).

(6) J. A. Prins, J. Schenk and L. H. J. Wachters, *Physica*, **23**, 746 (1957).

(7) Product of Stauffer Chemical Co. having the registered trade name of "Crystex."

(8) H. Krebs and E. F. Weber, *Z. anorg. allgem. Chem.*, **272**, 288 (1953).

(9) F. Fairbrother, G. Gee and G. T. Merrall, *J. Polymer Sci.*, **16**, 459 (1955); G. Gee, *Science Progress*, No. 170, 193 (1955).

(10) D. M. Gardner and G. K. Fraenkel, *J. Am. Chem. Soc.*, **78**, 3279 (1956).

ported conclusive paramagnetic resonance evidence for the existence of long-chain biradical poly-

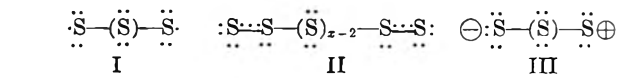

I II III

mers in *liquid* sulfur. In the present paper, we report our findings.

Results and Discussion

A determination on a carbon disulfide-insoluble sample of "supersublimation" sulfur showed a resonance signal at $g = 2.0044$, which is close to the g value of 2.0023 for a free electron.[11] This result constitutes definite evidence in favor of structure I. It should be noted that the line (Fig. 1) is asym-

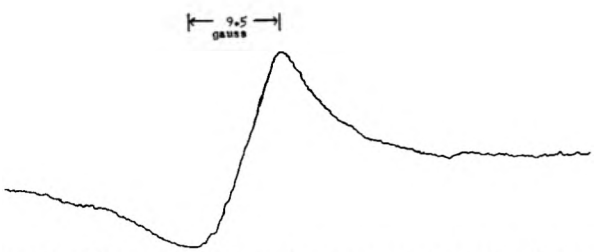

Fig. 1.—Electron paramagnetic resonance absorption line for carbon disulfide–insoluble supersublimation sulfur.

metric and thus unlike most organic free radical lines. This asymmetry is indicative of anisotropy in $g_\perp$ and $g_{\parallel}$ which is a result of an appreciable amount of spin–orbit coupling, the unpaired electron being localized on the sulfur in a p orbit. In comparison, the average g value found by Gardner and Fraenkel[10] for liquid sulfur was 2.024, a value which is shifted ever further from the g value for a free electron. The general interpretation has been made[10] that shifts in g-values for molecules in nondegenerate orbital ground states increase with the magnitude of the spin–orbit coupling and decrease with the separation between ground and excited states.

The absolute concentration of unpaired electrons was estimated to be about 1×10^{-5} mole/l. which can be compared with the value 1.1×10^{-3} found by Gardner and Fraenkel[10] for liquid sulfur at 300°. The number average chain length (p) of the sulfur helix polymers was calculated to be 1×10^7 using the relation:[10] $p = (1000/32)(\rho/C_c)$, where ρ the density was taken as 1.95 g./ml.[12]; the concentration of helix fragments (C_c) taken as 5×10^{-6} mole/l.,[13] assuming two independent electrons per helix fragment. The corresponding values obtained by Gardner and Fraenkel[10] for liquid sulfur were $(5.0 \pm 2.5) \times 10^4$ at 300° and a maximum value of $(1.5 \pm 0.7) \times 10^6$ at 171°. Thus, the value obtained in the present work appears to be in the right order of magnitude.

Based on the information that the sulfur particles are spheres with an average diameter of 2 to 4 μ,[13] an estimate of the average number of helix chains per sulfur particle ($\bar{n}_a$) can be calculated from the relation: $\bar{n}_a = NDVC_g/2$, where N = Avogadro's number, D = density, V = volume of the sulfur sphere, and C_g = absolute concentration of electrons in mole/g. The calculated value is $(2 \text{ to } 4) \times 10^4$ helix chains per sulfur particle, assuming two odd electrons per helix chain. Since X-ray diffraction patterns reveal a regular crystalline structure for this form of sulfur,[5,6] it is reasonable to postulate that the helix chains are oriented with their central axes parallel. This arrangement would of necessity locate the odd electron ends of the helix chains at opposite ends of the spherical particle and would result in the localization of the unpaired electrons which would explain the anisotropy suggested by the asymmetry in the absorption line noted above.

Experimental

The measurements were made on a Varian Associates Model V-4500 E-P-R Spectrometer. The g-value of the sample was calibrated by placing a small amount of 1,1-diphenyl-2-picrylhydrazyl in the sulfur sample. This mixture showed a slight shift from the known[11] g-value of 2.0036 for 1,1-diphenyl-2-picrylhydrazyl. The concentration of unpaired electrons was estimated by comparing the first moment of the line from a 500-mg. sample of sulfur with that from a 5×10^{-2} M solution of vanadyl sulfate (containing the VO^{++} ion), using one line of the 8-line spectrum of the latter. The concentration of unpaired electrons determined in this manner was 5×10^{-9} mole/g.

A sample of "supersublimation" sulfur[14] weighing 9.82 g. was extracted with 200 ml. of redistilled ACS grade carbon disulfide by means of a Soxhlet extractor. After three extractions (totaling 47 hours), the amount of insoluble material remaining after drying to constant weight *in vacuo* at room temperature was 80.3%.[15]

Acknowledgment.—Helpful discussions with Professor Charles E. Reeder of Baylor University are gratefully acknowledged.

(11) J. E. Wertz, *Chem. Revs.*, **55**, 829 (1954).

(12) The Stauffer Product Report No. 819 A lists this value for Crystex.

(13) Stauffer Product Report No. 819 A.

(14) Specifications and properties of this form of sulfur ("Crystex") are described in several Stauffer technical data sheets, product reports and a brochure entitled, "Stauffer Sulfurs." The authors thank the Stauffer Co. for an experimental sample.

(15) This does not necessarily represent extraction to constant weight since there was still a small percentage of material extracted during the third extraction. However, since according to the Stauffer Technical Data Sheet No. 717 Y, "Crystex" undergoes slow reversion to soluble sulfur (the rate increasing with increase in temperature), it is possible that this is the reason for the inability to attain a constant weight by repeated extraction.

COMPLEX FORMATION CONSTANTS OF LEAD AND CADMIUM IONS WITH CHLORIDE IN FUSED LITHIUM PERCHLORATE[1]

BY FREDERICK R. DUKE AND WALTER W. LAWRENCE

Institute for Atomic Research and Department of Chemistry, Iowa State University, Ames, Iowa

Received July 29, 1959

Complex formation constants involving lead and cadmium ions with chloride ion have been determined in a fused KNO_3–$NaNO_3$ eutectic.[2] It is of interest to compare the complex formation constants in a nitrate solvent with those in a perchlorate. Lithium perchlorate is the only stable fused perchlorate and it has been shown to dissolve insignificant amounts of water at low humidity.[3] Therefore the constants were determined in fused

(1) Contribution No. 780. Work was performed in the Ames Laboratory of the U. S. Atomic Energy Commission.

(2) F. R. Duke and M. L. Iverson, THIS JOURNAL, **62**, 417 (1958).

(3) F. R. Duke and A. Doan, *Iowa State College J. Sci.*, **32**, 451 (1958).

$LiClO_4$. The experiments paralleled exactly those reported in fused nitrates.[2]

Results and Discussion

The data are shown in Table I. The constants calculated from the data are listed in Table II.

TABLE I

SOLUBILITY OF METAL CHROMATE IN LITHIUM PERCHLORATE CONTAINING SODIUM CHLORIDE[a]

Sodium chloride, m	Solubility (mg./g. solv.) $PbCrO_4$ 275°	$PbCrO_4$ 300°	$CdCrO_4$ 250–275°
0.0	0.09	0.10	2.3
.02	.11	.14	3.1
.033	.13	.17	
.05	.16	.21	
.08	.21	.30	5.6
.125	.30	.44	7.1
.206	.51	.73	
.325	.85	1.20	
.413	1.10	1.60	
.5	1.35	2.00	
.75		3.25	

[a] $K_s = 9.6 \times 10^{-8}(M/1000\ \text{g.})^2$.

TABLE II

STABILITY CONSTANTS FOR METAL HALIDE COMPLEX IONS IN MOLTEN LITHIUM PERCHLORATE

(Concentration unit, molality)

Complex	Stability constant, 275°: $LiClO_4$	275°: K–$NaNO_3$	300°: $LiClO_4$	300°: K–$NaNO_3$
$PbCl^+$	30 ± 5	8 ± 2	50 ± 8	6 ± 2
$PbCl_2$	9 ± 5	3 ± 1.5	10 ± 5	3 ± 1.5
$PbCl_3^-$	5 ± 5	1 ± 1	4.5 ± 5	1 ± 1
$CdCl^+$	40 ± 15	22 ± 4	40 ± 15	24 ± 4

The high solubility of $CdCrO_4$ limits the range of chloride over which the solubility may be conveniently studied and results in lower precision for the value of the constant. It was observed, however, that, within experimental error, there was no temperature effect.

The higher constants than those found in nitrate solvent are a reflection of the lower polarizability of the perchlorate ion. It is interesting that the temperature effect in perchlorate is in the opposite direction, the constant formation being endothermic.

COMMUNICATION TO THE EDITOR

PHOTOLYSIS OF GAMMA-RAY PRODUCED FREE RADICALS IN ETHANOL AT LOW TEMPERATURES[1]

Sir:

Great interest recently has been evinced in the nature of the various species produced in organic solids irradiated at low temperatures.[2]

The absorption and Electron Paramagnetic Resonance spectra, as well as the effects of bleaching with visible and ultraviolet light, have been studied.[3]

The chemical consequences of bleaching the unstable intermediates in terms of the nature of the stable species produced after the sample is melted have not been studied. Such studies should provide valuable data as to the nature of these transient species. Preliminary to a general investigation of this phenomenon the consequences of both types of bleaching on γ-irradiated ethanol glasses have been studied. Degassed ethanol which was both anhydrous and benzene-free was sealed in thin Pyrex ampoules (5% transmission at 275 mμ) and irradiated with cobalt-60 γ-rays at liquid air temperature. The samples were warmed up in the dark or bleached at liquid nitrogen temperature with either visible or ultraviolet light[4] before warming. Analysis of the gaseous products was made by a modification of the Saunders–Taylor[5] method combined with vapor-phase chromatography for the less volatile fraction.

Dosages are based on the Fricke Dosimeter, using $G(Fe^{+3})$ of 15.6. A summary of experimental results is to be found in Table I.

TABLE I

YIELDS OF GASEOUS DECOMPOSITION PRODUCTS FROM ETHANOL IRRADIATED AT 83°K.

	Conditions of irradiation[b]	Apparent[a] G-values (100 ev. yields) $G(H_2)$	$G(CH_4)$	$G(CO)$	$G(C_2H_6)$	$G(C_2H_4)$
1	1×10^{19} ev./g., no bleach	4.71	0.28	0.01	0.29	0.32
2	1×10^{19} ev./g. vsb. light	5.87	0.46	0.30	0.28	0.33
3	1×10^{19} ev./g. A-H6 Arc[c]	25.20	7.83	4.20	4.62	0.38
4	0.5×10^{19} ev./g. A-H6 Arc[c]	33.98	12.14	8.85	7.16	1.45
5	0.25×10^{19} ev./g. A-H6 Arc	33.15	11.10	7.32	7.52	3.53

[a] Calculated on the assumption that sole source of energy for decomposition is gamma radiation. [b] Dose rate = 2×10^{17} ev./g./min. [c] A residual pink color observed.

A striking increase in the amount of gaseous decomposition products is observed when ultraviolet light is used. This agent by itself produces no significant decomposition. The yield-determining factor seems to be the extent to which the paramagnetic species are decomposed by the ultraviolet light (experiments 3, 4, 5).

It is conjectured that these increased yields are due to the photolysis of the ethanol free radical which under ordinary conditions would either dimerize or recombine with hydrogen atom. Support for this postulate is to be found in the work of V. V. Voevodsky[6] who reports that under ultraviolet illumination the ethanol quintet is replaced

(1) Based on work supported in part by USAEC contract AT-(40-1)2001.

(2) (a) M. C. R. Symons and M. Townsend, *J. Chem. Phys.*, **25**, 1299 (1956); (b) B. Smaller and M. S. Matheson, *ibid.*, **28**, 1169 (1958); (c) C. F. Luck and W. Gordy, *J. Am. Chem. Soc.*, **78**, 3240 (1956).

(3) (a) R. S. Alger, T. H. Anderson and L. A. Webb, *J. Chem. Phys.*, **30**, 695 (1959); (b) H. Zeldes and R. Livingston, *ibid.*, **30**, 40 (1959).

(4) An AH-6 mercury arc with quartz envelope and a water filter was used.

(5) K. W. Saunders and H. A. Taylor, *J. Chem. Phys.*, **9**, 616 (1941).

(6) V. V. Voevodsky, Abstracts, 4th International Symposium on Free Radical Stabilization, Washington, D. C., 1959.

by a quartet with hfs splitting similar to that found for the methyl radical.

$$CH_3\dot{C}HOH \xrightarrow{h\nu} CH_3\cdot + HCH{=}O$$

Bleaching of the color centers with visible light results in slightly increased yields of CO, H_2, CH_4 and CO_2. The yields of ethane and ethylene are unaffected. A likely reaction leading to these enhancements is the transformation of some photosensitive species to the ethanol free radical.

CHEMISTRY DEPARTMENT
FLORIDA STATE UNIVERSITY RUSSELL H. JOHNSEN
TALLAHASSEE, FLORIDA

RECEIVED SEPTEMBER 28, 1959

ADDITIONS AND CORRECTIONS

1956, VOL. 60

Donald G. Miller. An Analytical Proof that the Extremum of the Thermodynamic Probability is a Maximum.

Page 538. After equation (13), insert "Equation (13) may be written more simply as

$$\Delta_i^C = (-1)^i \sum_{j=1}^{t} \left[\sum_{i=1}^{t} \frac{(\epsilon_j - \epsilon_i)^2}{2} \prod_{\substack{l=1 \\ l=i,j}}^{t} \sigma_l^C \right]$$

DONALD G. MILLER.

Donald G. Miller. On the Stokes–Robinson Hydration Model for Solutions.

Page 1299. In the paragraph after equation (16), replace the three occurrences of z by s.—DONALD G. MILLER.

1958, VOL. 62

Richard F. Porter and Richard C. Schoonmaker. Gaseous Species in the Sodium Hydroxide–Potassium Hydroxide System.

Page 489. In Table V, in the reaction $Na_2(OH)_2(g) = 2NaOH(g)$, ΔH_T^0 (kcal.) should read "52.3" instead of "51.4."—RICHARD C. SCHOONMAKER.

Jean M. Stokes and R. H. Stokes. The Conductances of Some Electrolytes in Aqueous Sucrose and Mannitol Solutions at 25°.

Page 498. In Table I, the entries for HCl in 20% sucrose should read: "$\Lambda^0 = 287.4$, $R = 0.674_4$"; and those for HCl in 40% sucrose should read: "$\Lambda^0 = 153.8$, $R = 0.361$." —R. H. STOKES.

Donald G. Miller. The Validity of Onsager's Reciprocal Relations in Ternary Diffusion.

Page 767. In equation (1), "$ad - bc = 0$" should read "$ad - bc \neq 0$." In the equations below equation (1), there should be spaces before c, d, β and δ. In Table I, the headings LHS[3] and RHS[3] should read LHS (1), RHS (1). In footnote (8), M_1 and $\bar{V}_1$ should read M_i and $\bar{V}_i$. In footnote (9), line 5, the two subscript 1's should be replaced by i's.—DONALD G. MILLER.

B. J. Steel, Jean M. Stokes and R. H. Stokes. Individual Ion Mobilities in Mixtures of Non-electrolytes and Water.

Page 1515. The first entry in Table IV (for H^+ in 20% sucrose) should read "H^+, $\lambda^0 = 239.2$, $R = 0.684$ (see correction on p. 498).—R. H. STOKES.

1959, VOL. 63

Virginia D. Hogan and Saul Gordon. A Thermoanalytical Study of the Binary Oxidant System Barium Perchlorate–Potassium Nitrate.

Page 94. The authors state: "A value of −13.5 kcal./mole was given for the heat of the reaction $2KNO_3 + Ba(ClO_4)_2 \rightarrow Ba(NO_3)_2 + 2KClO_4$ at 325°C. The corrected value is −16.5 kcal./mole. The entropy change necessary to make the free energy change of this reaction zero was given as −22.5 cal./deg./mole, whereas the corrected value is −27.5 cal./deg./mole.—SAUL GORDON.

K. Bril, S. Bril and P. Krumholz. Separation of Metal Ions by Means of Ion Exchange Membranes. I. Separation of Rare Earth Mixtures, and of Thorium–Rare Earth Mixtures Using Ethylenediaminetetraacetic Acid.

Page 257. The numerator part of equation (3) should read "$(Me_1)/(Me_2)$."

Page 259. In Table I, the headings reading "α_{Nd}^{La} and β_{Nd}^{La}" should read "β_{La}^{Nd} and α_{La}^{Nd}." Also, in Table II, the headings reading "α_{Nd}^{La}, α_{Nd}^{Pr}, β_{Nd}^{La}, β_{Nd}^{Pr}," should read "β_{Pr}^{Nd}, β_{La}^{Nd}, α_{Pr}^{Nd}, α_{La}^{Nd}." Then in Table II, Expt. 12, last column, for "1.36" read "1.86."—P. KRUMHOLZ.

Concetto R. Giuliano, Newton Schwartz and W. K. Wilmarth. The Aqueous Chemistry of Inorganic Free Radicals. II. The Peroxydisulfate Induced Exchange of Oxygen Atoms between Water and Molecular Oxygen and Evidence Regarding the Acidity Constant of the Hydroxyl Radical.

Page 354. Equation (3) should read

$$\frac{1}{t} \ln (1 - F) = \frac{k}{[1 + (V_g/V_s\lambda)]}$$

Page 355. A revised Fig. 1 should be substituted:

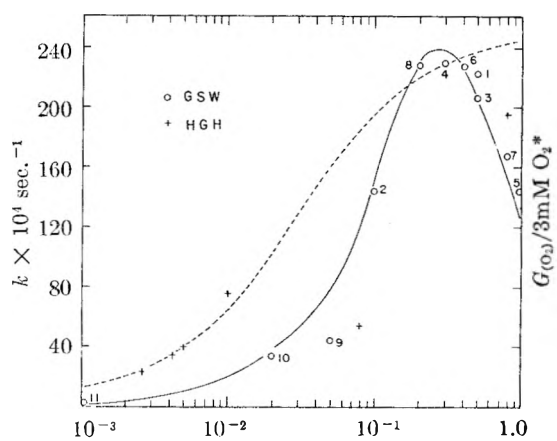

Fig. 1.

W. K. WILMARTH

Donald G. Miller. Ternary Isothermal Diffusion and the Validity of the Onsager Reciprocity Relations.

Page 570. The author notes that: "Equations 5, 13, 14 and 15, and the L_{ij} entries in Table III all have the wrong sign. This does not affect the conclusions nor the absolute numerical values of any tabulated quantities." In Tables II and V the roman numeral I should be supplied in the headings. In footnote a of Table V, $10^{-2}RT$ should read $10^{-8}RT$. In equation (11A) on page 578, j_i should read j_i. In the equalities (23A), the δ should be replaced by α.—DONALD G. MILLER.

Peter J. Dunlop. Data for Diffusion in a Concentrated Solution of the System NaCl–KCl–H_2O at 25°. A Test of the Onsager Reciprocal Relation for this Composition.

Page 612. In col. 1, last line of paragraph 3, for "ref. 1" read "ref. 2." In col. 2, line 3, for "D_A" read "$\mathfrak{D}_A$."

Page 614. In equation (6b) for subscript "$C_{k\neq 0,j}$," read "$C_{l\neq 0,j}$." In Table III, B_{12} should be 0.0573_2 and B_{21} should be 0.0389_2. The values in Table IV now become:

Γ_{11}	0.037_3	$\mu_{11}/(RT)$	1.243_3
Γ_{12}	0.013_1	$\mu_{12}/(RT)$	0.482_5
Γ_{21}	0.013_1	$\mu_{21}/(RT)$	0.450_0
Γ_{22}	0.005_7	$\mu_{22}/(RT)$	1.103_9
$(L_{12})_0 \times RT \times 10^9$	-3.9_3	$(L_{11})_0 \times RT \times 10^9$	13.1_5
$(L_{21})_0 \times RT \times 10^9$	-3.6_3	$(L_{22})_0 \times RT \times 10^9$	18.7_9
$\%\Delta_{exp}$	-7.9		

Page 615. In col. 2, line 19, for "7.4%" read "−7.9%." In col. 2, line 15 from the end, for "KCl-urea-H_2O" read "raffinose-urea-H_2O."—PETER J. DUNLOP.

C. Botré, V. L. Crescenzi and A. Mele. A Study on Micelle Formation in Colloidal Electrolyte Solutions.

Page 652. Equations (1) and (2) should read:

$$a = \gamma(C_0 + n\alpha C_m) \qquad (1)$$

$$\gamma_{ex} = \gamma\alpha + \frac{\gamma C_0(1 - \alpha)}{C} \qquad (2)$$

P. Krumholz. Spectroscopic Studies on Rare Earth Compounds. III. The Interaction between Neodymium and Perchlorate Ions.

Page 1314. In Table I, the term "$(\epsilon - \epsilon_0) \times 10^3$" in the table headings should read "$(\epsilon - \epsilon_0) \times 10^2$."—P. KRUMHOLZ.

Kurt A. Kraus and Richard J. Raridon. Temperature Dependence of Some Cation Exchange Equilibria in the Range 0 to 200°.

Page 1903. In col. 2, line 9 below Fig. 1, for "0.7%" read "0.04%."

Author Index to Volume LXIII, 1959

Subject Index to Volume LXIII, 1959

Interesting Research Positions for

CHEMISTS
AT LOCKHEED

Lockheed Missiles and Space Division has a number of important, research positions for experienced chemists at its new facilities in the Stanford Industrial Park, Palo Alto, and Sunnyvale, California. This location, on the beautiful San Francisco Peninsula, is one of the choicest living areas in the nation.

The Division is widely diversified in its work, with complete capability in more than 40 areas of science and technology—from concept to operation.

Career opportunities are available for chemists with the following background:

PHYSICAL-ORGANIC CHEMISTRY

Ph.D. required with post-doctoral experience in instrumental analytical techniques including infrared, ultraviolet and mass spectroscopy.

Experience in gas chromatography, X-ray and electron diffraction work desirable.

INORGANIC CHEMISTRY

Ph.D. with 5 years' experience in gas solid reaction kinetics, intermetallic compounds and electronic properties of matter.

ANALYTICAL CHEMISTRY

M.S. or Ph.D. with several years' experience in the development of microchemical techniques. Experience in X-ray and electron diffraction work desirable.

ELECTROCHEMISTRY

M.S. with background in corrosion effects. For work in the development of surface treatments of metals and basic work on surface reaction kinetics. Knowledge of X-ray and electron diffraction techniques desirable.

ORGANIC CHEMISTRY

M.S. or Ph.D. with background in formulation of elastomers. Should be thoroughly grounded in the molecular resistance of substances to various environments.

ORGANIC CHEMISTRY

Ph.D. with experience in reinforced plastic area. Should have ability to relate physical requirements to modifications in molecular structures.

***PHOTO CHEMISTRY**

Ph.D. with background in experimental techniques in the field of photo chemistry.

***PHYSICAL CHEMISTRY**

M.S. or Ph.D. with strong background in the theory of catalysis and experience in developing catalysts. Fundamental knowledge in solid state chemistry, physics or surface chemistry desirable.

***ELECTROCHEMISTRY**

Ph.D. required.

*For work on a high priority project in the field of energy conversion.

FOR INFORMATION regarding these positions, please write Research and Development Staff, Lockheed Missiles and Space Division, Dept. L-99, 962 West El Camino Real, Sunnyvale, California. U.S. citizenship required.

Lockheed / **MISSILES AND SPACE DIVISION**

Sunnyvale, Palo Alto, Van Nuys, Santa Cruz, Santa Maria, California
Cape Canaveral, Florida—Alamogordo, New Mexico—Hawaii